Freie Universität Berlin

Electrocatalytic Carbon Dioxide Reduction Using Cationic Cp*-Iridium Complexes Bearing Unsymmetrically Substituted Bipyridine Ligands

Inaugural-Dissertation

to obtain the academic degree

Doctor rerum naturalium (Dr. rer. nat.)

submitted to the Department of Biology, Chemistry and Pharmacy of the Freie Universität Berlin

by:

M.Sc. Fanni Daruny Sypaseuth

from Szombathely, Hungary

November 17, 2014

1. reviewer: Prof. Dr. C. C. Tzschucke

2. reviewer: Prof. Dr. C. Müller

Disputation on the 2nd February 2015

The described work was carried out within the time period of January 2012 until November 2014 under the supervision of Prof. Dr. C. C. Tzschucke at the Freie Universität Berlin.

"If we knew what it was we were doing, it would not be called research, would it?"
Albert Einstein

Contents

List of abbreviations, acronyms & symbols

ΔG	$\mathrm{J{\cdot}mol^{-1}}$	Gibbs free energy
ΔH	$\mathrm{J{\cdot}mol^{-1}}$	enthalpy
ΔS	$\mathrm{J{\cdot}mol^{-1} \cdot K^{-1}}$	entropy
δ	ppm	chemical shift
η	%	current efficiency
η_{corr}	%	corrected current efficiency
ν	$\mathrm{V{\cdot}s^{-1}}$	scan rate
μ	Pa·s	viscosity
σ_p^+		sensitivity constant
A	$\mathrm{m^2}$	area
Ac		acyl
Ar		aryl
APTES		3-aminopropyl-triethoxysilane
bpy		(substituted) bipyridine
c	$\mathrm{\mu mol{\cdot}mL^{-1}}$	concentration
$c_{(+/-)}$	$\mathrm{\mu mol{\cdot}mL^{-1}}$	concentration from cathodic and anodic half cells
calc.		calculated
cat		catalyst
CE		counter electrode
Cp*		η^5-pentamethylcyclopentadienyl
CV		cyclic voltammetry
Cy		cyclohexyl
D	$\mathrm{cm^2{\cdot}s^{-1}}$	diffusion coefficient
d	mm	diameter
dba		dibenzylideneacetone
DCM		dichloromethane
DFT		density functional theory
DMAE		dimethylaminoethanol
DMF		dimethylformamide
DNPH		2,4-dinitrophenylhydrazine

DPPA		diphenylphosphoryl azide
dppe		1,2-bis(diphenylphosphino)ethane
DPV		differential pulse voltammetry
E	V	potential
$E_{(1/2)}$	V	half-wave potential
E_{app}	V	applied potential in controlled potential electrolysis
EDC		1-ethyl-3-(3-dimethylaminopropyl)carbodiimid
EDG		electron donating group
EDOT		3,4-ethylenedioxythiophene
E_{p}	V	peak potential
E_{pa}	V	anodic peak potential
E_{pc}	V	cathodic peak potential
eq., equiv.		equivalent
Et		ethyl
EWG		electron withdrawing group
F	$= 9.64853399(24) \cdot 10^4$ C·mol^{-1}	Faraday's constant
Fc		ferrocene
FKM		designation for fluoroelastomer
GC		glassy carbon
GC-MS		gas chromatography - mass spectrometry
HMBC		heteronuclear multiple bond coherence
HMQC		heteronuclear multiple quantum coherence
HOBT		hydroxybenzotriazole
HPLC		high performance liquid chromatography
HRESI-MS		high-resolution electrospray ionisation mass spectrometry
I	A, mA, μA	current
ID	mm	inside diameter
Int		integrals in ^{1}H NMR spectra
i_{p}	A, mA, μA	peak current
i_{pa}	A, mA, μA	anodic peak current
i_{pc}	A, mA, μA	cathodic peak current

IR		infrared spectroscopy
J	Hz	coupling contant
k	$= 1.3806488(13)\cdot10^{-23}$ J·K^{-1}	Boltzmann constant
LA		Lewis acid
m	mg	mass
m/z		mass to charge ratio
Me		methyl
MLCT		metal to ligand charge transfer
n	mol, μmol	molar amount
$n_{(+/-)}$	mol, μmol	molar amount in the samples from the cathodic and anodic half cells
NBD		norbornadiene
nBu, Bu		butyl
NMP		N-methyl-2-pyrrolidone
NMR		nuclear magnetic resonance
NS		"Normschliff" which means ground glass joint
OD	mm	outside diameter
ox		oxidation
p	Pa	pressure
Ph		phenyl
pK_a		acid dissociation constant
pTol		para-tolyl
ppm		part per million
ppy		phenylpyridine
Py, pyr		pyridine
Q	C	charge
q		quartett
Q_{bckg}	C	background charge
Q_{corr}	C	corrected charge
R	$= 8.3144621(75)$ J·mol^{-1}K^{-1}	gas constant
r.d.s.		rate determining step

RE		reference electrode
red		reduction
R_i		molecular radius
r.t.		room temperature
s		singlet (NMR) *or* strong (IR)
SEC		spectroelectrochemistry
T	K	temperature
t	h	time
TBAP		tetrabutylammonium hexafluorophosphate
tBu		tert-butyl
TEA		triethylamine
TEOA		triethanolamine
THF		tetrahydrofuran
TM		transition metal
TMG		transmetalating group
TOF	min^{-1}	turnover frequency (per catalyst molecule)
TON		turnover number (per catalyst molecule)
tpy		(substituted) terpyridine
US		United States
UV-Vis		ultraviolet-visible light
V	mL	volume
v/v	%	volume ratio
$V_{\mathrm{NMR(+/-)}}$	mL	volume of NMR samples from cathodic and anodic cell compartments
V_tot	mL	total volume of the electrolyte
w		weak (IR)
w/o		without
WE		working electrode
$x_{\mathrm{CO_2}}$		molar ratio of CO_2 in solvent
X_max	%	maximum conversion
X_observed	%	observed converion
xyl		xylene
z		number of charge

Abstract in *English*

Due to environmental considerations and the limitation of fossil based energy resources, carbon dioxide reduction into liquid fuels and energy storage materials, such as formic acid, is one of the most important topics of recent research. Ir complexes play a significant role in both the hydrogenation and electrocatalytic conversion of CO_2. This thesis describes the synthesis of new Ir complexes and their elecrocatalytic activity in CO_2 reduction.

Unsymmetrically substituted bipyridine ligands were prepared by Pd catalyzed C−H bond arylation of pyridine *N*-oxides using halopyridines. This method was extended towards the formation of asymmetrically substituted terpyridines. The substituents on both the pyridine *N*-oxide and halopyridine rings played a crucial role in the yields of the formed products. The presence of the electron withdrawing ethoxycarbonyl group in the 4 position on the pyridine *N*-oxide ring was essential to drive the reaction to moderate to good yields. As for the arylating reagents, using 2-bromopyridine and 2-bromo-4-tert-butylpyridine resulted in the best yields. The bi- and terpyridine *N*-oxides were reduced to the corresponding bi- and terpyridines in excellent yields.

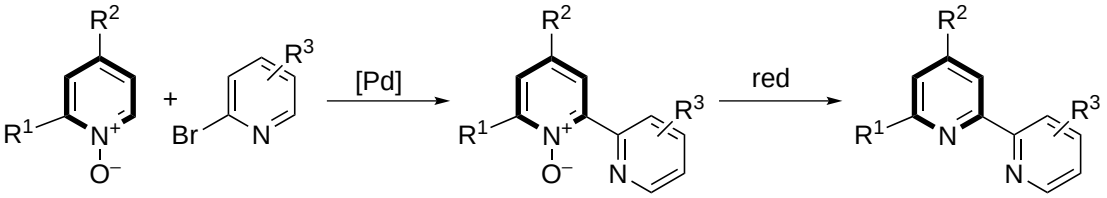

R^1 = H or (substituted) pyridyl
R^2 = CO_2Et
R^3 = H, Me, *t*Bu, OMe, CF_3, CN

$[Cp^*Ir(bpy)Cl]^+$-type complexes were subsequently prepared, bearing symmetrically and unsymmetrically substituted, as well as unsubstituted bpy ligands. The complexes were characterized by standard methods and their electronic properties were investigated by cyclic voltammetry. The expected trend was observed in the potentials of the Ir centered reduction event of the complexes: electron donating substituents shifted the reduction potentials to more negative values, whereas complexes bearing electron withdrawing CO_2Et group were reduced at more positive potentials. In CO_2 saturated $MeCN/H_2O$ 9:1, v/v mixture all complexes displayed a catalytic current wave between −1.80 and −2.05 V vs Fc/Fc^+.

To further test the catalytic behavior of the complexes, controlled potential electrolysis experiments

were carried out in a self-made two compartment cell. First, the electrolysis conditions were examined using [Cp*Ir(bpy)Cl]Cl complex bearing unsubstituted 2,2′-bipyridine. At −1.80 V vs Ag wire, formation of formate and formic acid were observed after electrolysis for 3 h in MeCN/H_2O 95:5, v/v and MeCN/MeOH 1:1, v/v solvent mixtures. Occasionally, another product, possibly formaldehyde was also obeserved, however its formation was not reproducible.

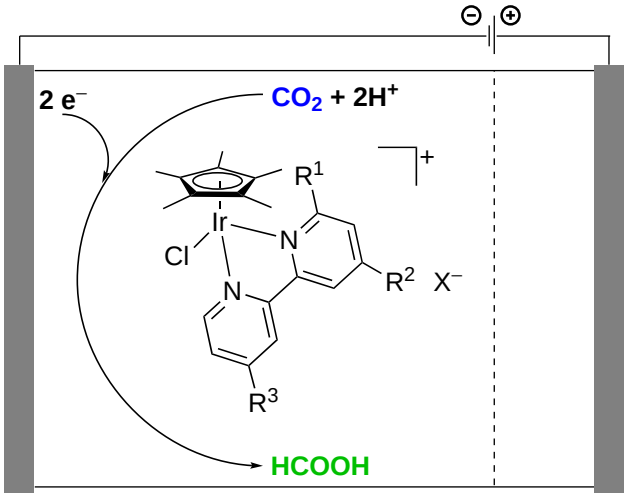

After optimization of the conditions, the catalysts were tested to determine turnover frequencies with respect to HCO_2H formation. Although a straightforward trend between electronic properties of the catalyst and their activity in the CO_2 reduction could not be observed, an influence of the ligand substituents on the activities was clear. All new complexes showed higher activities than the [Cp*Ir(bpy)Cl]Cl complex bearing unsubstituted 2,2′-bipyridine ligand.

Abstract in *German*

Durch zunehmende Umweltbedenken und die Begrenzung fossiler Ressourcen hat die Reduktion von CO_2 zu flüssigen Treibstoffen als Energieträger, wie zum Beispiel Ameisensäure, in der heutigen Forschung an großer Bedeutung gewonnen. Hierbei spielen Iridium-Komplexe eine wichtige Rolle in der Hydrierung sowie der elektrokatalytischen Umwandlung von CO_2. Die vorliegende Dissertation beschreibt die Synthese von neuen Iridium-Komplexen und ihre elektrokatalytische Aktivität zur CO_2-Reduktion.

Die Herstellung unsymmetrischer substituierter Bipyridin-Liganden erfolgte durch Palladium-katalysierte Arylierung der Kohlenwasserstoffbindungen in den Pyridin-*N*-oxiden durch Halopyridine. Diese Methode wurde auch zur Herstellung unsymmetrischer substituierter Terpyridine genutzt. Die Substituenten des *N*-oxid- und Halopyridinrings spielen dabei eine essentielle Rolle für die Ausbeuten der gebildeten Produkte. Die Anwesenheit der elektronenziehenden Ethoxycarbonylgruppe in der 4-Position am Pyridin-*N*-oxid war eine Grundvoraussetzung für gute Ausbeuten. Wie für Arylierungsreagenzien war die Ausbeute unter Verwendung von 2-Brompyridin und 2-Brom-4-*tert*-butylpyridin am höchsten. Die Bi- und Terpyridin-*N*-oxide wurden in sehr hohen Ausbeuten zu ihren korrespondierenden Bi- und Terpyridinen reduziert.

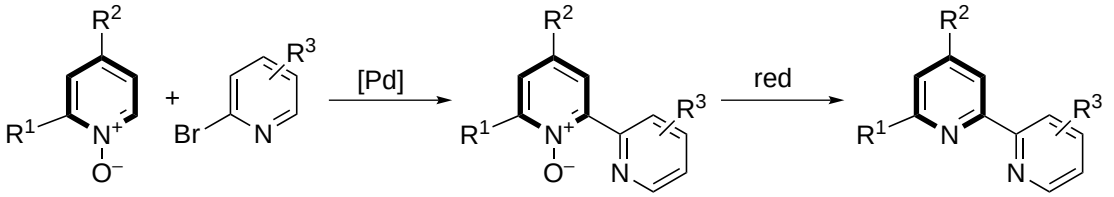

R^1 = H or (substituted) pyridyl
R^2 = CO_2Et
R^3 = H, Me, *t*Bu, OMe, CF_3, CN

$[Cp^*Ir(bpy)Cl]^+$-Komplexe wurden mit symmetrischen und unsymmetrischen Substituenten sowie mit nicht-substituierten bpy-Liganden hergestellt. Alle Komplexe wurden mit Standardmethoden charakterisiert sowie mit cyclischer Voltammetrie bezüglich ihrer Redoxpotentiale untersucht. Bei den Redoxpotentialen der Iridium-zentrierten Reduktionen wurde ein erwarteter Trend beobachtet: Elektronenschiebende Substituenten veränderten das Reduktionspotential zu negativeren Werten, während Komplexe mit elektronenziehenden CO_2Et-Gruppen bei positiveren Potentialen reduziert wurden. In CO_2-gesättigten MECN/H_2O 9:1, v/v zeigten alle Komplexe einen katalytischen Strom zwischen $-1{,}80$ und 2,05 V *vs* Fc/Fc^+.

Um das katalytische Verhalten der Komplexe besser charakterisieren zu können, wurden potentialkontrollierte Elektrolyseexperimente durchgeführt, in einer dafür eigens entwickelten zweiteiligen Zelle. Die Elektrolysebedingungen wurden unter Verwendung des $[Cp^*Ir(bpy)Cl]^+$-Komplexes mit nicht-substituiertem 2,2-Bipyridin untersucht. Bei $-1{,}80$ V *versus* Silberdraht, wurde nach 3 Stunden Elektrolyse in MeCN/H_2O 95:5, v/v die Bildung von Formiat und Ameisensäure beobachtet. In einigen Fällen wurde die Bildung eines weiteren Produktes beobachtet, möglicherweise Formaldehyd. Jedoch war die Bildung dieses Produktes nicht reproduzierbar.

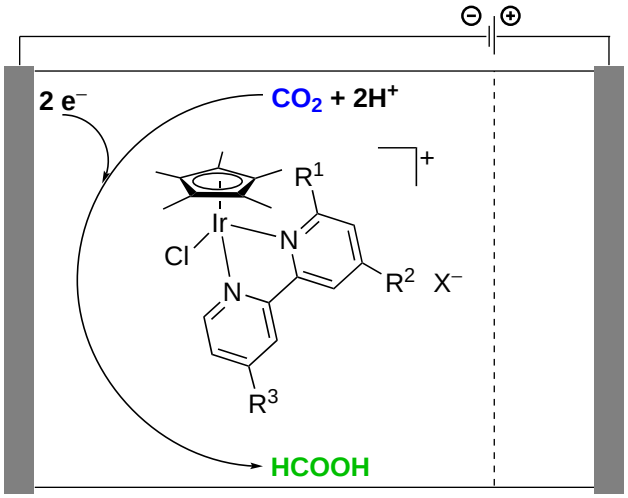

Nach der Optimierung der Reaktionsbedingungen wurden alle Katalysatoren bezüglich ihrer Wechselzahl für Ameisensäure untersucht. Obwohl kein klarer Trend zwischen elektronischen Eigenschaften der Katalysatoren und ihrer CO_2-Reduktionsaktivität beobachtet werden konnte, ist der Einfluss der verschiedenen Substituenten auf die Aktivität eindeutig. Alle hier neu synthetisierten Komplexe zeigten höhere Aktivitäten als der $[Cp^*Ir(bpy)Cl]^+$-Komplex mit nicht-substituiertem 2,2′-Bipyridin.

1 Introduction to the challenges in CO_2 conversion

1.1 Importance of CO_2 reduction

Carbon dioxide is a naturally abundant compound in Earth's atmosphere being part of the carbon cycle. Its amount was determined to be about 400 ppm in October 2014.[1] CO_2 is essential for life on Earth as it is the starting compound of photosynthesis that is the energy producing process of plants. Atmospheric CO_2 is produced by respiration from both plants and animals and decomposition of biomass. The amount of atmospheric CO_2 is fluctuating because there is a constant exchange between atmospheric CO_2 and terrestrial biosphere, ocean and fossil fuel reservoirs.
However, human activities significantly increase the amount of CO_2 in the atmosphere not only by using CO_2 emitting large scale industrial processes and transportation, but also by influencing the function of natural sinks, such as forests. Human induced CO_2 emissions were increasing by 2.5% anually over the past decade.[2]

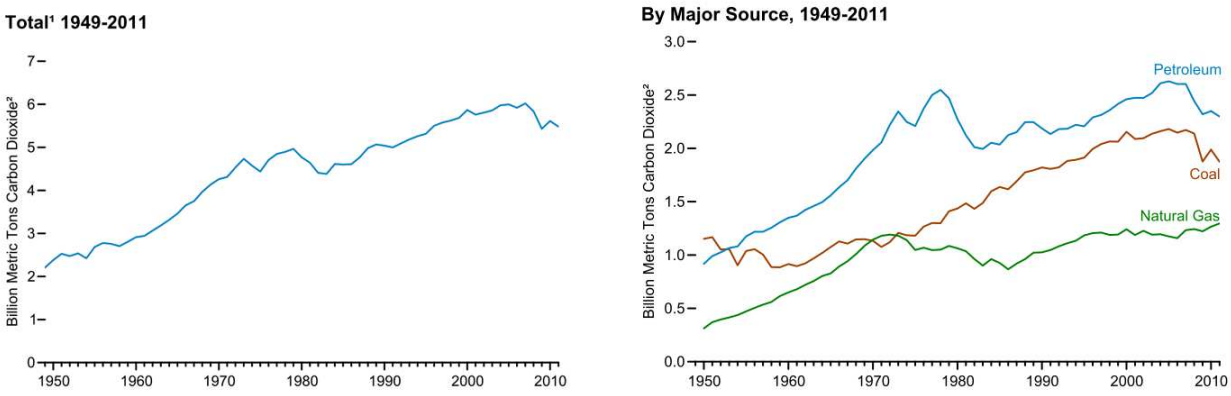

Figure 1: Total CO_2 emission from energy consumption between 1949-2011 (left) and emissions from the major sources of energy industry. Graphs are adopted from the Annual Energy Review by the US Energy Information Administration.[3]

Since energy production in today's world is dependent on the burning of the diminishing fossil fuel resources, CO_2 emissions are inevitably further increasing (see Figure 1). Several governments already took action to boost implementation of renewable energy sources, which will decrease CO_2 emissions of the energy sector in the long term. Besides, there are already several industrial technologies to tackle the CO_2 emission problem, such as separation and capture systems used in power plants and industrial processes.[4]
The growing emission values make CO_2 an abundant, cheap and ideal starting material for chemical

industry. Besides, CO_2 offers a powerful option for energy storage when converting it into liquid fuels using renewable energy sources (Scheme 1). This procedure has a very high potential considering the finite availability of fossil based resources. Therefore, development of energy efficient and cheap processes for the conversion of CO_2 are essential.

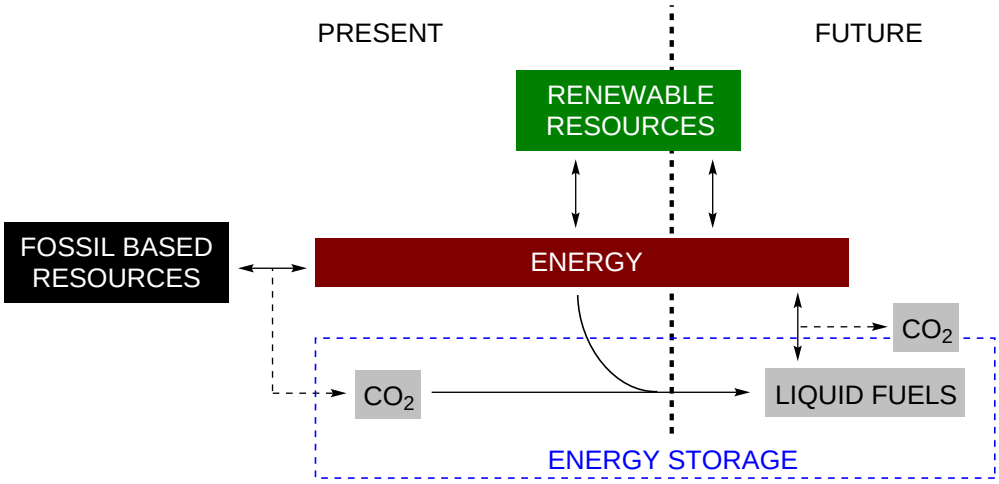

Scheme 1: CO_2 conversion as a potential tool for energy storage.

1.2 Stability of the CO_2 molecule

In general, independent from the catalytic system, the activation of the CO_2 molecule is very difficult due to its high thermodynamic and kinetic stability. As for the thermodynamics, the carbon-oxygen double bonds are strong (ΔH_f(C=O) = −803 kJ·mol^{-1}) and therefore substantial energy is needed to cleave them. However, when CO_2 reacts with a high energy content compound, such as H_2, the formation of more stable products can indeed make the overall reaction thermodynamically more favourable. For example, reaction of gaseous CO_2 and H_2 to formic acid has a Gibbs free energy ΔG^0 = 32.9 kJ/mol, whereas addition of a base such as NH_3 induces a substantial decrease in the ΔG^0 value to -9.5 kJ/mol by forming a salt with the formic acid product thereby lowering the enthalpy.[5]

	ΔH°_{298} kJ·mol^{-1}	ΔS°_{298} kJ·mol^{-1}·K^{-1}	ΔG°_{298} kJ·mol^{-1}
CO_2 (g) + H_2 (g) ⟶ HCO_2H (l)	–31.6	–0.215	+32.9
CO_2 (g) + H_2 (g) + NH_3 (aq) ⟶ HCO_2^- (aq) + NH_4^+ (aq)	–84.3	–0.250	–9.5

Scheme 2: Thermodynamics of CO_2 hydrogenation in the abscence and presence of a base.[5]

In accordance with the above example, in electrochemical processes, proton-coupled multielectron steps are more favourable than the single electron reduction of CO_2 to $CO_2^{\bullet-}$, since the formed

molecules are thermodynamically more stable.[6] The challenge in converting CO_2 into more complex molecules lies not only in the overall unfavourable thermodynamics but also the high kinetic barriers. It is not straightforward to find a single catalyst that can go through all the steps to convert CO_2 into HCO_2H, HCHO, MeOH and CH_4 at low activation energies without the use of stochiometric amounts of high energy reactants.[7,8,9]

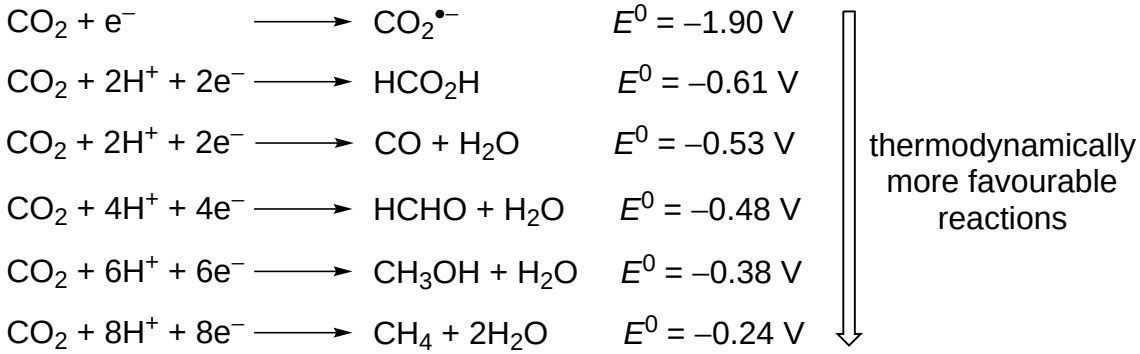

Scheme 3: Standard potentials of different electrochemical CO_2 reduction processes in pH = 7 aqueous solutions under 1 atm CO_2 pressure and 1 M solute concentration *vs* NHE.[6]

1.3 Catalytic approaches towards CO_2 conversion

Catalytic CO_2 conversion can be categorized into several branches depending on the energy source used: chemical, electrical, solar; the nature of the catalytic process: homogeneous, heterogeneous; and the catalyst material or molecule: transition metal (TM) based or TM free.

Table 1: Catalytic approaches towards CO_2 reduction and the most recent reviews highlighting these approaches.

		Catalyst		
		Homogeneous		Heterogeneous
		TM based	TM free	
Energy source	Chemical	Ref[10,5,11]	Ref[10,8]	Ref[10,12]
	Electrical	Ref[6,13,14,15,16,17]	Ref[13]	Ref[13,18,19]
	Solar	Ref[20,21,22]		Ref[23,24,18,25,22]

Electrocatalytic processes are particularly interesting, because electricity can be derived from solar or wind power as sustainable energy sources. In the last decades, many approaches towards CO_2 conversion using homogeneous hydrogenation, as well as photocatalytic, and electrocatalytic reductions were reported. However, achieving high product selectivity and catalyst activity remains a challenge.

Depending on the catalytic system, the reduction of CO_2 typically results in the formation of carbon monoxide[26,27,28,29,30,31,32,33,34,35,36] or formate[37,38,39,40,41,42,43,44] but other products such as formaldehyde,[45,46] methanol[47,48] and methane[49,50] have also been observed. The formation of formic acid is especially interesting, because it could serve as a hydrogen storage compound for fuel cells.[51,52,53,54,55] A large number of transition metal based procedures has been developed including numerous iridium based catalysts for homogeneous hydrogenation and electrocatalytic reduction of CO_2.

1.3.1 Iridium catalyzed CO_2 reduction

Homogeneous hydrogenation of CO_2 and bicarbonate in water using half-sandwich complexes has been extensively studied by Himeda *et al.*[56,57,58,59] Initially they investigated Ir, Rh and Ru complexes, and observed that deprotonated 4,7-dihydroxy-1,10-phenanthroline ligands under the basic reaction conditions significantly accelerated the hydrogenation reaction compared to when unsubstituted or MeO substituted phenanthrolenes were used as ligands. The observations implied that the electron donating ability of the ligand directly influenced the catalytic activity. They also detected the Ir(III)-hydride species (on the right in Scheme 4, M = Ir) by ^{1}H NMR after stirring the Ir(III)−Cl complex under H_2 pressure. This hydride species showed high activity towards the formation of HCO_2^- after addition of $KHCO_3$ under atmospheric pressure of H_2, indicating that the hydride species can be an intermediate in the catalytic cycle (Scheme 4).

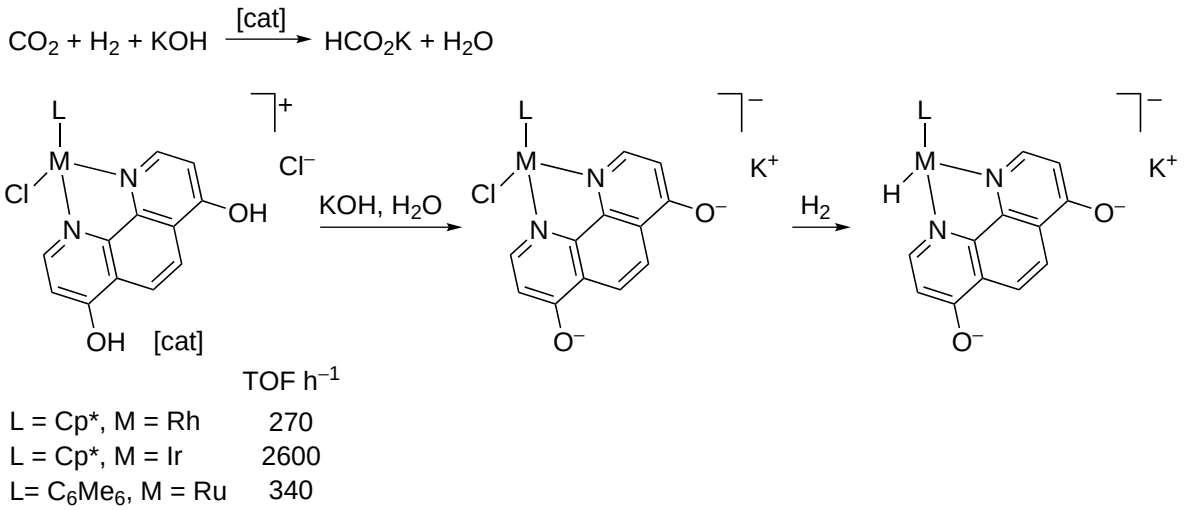

Scheme 4: Water soluble half-sandwich complexes in the hydrogenation of CO_2 under basic conditions: 1 M aq. KOH, 4 MPa CO_2:H_2 1:1, $c_{cat} = 0.01$ mM, $T = 80$ °C.[56]

Inspired by these studies and additional theoretical work by Sakaki,[60] Himeda *et al.* further examined the influence of the electronic effects on the catalytic activity using a series of $[Cp^*Ir(bpy)Cl]^+$

complexes (Scheme 5). They evaluated the Hammett plot of the initial turnover frequencies log(TOF) *vs* the σ_p^+ values of the bpy substituents under basic conditions and obtained a good correlation with the following trend in reactivity: O^->OMe>Me>CO_2^->H.[58]

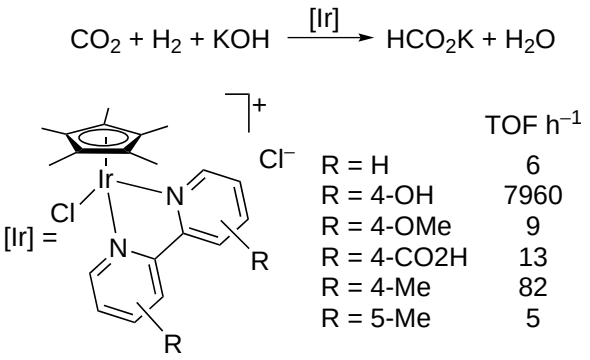

Scheme 5: $[Cp^*Ir(bpy)Cl]^+$-type complexes containing differently substituted bpy ligands in the hydrogenation of CO_2 under basic conditions: 1 M aq. KOH, p = 4 MPa CO_2:H_2 1:1, c_{cat} = 0.02 mM, T = 80 °C.[58]

Iridium(III) pincer complexes were also studied in CO_2 hydrogenation reactions.[61,62,63,64] Nozaki obtained the highest activity when using Ir(III)-trihydride complex (TOF = $1.5{\cdot}10^5$ h^{-1}, Scheme 6) and observed that the chloro derivatives resulted in worse yields than their hydride analogues. Using Ir(III)-trihydride as catalyst, he also examined the use of K_3PO_4 as weaker base than KOH in the CO_2 hydrogenation, but they obtained considerably lower activity with a TOF = $2.0{\cdot}10^4$ h^{-1}. Nozaki speculated that the Ir(III)-trihydride complex showed such a high activity due to accelerated HCO_2^- dissociation brought about by simultaneous ligand deprotonation-dearomatization (see discussion in 1.3.2). The authors emphasized that this catalyst system delivered to date the highest TOF. However, it should be noted that considerably harsher conditions were used in these experiments than in the studies by Himeda *et al.*[58]

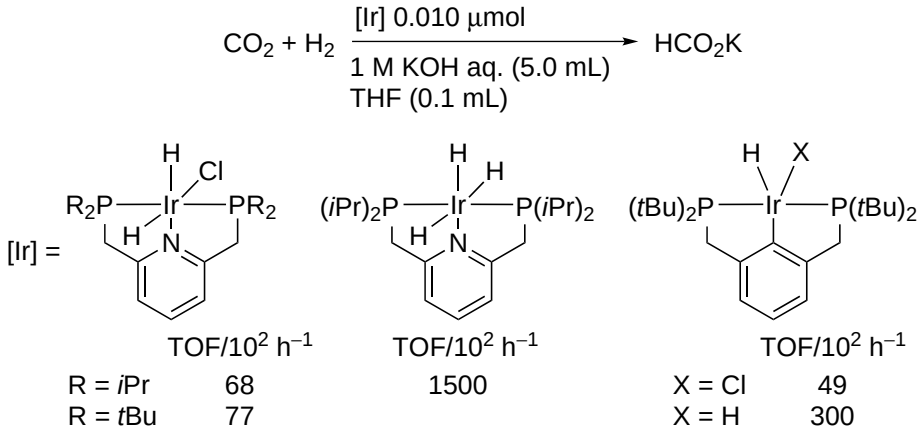

Scheme 6: Iridium(III) pincer complexes in the hydrogenation of CO_2 under basic conditions: p = 5 MPa CO_2:H_2 1:1, c_{cat} = 0.002 mM, T = 200 °C.[61]

The successful immobilization of Ir catalyst for CO_2 hydrogenation was demonstrated by Hicks, who recently reported on an Ir species attached to a polyethyleneimine backbone with an iminophosphine ligand. The same group also described the immobilization of the same Ir species on silica support. Using this system, they obtained HCO_2H with a TON of 2800 after 20 h reaction under 4 MPa CO_2/H_2 1:1 at 60 °C.[65,66]

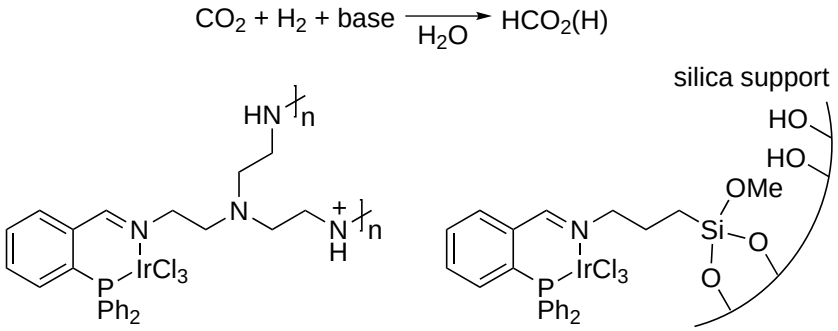

Scheme 7: Immobilized Ir species for the hydrogenation of CO_2 in water in the presence of base.[65,66]

Electrocatalytic reduction of CO_2 using an iridium complex was first mentioned by Meyer, who observed enhanced current in the CV of $[Ir(bpy)_2(PPh_3)H][PF_6]_2$ in CO_2 saturated MeCN compared to the current in the absence of CO_2.[44] Some years later Deronzier investigated the formate selective electrocatalytic reduction of CO_2 using $[Cp^*M(bpy)Cl]^+$ complexes (M = Ir, Rh in Scheme 8). He used an aqueous-organic medium with Bu_4NPF_6 conductive salt and noted that 10-20% H_2O content played an important role resulting in higher product amounts. Current efficiencies of the HCO_2^- formation were up to 50%. He proposed the formation of an M(III)-hydride as intermediate in the catalytic cycle (see 1.3.2).[42] Surprisingly, despite their extensive use in homogeneous CO_2 hydrogenation reactions, there are no other reports to date on the electrocatlayitic reduction of CO_2 using $[Cp^*Ir(bpy)Cl]^+$-type complexes.

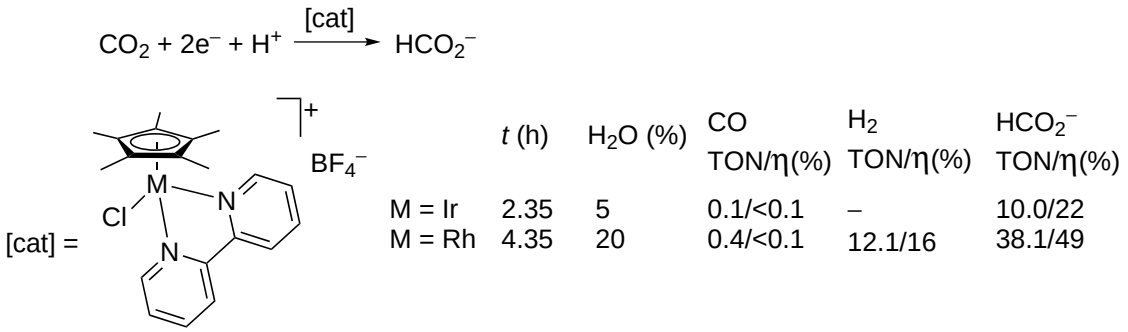

	t (h)	H_2O (%)	CO TON/η(%)	H_2 TON/η(%)	HCO_2^- TON/η(%)
M = Ir	2.35	5	0.1/<0.1	–	10.0/22
M = Rh	4.35	20	0.4/<0.1	12.1/16	38.1/49

Scheme 8: $[Cp^*M(bpy)Cl]^+$ complexes in the electrocatalytic reduction of CO_2 reported by Deronzier.[42]

Meyer and Brookhart studied water stable Ir(III) pincer dihydride complexes for the insertion and

electrocatalytic reduction of CO_2. Controlled potential electrolysis experiments were carried out at $E_{app} = -1.45$ V *vs* NHE in MeCN/H_2O 95:5, v/v and a TON of 40 regarding HCO_2H product and a high current efficiency of 85% were obtained. Background reduction of H_2O to H_2 was described as side-reaction, but CO product was not detected. The current was decreasing gradually during the electrolysis and the solution became basic (pH $>$ 9).[67] Motivated by the good selectivity towards HCO_2H formation over the reduction of H_2O in MeCN/H_2O mixture, the same group developed a water soluble derivative of the Ir(III) pincer complex by tethering a quaternary amine moiety on the phosphinite pincer ligand (Scheme 9). In pure H_2O high selectivity towards HCO_2^- over H_2 (up to 93 *vs* 7%) was achieved between $E_{app} = -1.35$ and -1.45 V. At lower potentials, H_2O reduction became more dominant. Addition of 1% MeCN was essential in the electrocatalysis, for the displacement of the coordinated HCO_2^- with MeCN to form the product and regenerate the Ir catalyst. The authors speculate that this special selectivity was due to a less hydridic Ir-hydride species which was not reactive to the formation of H_2, but sufficiently reactive to reduce CO_2. However, they did not elaborate further on this idea.[68]

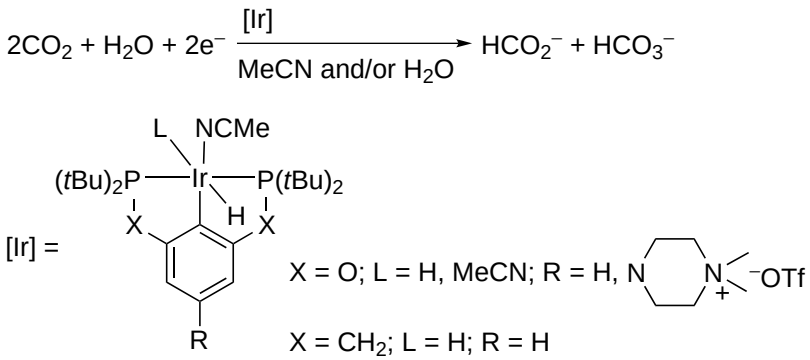

Scheme 9: Iridium(III) pincer complexes in the electrocatalytic CO_2 reduction reported by Meyer and Brookhart.[67,68]

Very recently Meyer and Brookhart immobilized a pyrene modified iridium pincer dihydride catalyst on gas diffusion electrodes using non-covalent binding by π-π interactions. The gas diffusion electrode was first coated with carbon nanotubes which were then impregnated with the iridium catalyst. A PEG overlayer provided the hydrophilicity of the surface. The supported catalyst showed very good stability and selectivity (83% yield towards HCO_2^-) up to a TON of 54200 at $E_{app} = -1.40$ V *vs* NHE.[69]

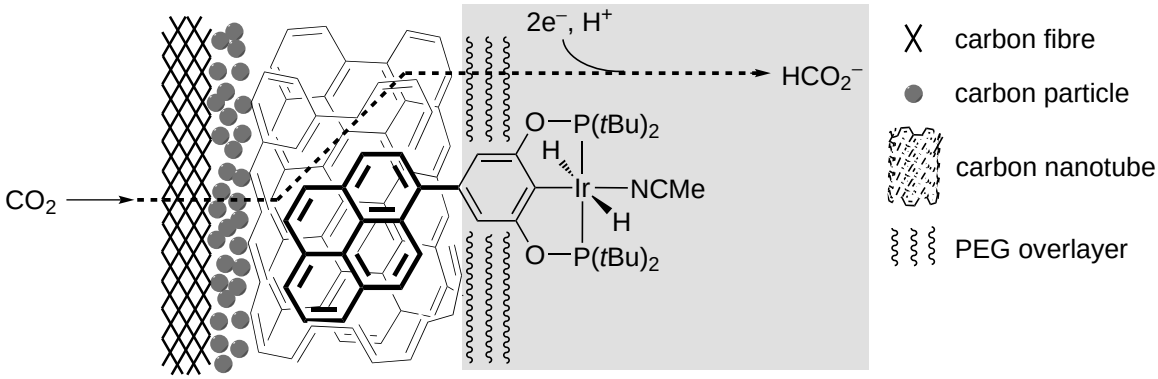

Scheme 10: Carbon nanotube coated gas diffusion electrode with surface bound Ir pincer dihydride catalyst for electrochemical reduction of CO_2 to formate developed by Meyer and Brookhart.[69]

Photocatalytic reduction of CO_2 by iridium complexes is limited to only a few examples despite their potential in photocatalytic applications due to their high absoprtion coefficients in the visible region of the solar spectrum and the long lifetime of the triplet excited state.[70,35] Ishitani tested the first mononuclear Ir complex photocatalyst in the reduction of CO_2. The procedure was selective towards CO product, which was obtained in up to TON = 50 under irradiation at $\lambda = 480$ nm with a quantum yield of $\Phi = 0.21$. After 30 min irradiation, $[Ir(tpy)(ppy)H]^+$ complex was formed and the starting chloride species disappeared, indicating that $[Ir(tpy)(ppy)H]^+$ was the active photocatalyst rather than the chloride species (left in Scheme 11).[35] Luo developed a coordination polymer containing an Ir complex, $(Y[Ir(ppy)_2(dcbpy)]_2[OH])$, which is a stable heterogeneous photocatalyst for CO_2 reduction acting both as light harvesting and CO_2 activation unit. Interestingly, in this catalyst system HCO_2^- was obtained as main product with a TOF = 118.8 μmol (g of cat.)$^{-1}$h^{-1} and $\Phi = 1.2\%$ under irradiation at $\lambda = 475$ nm. The catalyst could be recycled five times in reactions conducted for six hours without significant loss of activity.[70]

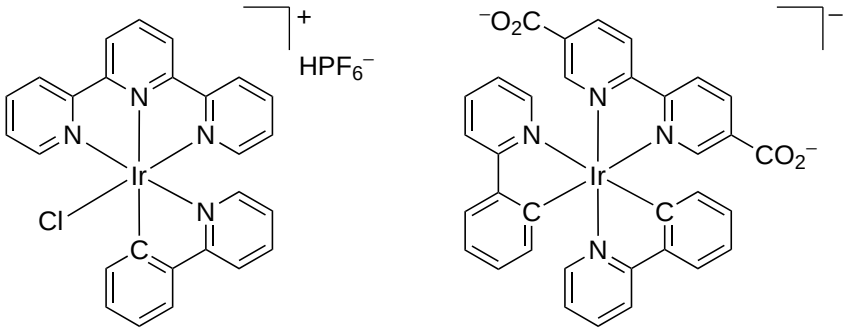

Ishitani 2013 Luo 2014

Scheme 11: Photocatalytic reduction of CO_2 using Ir complexes.[35,70]

1.3.2 Mechanistic considerations

Insertion of an unsaturated molecule into a M−H bond is a fundamental step in many catalytic reduction cycles. Accordingly, in the formation of HCO_2H from CO_2, M−H intermediates play a crucial role. The first examples of CO_2 insertion into M−H bonds to form M−O_2CH species were reported in the 80's by Sullivan and Meyer using *fac*-Re(bpy)$(CO)_3$H complex.[71,72] The same group suggested the formation of Ru−H in the electrocatalytic CO_2 reduction with *cis*-$[Ru(bpy)_2(CO)(NCMe)]^{2+}$ complex (Scheme 12). In the first step of the mechanism, which was proposed based on observations from the CVs of the catalyst in the presence of CO_2 and H_2O, the Ru complex undergoes a bpy centered one electron reduction. This makes the the Ru−H bond more nucleophilic and therefore more reactive towards CO_2 insertion. The reduction of the second bpy ring is accompanied by the dissociation of the formate anion and association of MeCN to the Ru center. The Ru−H is regenerated by reduction of H_2O to bicarbonate. The authors emphasized the possibility of other pathways, since catalytic formation of CO was also detected.[73] Later Deronzier proposed a similar mechanism for the electrocatalytic CO_2 reduction using $[Cp^*Ir(bpy)Cl]^+$ as catalyst (*vide infra*).[42]

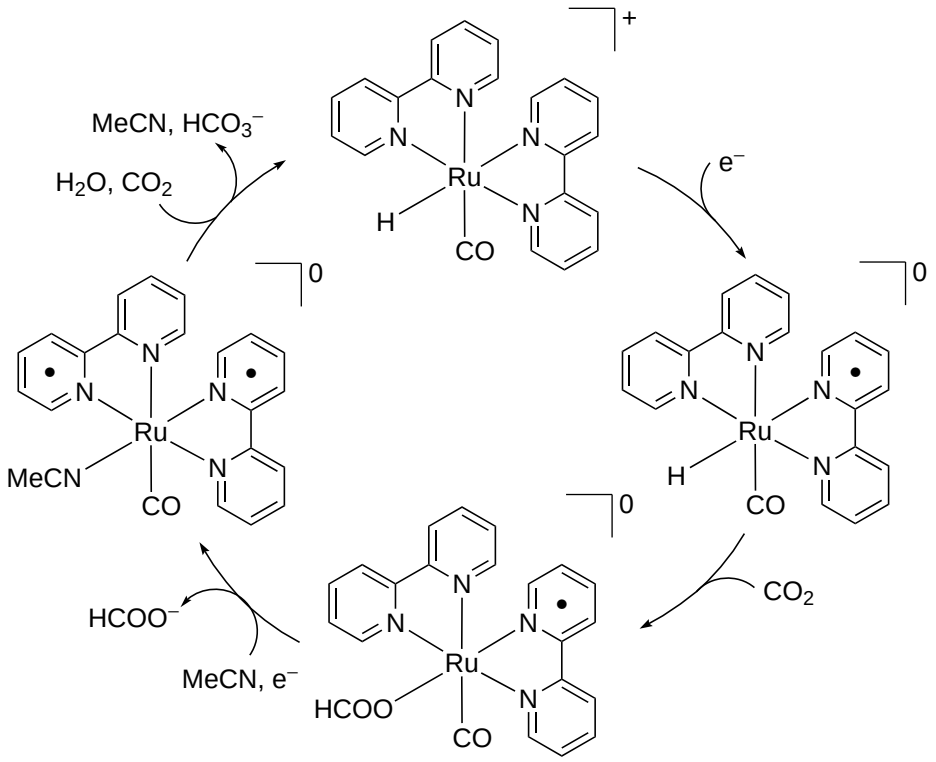

Scheme 12: Proposed mechanism of the electrocatalytic CO_2 reduction using *cis*-$[Ru(bpy)_2(CO)(NCMe)]^{2+}$ complex by Meyer *et al.*[73]

In the early 1990's Nicholas and Leitner discussed Rh−H in the hydrogenation of CO_2.[74,75] The work by Nicholas was the first example to study the mechanism of TM catalyzed CO_2 hydrogenation

to HCO_2H.[75] Nicholas and co-workers performed extensive mechanistic investigations using ^1H, ^{31}P NMR and *in situ* IR measurements in the presence of $[Rh(NBD)(PMe_2Ph)_3]BF_4$ catalyst. The analytical measurements showed the formation of several Rh−H, as well as two Rh-formato species in η^1_O and $\eta^2_{O,O}$ coordination modes. Added H_2O accelerated the reaction five fold. The proposed catalytic cycle involves CO_2 insertion, reductive HCO_2H elimination and oxidative addition of H_2 steps (Scheme 13).The kinetic and spectroscopic studies suggested reductive elimination to be rate-determining.[75]

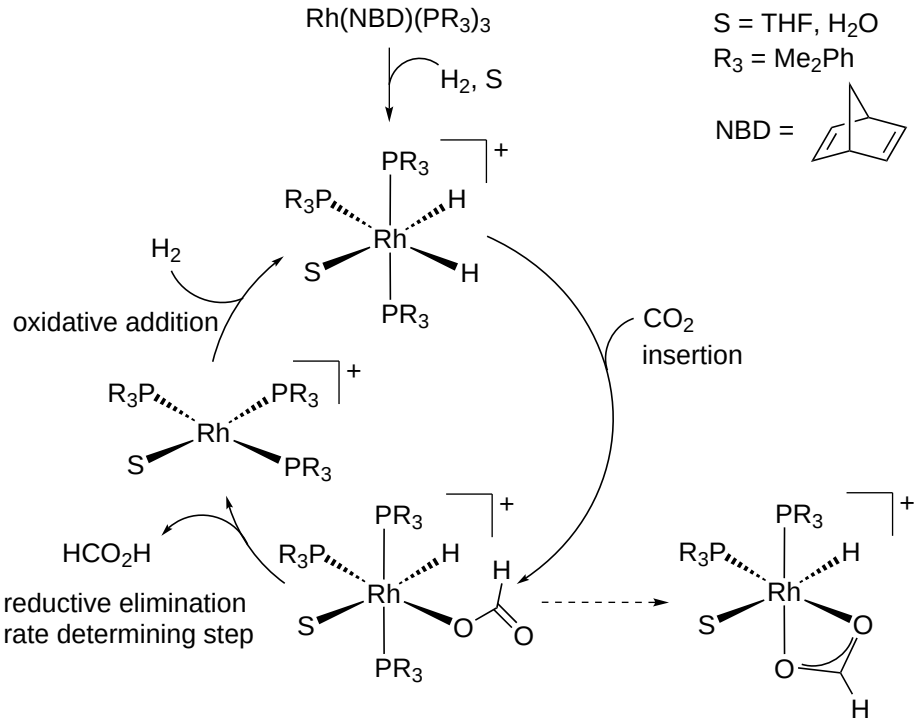

Scheme 13: The first proposed mechanism of CO_2 hydrogenation to HCO_2H by Nicholas *et al.*[75]

Darensbourg studied the tungsten catalyzed reaction of NaOMe with CO_2 at 125 °C and 2.76 MPa to form HCO_2Na and HCHO after 24 h with a total TON of 10.[76] He proposed the formation of a W−OMe species which would undergo a β-hydride elimination to yield formaldehyde and an anionic W−H species that inserts CO_2 consecutively. Finally, reaction with NaOMe regenerates the W−OMe species and yields HCO_2Na product (Scheme 14).

Given the importance of the reaction of a M−H species with CO_2, this elementary step as well as the whole catalytic cycle of the CO_2 reduction with different TM species have been computationally studied. Sakaki performed theoretical investigations on the *cis*-$Ru(H)_2(PMe_3)_3$ catalyst in the hydrogenation of CO_2 to formic acid. He suggested that the rate determining step of this reaction was the insertion of CO_2 into the Ru−H bond, which would be favoured by strongly electron donating

ligands and polar solvents.[60]

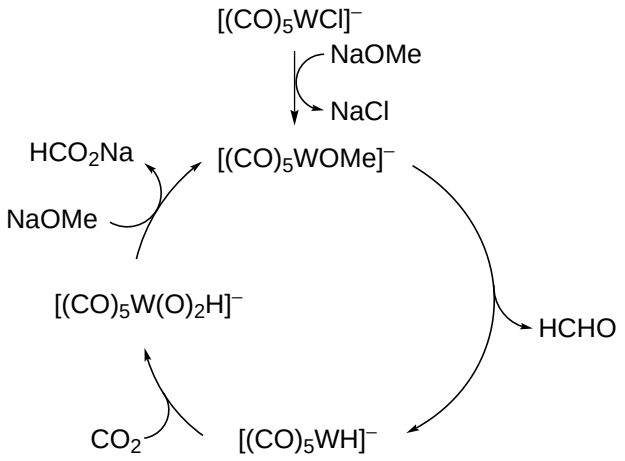

Scheme 14: Reaction of NaOMe with CO_2 in the presence of $[(CO)_5WH]^-$ to HCHO and HCO_2Na.[76]

Nozaki first investigated the mechanism of the CO_2 hydrogenation using an Ir(III) pincer complex, involving insertion of CO_2 into the Ir−H bond and an accelerated formate dissociation by deprotonation-dearomatization of the ligand. The catalyst was regenerated by hydrogenation of the dearomatized species (Scheme 15).[61] Later the same research group as well as Ahlquist and Yang carried out theoretical investigations on the mechanism of this reaction.[77,63,78]

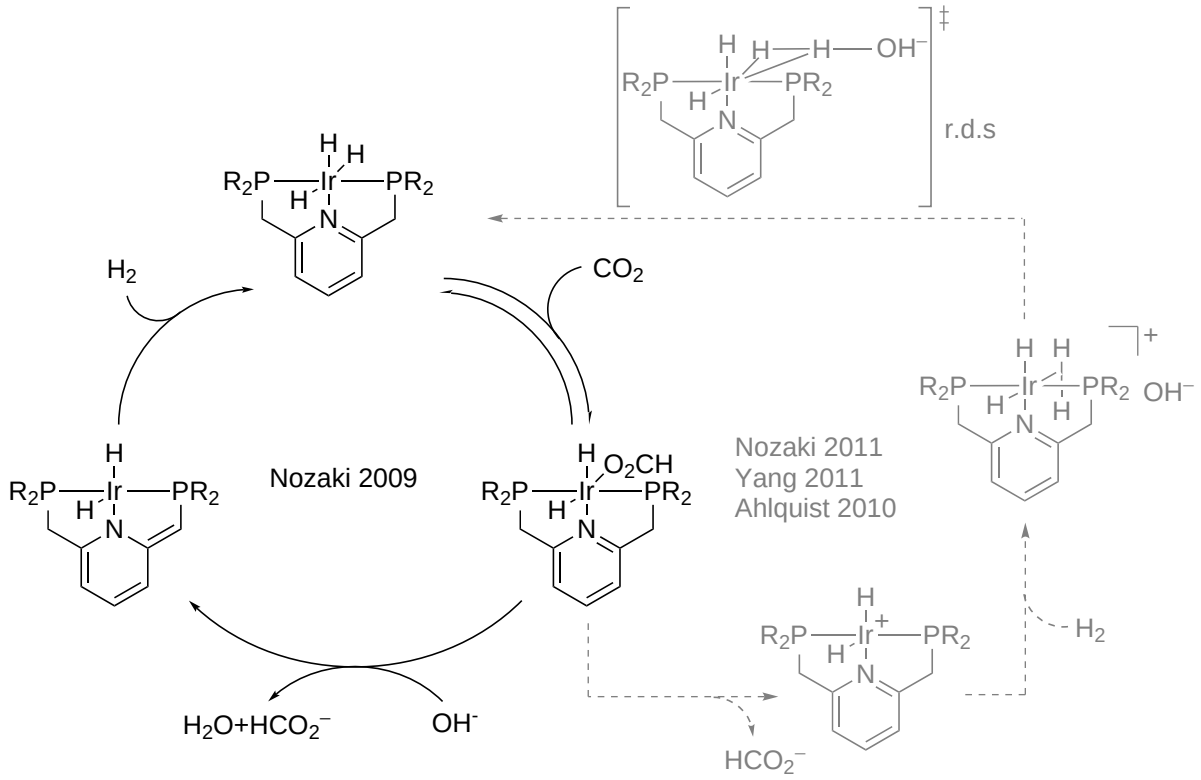

Scheme 15: Mechanism of the CO_2 hydrogenation by an Ir(III) pincer complex proposed by Nozaki (left),[61] Yang and Ahlquist (right).[77,78]

Yang and Ahlquist debated the ligand dearomatization step as they found catalytic cycles not involving the ligand energetically more favourable.[77,78] In the computational studies Nozaki also found two competing catalytic cycles only one involving the formation of a dearomatized ligand.[63] These theoretical studies, however, agree that in the cycles not involving ligand deprotonation, the rate determining step is the heterolysis of the H_2 in the presence of a base to regenerate the $Ir(H)_3$ species. Hazari proposed a similar mechanism earlier in which displacement of HCO_2^- by H_2 was rate determining. The group designed a ligand capable of secondary coordination sphere interactions, which resulted in more favourable kinetics for the CO_2 insertion and suggested an outer sphere mechanism for this step (Scheme 16).[64]

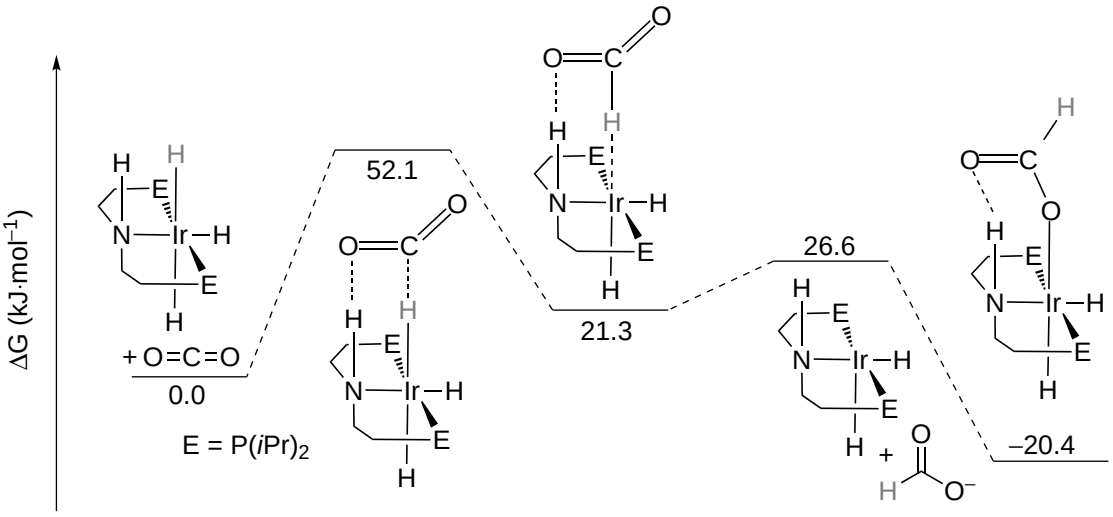

Scheme 16: Insertion of CO_2 into Ir−H by outer sphere mechanism supported by secondary coordination sphere interactions.[64]

Himeda *et al.* speculated the influence of secondary coordination sphere interactions in the hydrogenation of CO_2 under mild conditions using $[Cp^*Ir(bpy)(OH_2)]SO_4$ complexes. When 6,6′ OH substituted bpy was used as ligand, the reaction was accelerated two-fold compared to when 4,4′ OH bpy was applied. DFT calculations indicated that the H_2 heterolysis was rate determining just like with the Ir pincer complexes. According to the calculations in this study, the H_2 heterolysis step was assisted by the pendant base on the bpy ligand on the 6,6′ position rather than OH^- from the basic solution (Scheme 17a).[59] Interestingly, kinetic data presented by Fukuzumi indicated that under acidic conditions (pH = 3.0) the CO_2 hydrogenation using $[Cp^*Ir(bpy)(OH_2)]^{2+}$ complexes was limited by the CO_2 insertion step into the Ir−H species in a similar catalytic cycle, involving formation of an Ir−H, CO_2 insertion and replacement of the HCO_2^- by solvent.[79]

Very recently, Zhao performed DFT calculations to verify the possible steps in the catalytic cycle

depicted in Scheme 17a using $[Cp^*Ir(bpy)(OH_2)]^{2+}$ catalyst containing hydroxyl groups in the 6,6′ positions.[80] The authors clarified the role of the pendant base in the H^- transfer to CO_2 step, which Himeda previously indicated to be assisted by the O^- substituent on the bpy ring (see **TS1** in Scheme 17a), a rather surprising suggestion, considering that H-bonding between O^- and Ir−H hydride is unexpected and if present it would most likely hinder the nucleophilicity of the hydride instead of accelerating its attack on the electrophilic carbon in the CO_2 molecule.

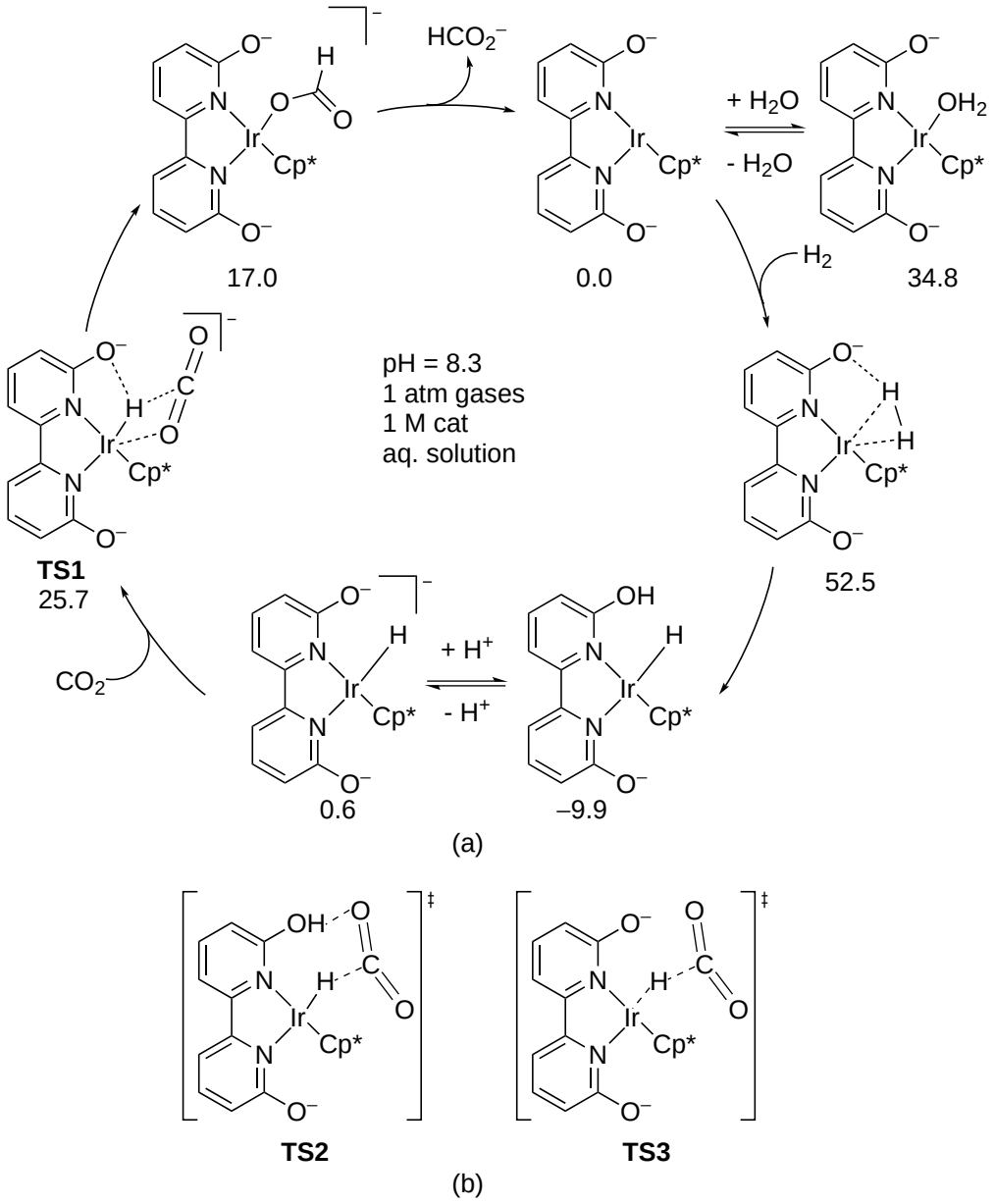

Scheme 17: (a) Catalytic cycle of the CO_2 hydrogenation using a $[Cp^*Ir(bpy)(OH_2)]SO_4$ complex determined by DFT calculations by Himeda. Computed free energies are indicated in $kJ{\cdot}mol^{-1}$.[59] (b) Transition states for the insertion of CO_2 into Ir−H in the presence of hydroxyl functional group on the 6,6′ positions of the bpy ligand proposed by Zhao.[80]

The idea of the pendant base's positive effect is better explained by Zhao, who considered two plau-

sible transitions states for the CO_2 activation step in this system (Scheme 17b). Zhao and co-workers excluded the possibility of an inner sphere hydride transfer, which is common in the hydrogenation of C=O double bonds using Ru−H complexes,[81] owing to high activation barriers of the ring slip of the Cp* ligand to an η-3 coordination mode as well as the bpy rotation to create a free coordination site. They found the outer sphere routes energetically more favourable, giving transition states for a ligand assisted (**TS2**) and a direct attack (**TS3**) depicted in Scheme 17b, where the ligand assisted pathway (**TS2**) was 4.1 kcal·mol^{-1} more favourable than the direct attack (**TS3**). These studies also confirmed heterolytic cleavage of H_2 to be rate limiting.

Meyer and Brookhart discussed a possible mechanism for the electrocatalytic reduction of CO_2 using Ir(III) pincer complexes. The cycle involves three steps, the insertion of the CO_2 into the Ir−H bond, the dissociation of the HCO_2^- product and the regeneration of the catalyst by 2e$^-$ reduction of the cationic Ir species and subsequent protonation of the reduced Ir center. H_2O plays the role of the H^+ source and the formed OH^- ion reacts with CO_2 to form HCO_3^- (Scheme 18).[67] The presented catalytic cycle was later confirmed by DFT calculations by Cao, which supported that the CO_2 insertion step is rate determining.[82]

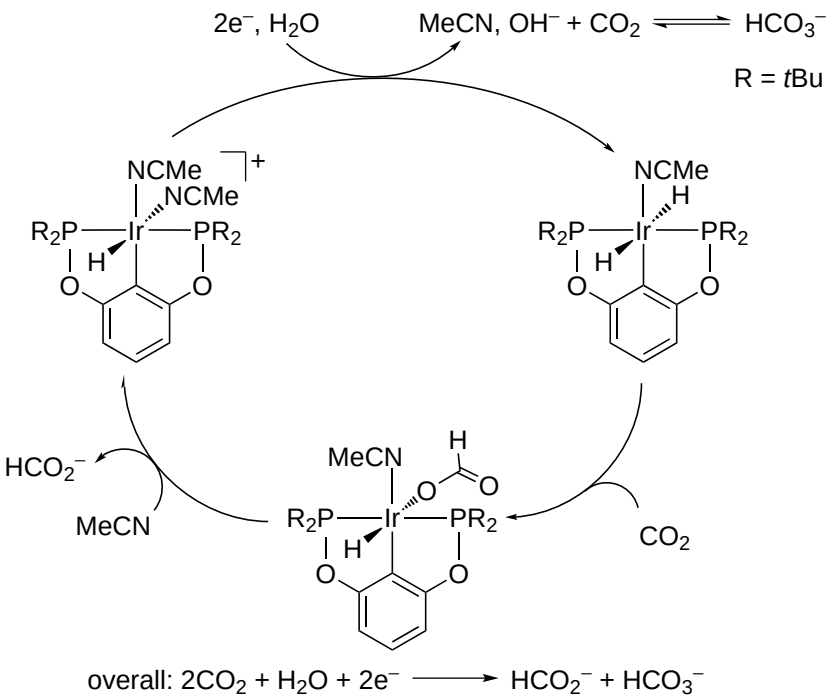

Scheme 18: Proposed mechanism of the electrocatalytic reduction of CO_2 by Ir pincer complex in MeCN/H_2O 95:5, v/v.[67]

Ishitani discussed a rather rough idea on the mechanism of photocatalytic CO_2 reduction using the

mononuclear Ir complex $[Ir(tpy)(ppy)Cl]^+$ as photocatalyst (Scheme 19).[35] They deduced structural changes of the Ir catalyst based on absorption spectra under irradiation in the presence of CO_2, which did not occur in the absence of TEOA. ^1H NMR studies indicated the disappearance of the starting complex and the formation of an Ir−H species after 30 min of irradiation. The ground state of the Ir−H was not reactive towards CO_2. After 300 min irradiation, the hydride species was consumed and a third Ir complex was generated. At the same time, CO production levelled off, indicating that this new Ir species was inactive towards CO_2 conversion. Based on ESI-MS data the authors speculate that the third Ir complex could be a dimer. As a result of these investigations, a catalytic cycle was proposed (Scheme 19), starting with reductive quenching of the lowest excited state of the starting Ir complex by TEOA, giving the one electron reduced species. Upon Cl^- elimination, the Ir−H species is formed, which undergoes further photoexcitation and reductive quenching to allow the activation of CO_2 and the subsequent formation of CO.

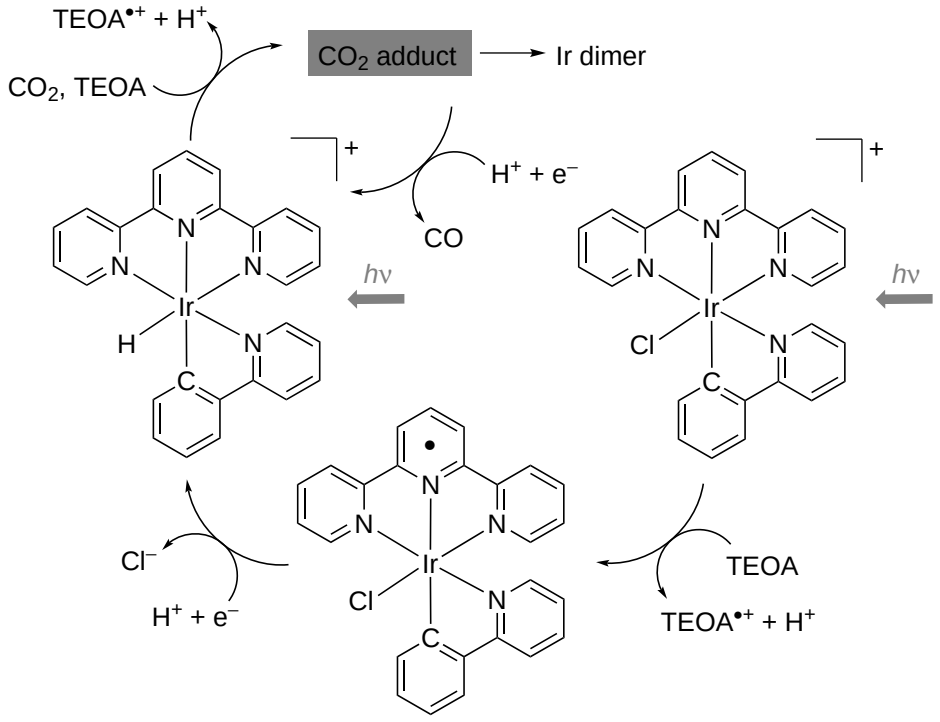

Scheme 19: Mechanism of the photocatalytic CO_2 reduction using a mononuclear Ir catalyst reported by Ishitani.[35]

1.3.3 Application in H_2 storage

The application of H_2 as energy carrier is desirable, since it can be utilized as fuel in a clean and environmentally friendly way without the formation of harmful products. However, the handling of sufficient amounts of H_2 is a challenge, since it is a flammable gas with a low energy content per

volume ratio, which cause safety issues in both storage and transportation. In contrast, HCO_2H is a liquid that is easy and safe to handle, offering an attractive option as H_2 storage material. The viability of this strategy has been investigated in both the HCO_2H production (*vide supra*) and H_2 generation steps.[51,83,52,84,53,85,54,55,86] However, there are only three examples of reversible H_2 storage using HCO_2H to date. Beller and Joó independently reported on the Ru catalyzed bicarbonate hydrogenation to HCO_2Na at high pressures (5-8 MPa) and 70 °C for the reversible storage of H_2.[87,88] Hull, Himeda and Fujita recently described the first sequence for reversible H_2 storage in aqueous media under mild conditions.[89] Interestingly, using pH and tempreature as trigger, the equilibrium could be switched between the bicarbonate/CO_2 hydrogenation and HCO_2^- decomposition/H_2 generation pathways (Scheme 20). Hydrogenation of CO_2 and HCO_3^- was achieved at 0.1 MPa CO_2/H_2 1:1 pressure at 25 °C with an initial TOF of 70 h^{-1} and TON of 7200. At pH = 3.5 and $T = 60-80$ °C, H_2 evolution was observed with TOFs up to 228000 h^{-1} and TONs up to 308000, the highest reported activities to date.

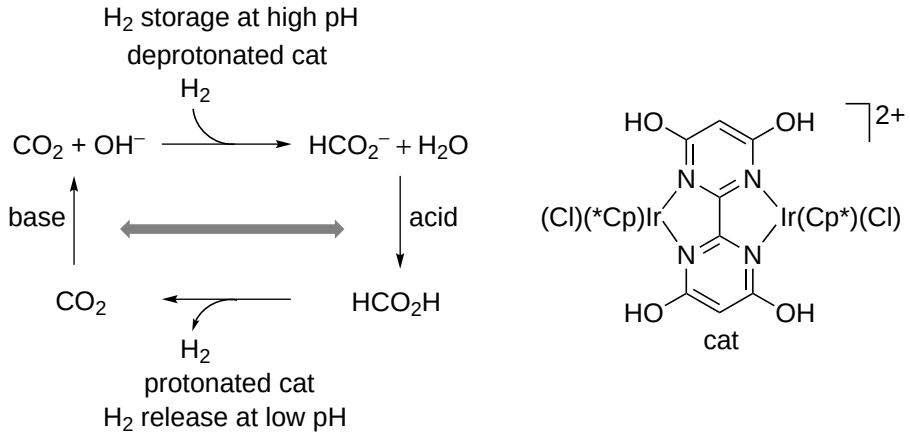

Scheme 20: Reversible H_2 storage controlled by pH demonstrated by Hull, Himeda and Fujita.[89]

Although, the hydrogenation of CO_2 to HCO_2^- and HCO_2H using $[Cp^*Ir(bpy)L]^{n+}$ type complexes has been extensively studied, electrocatalytic reduction with such complexes has not received as much attention. Electrocatalytic procedures are advantageous, if the electricity is derived from sustainable resources, because they do not require H_2 as reagent but utilize H_2O as proton source and they proceed at ambient temperature and CO_2 pressure.

1.4 Objective

The goal of the presented work was the synthesis and characterization of new $[Cp^*Ir(bpy)Cl]^+$ type complexes containing unsymmetrically substituted bpy ligands and the screening of their activity in

the electrocatalytic CO_2 reduction towards HCO_2^-/HCO_2H. Depending on the electron withdrawing and donating abilities of the complexes, a trend in the CO_2 reduction activity was expected. The design and optimization of a small volume cell was envisaged to enable the screening of small amounts of the catalyst solutions. Product selectivities as well as the relationship between activities and catalyst structure and electronic properties would give us further information on the most crucial features of the Ir complexes to facilitate further catalyst design and ideas for plausible mechanistic steps.

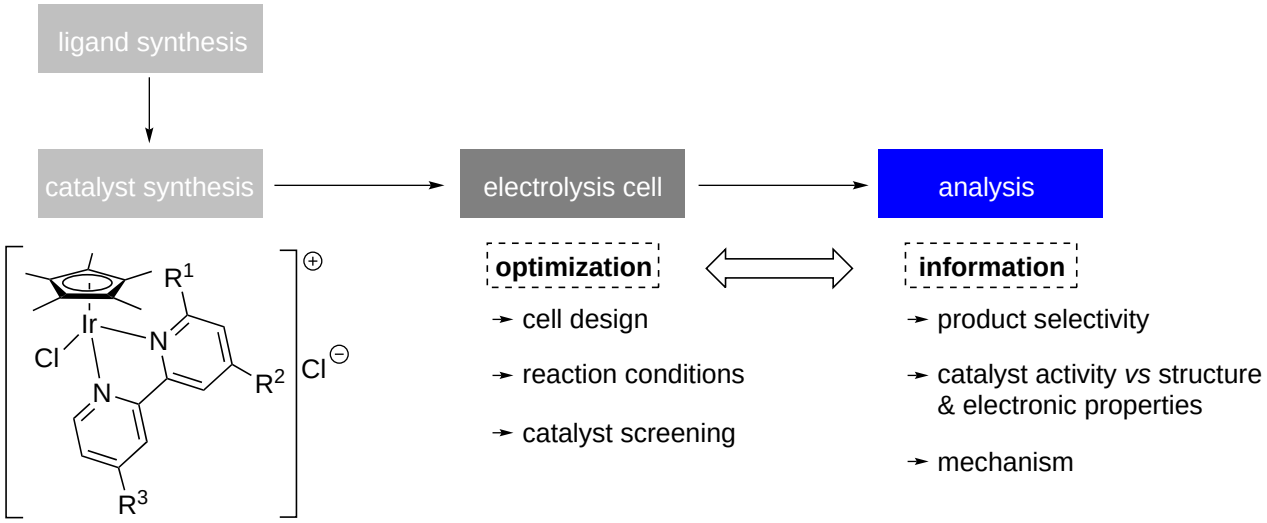

Scheme 21: The strategy to investigate the viability of $[Cp^*Ir(bpy)Cl]^+$ type complexes in the electrocatalytic reduction of CO_2 into HCO_2H.

2 Synthesis of the iridium catalysts

2.1 Ligand synthesis

2,2′-bipyridines and 2,2′:6′,2″-terpyridines constitute two important classes of chelating heterocyclic ligands. They form stable complexes with many metals[90] and have a wide range of applications in transition metal catalysis,[91,92,93,94,95,96,97,33] photochemistry,[98,99,100,101,102] analytical[103,104,105] and supramolecular[106,107,108,109] chemistry. Due to their manifold applications, the demand on synthetic routes towards differently substituted bi- and terpyridines is high.

2.1.1 Common procedures for the synthesis of 2,2′-bipyridines

Generally, there are two strategies to prepare substituted bpy ligands: 1. heterocycle synthesis and 2. metal mediated homo- or cross-coupling of two pyridine rings.

Heterocycle synthesis

Kröhnke developed the first condensation reaction towards symmetrically and unsymmetrically substituted 2,2′-bipyridines. The synthesis is based on the Michael addition of the deprotonated pyridinium salt to the α,β-unsaturated ketone, followed by the elimination of pyridinium bromide and condensation in the presence of ammonium acetate (Scheme 22). Depending on the substitution pattern, the overall fair yields varied between 19 and 92%.[110]

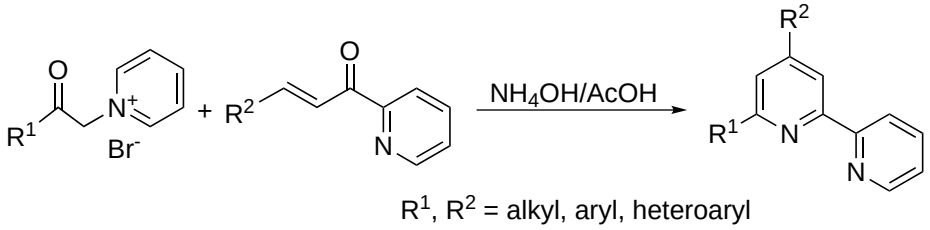

Scheme 22: Synthesis of 2,2′-bipyridines by the Kröhnke method.[110]

Another synthetic approach is the [2+2+2] cyclization between two alkyne and a nitrile functional groups.[111,112,113,114,115] These cobalt catalyzed reactions are based on the pioneering work by Yamazaki and Wakatzuki,[116] as well as Bönnemann[117] towards the synthesis of functionalized pyridines. A recent example of this type of synthesis is shown in Scheme 23 reported by Okamoto *et al.*[115] Bpy structures were obtained in 47-91% yields with excellent regioselectivities.

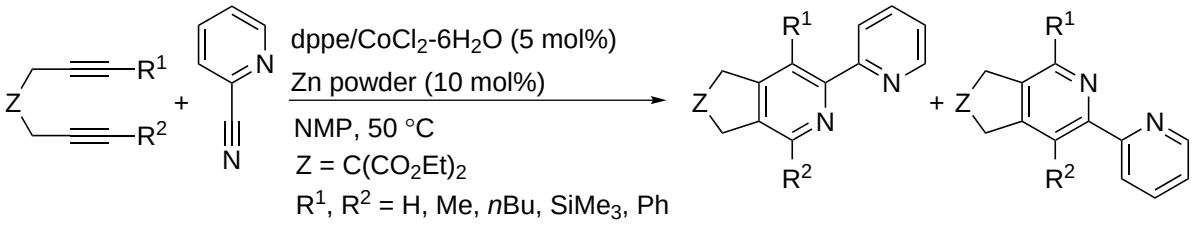

Scheme 23: Synthesis of 2,2′-bipyridines by [2+2+2] cycloaddition.[113]

In the late 1990's, Pabst and Sauer developed the so called LEGO-system for the synthesis of oligopyridines.[118,119,120,121] This reaction involves the formation of an electron poor 1,2,4 triazine that reacts with dienophiles in a Diels-Alder reaction followed by a retro Diels-Alder sequence with loss of N_2 and cyclopentadiene. Regarding the substrate scope of this reaction, both triazines and oligopyridynes were obtained in fair to good yields. The obvious disadvantage of this procedure is that the triazine synthesis is a multistep process considering the preparation of the functionalized starting materials.[122,123,124,125]

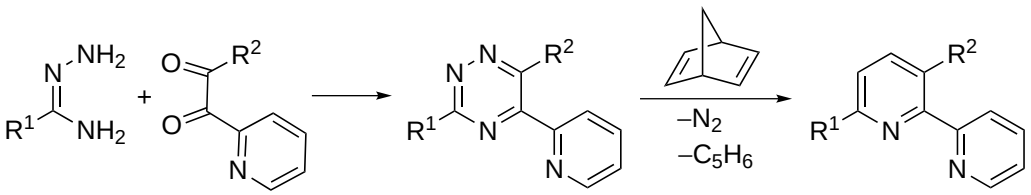

Scheme 24: Synthesis of 2,2′-bipyridines by Diels-Alder and subsequent retro-Diels-Alder reaction between a triazine and a dienophile.[119]

Very recently, Reissig and co-workers developed a new method towards unsymmetrically substituted 2,2′-bipyridines.[126,127] Despite the general good yields of the reactions involved in this synthetic route, the multi-step nature inevitably limits its applicability and the overall yields.

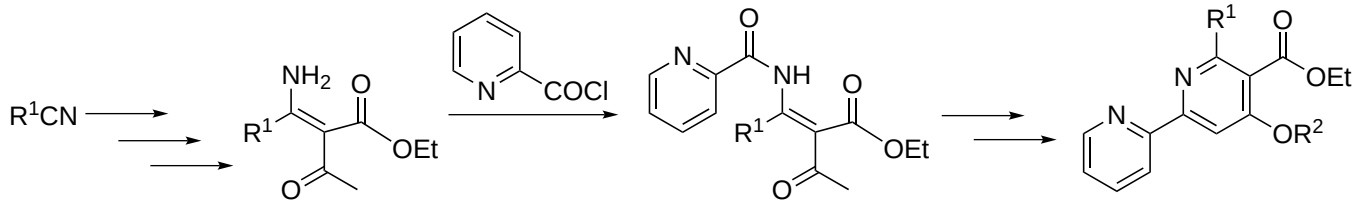

Scheme 25: Synthesis of unsymmetrically substituted 2,2′-bipyridines developed by Reissig *et al.*[126,127]

Metal mediated coupling of pyridines

Since the discovery of the Ullmann reaction in 1901, related homo- and cross-coupling reactions have been extensively studied for the synthesis of biaryls and bipyridines.[128,129] There are several

examples describing the Ullmann-type homo-coupling in the synthesis of symmetrically substituted bipyridines.[130,131] Regarding cross-coupling reactions, the Stille, Negishi and Suzuki-Miyaura reactions are most commonly used in bpy synthesis. The main disadvantages associated with this type of couplings are possible product inhibition caused by coordination of the formed bpy to the Pd or Ni catalyst and the usage of often unstable or toxic pyridyl derivatives containing a transmetalating group. The overview of such reactions is shown in Scheme 26.

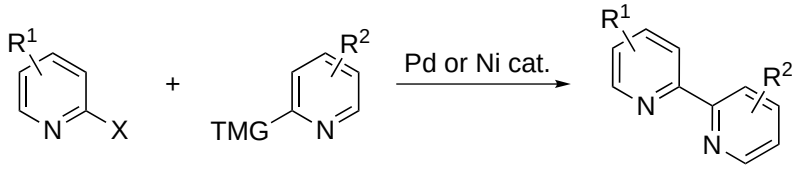

X = halide or triflate
TMG = SnR_3, ZnX, $B(OR)_2$, BR_2, BF_3K

Scheme 26: Synthesis of unsymmetrically substituted 2,2′-bipyridines by the metal mediated cross-coupling approach.

The **Stille coupling** was investigated in bpy synthesis by Schubert *et al.*[132] Dimethyl substituted bpys were obtained in very good yields. Panetta *et al.* studied the synthesis of methoxycarbonyl substituted bpys using Stille coupling.[133]

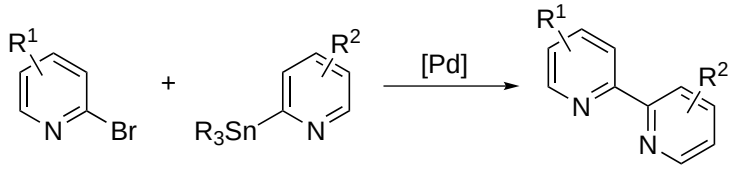

Schubert *et al.*	R^1	R^2	
[Pd] = $Pd(PPh_3)_4$	5-Me	5′-Me	87%
R = $(n\text{Bu})_3$	4-Me	5′-Me	80%
	5-Me	6′-Me	72%
	5-Me	H	64%

Panetta *et al.*	R^1	R^2	
[Pd] = $Pd(PPh_3)_2Cl_2$	4-CO_2Me	H	52%
R = $(CH_3)_3$	5-CO_2Me	H	84%
	6-CO_2Me	H	61%

Scheme 27: Synthesis of unsymmetrically substituted 2,2′-bipyridines using the Stille cross-coupling approach presented by Schubert and Panetta *et al.*[132,133]

Moreover, this method also facilitates the formation of halogenated bipyridines from the reaction of dihalopyridine and stannylpyridine.[134] Although the stannyl derivatives are air and moisture stable and relatively easy to prepare staring from the halopyridine compounds, their use is limited due to

their high toxicity and the formation of tin by-products that are difficult to remove.

The **Negishi coupling** was first described in 1977.[135] Since then, examples using this protocol in the synthesis of heteroaryl structures,[136] opticially active bpys,[137,138] fungicides[139] and natural products[140,141,142] have been described. The first systematic investigation on the synthesis of 2,2′-bpys using this method was carried out by Savage *et al* (Scheme 28).[143] In the coupling between 2-pyridyl triflates and 2-halopyridines, they obtained monomethylated 2,2′-bpys in very good yields. A couple of years later Lützen *et al.* demonstrated the substrate scope of this type of cross-coupling between two 2-halopyridine rings and observed a significant dependence of the yields on the substituent (Scheme 28).[144]

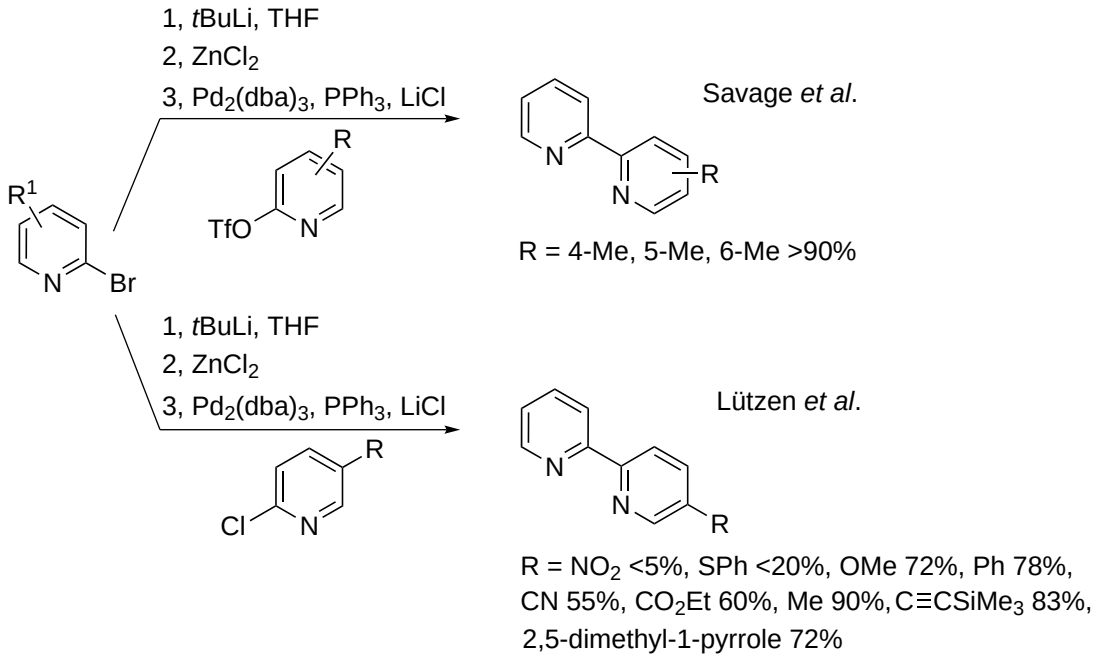

Scheme 28: Synthesis of unsymmetrically substituted 2,2′-bipyridines using the Negishi cross-coupling approach presented by Savage and Lützen *et al.*[143,144]

The major limitation of the **Suzuki-Miyaura coupling** in the synthesis of 2,2′-bipyridines is the preparation of suitable 2-pyridyl boronic reagents, because they can undergo protodeboration under protic conditions.[145] The first examples of the preparation of dimethyl-2-pyridyl boronate and its use in the synthesis of 2,2′-bipyridines were described in the early 1990's.[146] This reagent was later further explored by Ogawa and Matondo (Scheme 29).[147,148] From 2000 on, more synthetic routes were described towards different 2-pyridyl borane derivatives.[149,150] A stable reagent, 2-(6-phenyl-1,3,6,2-dioxazaborocan-2-yl)pyridine was used by Stevens[151] and Lützen[152] to investigate the substrate scope of this reaction (Scheme 29). The cross-coupling tolerated Me, OMe, CF_3, CO_2Me, NO_2, CHO and

2,5-dimethyl-1-pyrrole substituents on the pyridyl halide and Me and OMe groups on the pyridyl borane reagent resulting in good to excellent yields of the desired bpy products. However, amino substituted bpys could not be obtained using this method.

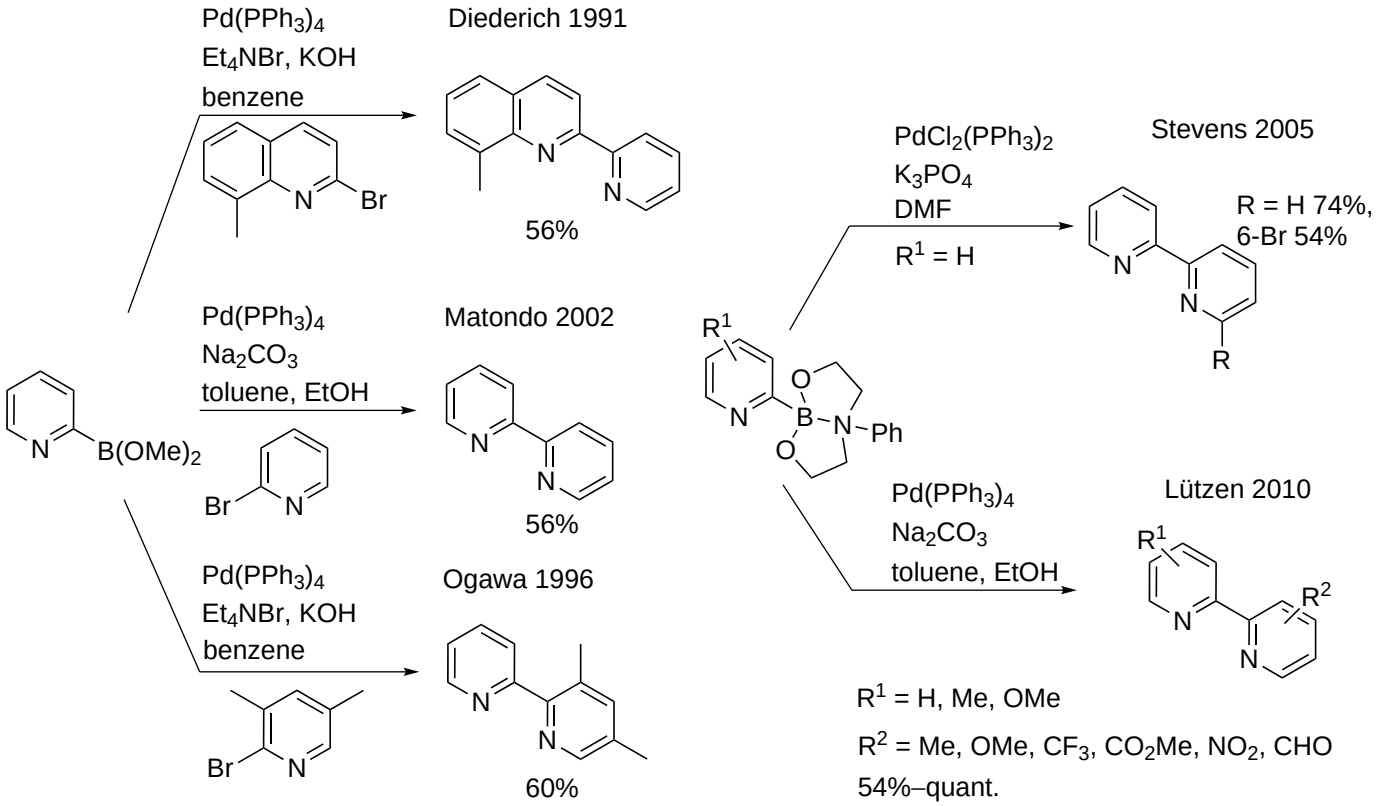

Scheme 29: Synthesis of 2,2′-bipyridines using the Suzuki-Miyaura coupling.[146,148,147,151,152]

2.1.2 Common procedures for the synthesis of 2,2′:6′,2″-terpyridines

In contrast to 2,2′-bpy synthesis, relatively few heterocycle synthesis and cross-coupling routes to terpyridines have been described, most of which apply to symmetrically substituted derivatives.[153,154,155,156,157] In this context Schubert studied the use of Stille cross-coupling between A) a dihalopyridine and two trialkylstannylpyridine units and B) a bis(trialkylstannyl)pyridine and two halopyridines (Scheme 30).[132]

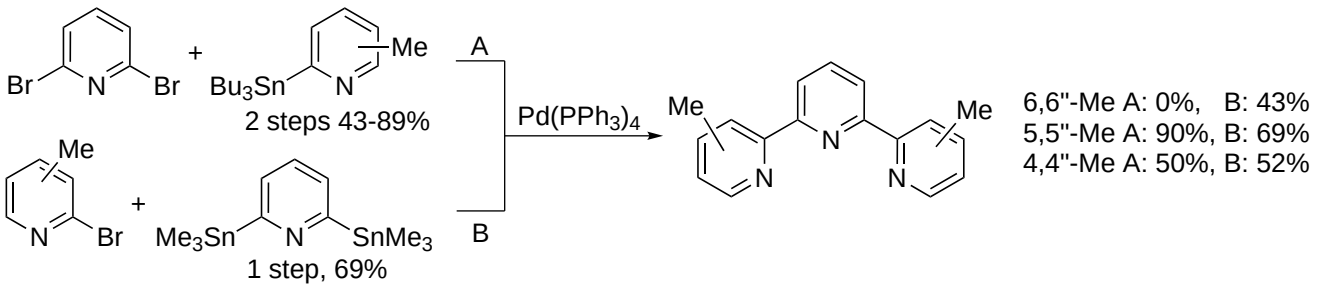

Scheme 30: Synthesis of symmetrical 2,2′:6′,2″-terpyridines by Schubert.[132,158,159]

The synthesis of asymmetrically substituted terpyridines is more challenging and has been so far limited to a few examples of coupling reactions between 6-bromo-2,2′-bipyridines and 2-trialkylstannyl pyridines and modifications of symmetrically substituted tpys.[160,161,154] As shown in Scheme 31, in these procedures several synthetic steps were applied, which substantially limited the overall yields. Besides, due to the synthetic effort required for the preparation of these structures, a modular route towards arbitrarily substituted tpys has not yet been used.

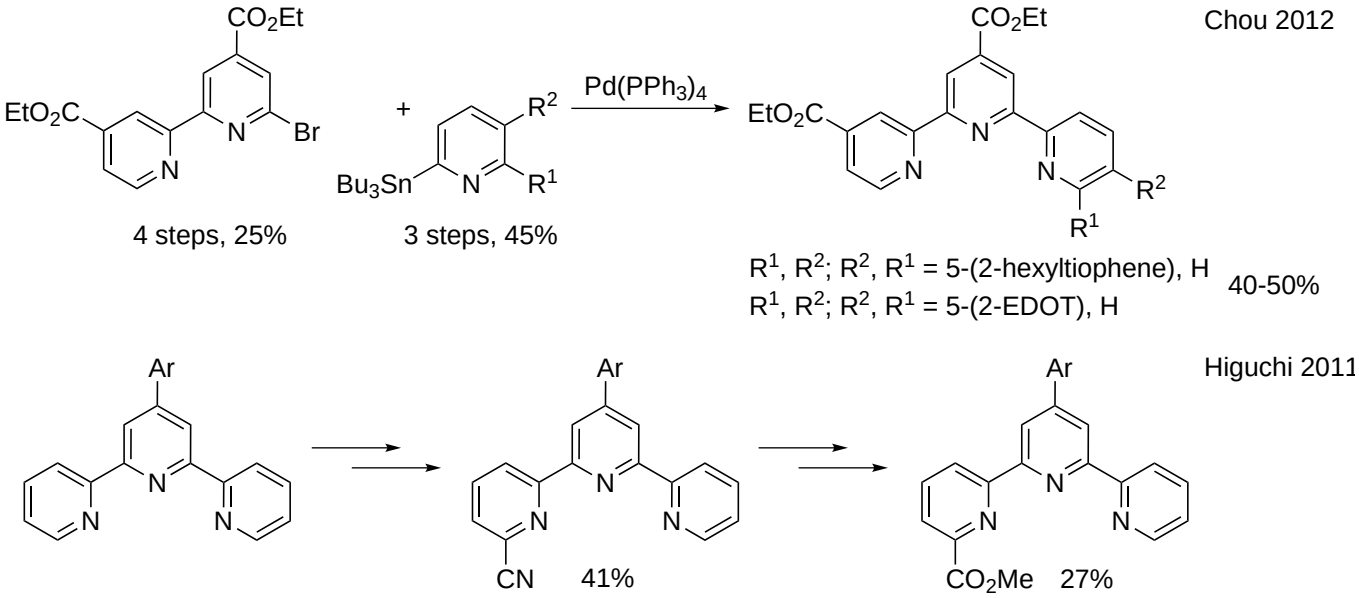

Scheme 31: Synthesis of asymmetrically substituted 2,2′:6,6″-terpyridines by Chou and Higuchi.[161,154]

2.1.3 The importance of C−H activation of pyridine *N*-oxides for bi- and terpyridine synthesis

The above described multi-step procedures are time consuming, result in low overall yields and complicate variation of the substitution pattern on the pyridyl rings. To overcome these limitations, transition-metal-catalyzed C−H activation reactions offer a powerful route for C−C bond formation as they do not require a functional group at the coupling site.[162,163,164,165,166,167,168,169] Pyridine *N*-oxides have been established as easily available and stable substrates for direct arylation and related cross-coupling reactions.[170,171,172,173] The C2-selective Pd-catalyzed direct arylation of pyridine *N*-oxides with aryl bromides was first investigated by Fagnou, describing good to excellent yields with a variety of substituents on both the pyridine *N*-oxide and halopyridine.[174]

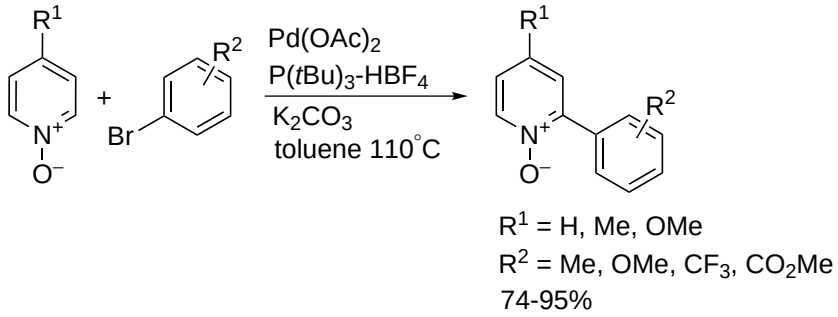

Scheme 32: C−H arylation of pyridine *N*-oxides by aryl-halides first presented by Fagnou.[174]

The kinetics of the palladium-catalyzed arylation of pyridine *N*-oxide have been investigated in some detail and two different mechanisms have been proposed.[175,176,177,178] Fagnou's group proposed a catalytic cycle in which fast oxidative addition of the aryl halide to a palladium(0) complex **A** leads to a palladium(II) aryl intermediate **B** (Scheme 33). After exchange of the halide ion for an acetate ion, aryl palladium complex **C** induces the rate-limiting C−H activation of the pyridine *N*-oxide, resulting in a bisaryl palladium complex **D**, which undergoes fast reductive elimination of the coupling product, regenerating the palladium(0) catalyst.

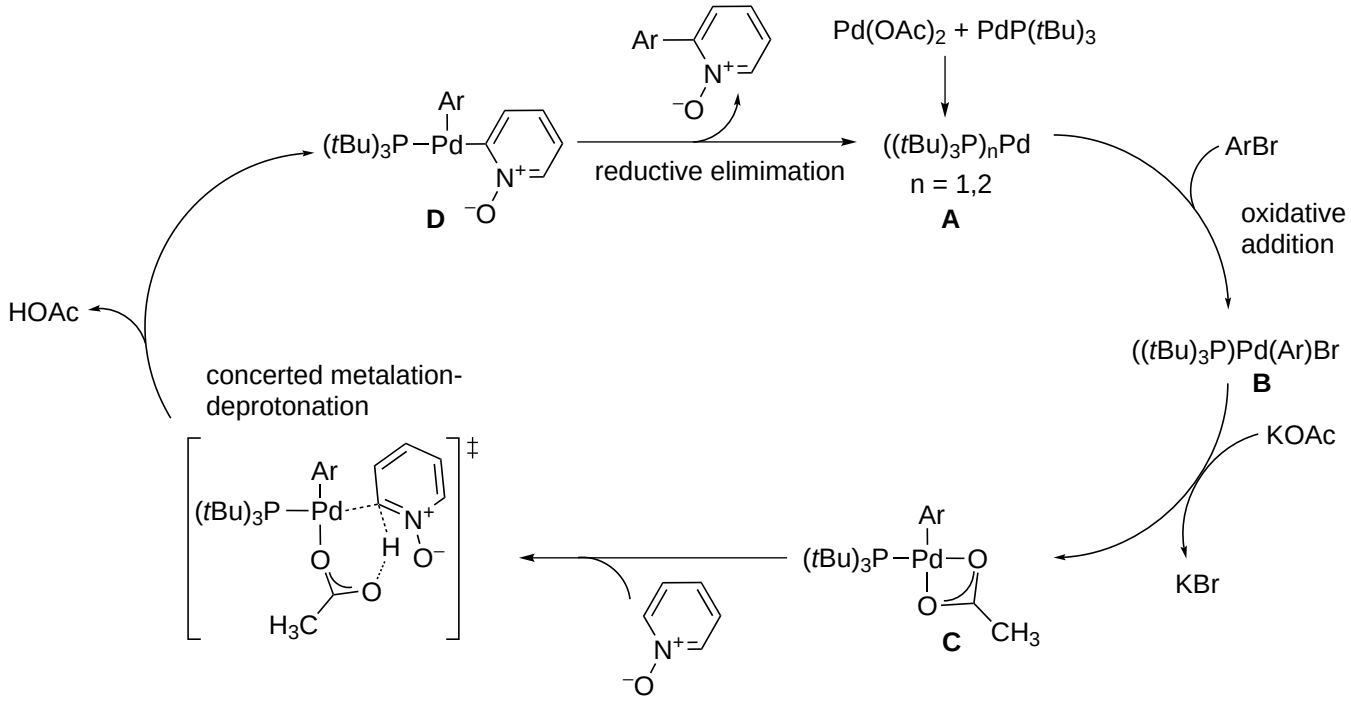

Scheme 33: The catalytic cycle for the direct arylation of pyridine *N*-oxides proposed by Fagnou *et al.*[176]

Hartwig and co-workers found that the isolated proposed aryl palladium intermediate **C** reacts with pyridine *N*-oxide only after an induction period and is therefore not kinetically competent for activating the C−H bond.[178] However, reaction of $Pd(OAc)_2$ and $P(tBu)_3$ rapidly forms cyclometaled

complex **E**, which was found to react with pyridine *N*-oxide without an induction period. They proposed a revised mechanism involving two interlocking catalytic cycles (Scheme 34). Dimeric cyclometalated complex **E** is in equilibrium with an undetected monomeric species **E′**, which induces C−H activation of the pyridine *N*-oxide, giving intermediate **F**. At the same time, a second aryl palladium complex **C** is formed by oxidative addition of the aryl bromide to palladium(0) complex **A**. These two aryl palladium complexes, **F** and **C**, react with each other, probably in a transmetalation reaction, transferring the pyridine *N*-oxide ring to **C**, which regenerates the cyclometalated complex **E′**. The concomitantly formed bisaryl palladium complex **D** undergoes fast reductive elimination to form the biaryl product and regenerate the palladium(0) catalyst **A**.

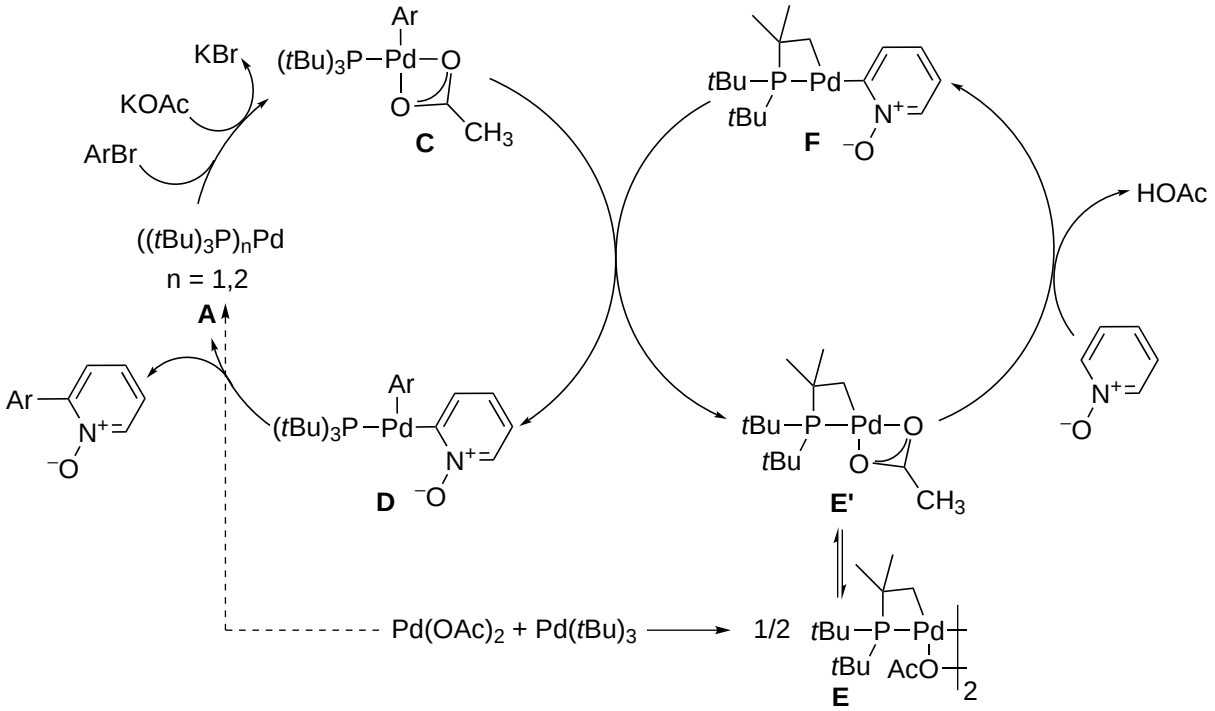

Scheme 34: The cooperative mechanism for the direct arylation of pyridine *N*-oxides proposed by Hartwig *et al.*[178]

2.1.4 Synthesis of bipyridines

Arbitrarily substituted bi- and terpyridines were synthesized using the Pd-catalyzed C−H arylation method described in section 2.1.3. The advantages of this procedure are that in most cases commercially available starting materials are used and that the lengthy preparation of unstable organometallic reagents is not necessary. Pyridine *N*-oxide **2a**, starting material for the coupling reactions, was easily obtained in excellent yield by oxidizing commercially available ethyl isonicotinate **1a** with H_2O_2 on the 10 g scale (Scheme 35).[179]

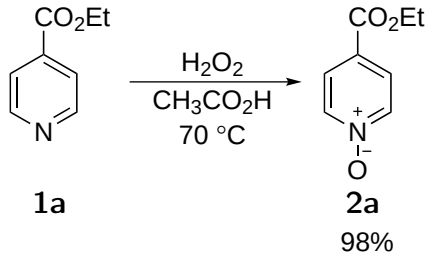

Scheme 35: Synthesis of pyridine *N*-oxide: the starting material for the Pd-catalyzed C−H activation.

Halopyridines used for the preparations of bipyridine *N*-oxides were purchased from commercial sources, except for 2-bromo-4-*tert*-butylpyridine, which was prepared according to a literature procedure (Scheme 36).[180]

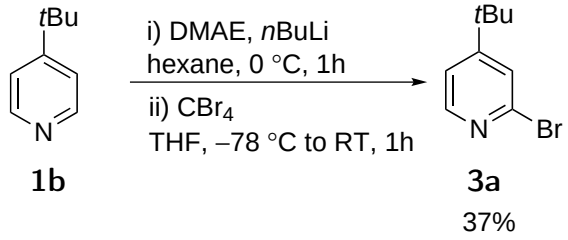

Scheme 36: Synthesis of 2-bromo-4-*tert*-butylpyridine.

The Pd-catalyzed C−H arylation was conducted using **2a** as starting material and different halopyridines. In the coupling reactions an excess of pyridine *N*-oxide (2 equivalent) relative to halopyridine was used in the presence of 5 mol% Pd catalyst and 6 mol% P*t*Bu$_3$ ligand. Using K_2CO_3 and K_3PO_4 bases in toluene delivered the highest yields of product **4**. Terpyridine *N*-oxides **8** originating from the double arylation of **2a** were observed in up to 20% yield. Scheme 37 summarizes the conditions of the reaction and the yields of the obtained bipyridine *N*-oxide and bipyridine products. Compound **2a** was chosen because the ethoxcarbonyl group offers at a later stage the possibility of further functionalization, for example for the immobilization of catalysts on surfaces.[181,182,183] Additionally, it has been previously established that electron withdrawing substituents on the pyridine *N*-oxide substrate result in increased reactivity in arylation reactions.[175,176,184] The reduction of pyridine *N*-oxides to the corresponding pyridines has considerable precedent.[185,186,187,188] For this final step, we used reduction with hydrogen and palladium on charcoal as the catalyst, which gave the corresponding bipyridines in high yields. The same conditions were also used to obtain terpyridines from their corresponding terpyridine *N*-oxides (see Section 2.1.5).

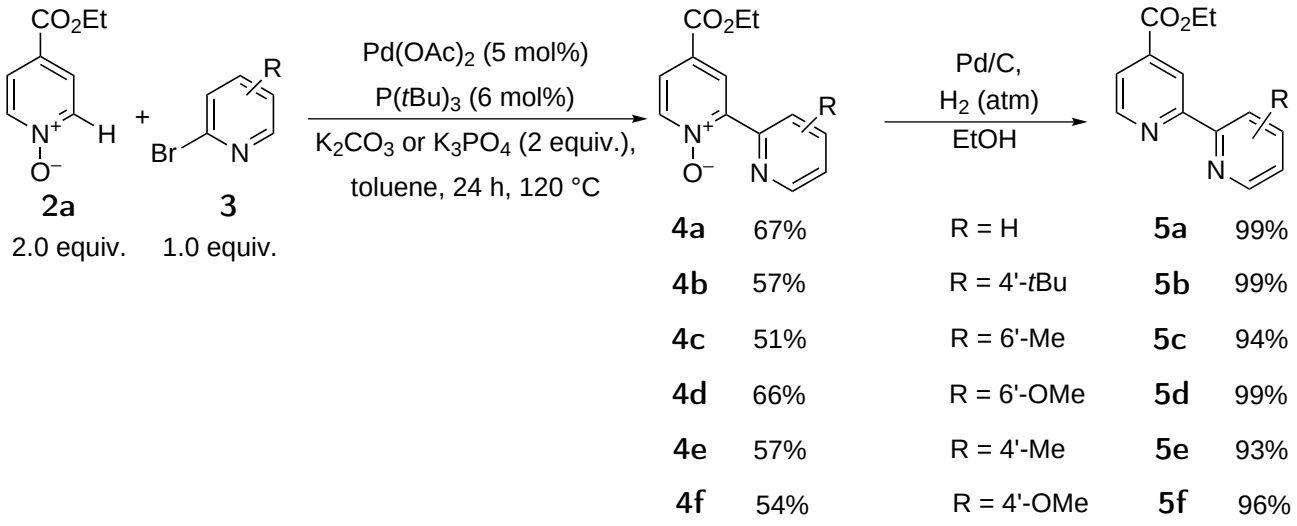

Scheme 37: Synthesis of unsymmetrically susbstituted bipyridine ligands.

To demonstrate the viability of further conversion of the unsymmetrically substituted bpy ligands, **5b** was converted into its bipyridine acid derivative **6b** in good yield, which was then coupled with *p*-toluidine to afford **5g** in 80 % yield.

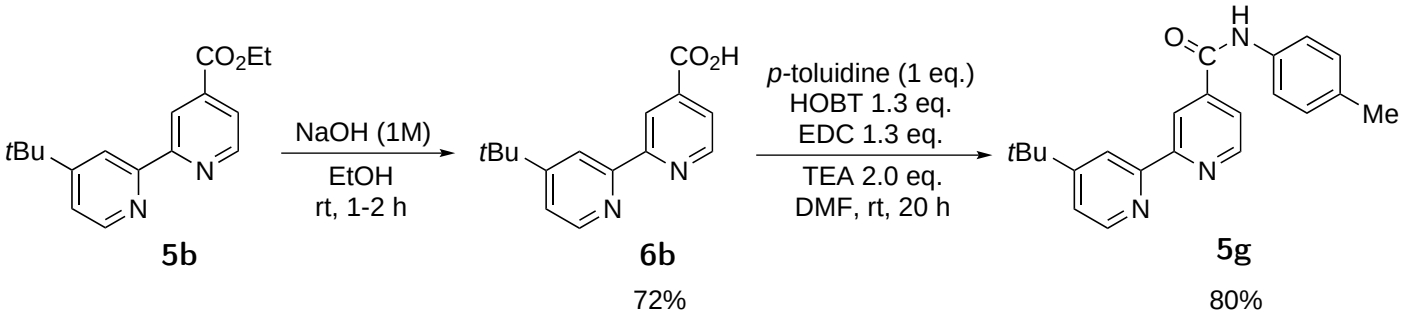

Scheme 38: Synthesis of **5g** from **5b**.

Ligands containing substituents prone to H-bond formation are especially interesting for various catalytic reactions, because they can facilitate catalyst-substrate interactions via secondary coordination sphere interactions.[64,59,189] Ligand **5h** was synthesized from bipyridine *N*-oxide **4g** through a stable tetrazole **7**,[190] which was reduced to **5h** using 1 atm H_2 and Pd on charcoal catalyst.[191]

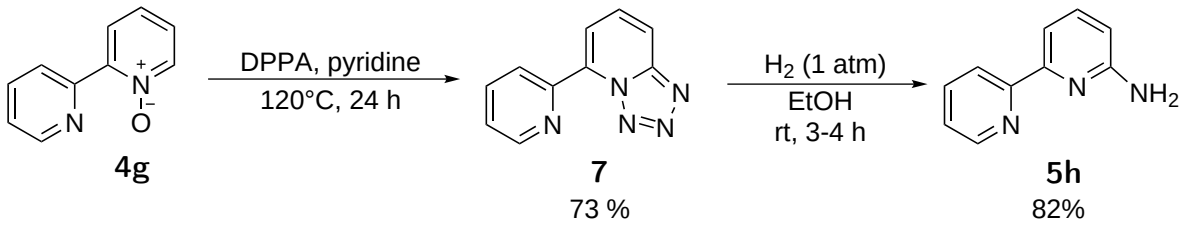

Scheme 39: Synthesis of **5h** from **4g**.

2.1.5 Synthesis of terpyridines

The possibility of extending the Pd-catalyzed C−H arylation reaction to the one-pot double arylation of pyridine *N*-oxide towards symmetrically substituted terpyridine *N*-oxides, and to the further arylation of unsymmetrically substituted bipyridine *N*-oxides towards asymmetrically substituted terpyridine *N*-oxides was also investigated. This work was published together with additional results; S. Duric, F. D. Sypaseuth, S. Hoof, E. Svensson, C. C. Tzschucke, *Chem. - Eur. J.* **2013**, *19*, 17456-17463.

Starting from our reported reaction conditions discussed above,[184] we investigated the double arylation of pyridine *N*- oxide **2a**. Whereas previously an excess of *N*-oxide was used, we now employed pyridine *N*-oxide **2a** as the limiting reagent. This substantial change makes full conversion of the *N*-oxide, and thus high yields of the arylated product, considerably more challenging because the rate of the reaction is first-order with respect to *N*-oxide concentration and the C−H activation step is rate-limiting.[176] Consistent with the mechanistic proposal by Hartwig *et al.*, we observed the highest yields of **8** when using phosphine ligands P(*t*Bu)$_3$ and P(*o*Tol)$_3$, which can form cyclometalated Pd complexes.[192,193] K_3PO_4 as the base resulted in better yields than K_2CO_3. Among the solvents tested, toluene, DMF, *N*-methylpyrrolidone (NMP), and THF gave similar results.[194] We chose toluene as the solvent because of its suitably high boiling point and nonpolar nature, which makes separation of the product mixture by column chromatography possible, without additional workup steps for removal of the solvent or the base.

The bipyridine *N*-oxides **4** were used as starting materials for subsequent investigations. The optimized conditions were applied in the synthesis of asymmetrically substituted terpyridine *N*-oxides **8** (Scheme 40). The best results were achieved by starting from bipyridine *N*-oxides with an ethoxycarbonyl substituent in the 4-position, and such terpyridine *N*-oxides were obtained in up to 77% yield.[194] However, substrates containing a cyano substituent gave no or little product regardless of the position of the cyano group. The most effective arylating agents were 2-bromopyridine and 2-bromo-4-(*tert*-butyl)pyridine. In several examples, the yields depended on the order of the introduction of the pyridyl rings.

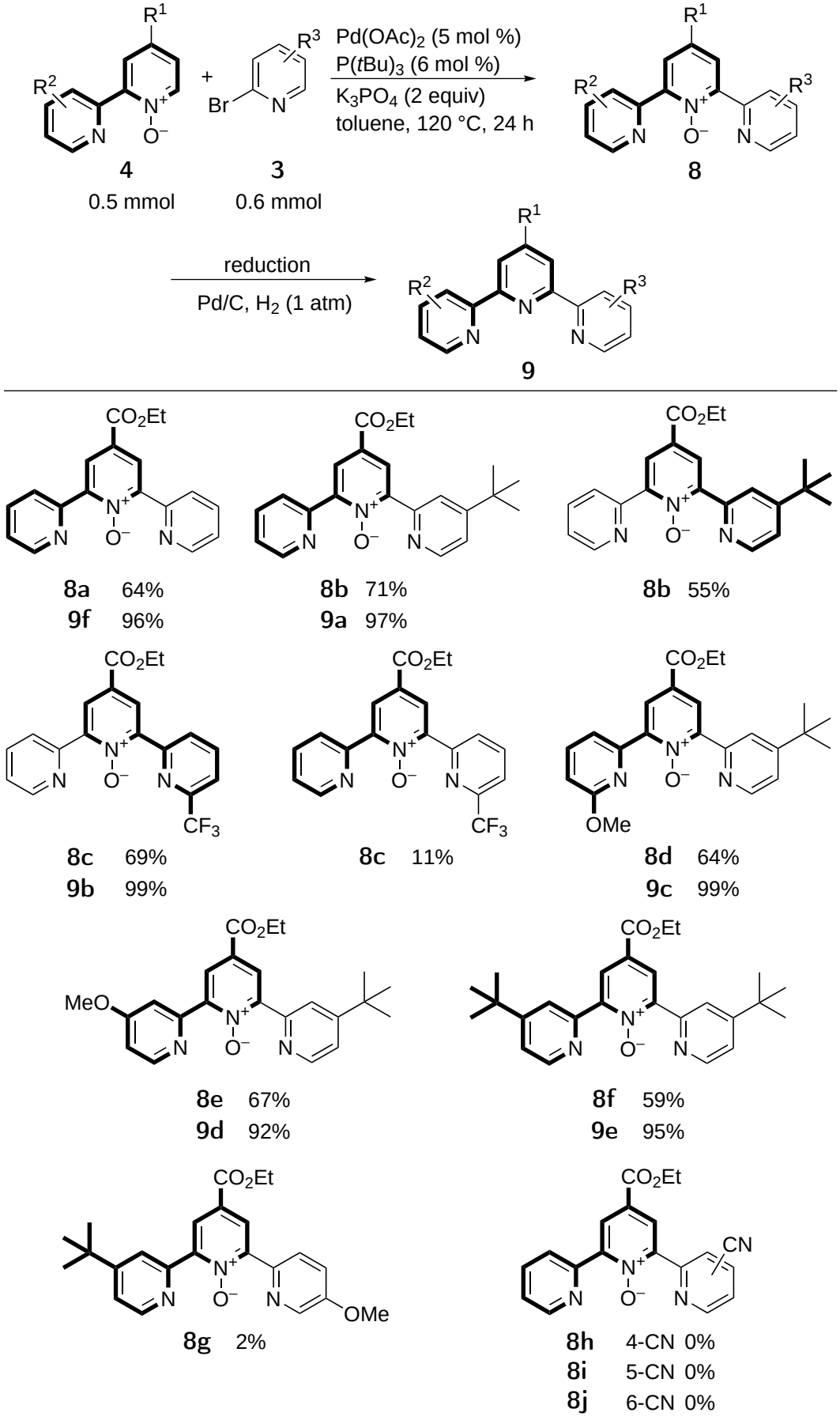

Scheme 40: Synthesis of asymmetrically substituted terpyridine ligands.

After optimization of the double arylation of compound **2a** using 2-bromopyridine, a variety of substituted halopyridines were tested for this one-pot synthesis (Scheme 41). In these reactions pyridine *N*-oxide was the limiting reagent and terpyridine *N*-oxides were obtained in low to moderate yields, usually affording bipyridine *N*-oxide as main product. The best yield was achieved using pyridine *N*-oxides containing -CO_2Et and -CF_3 electron-withdrawing substituents, 44 and 37%, respectively.[194] Compared to other routes towards symmetrically substituted tpys described in 2.1.2, our method offers much less synthetic effort and readily available starting materials resulting in very similar overall yields to those reported. Thus, despite the relatively low yield, the one-step double arylation might still be the most economic way to access a specific, symmetrically substituted terpyridine.

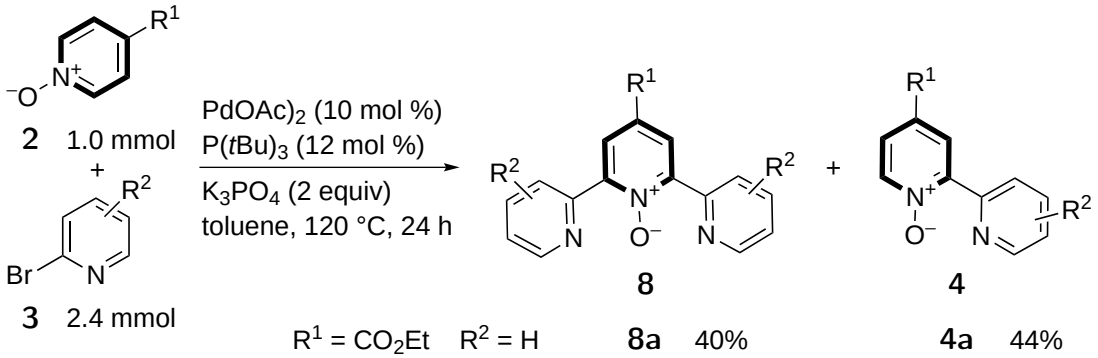

R^1 = CO_2Et	R^2 = H	**8a**	40%	**4a**	44%
R^1 = CO_2Et	R^2 = *t*Bu	**8f**	9%	**4b**	50%
R^1 = NO_2	R^2 = H	**8k**	3%	**4h**	22%
R^1 = H	R^2 = H	**8l**	26%	**4g**	50%

Scheme 41: One-pot synthesis of symmetrically substituted terpyridines.

From the ligand synthesis experiments we conclude that

- Pd-catalyzed direct arylation of pyridine *N*-oxides with halopyridines is a convenient method for the synthesis of substituted 2,2′-bipyridines and 2,2′:6′,2″-terpyridines
- the presented synthetic route significantly reduces the number of steps compared to conventional synthetic methods
- the best results were obtained using electron deficient pyridine *N*-oxides
- our results are not entirely consistent with the mechanistic proposal by Hartwig *et al.*, since the limitations observed with electron rich *N*-oxides cannot be explained by this catalytic cycle

- kinetic studies are being performed in our labs to enable further mechanistic understanding of this reaction and thereby allow the extension of the substrate scope

2.2 Complex synthesis

The $[Cp^*Ir(bpy)Cl]^+$-type complexes **10a** and **10b** were prepared from commercially available bpys whereas ligands for complexes **10c**-**10j** were synthesized as described in Section 2.1.4. The ligand and the $[Cp^*IrCl_2]_2$ precursor were stirred together in DCM from which the complexes were isolated by filtration (**10a**, **10b** and **10j**) or via an aqueous work-up after removal of the DCM (**10d**-**10i**) in very good yields as bright yellow to brownish solids and fully characterized (Scheme 42). Since **10c** could not be separated from the ligand through an aqueous work-up, it was purified after evaporation of the DCM by washing it with hexane to remove the excess ligand.

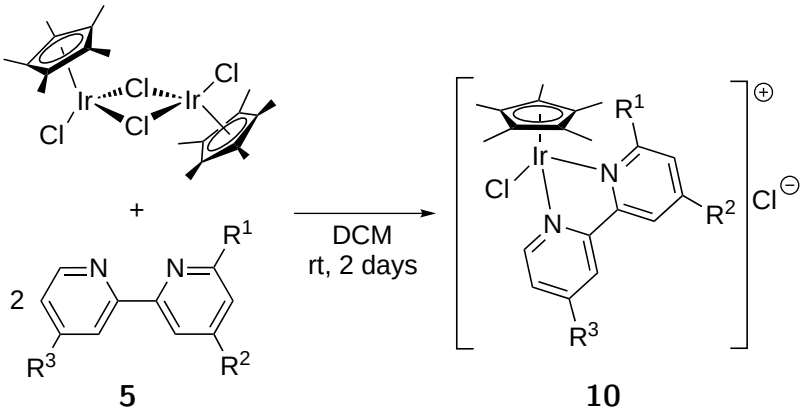

5 **10**

Complex	R^1	R^2	R^3	yield %
10a	H	H	H	99
10b	H	OMe	OMe	99
10c	H	H	COOEt	89
10d	H	OMe	COOEt	97
10e	OMe	H	COOEt	99
10f	H	Me	COOEt	99
10g	Me	H	COOEt	99
10h	H	*t*Bu	COOEt	99
10i	H	*t*Bu	CONH(*o*Tol)	99
10j	NH_2	H	H	83

Scheme 42: Synthesis of $[Cp^*Ir(bpy)Cl]^+$-type complexes.

The air stable complexes are all soluble in water as well as DCM, MeCN, MeOH organic solvents and they are poorly soluble in THF, Et_2O and hexane. Water stability of the complexes was examined

by HRESI-MS after stirring them in water under air at 70°C for 6 h. Complexes **10e**, **10g** and **10h** had a peak in the HRESI-MS spectra with a mass difference of 28, showing hydrolysis of the ethoxycarbonyl group in the bpy ligands. Complexes **10c**, **10d**, **10f** and **10i** did not undergo hydrolysis during the stability measurements. **10a** and **10h** also showed some unexpected signals which could not be identified. In case of **10f** and **10j** a signal at $m/z = 363.04$ was observed corresponding to a $[Cp^*Ir(Cl)]^+$ fragment after the loss of the bpy ligand. **10b** was completely stable under these conditions and no change in the HRESI-MS spectrum was observed after the stability experiment.

As expected, the ^{1}H NMR signals of the ligand protons shifted down field upon complexation due to the de-shielding effect of the cationic iridium (Figure 2). Protons on the 5,5′ and 6,6′ positions on the bpy shifted down field with about 0.5 and 0.3 ppm, respectively, whereas the positions of the signals of H-3,3′ changed only slightly.

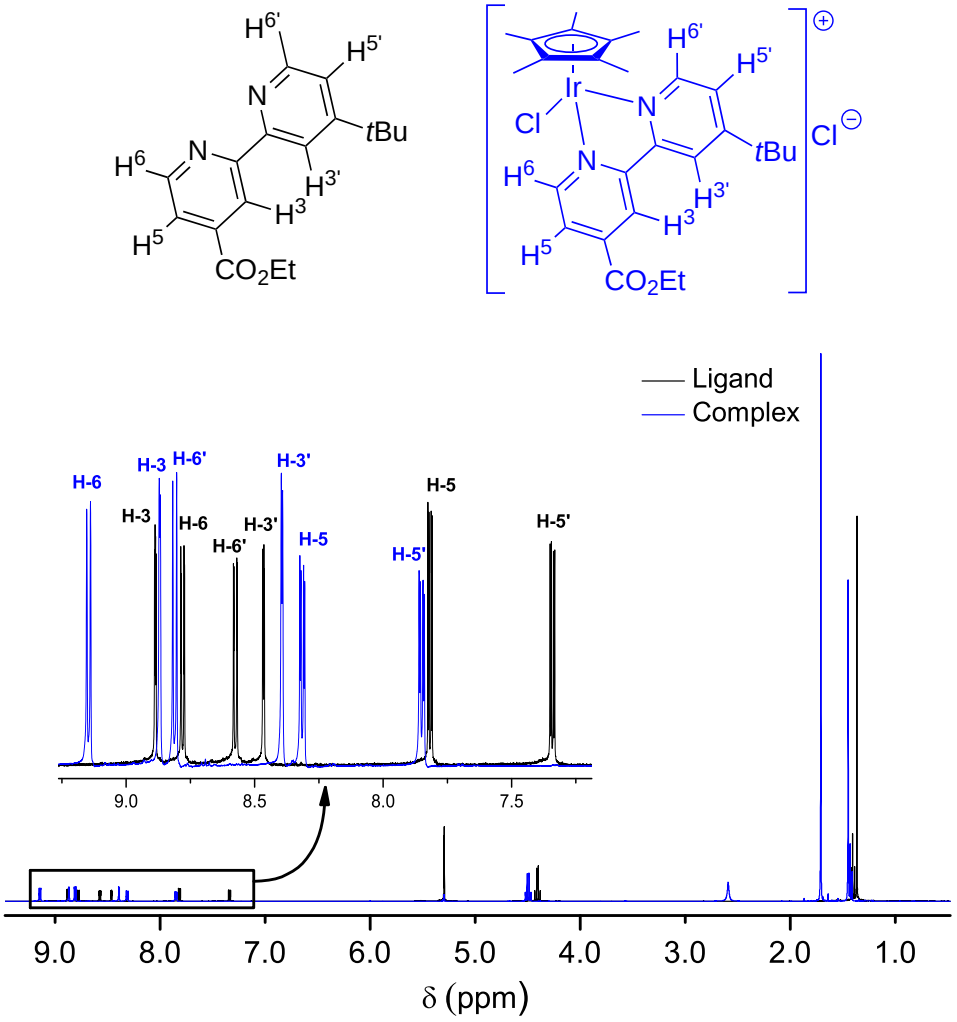

Figure 2: ^{1}H NMR spectra of ligand **5b** and complex **10h**.

Single crystals of **10a** and **10j** suitable for X-ray structure determination were obtained by slow diffusion of Et_2O into a solution of the complexes in EtOH/MeCN 1:4. Both, **10j** and known complex **10a**[195] are essentially isostructural and display a piano-stool configuration (Figure 3). In both complexes, the two Ir−N bonds have the same length (ca. 2.1 Å) and the N−Ir−N angles are also similar. The Ir−Cl bond is approximately perpendicular to the plane of the bipyiridine ligand in both structures and has a similar length (ca. 2.4 Å).

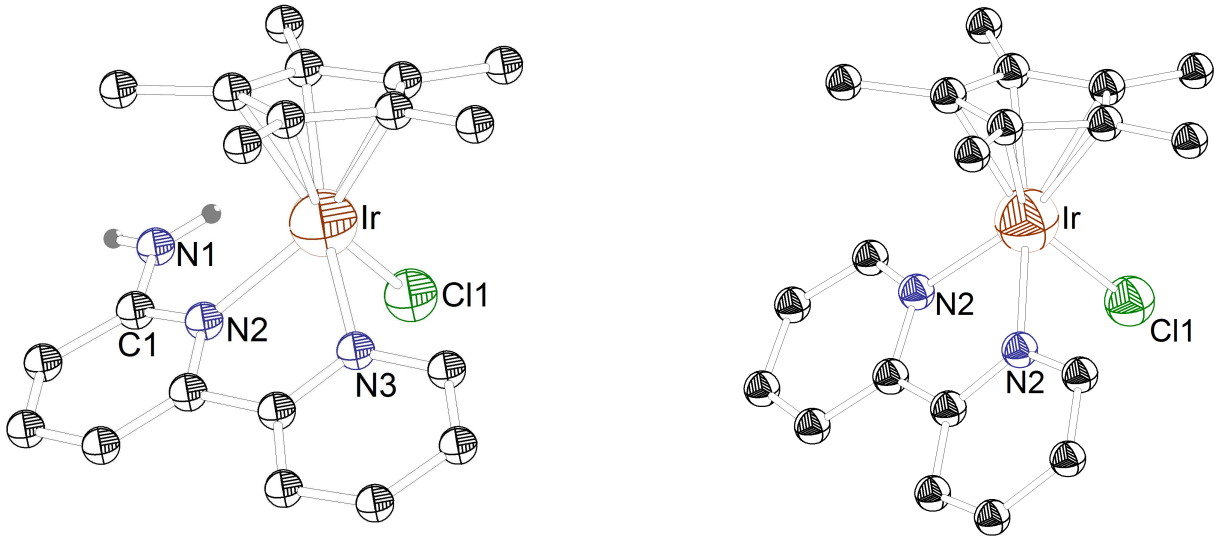

(a) **10j** (b) **10a**

Figure 3: Crystal structures of complexes **10j** and **10a**. Ortep drawings at 50% probability level. Hydrogen atoms are omitted for clarity. The structure of **10a** has been reported before.[195] Selected bond lengths (Å) and angles (deg) of complex **10j**: N(1)−C(1) = 1.34(1), Ir−N(2) = 2.096(6), Ir−N(3) = 2.100(6), Ir−Cl(1) = 2.400(2); N(2)−Ir−N(3) = 75.0(2), N(2)−Ir−Cl(1) = 89.0(2), N(3)−Ir−Cl(1) = 89.7(2) and of complex **10a**: Ir−N(2) = 2.094(4), Ir−Cl(1) = 2.391(2); N(1)−Ir−N(2) = 76.7(1), N(1)−Ir−Cl(1) = 85.61. CCDC 1013175 and 1013309 contain the crystallographic data for **10j** and **10a**.

The complexes were investigated by ultraviolet-visible light (UV-Vis) spectroscopy to reveal the influence of the ligand substitution pattern on the optical properties of the compounds. The UV-Vis spectra were recorded at room temperature using diluted solutions ($c_{Ir} = 5 \cdot 10^{-6}$; $9 \cdot 10^{-6}$; $5 \cdot 10^{-5}$ M) of the complexes in acetonitrile (see example in Figure 4). All complexes show absorption bands for the ligand centered allowed π-π^* transitions of the bipyridine ligands between 250 and 405 nm. The typical bands corresponding to metal-to-ligand charge transfer (MLCT) were not present in any of the spectra. These MLCT transitions in related iridium (III) complexes are observed between 450 and 500 nm.[196,197,198]

The results of the measurements are summarized in Table 2. Absorption maxima and extinction

coefficients of **10a** are similar to reported values.[195] As expected, the presence of EDGs on both rings of the bpy ligand resulted in blue shifted absorptions of **10b** compared to **10a**. On the contrary, the CO_2Et EWG caused red shift of the lower energy (> 300 nm) absorption bands of **10c**. In the case of unsymmetrically substituted bpys, the lower energy absorptions were dominated by the EWG on the bpy, causing red shifted bands of **10d-10i**. Interestingly, **10j** displayed only two blue shifted absorption bands at 235 and 287 nm, whereas the lower energy bands were red shifted compared to **10a**.

Table 2: Absorption spectra of complexes **10a-10j** in acetonitrile. Extinction coefficients were obtained from measueremnts of three complex concentrations.

Entry	Complex	λ_{max} nm ($\varepsilon \cdot 10^{-3}$ dm$^3 \cdot$ mol$^{-1} \cdot$ cm^{-1})			
1	**10a**	252 (17.4)	293(11.0)	315 (sh)	353 (2.2)
2	**10b**	230 (34.2)	265 (sh)	300 (8.0)	345 (3.8)
3	**10c**	229 (22.2)	301 (13.3)	323 (sh)	366 (3.3)
4	**10d**	220 (31.1)	303 (10.6)	323 (5.6)	366 (3.1)
5	**10e**	313 (sh)	326 (4.1)	341 (3.6)	376 (0.9)
6	**10f**	230 (16.6)	304 (12.2)	327 (sh)	367 (3.6)
7	**10g**	287 (4.2)	312 (4.3)	321 (4.2)	362 (1.0)
8	**10h**	231 (23.3)	300 (5.2)	329 (sh)	353 (2.2)
9	**10i**	231 (25.6)	299 (2.3)	323 (1.5)	358 (0.8)
10	**10j**	235 (44.2)	287 (1.3)	369 (1.0)	403 (1.6)

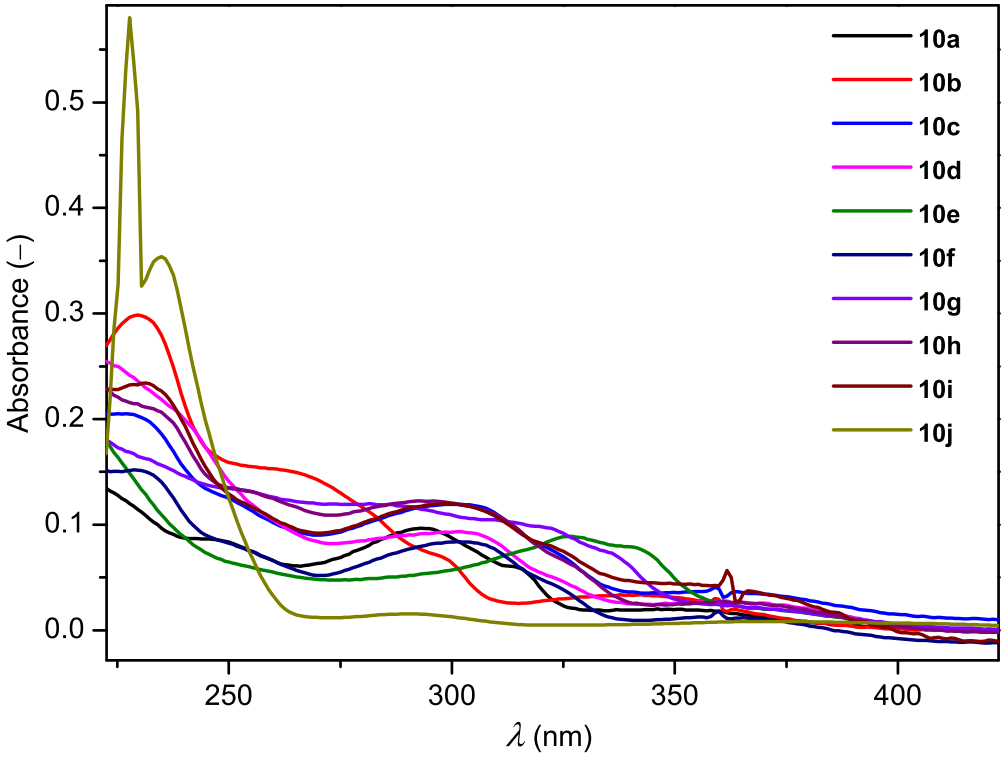

Figure 4: UV spectra of acetonitrile solutions of **10a** - **10j**, $c_{\mathrm{Ir}} = 9 \cdot 10^{-6}$ M.

From the synthesis and characterization studies of the complexes we conclude that

- the [Cp*Ir(bpy)Cl]$^{+}$-type complexes were obtained in excellent yields in an easy synthetic step
- the complexes were air and moisture stable at room temperature and underwent no decomposition or ester hydrolysis when heated in water for 6 h at 70 °C
- structures of complexes **10a** and **10j** are isostructural and display a piano-stool configuration with the coordinating chloride approximately perpendicular to the plane of the bpy ligand
- in the UV-Vis measurements all complexes show absorption bands for the ligand centered allowed π-π^* transitions of the bpys and no MLCT transitions were observed
- the new [Cp*Ir(bpy)Cl]$^{+}$-type complexes display ideal catalyst properties such as excellent solubility, stability and possibility for further functionalization, making them promising candidates for the testing of electrocatalytic CO_2 reduction

3 Electrochemical behavior and CO_2 reduction activity of the iridium (III) complexes

To investigate the viabilty of complexes **10a-10j** as catalysts in the electrocatalytic CO_2 reduction, a suitable experimental setup had to be designed and constructed. Cyclic voltammetry is a convenient technique extensively used for determination of redox behavior of transition metal complexes. However, in terms of catalysis, complicated calculations are required to determine catalyst activities from wave currents in the CVs associated with the catalytic process.[15] Therefore, we used a different method, controlled potential electrolysis, to gain insight into the activity of the complexes. Controlled potential electrolysis experiments are typically done in a divided cell using a high surface/electrolyte volume ratio (A/V) and vigorous stirring. However, considering the initially produced catalyst amounts in this project (100 mg scale), we decided to design a cell that requires low electrolyte volume and catalyst amount per reaction. In this chapter, the results from the characterization and catalysis experiments, as well as description of the electrolysis cell design are summarized.

3.1 Short description of the cyclic voltammetry setup and standard measurements

To investigate the ligand influence on the redox behavior of the metal center, the [Cp*Ir(bpy)Cl]Cl complexes **10a-10j** were studied by cyclic voltammetry. All CVs were recorded using glassy carbon working electrode (WE, $d = 3.0$ mm), non-aqueous $Ag/AgNO_3$ reference electrode (RE) and Pt wire counter electrode (CE). CVs of complex solutions (0.3-0.6 mM + 0.1 M Bu_4NPF_6) were recorded at 100 mV/s scan rate with negative step potential. The CV setup is depiceted in Scheme 43: Ar or CO_2 were bubbled through the blank or complex solutions for about 10 min via a Teflon tube inlet. After saturation, the tube was removed from the solution and fixed on top to maintain the required atmosphere above the solution. In case of substantial volume loss the electrolyte was refilled with the appropriate solvent mixture so that the volume remained 10 mL. Complexes were investigated under four different conditions: Ar saturated MeCN (A); CO_2 saturated MeCN (B); CO_2 saturated MeCN/H_2O, 9:1, v/v (C) and Ar saturated MeCN/H_2O, 9:1, v/v (D). At first, the redox potential of the reference Fc/Fc^+ couple was measured *vs* $Ag/AgNO_3$ RE (with inner electrolyte: 0.01 M $AgNO_3$ and 0.1 M TBAP in MeCN) in the different electrolytes used (Table 3). In Ar saturated MeCN (A), the potential of the Fc/Fc^+ redox couple was 0.088 V *vs* $Ag/AgNO_3$, identical to the reported value.[199] Clearly, saturation with CO_2 did not have a significant effect on the $E_{1/2}$ of the Fc/Fc^+

redox couple in the two solvent mixtures investigated (compare conditions A with B and C with D), but rather the presence of H_2O played a role, shifting the potentials towards lower values (compare conditions A and B with C and D, Figure 5). Potentials of solvent decompositions and the redox events in the presence of the iridium complexes are reported relative to Fc/Fc^+ redox couple if not otherwise noted and were calculated according to Equation 1:

$$E(vs\ Fc/Fc^+) = E(vs\ Ag/Ag^+) - E_{Fc/Fc^+}(vs\ Ag/Ag^+)\ (V) \quad (1)$$

where $E(vs\ Fc/Fc^+)$ is the potential against the Fc/Fc^+ redox couple, $E(vs\ Ag/Ag^+)$ is the potential measured with the Ag/Ag^+ RE and $E_{Fc/Fc^+}(vs\ Ag/Ag^+)$ is the half potential $E_{1/2}$ of the Fc/Fc^+ redox couple against the Ag/Ag^+ RE.

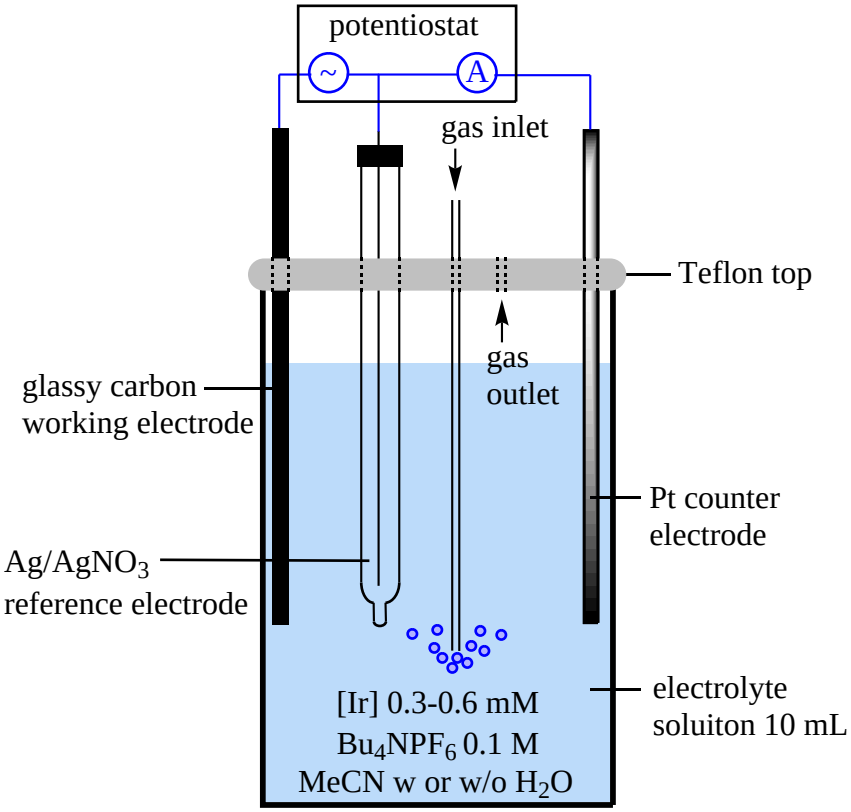

Scheme 43: Cyclic voltammetry setup.

As expected, electrolyte decomposition in the blank solutions containing ferrocene was dependent on the solvent mixture components. The Ar saturated MeCN solution was the most stable, followed by the Ar saturated $MeCN/H_2O$ mixture. When CO_2 was present, the decomposition started at more positive potentials, thus the CO_2 saturated MeCN and $MeCN/H_2O$ mixtures were electrochemically less stable. However, the redox events in the presence of the iridium complexes fitted well in the observed solvent decomposition windows and so we could identify all of the expected events in

the cyclic voltammograms. In Figure 5, CVs of the blank solutions containing ferrocene are shown. Decomposition potentials *vs* Fc/Fc^+ and Fc/Fc^+ potentials *vs* $Ag/AgNO_3$ are summarized in Table 3.

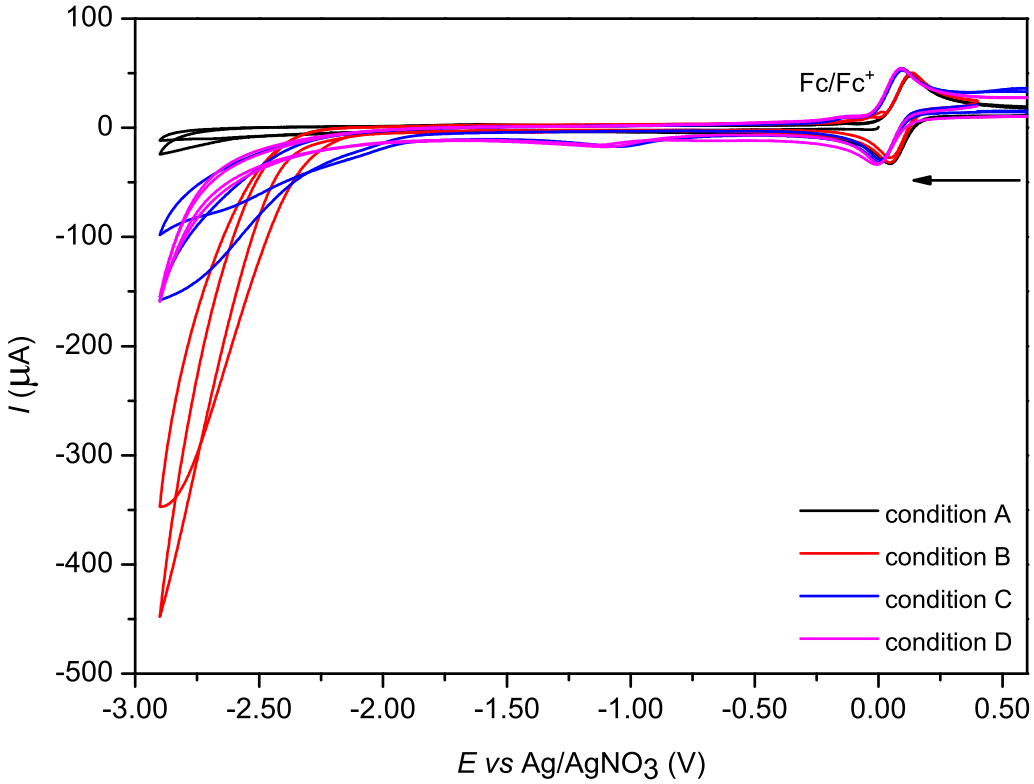

Figure 5: Reductive electrolyte decomposition and Fc/Fc^+ redox couples under different conditions. Ar saturated MeCN (A); CO_2 saturated MeCN (B); CO_2 saturated MeCN/H_2O, 9:1, v/v (C) and Ar saturated MeCN/H_2O, 9:1, v/v (D). CVs were recorded using glassy carbon working electrode (WE, d = 3 mm), non-aqueous $Ag/AgNO_3$ reference electrode (RE) and Pt wire counter electrode (CE) with a scan rate of 100 mV/s and negative initial step potential.

Table 3: Summary of solvent decomposition potentials and Fc/Fc^+ half potentials measured under different conditions.

Condition	Electrolyte dec. *vs* Fc/Fc^+(V)[a]	E_{Fc/Fc^+} *vs* $Ag/AgNO_3$(V)[b]	Nr. of measurements
A: Ar saturated MeCN	−2.62	0.088 ± 0.002[199]	10
B: CO_2 saturated MeCN	−2.25	0.090 ± 0.002	8
C: CO_2 saturated MeCN/H_2O, 9:1, v/v	−1.93	0.045 ± 0.008	7
D: Ar saturated MeCN/H_2O, 9:1, v/v	−2.38	0.043 ± 0.006	6

[a] Absolute error of the measurements is ± 0.02 V. [b] Errors calculated from standard deviations.

3.2 Redox behavior of the Ir complexes

Redox behaviour of complex **10a** was already studied by Ziessel and Kaim *et al.* using cyclic voltammetry.[200,201] First, an iridium centered two electron reduction takes place, which is an irreversible process displaying a distinct separation between the reduction and oxidation peaks (events *a* and *c* in Figure 6). The Ir(III)/Ir(I) reduction is followed by a one electron reduction of the bpy ligand (event *b* in Figure 6). At positive potentials (0.70 V), an irreversible oxidation was observed (not shown in Figure 6) assigned to the Cp* ligand oxidation.

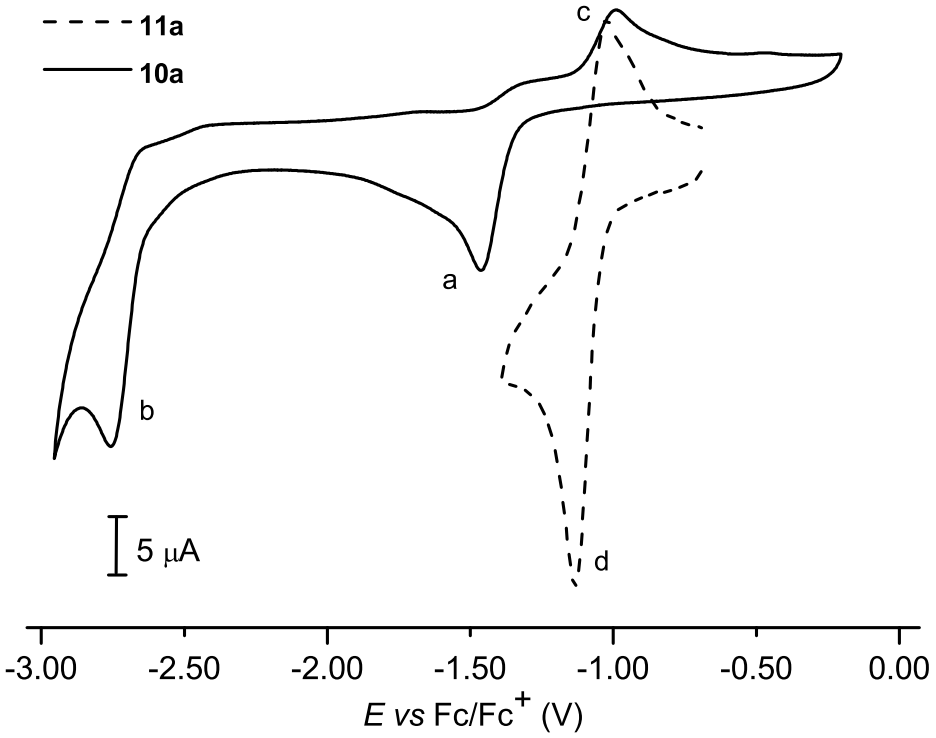

Figure 6: Redox behavior of complexes **11a** and **10a** in MeCN under Ar atmosphere. For CV parameters see caption to Figure 5.

Kaim *et al.* argued that the irreversible metal centered redox event is due to the stabilization of the reduced, coordinatively unsaturated Ir(I) species by π-back donation from the d^8 iridium to the π^* orbital of the ligand. This would make the iridium center less electron rich and thereby more difficult to oxidize. The strong π-back donation was confirmed by the more negative reduction potential of the bpy ligand in the complex, than the free bpy. However, we assumed that the large peak separation of the Ir(III)/Ir(I) redox couple was due to formation of a solvato complex instead of regeneration of the chloro complex on the reverse scan. Therefore, we prepared the tentative product, complex **11a**, and compared its electrochemical behavior with that of **10a** using cyclic voltammetry (Scheme 44). As expected, double cationic complex **11a** was more easily reduced than **10a** and displayed a reversible reduction event at -1.08 V (Figure 6, event *d*). The anodic peak potentials were essentially

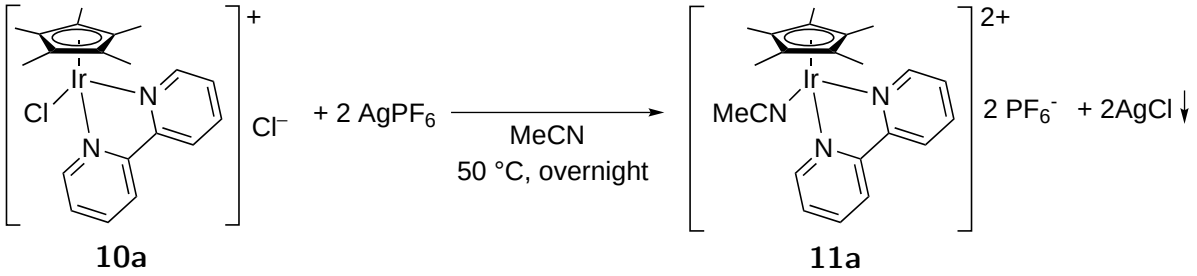

Scheme 44: Synthesis of complex **11a**.

the same for both complexes (−1.02 V and −0.99 V for **11a** and **10a**, respectively) compatible with the assumption that in both cases the same Ir(I) species is formed upon two-electron reduction of the starting complex (Scheme 45). Since CV measurements were recorded in MeCN solutions at low complex concentrations (0.2−0.3 mM), the chloride ion concentration is much lower than the electrolyte concentration.

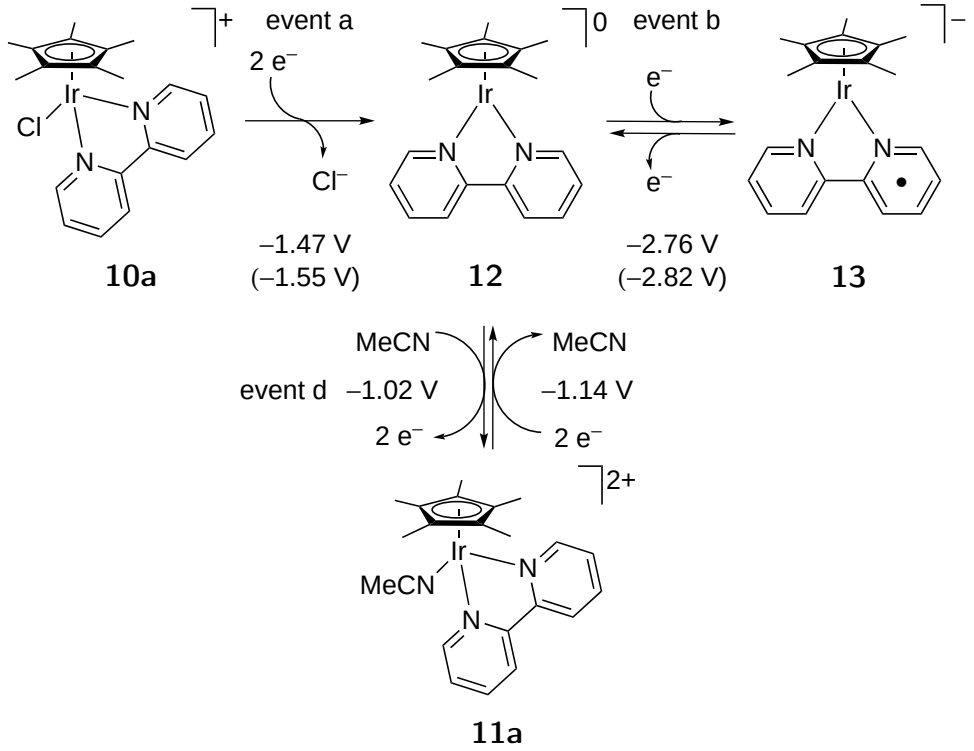

Scheme 45: Redox behavior of $[Cp^*Ir(bpy)Cl]^+$ complex **10a** first investigated by Kaim.[201] Measured reduction potentials are given under the arrows. Reported values are in parentheses. Compound **11a** was newly prepared to investigate the cause of irreversibility of the Ir(III)/Ir(I) redox couple.

Therefore upon oxidation of **12** coordination of the solvent to give **11a** is much faster than association with chloride leading back to **10a**. If Kaim's hypothesis were true for the first reduction event, we would have observed an irreversible behavior for complex **11a** as well. Therefore we could confirm the role of Cl^- anion dissociation in the irreversibility of this Ir centered redox peak.

The reversibility of event *d* in Figure 6 was proved by standard analysis methods.[202] For Nernstian reversible systems the following three conditions apply:

1. E_p is independent from the scan rate (ν) and the current is proportional to $\nu^{1/2}$
2. $|E_\mathrm{pc} - E_\mathrm{pa}| = 2.20 \cdot \frac{R \cdot T}{z \cdot F} = \frac{56.5}{z}$ mV at 25 °C
3. $\frac{i_\mathrm{pc}}{i_\mathrm{pa}} = 1$

Redox event *d* fulfilled criteria 1 and 3 as shown in Figure 7 and regarding criterium 2, an average peak separation of about 12 mV was obtained, which would correspond to $z = 4.7$. It is difficult to explain where the huge deviation in $|E_\mathrm{pc} - E_\mathrm{pa}|$ comes from compared to the expected value of 28 mV. It cannot be a temperature effect, since a 5 °C decrease of temperature would cause a 0.99 mV difference in the measured value according to the calculation described in point 2.

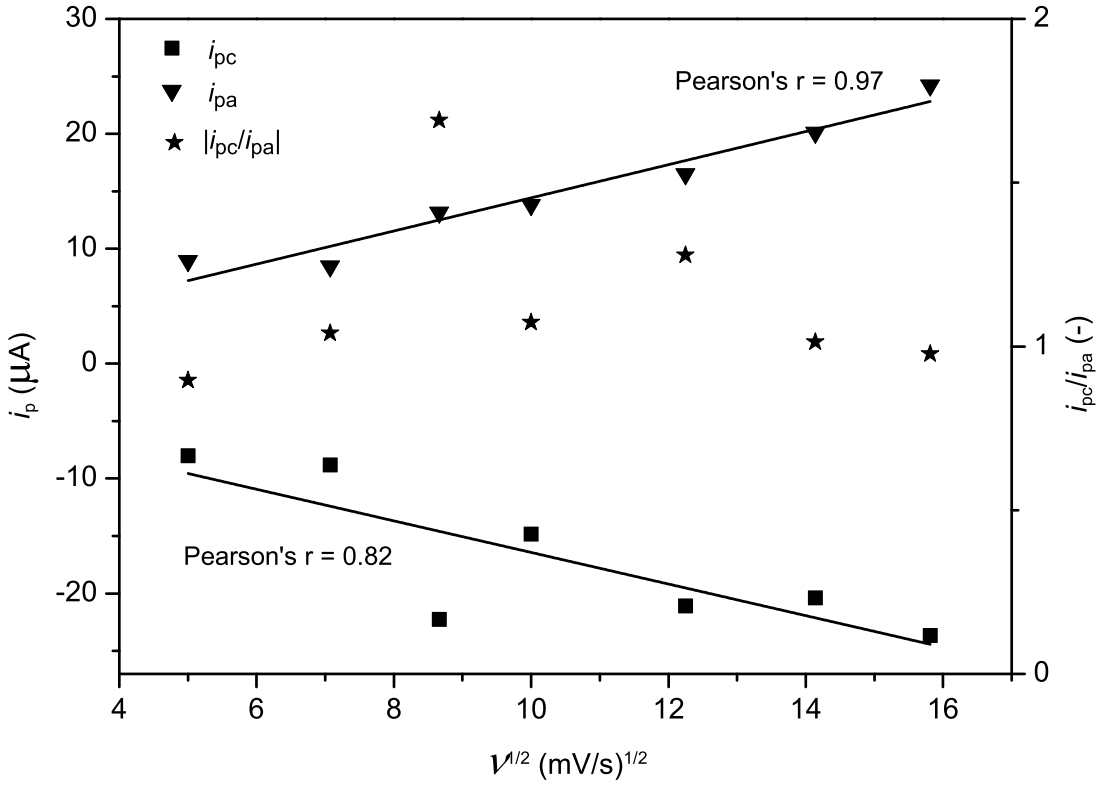

Figure 7: Reversibility analysis of the redox event *d* in Figure 6 of compound **11a**.

The role of the chloride anion dissociation and solvent association in the irreversibility of the Ir(III)/Ir(I) redox couple of the [Cp*Ir(bpy)Cl]$^+$-type complexes was also confirmed by spectroelectrochemistry measurements of complexes **10d** and **10g**. In these measurements a very small volume of about 0.1 mL was applied, allowing the association of the Cl^- anion on the anodic scan after formation of **12** thus resulting in a reversible Ir(III)/Ir(I) redox couple under spectroelectrochemical

conditions. Figure 8 shows the change in the absorption spectra of **10d** and **10g** duirng the iridium centered reduction process, event *a*. A new peak appears at 579 and 597 nm for **10d** and **10g**, respectively, which is typical for MLCT transitions from a d^8-iridium center to the π^* orbital of the ligand.[201]

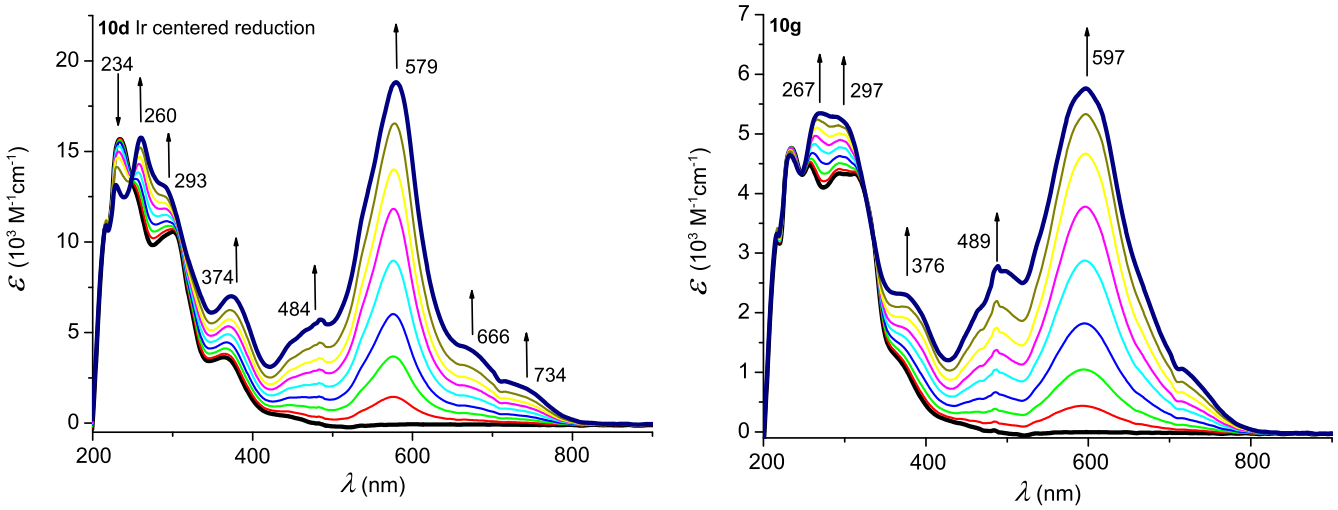

Figure 8: UV-Vis absorption spectra recorded in a SEC cell for the iridium centered reduction event of **10d** and **10g**.

After reproducing the redox behavior of **10a**, we measured CVs of all the complexes under conditions A, B, C and D. The complexes all showed similar behavior in Ar saturated MeCN (A). The peak potentials of events *a* and *c* corresponding to the Ir(III)/Ir(I) couple are depicted in Figure 9 for each complex. As expected, **10j** and **10b** containing only electron donating substituents shift the reduction potentials to more negative values, whereas **10c** is the easiest to reduce, confirming that the reduction potential of the iridium center is determined by the substitution pattern of the ligand. Complexes **10d-10h**, constituting both an electron withdrawing ethoxycarbonyl and an electron donating substituent were reduced at very similar potentials indicating that the reduction potential of the metal center is mainly influenced by the ethoxycarbonyl group on the bipyridine and the Cp* ligand present in each complex. This behavior can be explained by the stabilizing effect of the π-back donation in the reduced species **12**. In this d^8-Ir species the energy of the d orbitals is higher than in **10a** and therefore closer to the energy of the bipyridine π^* orbitals. Since the energy of the π^* orbital in the ethoxycarbonyl substituted pyridine ring is lower compared to the pyridine ring bearing an electron donating group, the stabilizing effect is mainly influenced by the Ir d^8-PyCO_2Et π^* interaction. The anodic peak potentials (E(ox)) corresponding to the oxidation of Cp*Ir(I)(bpy) species showed a similar trend, except for compounds **10a** and **10h**, which displayed higher E(ox) than expected from the trend in the reduction potential values. In case of electron

donating substituents, *i.e.* in **10j** and **10b**, the π-back donation from the Ir(I) center to the π^* orbital of the ligand is weaker, therefore oxidation occurs at more negative potentials. Peak separations (E(ox)$-E$(red)) varied between 0.28 and 0.41 V at 100 mV/s scan rate; the largest separations were observed for compounds **10a** and **10h** (0.41 V and 0.40 V) whereas the rest showed very similar values (around 0.30 V).

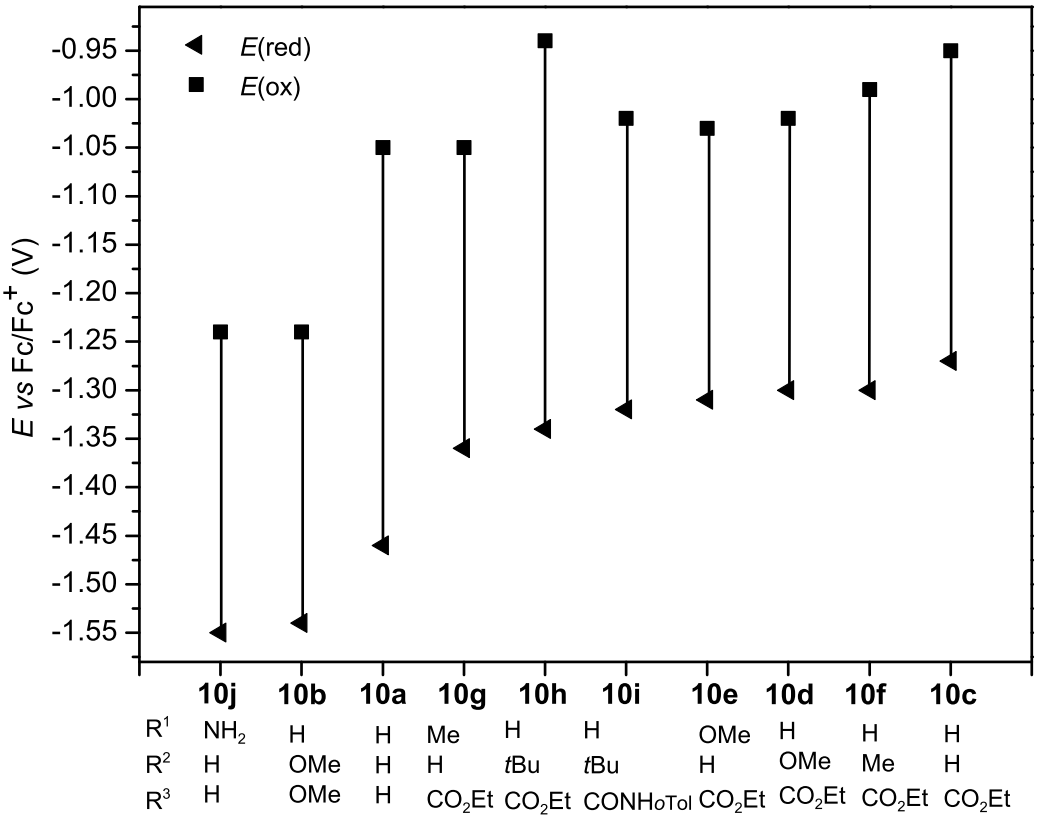

Figure 9: The Ir(III)/Ir(I) reduction-oxidation couple of the [Cp*Ir(bpy)Cl]$^+$ type complexes in MeCN under Ar atmosphere. For CV parameters see caption to Figure 5.

First experiments on the electrocatalytic activity of the complexes were done by cyclic voltammetry in CO_2 saturated MeCN/H_2O (9:1, v/v). Water was added because of earlier reports that the activity of **10a** was increased considerably by addition of a proton source to the reaction mixture.[42] Complex **10d** depicts the typical behavior of the complexes under these conditions (Figure 10). We observed the same reduction events as Deronzier, and assigned them according to their mechanistic proposal for **10a** (see Scheme 46).

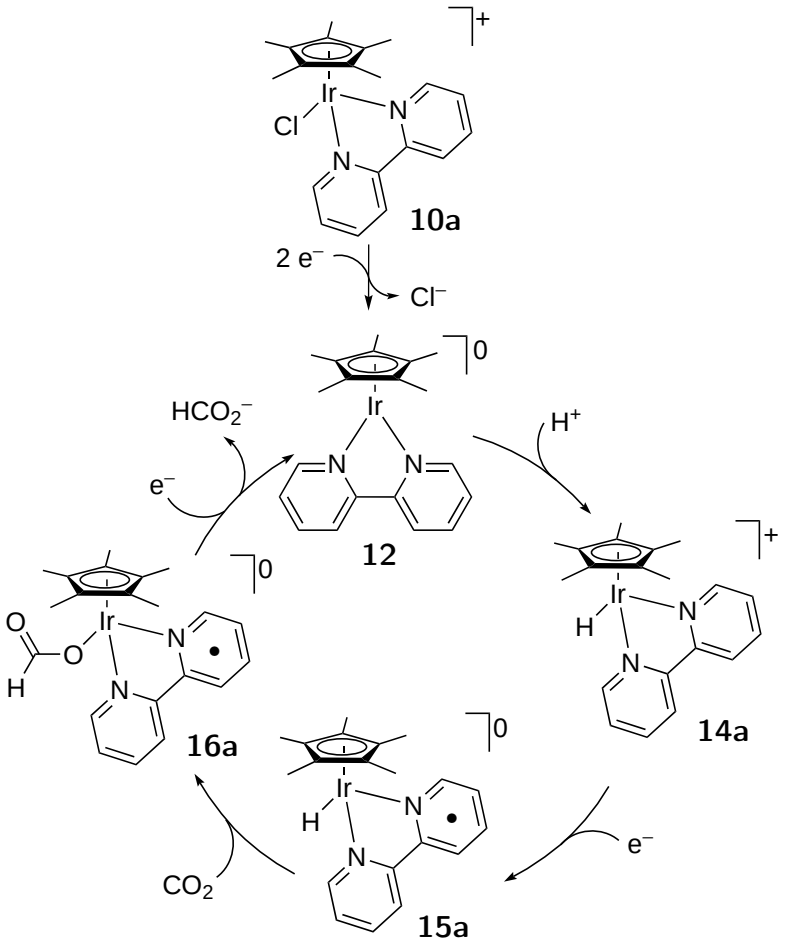

Scheme 46: Possible mechanism for the electrocatalytic reduction of CO_2 by **10a** proposed by Deronzier.[42]

Following an initial two-electron reduction of **10a** (event *a*, CV C in Figure 10), the resulting Ir(I) species **12** is proposed to be protonated to form Ir(III)-hydride **14a**, which undergoes a bipyridine centered one electron reduction (event *e*, CV C in Figure 10) before the hydride is transferred from **15a** to CO_2. Dissociation of formate from **16a** requires another one electron reduction, which closes the cycle and regenerates **12** (event *f*, CV C in Figure 10).[42] An analogous mechanism had been proposed earlier by Meyer and co-workers for a Ru-bipyridine complex used in the electrocatalytic reduction of CO_2 (Scheme 12).[73]

Control experiments in CO_2 saturated MeCN in the absence of H_2O as well as in MeCN/H_2O (9:1, *v*/*v*) in the absence of CO_2 were carried out for each compound, as depicted in Figure 10 for a selected example, compound **10d** (see all CVs in the Experimental Part). In neat MeCN solution, the CVs in the presence and absence of CO_2 were essentially the same apart from a slight shift of the peak potential values (CVs A and B in Figure 10), which shows that no reaction is taking place

and confirms the need of a proton source for CO_2 reduction.

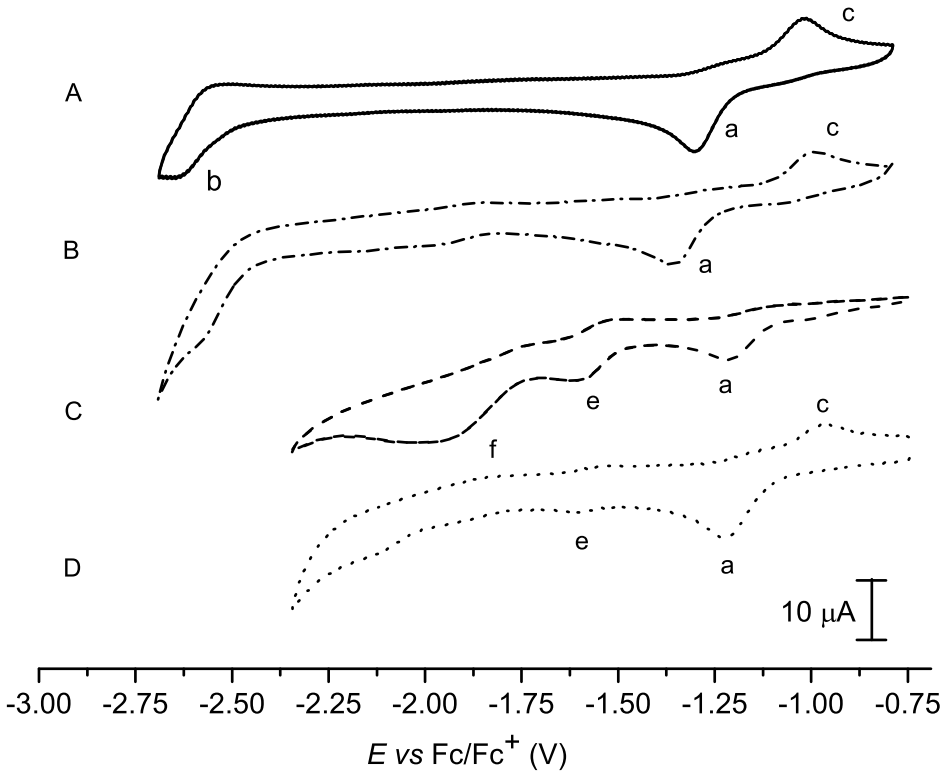

Figure 10: CVs of complex **10d** under different conditions. For conditions and CV parameters see caption to Figure 5.

In the presence of H_2O, however, CVs under CO_2 and Ar were clearly different. As expected, the additional peak *f* assigned to a CO_2 reduction event was only observed in the presence of CO_2. However, the reversible peak *e* at −1.56 V, assigned previously to the one electron reduction of an Ir-hydride species **14**, was almost negligible under Ar atmosphere, and the anodic event *c* at −0.97 V still occurred at the same potential as observed under anhydrous conditions (CV D, Figure 10). This behavior of **10d** is unexpected with respect to previous reports on **10a** that an Ir-hydride species is formed quantitatively from **12** in the presence of a proton source like H_2O.[42,200] In our measurements of **10a**, we observed only non-quantitative formation of the Ir-hydride under Ar atmosphere in the presence of water. Compound **10d** displayed the additional peak *e* more pronounced only when both H_2O and CO_2 were present (CV C in Figure 10).

Similar behavior was observed for complexes **10c**, **10e**, **10f**, **10h** and **10i**, which display reduction potentials higher than −1.33 V. On the contrary, compounds **10a**, **10b**, **10g** and **10j**, which have reduction potentials below −1.33 V, displayed a redox event *e* in the presence of H_2O under Ar as well as in CO_2 saturated solutions. Furthermore, for complexes **10b**, **10g** and **10j** the anodic peak

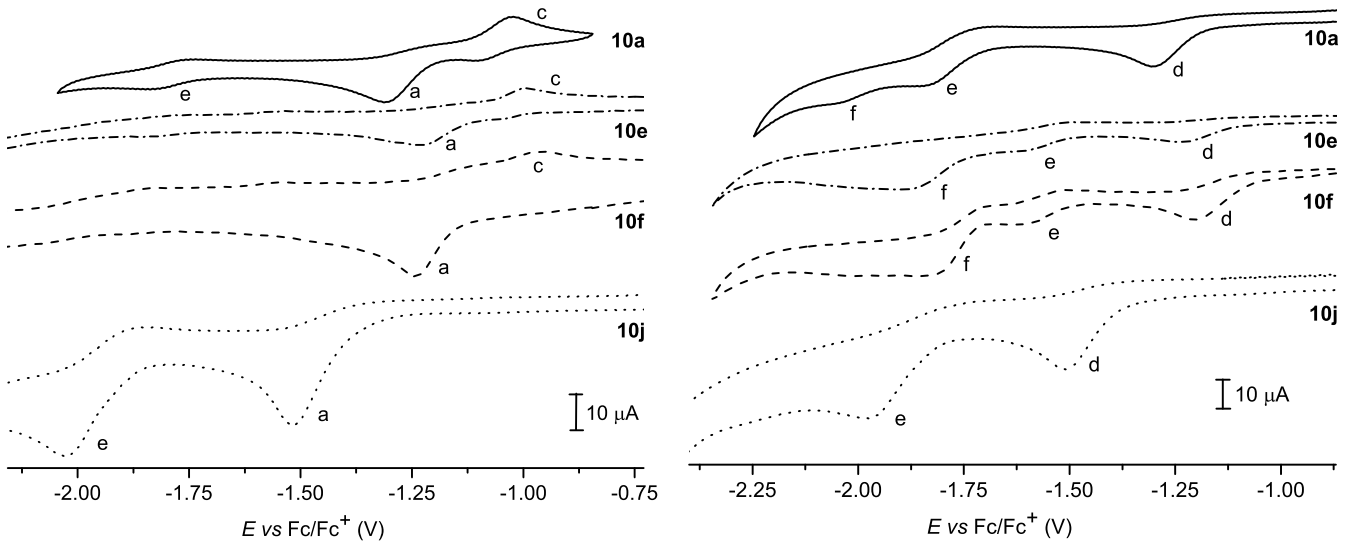

(a) (b)

Figure 11: Cyclic voltammograms of selected complexes in MeCN/H_2O (9:1, v/v) under (a) Ar and (b) CO_2 atmosphere. For CV parameters see caption to Figure 5.

c assigned to the oxidation of Ir(I) to Ir(III) entirely disappeared. Figure 11a shows the behavior of selected complexes in MeCN/H_2O (9:1, v/v) under argon atmosphere while Figure 11b demonstrates the behavior under CO_2 atmosphere. The absence of event c on the reverse scan suggests quantitative transformation of the neutral Ir(I) species to a new compound, an Ir(III)-hydride. Based on these observations, we suggest that the amount of the Ir-hydride species formed is influenced by the acidity of the electrolyte, which depends on the presence or absence of CO_2, and the reduction potential of the complex, which in turn depends on the nature of the bipyridine ligand.

To confirm that the hydride formation by protonation of the reduced Ir(I) species is dependent on the acidity of the electrolyte as well as the nature of the bpy ligand, we further investigated complexes **10d** and **10g**, which showed none or quantitative formation of the hydride, respectively in Ar saturated MeCN/H_2O, 9:1, v/v (condition D). After addition of HPF_6 (5 equivalents) we expected quantitative formation of the hydride in both cases, because of increased acidity of the electrolyte (see Figure 12a and 12b). When HPF_6 was added to the solution of **10d**, a broad and intense peak was observed in the potential region where the one electron reduction of the iridium hydride is expected (see box in Figure 12a). This event was also present when HPF_6 solution was probed in the absence of Ir catalyst (dotted line in Figure 12a) and might correspond to the iridium hydride reduction as well as simultaneous reduction of protons due to increased H^+ concentration.[203] Nevertheless, in both cases event c was not observed after the addition of excess acid, confirming

quantitative transformation of the reduced iridium (I) species. The higher i_p of event *a* under acidic conditions in both cases could be due to the higher mobility of the electrolyte after addition of H^+-s, which causes higher conductivity and therefore a higher observed current.

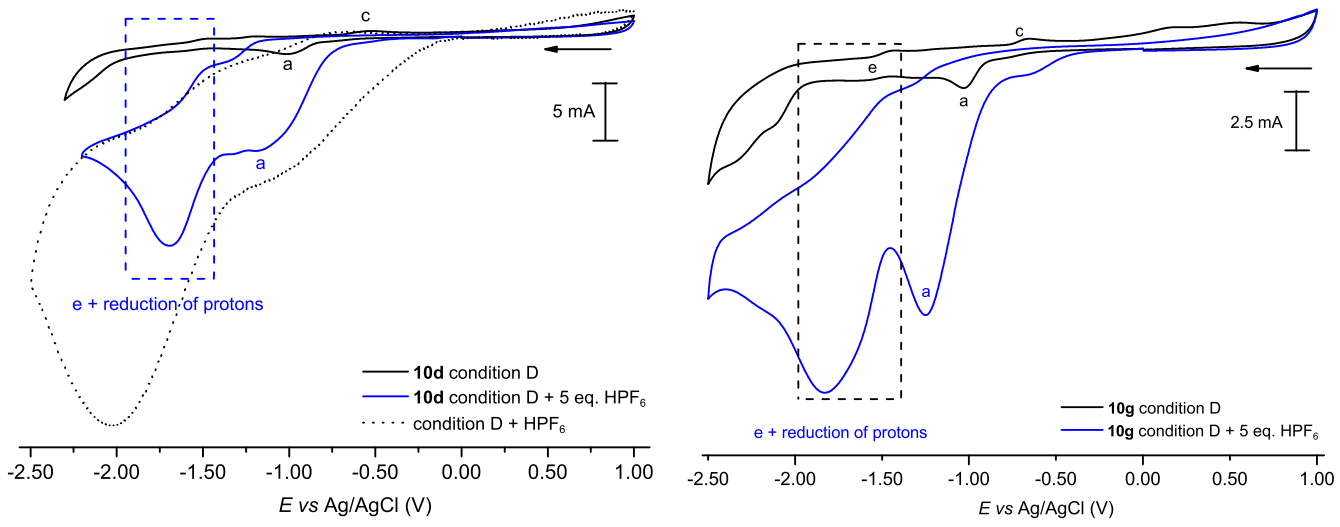

Figure 12: CVs of compound **10d** (a) and **10g** (b) in Ar saturated $MeCN/H_2O$, 9:1, v/v (D) (in black) and under the same conditions in the presence of five eqivalents of HPF_6 (in blue).

From these initial studies we can conclude that

- the new $[Cp^*Ir(bpy)Cl]^+$-type complexes show similar CV behavior to **10a** under all tested conditions
- the reduction potential of the metal centre could be fine-tuned by the substituents on the bpy ligands
- the irreversible Ir(III)/Ir(I) behavior of the complexes is due to Cl^- dissociation on the reduction scan and MeCN association on the oxidation scan
- a reduction peak corresponding to interaction of the complexes with CO_2 was observed for each compound under condition C
- the formation of the iridium hydride is dependent on the acidity of the electrolyte and the nucleophilicity of the iridium (I) species
- the number of electrons involved in events *a*, *c* and *d* could not be determined conclusively

3.3 Catalytic activity of the Ir complexes in CO_2 reduction

To validate that the interaction between the iridium complexes and CO_2 observed in the CVs leads to actual conversion of CO_2, a thorough study by controlled potential electrolysis experiments was required, with sufficient product analysis. For this, a two-compartment divided air-tight cell was designed with a small volume. Scheme 47 shows the schematic representation of the first cell design with a total volume of $V_{tot} = 1.2$ mL (for each compartment). The compartments were made of glass and seperated by Nafion membrane, which was pre-treated by soaking in milli-Q water. Care was taken that the H^+ permeable side of the membrane faced the anodic cell compartment, where the oxidation occured. In initial experiments, glassy carbon WE, Pt sheet CE and Ag wire reference electrodes were used. The WE and CE were sealed to the glass edges by Teflon seals. The cell could be flushed with CO_2 or inert gas through a needle and closed air-tight with septa. The thin RE was simply placed through the septum closing the cathodic half cell.

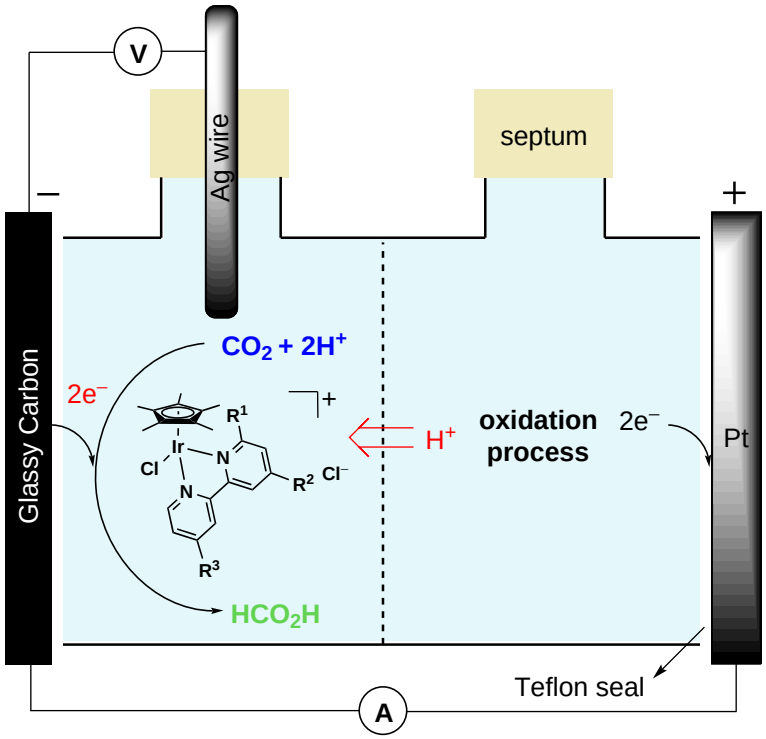

Scheme 47: Schematic representation of the first cell design used in controlled potential electrolysis experiments.

The disadvantages of this design were that the sharp edges of the glass pieces damaged the membrane and therefore occasional leakage was observed during the electrolysis experiments; the Teflon seals did not always work perfectly, sometimes the cell had to be disassembled and reassembled again to obtain proper sealing; the Ag wire is not a stable reference electrode; the glass pieces were prone to break after extensive usage due to the force that was applied to press the pieces together with a

frame.

To address these problems, a second generation of the cell was developed. Cell compartments made of Teflon were used with a total volume of V_{tot} = 1.5 mL (for each compartment). This design did not require Teflon seals but rather O-rings towards both the electrode and the membrane sides and appeared to be less damaging for the membrane material. A thin leak-free Ag/AgCl reference electrode was used in this setup. The new cell design was reliably tight except for occasional leakage when experiments were conducted for 15 h.

3.3.1 Product analysis

After the design of the electrolysis cell, the second challenge was to find a suitable methodology for the quantification of the products. We anticipated based on the work by Deronzier *et al.* that our systems would be selective towards the formation of formic acid or formate anion.[42] They quantified the formate product using HPLC with a Bio Rad HPX-87 cation exchange resin column eluted with 10^{-2} M H_2SO_4 solution. In these experiments a considerably larger amount of the electrolyte was used for catalytic experiments and after the electrolysis the samples were treated prior to analysis to remove the conductive salt. Considering the small volume and low catalyst and product concentrations of our samples, we had to use an analytical method that could be applied directly on the electrolysis samples without work up.

Several methods have been reported for the quantification of formic acid by HPLC,[204] GC[205,206] and ^{1}H NMR[207,208,209,210] techniques. The former two methods would be problematic to use for our analysis, because high concentration of the conductive salt used in the electrolysis experiments would not only damage the column, but also make product detection difficult. Therefore ^{1}H NMR spectroscopy with WET solvent suppression method was studied to investigate the possibility of the product analysis of these reactions.[211]

In the controlled potential experiments, a catalyst concentration of c_{Ir} = 1.34 mM was used, which corresponds to a molar amount of n_{Ir} = 1.60 μmol using cell type 1. Before optimization, we conducted solvent suppression ^{1}H NMR experiments with solutions of known amounts of authentic formic acid in MeCN/H_2O using *p*-xylene as internal standard to determine the absolute error of this quantification method. The amounts of formic acid were chosen to correspond to TONs of about 10. In Equation 2 the calculation of the formic acid amount is shown from the ^{1}H NMR integration data.

$$n_{\mathrm{HCO_2H}} = \frac{Int_{\mathrm{HCO_2H}}}{Int_{\mathrm{xyl}}} \cdot 4 \cdot n_{\mathrm{xyl}}\ (\mu\mathrm{mol}) \tag{2}$$

where n_{i} is the molar amount of formic acid (i = HCO_2H) and *p*-xylene (i = xyl) and Int_{i} are the integrals of the ^{1}H NMR spectra. Figure 13 shows the calculated formic acid amounts as a function of the actual amounts weighed in the different dilutions. After a least squares fit on the four data points it can be concluded that this method is suitable for the product amount determination in this concentration range and that the error from the ^{1}H NMR sample preparation, measurement and integration is about $slope_{\mathrm{error}}/slope \cdot 100 = 7\%$.

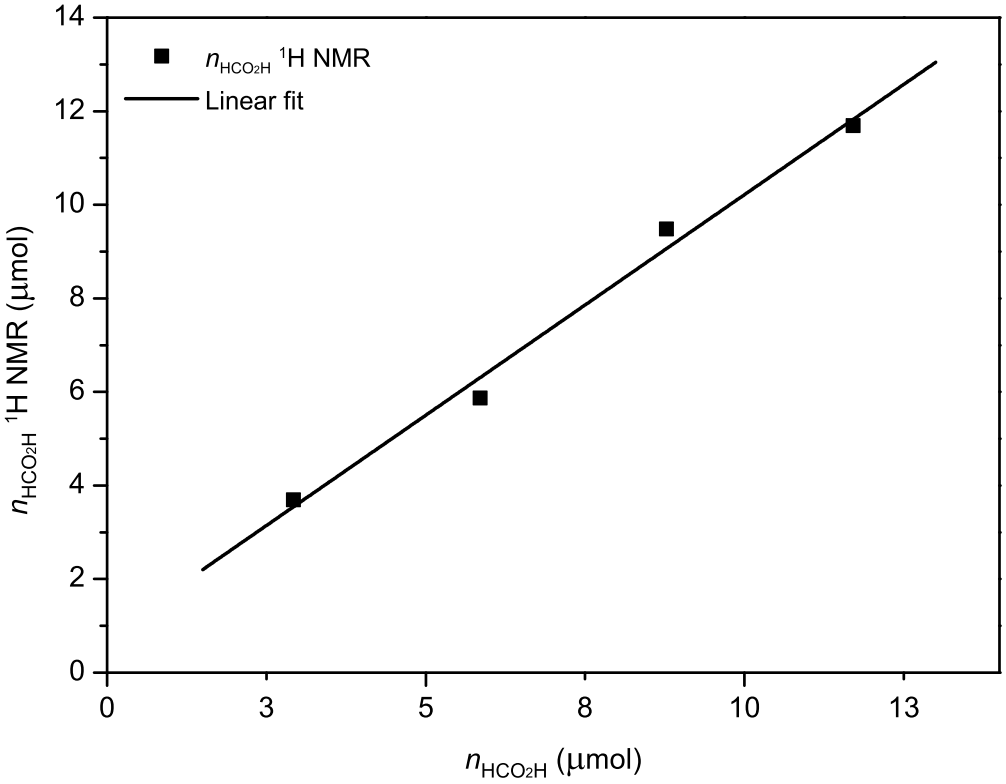

Figure 13: Validation of the WET solvent suppression ^{1}H NMR measurements as analytical tool for the electrolysis experiments: the calculated *vs* actual amounts of formic acid.

3.3.2 Optimization using catalyst 10a

After having cell type 1 and a suitable analytical method in hand, optimization experiments were conducted using complex **10a**. For comparison of the different investigated conditions, formic acid amount ($n_{\mathrm{HCO_2H}}$), turnover numbers (TON) and current efficencies (η) were determined using equations 3, 4, 5.

$$n_{\mathrm{HCO_2H}} = \frac{Int_{\mathrm{HCO_2H}}}{Int_{\mathrm{pxyl}}} \cdot 4 \cdot n_{\mathrm{pxyl}} \cdot \frac{V_{\mathrm{tot}}}{V_{\mathrm{NMR}}}\ (\mu\mathrm{mol}) \tag{3}$$

$$\mathrm{TON} = \frac{n_{\mathrm{HCO_2H}}}{n_{\mathrm{Ir}}} \tag{4}$$

$$\eta_{\mathrm{HCO_2H}} = \frac{n_{\mathrm{HCO_2H}} \cdot z \cdot F}{Q} \cdot 100\ (\%) \tag{5}$$

where V_{tot} is the volume of the electrolysis sample, V_{NMR} is the volume of the ^{1}H NMR sample taken from the electrolysis sample for analysis, z is the number of electrons involved in the process (for HCO_2H it is 2), Q is the total amount of charge passed and F is Faraday's constant (F = 9.64853399(24)·10^4 C·mol^{-1}). In Equation 5 the maximum amount of product is directly derived from Faraday's law (see Equation 6) and Q was determined by integration of the time-current graphs of each measurement.

$$Q = n \cdot z \cdot F\ (\mathrm{C}) \tag{6}$$

$$Q = \int I(t)\ \mathrm{d}t\ (\mathrm{C}) \tag{7}$$

To explore the effect of different conditions and additives, chronoamperometric measurements were carried out at −1.80 V *vs* Ag wire for a total of t = 3 h. In both half-cells, a solution of complex **10a** was used. In the cathodic half-cell the CO_2 reduction took place while in the anodic half-cell oxidative solvent decomposition occurred, presumably water oxidation catalyzed by **10a**, which is known to act as catalyst precursor for this reaction.[212,213,214] In the cathodic half cell some gas formation (bubbles) was observed during the reaction, which was not analyzed for the optimization reactions. With **10a** as the catalyst, we attempted to optimize the reaction conditions to obtain the highest possible amount of HCO_2^- product in our system (Table 5).

Samples from both half cells were taken for analysis. Unexpectedly, two singlets at 8.46 and 8.13 ppm were observed in the ^{1}H NMR spectra of the electrolytes from the cathodic and anodic compartments, respectively. Both signals are within the range of chemical shifts observed for formic acid at different pH values by Berregi 8.2−8.4 ppm[208] and Burakevich 8.0−9.0 ppm.[210] We assumed that the peaks at 8.46 and 8.13 ppm correspond to the chemical shifts of the HCO_2^- and HCO_2H in the cathodic and anodic half cells, respectively. This is also in good agreement with ^{1}H NMR spectra of authentic ammonium formate and formic acid displaying peaks at 8.37 and 8.12 ppm in CD_3CN.

To verify whether both peaks belonged to HCO_2H, the samples were spiked with known amount of HCO_2H solutions.

Figure 14 shows the ^1H NMR spectra of the samples before and after addition of formic acid. After addition only one combined signal was observed. For the solution from the cathodic half-cell, the singlet at 8.48 ppm corresponding to HCO_2^- product shifted up field to 8.32 ppm after the addition of HCO_2H. In the case of the anodic half-cell the singlet at 8.13 ppm remained at the same position. These results suggest a slightly higher pH in the cathodic half cell where protons are consumed in the CO_2 reduction, whereas solvent decomposition in the anodic half cell, *e.g.* water oxidation, produces protons and thus explains the acidic pH in this compartment. Table 4 shows the amounts of product before and after the addition of known amount of formic acid and the differences between the calculated and actual values. The relatively high error for the cathodic half cell's sample might be due to a broader peak that results in less accurate integration even when line fitting was applied on the spectrum.

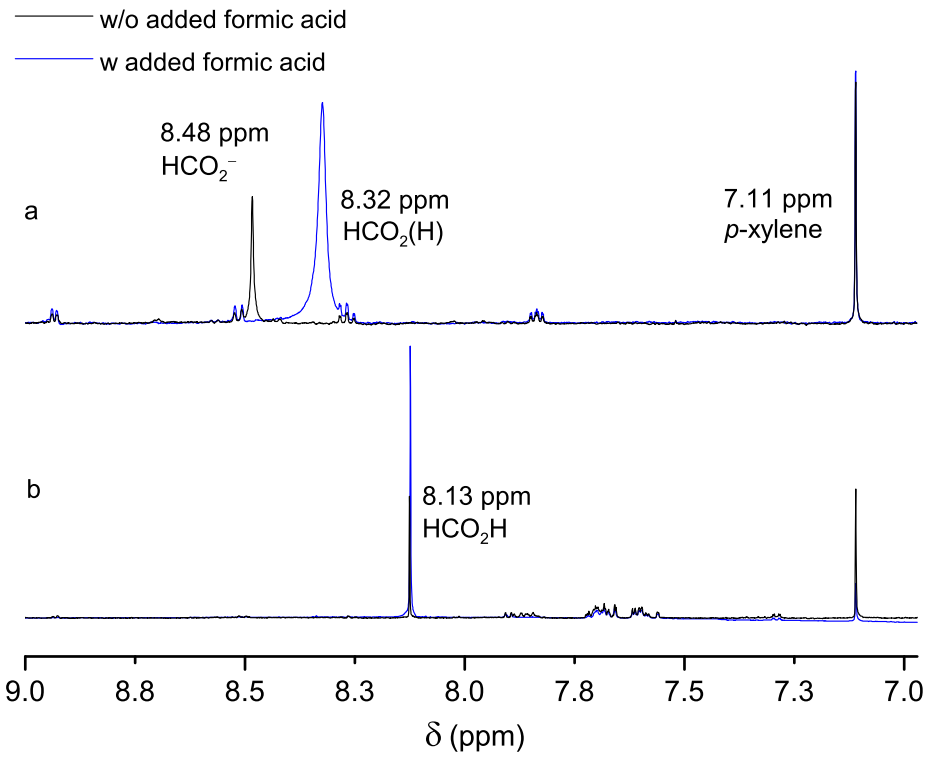

Figure 14: ^1H NMR spectra of the products in the cathodic (a) and anodic (b) half-cells before and after addition of HCO_2H solution.

Table 4: The amounts of formic acid/formate in the ^{1}H NMR samples (V_{NMR} = 0.7 mL) from the cathodic and anodic half cells before and after the addition of a known amount of formic acid. Product amounts are given in μmol. Samples were taken from the experiment described in Table 5, entry 3.

	n_{HCO_2H}	n_{HCO_2H}added	n_{HCO_2H}sum	n_{HCO_2H} ^{1}H NMR	Δn_{HCO_2H}
cathodic	3.1	11.0	14.1	15.6	1.5
anodic	1.7	11.0	12.7	13.1	0.4

Different amounts of H_2O were added to the electrolyte to determine the influence of the concentration of protic solvent on the catalytic activity. The highest yield of HCO_2^- and a TON of 5.1 was obtained with 5% H_2O content (Table 5, entries 2−5). Increasing the H_2O concentration led to lower yields. When no water (except for residual water from the Nafion membrane) was added, still some formation of formate was observed albeit with slightly lower TON. Lowering the concentration of Bu_4NPF_6 as conductive salt from 100 mM to 25 mM afforded a slight improvement in yield and current efficiency (Table 5 entries 3, 6).

Considering the proposed mechanism,[42] namely the protonation of **12** to form the Ir(III) hydride (**14a**), we were interested in the influence of proton concentration on the catalysis. However, addition of HBF_4 did not improve the outcome of the reaction resulting in TONs of 2.6 and 2.4 (Table 5 entries 7, 8 and 3). This result was expected because protonation of the iridium complex should be a fast reaction and not the rate limiting step of the catalytic cycle.

Because formation of the catalytically active species presumably involves chloride dissociation, the effect of added chloride as well as the abstraction of the coordinated chloride were studied. The addition of excess chloride (3.75 equivalents) clearly inhibited the catalytic process. Whereas when the catalyst solution was pre-treated with 1.75 equivalents of $AgPF_6$ to remove the chloride ions, formation of acetaldehyde due to reduction of MeCN was observed besides smaller amounts of formate.

Acetaldehyde could be unambiguously identified by its characteristic ^{1}H NMR signal at 9.73 ppm displaying a quartet with J = 2.9 Hz (Figure 15, *b*).[215] When MeCN/MeOH/H_2O (20:72:8, v/v) was used as electrolyte only a small amount of formate was obtained and unexpectedly a new signal was also observed at 8.34 ppm, which could not be assigned (Figure 15, *c*). When MeOH/MeCN mixture

(1:1, v/v) was used as electrolyte, the formation of a substantial amount of new product displaying a singlet at 8.60 ppm (Figure 15, *a*) was observed next to HCO_2H. We suspected that the singlet at 8.60 ppm belongs to formaldehyde, which is a product of the four electron reduction of CO_2.

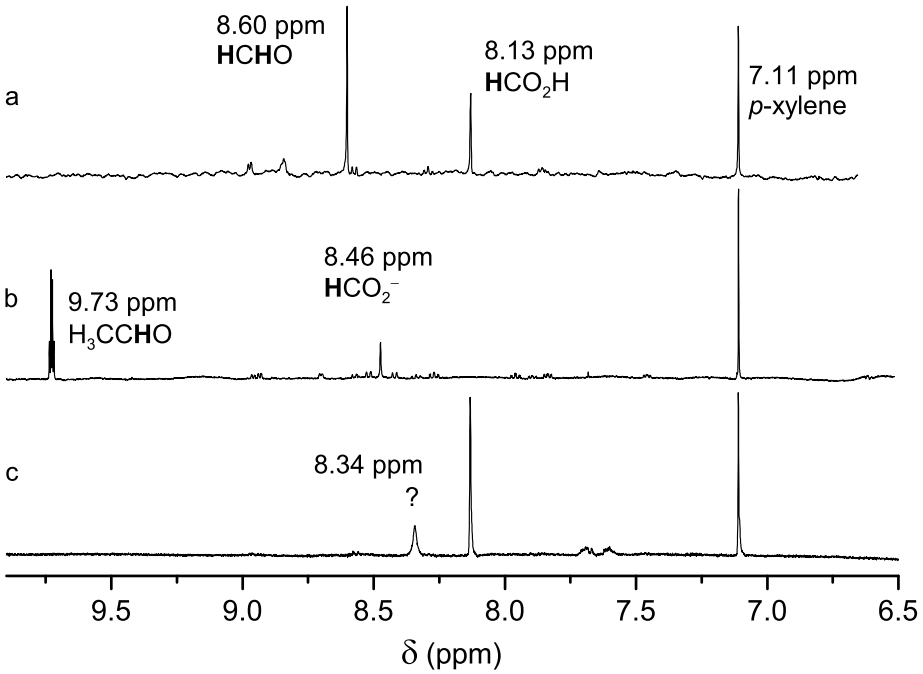

Figure 15: ^{1}H NMR spectra of reaction mixtures taken from the cathodic cell compartment after electrolysis under conditions described in Table 5 entries 12 (spectrum a), 10 (spectrum b) and 11 (spectrum c).

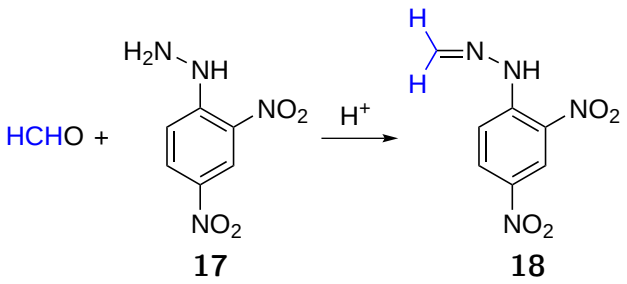

Scheme 48: Formaldehyde-2,4-dinitrophenylhydrazine **18** was prepared for analysis by GC-MS and prove the presence of HCHO in the electrolysis mixture.

To confirm this, after the electrolysis experiment a sample was taken to convert the carbonyl product, possibly HCHO, to a hydrazone derivative (Scheme 48). After precipitation of the conductive salt and extraction of the product from the aqueous phase by toluene, the analyte was measured by GC-MS. Indeed, compound **18** was detected by GC-MS and the spectrum was identical to that found in the database for this compound (see Experimental Part Figure 38). Additionally, Sabo-Etienne also reported a ^{1}H NMR chemical shift of 8.74 ppm for formaldehyde in *d*-benzene, further supporting that the singlet in our sample at 8.60 ppm can be assigned to this product.[46]

Table 5: Controlled potential electrolysis experiments. Conditions: t = 3 h, V_{tot} = 1.2 mL, E_{app} = −1.80 V *vs* Ag wire, n_{Ir} = 1.6 μmol, MeCN/H_2O mixture as solvent, at r.t. Estimated error of TON amounts is ± 0.25[a].

Entry	Bu_4NPF_6 /Bu_4NCl (mM)	H_2O (*v/v%*)	HBF_4 /$AgPF_6$ (μmol)	TON[b]	*Q (C)*	η[c] (%)
1[d]	100/−	10	−/−	−	−0.9	2.1
2	100/−	0	−/−	4.3	−3.0	44.1
3	100/−	5	−/−	5.1	−11.5	13.9
4	100/−	10	−/−	2.1	−2.3	29.0
5	100/−	20	−/−	0.8	−2.9	8.7
6	25/−	5	−/−	6.1	−7.0	27.0
7	100/−	5	8.0/−	2.6	−5.1	16.0
8	100/−	5	16.0/−	2.4	−4.0	18.7
9	20/5	5	−/−	0.3	−0.7	10.2
10 [e]	25/−	5	−/3.2	2.7	−2.2	37.9
11 [f][g]	25/−	8	−/−	0.9	−10.8	1.8
12 [g][h]	25/−	−	−/−	5.4	−18.0	9.3

[a] Errors were calculated from standard deviations of TONs in duplicate measurements of entries 1 and 3. [b] TON refers to the amount of product formed per molecule of precatalyst after t = 3 h as shown in Equation 4. [c] Calculated assuming a consumption of 2 e^- per CO_2 molecule as shown in Equation 5. [d] No catalyst was added. 0.3 μmol product was formed. [e] Acetaldehyde formation was observed. [f] A solvent mixture of MeCN/MeOH/H_2O (20:72:8, v/v) was used. [g] Formaldehyde formation was observed. [h] MeCN/MeOH (1:1, v/v) solvent mixture was used.

To verify that products indeed originated from the conversion of CO_2 substrate, reaction with **10a** was repeated with $^{13}CO_2$ under conditions summarized in Table 5, entry 12. $H^{13}CHO$ and $H^{13}CO_2H$ products indeed displayed doublets in the ^{13}C coupled ^1H NMR spectra at 8.60 and 8.13 ppm with coupling constants of $^1J_{C-H} = 188$ Hz and $^1J_{C-H} = 227$ Hz, respectively in the WET solvent suppression measurements (Figure 16).

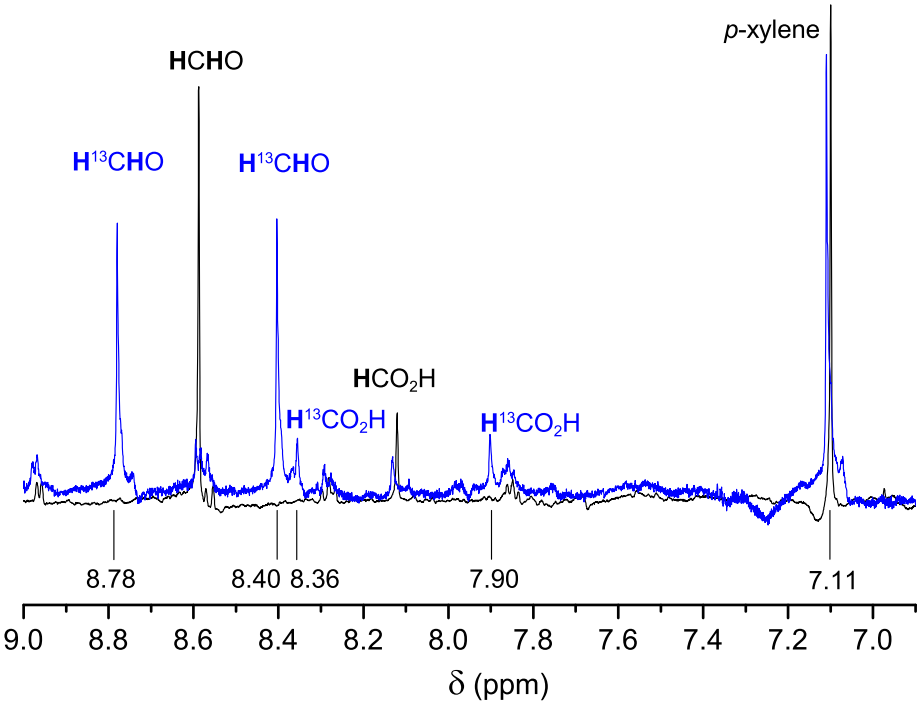

Figure 16: ^1H NMR spectra of the formed products after electrolysis using CO_2 (black) or $^{13}CO_2$ (blue) as substrate, determined by WET solvent suppression measurements.

The spectral properties observed in our experiment are similar to reported values, except for the ^{13}C chemical shift of $H^{13}CHO$, which we observed at $\delta = 169$ ppm as opposed to Sabo-Etienne's reported value of 193.0 ppm (Table 6).[46,216] This raises doubts about the identity of the observed product at 8.60 ppm in the ^1H NMR spectrum and thus we cannot exclude that another compound is responsible for its presence.

Table 6: ^1H and ^{13}C NMR shifts of ^{13}C labeled products of the electrocatalytic experiments.

	Ref[46]	This work	Ref[216]	This work
	$H^{13}CO_2H$		$H^{13}CHO$	
^1H NMR δ (ppm)	8.15	8.15	8.74	8.59
^{13}C NMR δ (ppm)	163.3	162	193.0	169
$^1J_{C-H}$ (Hz)	215	227	176.6	188

However, we find the formation of HCHO most plausible not only for mechanistic considerations, since it is a known product of the four electron reduction of CO_2,[217,45,46] but also because the GC-MS and ^{1}H NMR spectra obtained from the electrolysis samples support its formation.

Figure 16 displays the solvent suppressed ^{1}H and ^{13}C NMR spectra of the experiments conducted under the same conditions (Table 5, entry 12) using CO_2 and $^{13}CO_2$ as substrate. We attempted to reproduce this experiment in deuterated solvent mixture of CD_3CN/CD_3OH 1:1 v/v to obtain better quality HMQC spectra. However, in later experiments the formation of formaldehyde could not be observed. $H^{13}CO_2H$ product was formed exclusively and the HMQC spectrum in CD_3CN:CD_3OH was identical to the spectrum recorded with WET solvent suppression technique (see Figure 17).

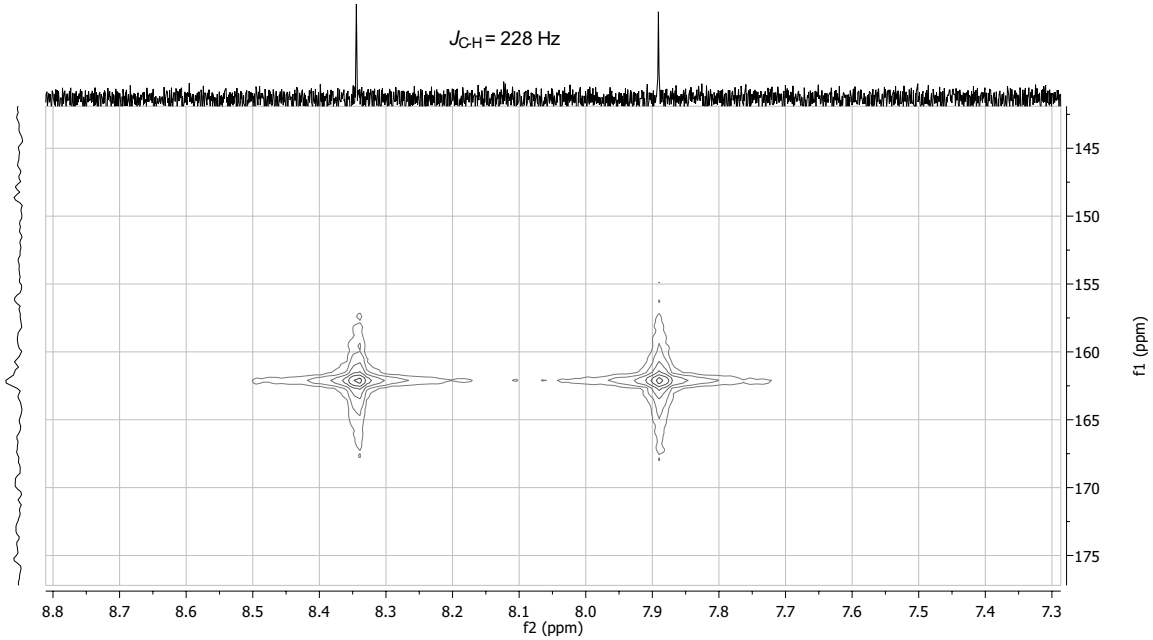

Figure 17: HMQC spectrum of $H^{13}CO_2H$ in CD_3CN/CD_3OH 1:1 v/v.

To explore the catalytic activity of this system and the viability of our methodology, we compared our optimization data with previous results from Deronzier in electrocatalytic reduction of CO_2 using **10a**.[42] In our experiments, two solvent mixtures were investigated: MeCN/H_2O (95:5, v/v) and MeCN/MeOH (1:1, v/v). Not taking into account the influence of different experimental setups, conditions given in Table 5, entry 3 are the best to compare with Deronzier's experiments, since they used 0.1 M Bu_4NPF_6 in MeCN/H_2O (95:5, v/v). After 250 min of electrolysis at $E_{app} = -1.70$ V *vs* Fc/Fc^+, they observed selective formate formation with a TON of 10 and 22% current efficiency. We obtained slightly lower TON = 5.1 and $\eta = 14\%$ after 180 min of electrolysis.

To sum up the results from the initial electrolysis experiments and product analysis:

- a small volume divided electrolysis cell was designed and further developed
- WET solvent suppression ^{1}H NMR spectroscopy was validated as suitable method for the analysis of the electrolysis products with 7% of measurement error
- two solvent mixtures were investigated: MeCN/H_2O and MeCN/MeOH
- in solvent mixture MeCN/MeOH 1:1, v/v formaldehyde was obtained as well as formic acid
- when $^{13}CO_2$ was used as substrate ^{13}C labeled products were formed confirming that the products originated from CO_2

3.3.3 Catalyst screening

In the following section electrolysis experiments using catalysts **10a-10j** will be discussed. The **first set of experiments** were conducted for $t = 3$ h in solvent mixtures MeCN/H_2O 95:5, v/v (*i*) and MeCN/MeOH 1:1, v/v (*ii*) according to conditions in Table 5 entries 6 and 12. The **second set of experiments** were conducted in solvent *ii* for $t = 5$ and 15 h. Due to different cell setups, analysis and calculations applied in these sets of experiments, they will be described separately.

3.3.3.1 Experiments conducted for $t = 3$ h Selected complexes were tested in solvent mixtures *i* and *ii* using cell type 1. Surprisingly, in solvent *i* complex **10a** showed the best activity towards HCO_2^- product and no formation of significant amounts of H_2 and CO was observed. A trend in the catalytic activity relative to the reduction potential of the complexes was not observed, emphasizing the complexity of the catalytic system and the manifold nature of the determining factors. In solvent *ii*, most complexes showed a better activity towards HCO_2H formation than in solvent *i*. HCHO was also observed and only formed in the presence of catalyst indicating that it was not an uncatalyzed further transformation of HCO_2H under reductive conditions. TONs were calculated as given in Equation 4 and n_{HCHO} was determined as shown in Equation 8. Current efficiencies were calculated for HCO_2H as given in Equation 5 and for HCHO as given in Equation 9, where $z = 4$.

$$n_{HCHO} = \frac{Int_{HCHO}}{Int_{pxyl}} \cdot 2 \cdot n_{pxyl} \cdot \frac{V_{tot}}{V_{NMR}} \ (\mu mol) \tag{8}$$

$$\eta_{HCHO} = \frac{n_{HCHO} \cdot 4 \cdot F}{Q} \cdot 100 \ (\%) \tag{9}$$

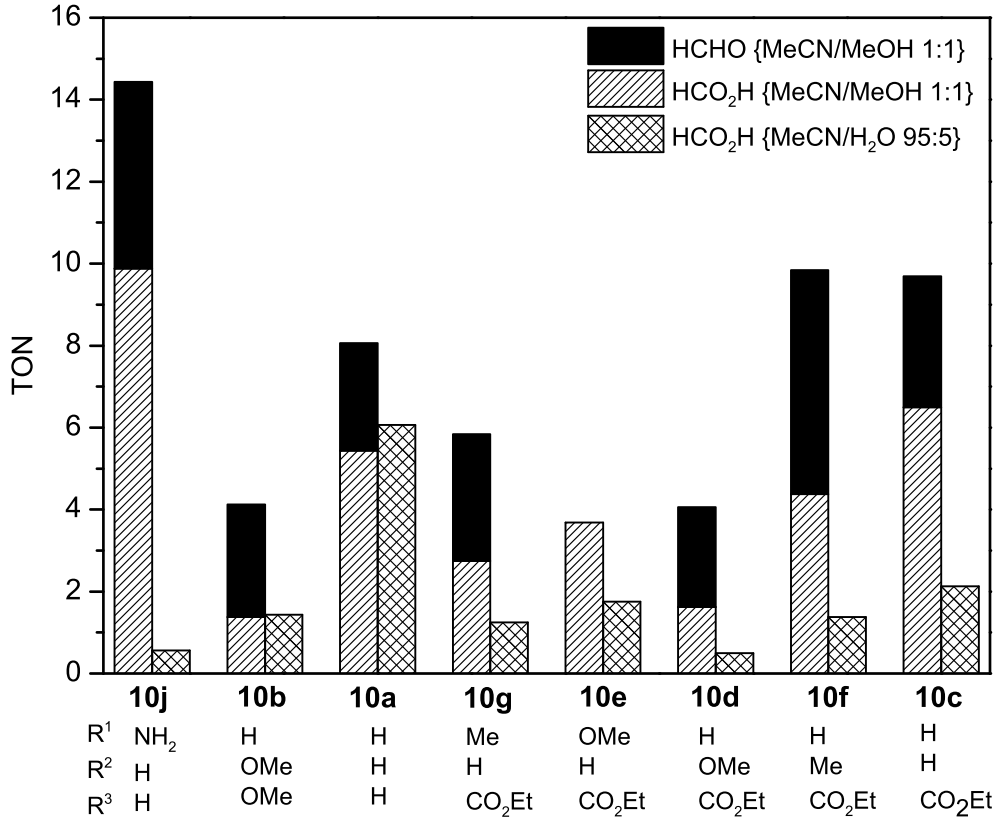

Figure 18: TONs of catalysts related to HCHO and HCO_2H products in solvents *i* and *ii* after t = 3 h electrolysis at $E_{app} = -1.80$ V *vs* Ag/AgCl. Complexes are ordered with growing reduction potential.

Highest turnover numbers of 9.8, 10.0 and 14.4 were achieved in solvent *ii* with complexes **10c**, **10f** and **10j**, respectively (Figure 18). Complexes **10c** and **10f** display the most positive reduction potential for the Ir(III)/Ir(I) transformation, whereas complex **10j** is the most difficultly reduced. This further suggests that the electronic properties do not linearly influence the catalytic activity of the complexes. However, it is important to point out that complexes **10c** and **10f** are structurally related, whereas complex **10j** displays a potential H-bond donor in the coordination sphere of the metal center, which may result in enhanced activity through secondary coordination sphere interactions.[59] The fourth most active catalyst in solvent *ii* was **10a**, displaying a relatively low reduction potential in our series, further suggesting that not only electronic properties of the iridium center play a role in catalysis, and that lower substituted bipyridine ligands may contribute to greater stability and therefore activity of the Cp* complexes. Interestingly, the lowest ativities were achieved by complexes containing methoxy-substituted bipyridine ligands. For precise data from the experiments cunducted for $t = 3$ h see Table 7.

Table 7: TON of complexes to HCO_2H, CO, H_2 and HCHO formation in controlled potential electrolysis experiments for $t = 3$ h in solvent mixtures *i* and *ii*. $E_{app} = -1.80$ V *vs* Ag/AgCl, $V_{tot} = 1.2$ mL. Estimated error of TON values is ±0.25.

	Solvent mixture *i*						Solvent mixture *ii*							
Catalyst	HCO_2H[a]		CO[b]		H_2[b]		HCO_2H[a]		CO[b]		H_2[b]		HCHO[a]	
	TON	η (%)	TON	η (%)	TON	η (%)	TON	η (%)	TON	η (%)	TON	η (%)	TON	η (%)
–[c]	0.2	5.9	0	0	0	0	0.6	10	0.1	0.4	0	0	0	0
10a	6.1	27	0	0	0.7	<1.0	5.4	9.3	0.3	1.1	1.3	<1.0	2.6	16.4
10b	1.5	26.2	n.d.	n.d.	n.d.	n.d.	1.4	4.7	n.d.	n.d.	n.d.	n.d.	2.8	18.3
10c	2.1	34.8	n.d.	n.d.	n.d.	n.d.	6.6	19.7	n.d.	n.d.	n.d.	n.d.	3.2	19.3
10d	0.5	4.9	n.d.	n.d.	n.d.	n.d.	1.6	5.6	0	0	0	0	2.4	16.6
10e	1.8	6.2	n.d.	n.d.	n.d.	n.d.	3.7	11	n.d.	n.d.	n.d.	n.d.	0	0
10f	1.4	20.4	n.d.	n.d.	n.d.	n.d.	4.5	12.9	n.d.	n.d.	n.d.	n.d.	5.5	32.3
10g	1.3	14.1	0	0	0	0	2.7	4.9	<0.1	<0.1	1.1	<0.1	3.1	10.9
10j	0.5	6.6	0	0	0	0	9.8	21.9	0.3	0.5	2.2	<0.1	4.6	20.2

[a] Determined by ^{1}H NMR analysis using *p*-xylene as standard. [b] Determined by GC analysis.
[c] Entry 1 shows hypothetical TONs for 1.6 μmol Ir precatalyst.

Figure 19 shows the CVs of the electrolyte before and after electrolysis as well as the time-current graph during the controlled potential electrolysis at $E_{app} = -1.80$ *vs* Ag/AgCl in CO_2 saturated MeCN/MeOH 1:1, *v*/*v* (solvent *ii*) using complex **10f**. Clearly, in the time frame of the CV experiment, the solution was stable at the applied potential (black trace). Actually, solvent decomposition appeared only at −2.11 V. Interestingly, as shown by the dashed trace, the CV changed considerably after catalysis. This could be attributed to the change in electrolyte composition, since the initial Ir complex was converted into the catalytically active species and HCO_2H was formed. The blue area

in Figure 19 (a) shows the potential range between the hydride reduction and the applied electrolysis potential (E_{app}), where catalytic wave current was observed.

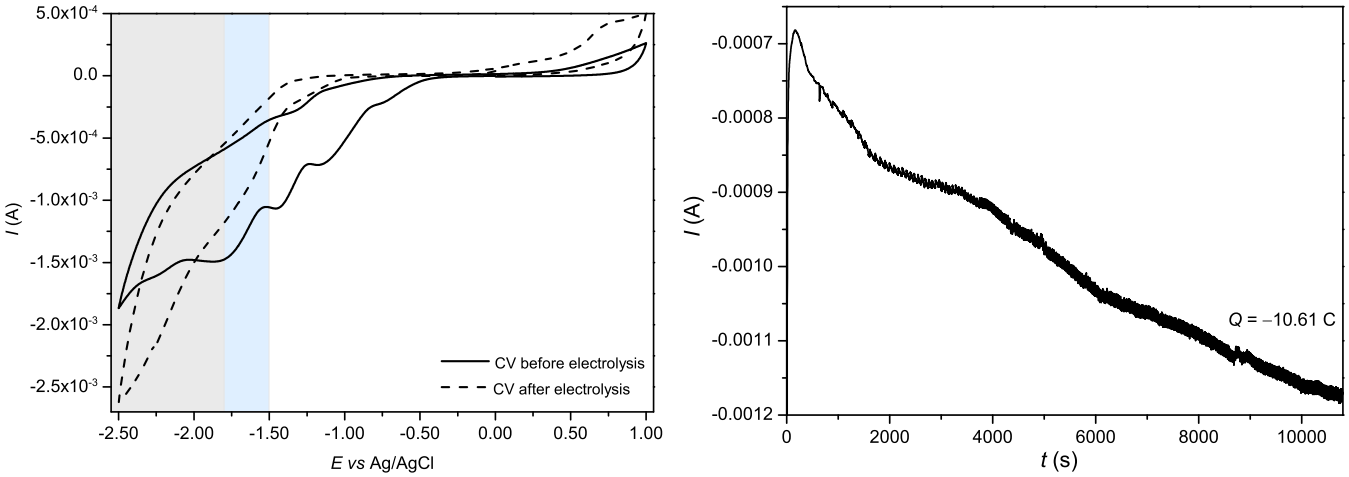

(a) (b)

Figure 19: (a) CVs of the electrolyte before (solid line) and after (dashed line) electrolysis and (b) the current *vs* time plot during electrolysis using **10f** in CO_2 saturated MeCN/MeOH 1:1, v/v (solvent *ii*). The grey area in (a) showes the potential range below −1.80 V where solvent decomposition might happen and the blue area shows the potential range between the hydride reduction and E_{app}.

3.3.3.1.1 Evaluation of efficiencies and time-current graphs from the experiments conducted for $t = 3$ h. In the electrocatalytic reduction of CO_2, electrons are a reagent and therefore the charge passed through the electrolyte during the experiment should directly relate to the amount of products formed. Since a substantial background current in the two investigated electrolytes under electrolysis conditions was observed, maximum conversion (X_{max}) and corrected current efficiency η_{corr} were defined, which take into account the loss of charge due to background current in the electrolysis experiments and thus give a more appropriate picture on the efficiencies of the catalysts rather than the whole electrolysis cell.

$$CO_2 + 2H^+ + 2e^- \rightarrow HCO_2H \tag{10}$$

$$CO_2 + 4H^+ + 4e^- \rightarrow HCHO + H_2O \tag{11}$$

Equations 10 and 11 show the overall redox process for the electrocatalaytic reduction of CO_2 into HCO_2H and HCHO. Both processes may be dependent on the CO_2 and H^+ concentrations, as well as the flux of electrons. To determine the amount of electrons available in the electrocatalytic CO_2 reduction process in these experiments, the loss of electrons that are consumed in background

electrolysis, possibly due to solvent decomposition, has to be considered. Therefore we defined the background charge Q_{bckg} which is the charge consumed in the electrolysis of solutions *i* and *ii* in the absence of the catalyst at E_{app} for $t = 3$ h (Equation 12). The background charge was three times larger in solvent mixture *ii* than in *i*, suggesting less stability of electrolyte *ii*. Consequently, Q_{corr} is the corrected charge passed through the electrolysis mixture and is given in Equation 13.

$$Q_{\mathrm{bckg}}(i) = -1.0 \text{ C and } Q_{\mathrm{bckg}}(ii) = -3.0 \text{ C} \tag{12}$$

$$Q_{\mathrm{corr}} = Q - Q_{\mathrm{bckg}}(i/ii) \text{ (C)} \tag{13}$$

Defining Q_{corr} enables us to determine the maximum conversion of CO_2 assuming that all the electrons that are not consumed in the background current are available in the catalytic CO_2 reduction process (Equation 14). For this, the initial CO_2 concentrations had to be estimated, which were calculated as shown in Equation 15 using solubility values reported in literature (Table 8). Equation 16 gives the conversion calculated from the products observed in the ^{1}H NMR spectra (n_{products}) of the electrolytes after electrolysis for $t = 3$ h.

$$X_{\mathrm{max}} = \left(1 - \frac{c_{\mathrm{CO_2}} \cdot V_{\mathrm{tot}} - \frac{Q_{\mathrm{corr}}}{2 \cdot F}}{c_{\mathrm{CO_2}} \cdot V_{\mathrm{tot}}}\right) \cdot 100 \text{ (\%)} \tag{14}$$

$$c_{\mathrm{CO_2}} = \frac{1}{\sum V_{\mathrm{S}}} \cdot \sum V_{\mathrm{S}} \cdot c_{\mathrm{CO_2S}} \qquad c_{\mathrm{CO_2}}(i) = 0.27 \text{ and } c_{\mathrm{CO_2}}(ii) = 0.29 \text{ mol/L} \tag{15}$$

$$X_{\mathrm{observed}} = \left(1 - \frac{c_{\mathrm{CO_2}} \cdot V_{\mathrm{tot}} - n_{\mathrm{products}}}{c_{\mathrm{CO_2}} \cdot V_{\mathrm{tot}}}\right) \cdot 100 \text{ (\%)} \tag{16}$$

Table 8: Solubility of CO_2 in the applied solvents.

Solvent	T (K)	p (kPa)	Solubility		Lit.
			$x_{\mathrm{CO_2}}$ (−)	$c_{\mathrm{CO_2S}}$ (M)	
MeCN	298	101.325	−	0.28	ref[218]
H_2O	298	101.325	$6.09 \cdot 10^{-4}$	0.035[a]	ref[219]
MeOH	299	103±5	$5.37 \cdot 10^{-3}$	0.30[a]	ref[220]

[a] Calculated using $x_{\mathrm{i}} = n_{\mathrm{i}} / \sum n_{\mathrm{i}}$

Comparison between X_{max} and X_{observed} gives a better insight on the efficiency of the catalysts

because this way the charge consumed due to background electrolysis is considered. Subsequently, corrected current efficiencies η_{corr} can be rationalized, as given in Equation 17.

$$\eta_{corr} = \frac{X_{observed}}{X_{max}} \cdot 100\ (\%) \tag{17}$$

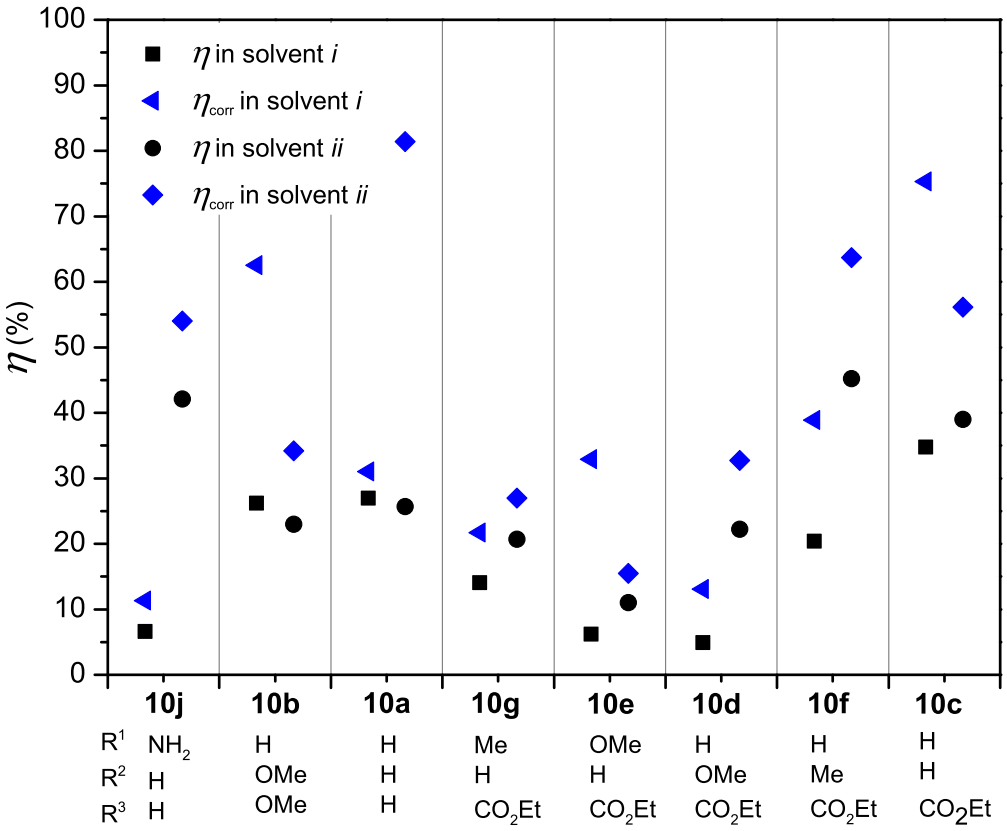

Figure 20: Maximum (η_{corr}) and observed η current efficiencies of CO_2 using selected catalysts in the electrolysis experiments in solvents *i* and *ii*.

Figure 20 shows how the current efficiencies regarding (η_{corr}) and disregarding (η) the background current during electrolysis compare to each other in solvent mixtures *i* and *ii*. Consequently, η_{corr} is always higher than η and the difference between the two values depends on the amount of charge (Q) consumed during electrolysis. The more charge is consumed, the less pronounced the difference is between η and η_{corr}, because the relative difference between Q and Q_{corr} is smaller. In several cases, independent from the solvent mixture used, the difference between the overall (η) and corrected (η_{corr}) efficiencies was substantial up to over two-fold (see Figure 20, compounds **10b**, **10c** and **10e** in solvent *i* and **10a** in solvent *ii*).

It is also interesting to note that Q was always much larger in solvent *ii* than in solvent *i* independent from the catalyst used. In case of **10j** the consumed charge was more than five times higher in *ii*

than that in *i* (Figure 21). Accordingly, in sovent *ii* X_{observed} was higher than in solvent *i* in case of each catalyst. This trend, however, did not necessarily result in higher overall current efficiencies (η) in solvent *ii* (see compounds **10b** and **10a**).

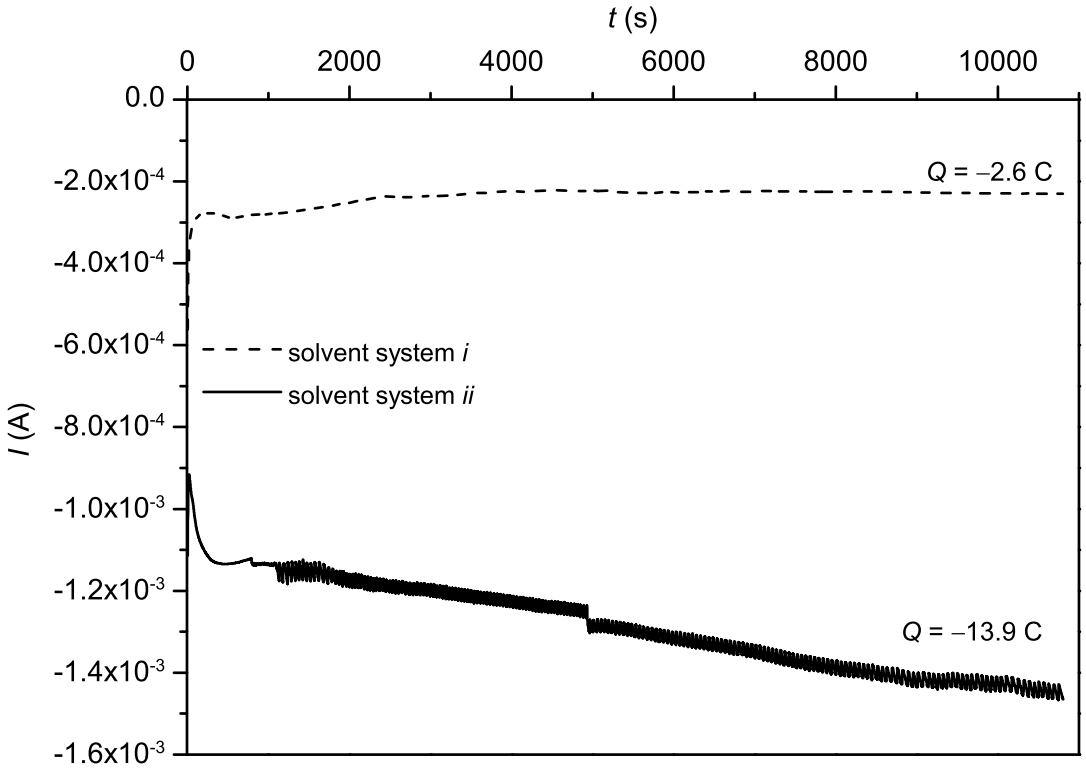

Figure 21: Time-current graphs of the electrolysis experiments using **10j**.

Interestingly, when the product formation over time was investigated, HCHO formation could not be detected any more. To determine the factors that previously led to the formation of formaldehyde and to ensure reproducibility of the system, we investigated the effects of using both sides of the previoulsy applied glassy carbon electrodes (as well as fresh ones), different sources of MeCN and MeOH solvents, a new batch of Bu_4NPF_6, and conditioning of the electrodes with *cc*HNO_3 or polishing with alumina suspension and polishing cloth. However, formaldehyde formation could not be reliably reproduced. Since the date from which formaldehyde was not anymore observed coincided with the date when a new bottle of MeCN solvent was used for the electrolysis experiments, it is very likely that previously a solvent impurity played a role in the irreproducible catalytic activity. Water was excluded from the role of such impurity by electrolysis measurements in the presence of 1, 3 and 5% H_2O in MeCN/MeOH 1:1 v/v that did not deliver any HCHO product (see Experimental part Figure 36).

According to the electrolysis experiments conducted for $t = 3$ h in solvent mixture *ii*, the best pre-

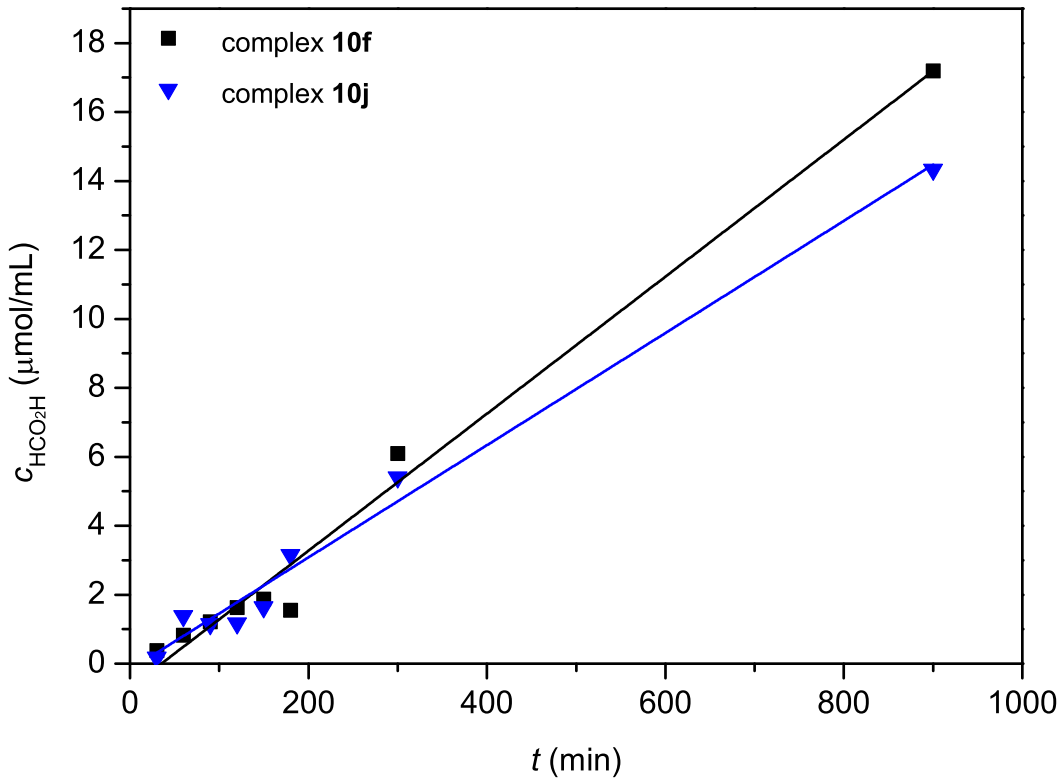

Figure 22: Concentration of formic acid product as a function of time in solvent mixture *ii*.

catalysts were **10f** and **10j**, and hence these were used to examine the product formation over longer time periods. As depicted in Figure 22, formation of HCO_2H was constant over time indicating the stability of the catalytically active Ir species in the time frame of 15 h. However, a relatively large scatter of the concentration values was observed at shorter reaction times. Therefore comparison of the catalysts by their performance in $t = 3$ h electrolysis measurements may be misleading. As shown in Figure 22, according to the single data points at $t = 3$ h, catalyst **10j** produces more HCO_2H than catalyst **10f**, whereas linear regression on all data points shows that catalyst **10f** is actually more active. Experiments for different times were conducted in cell type 2 using a fresh membrane in each measurement to circumvent any changes which might result in lower overall accuracy. The product concentrations were calculated as follows.

$$n_{(-/+)} = \frac{Int_{HCO_2H}}{Int_{xyl}} \cdot 4 \cdot c_{xyl} \cdot V_{xyl} \ (\mu mol) \tag{18}$$

$$c_{tot} = \frac{n_{(-)} + n_{(+)}}{V_{NMR(-)} + V_{NMR(+)}} \ (\mu mol \cdot mL^{-1}) \tag{19}$$

where $n_{(-/+)}$ is the amount of HCO_2H in the NMR samples and $V_{NMR(-/+)}$ is the volume of the NMR samples taken from the cathodic $(-)$ and anodic $(+)$ half cells.

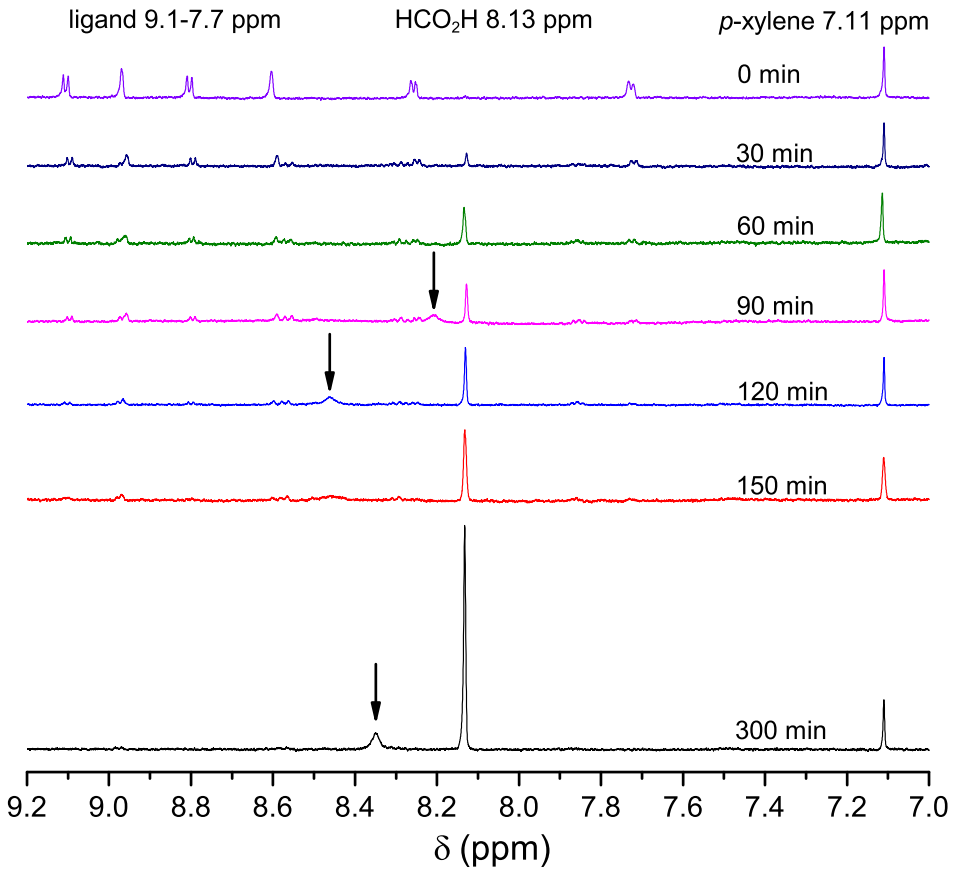

Figure 23: ^{1}H NMR spectra of the samples taken from the cathodic half cell after electrolysis for different times using **10f**.

Figure 23 shows the solvent suppression ^{1}H NMR spectra of the catalytic experiments after different electrolysis time using complex **10f**. In the first 2.5 h a change in the ligand chemical shifts was not observed and in longer experiments, this aromatic region of 9.1−7.7 ppm in the ^{1}H NMR spectra could not be evaluated to conclusively deduce any structural changes. Nevertheless, no signals of the free bpy ligand were observed, suggesting that the iridium catalyst was stable under these reductive conditions and catalyst decomposition *via* bpy dissociation is unlikely. At t = 90, 120 and 300 min a broader peak−possibly due to traces of formaldehyde−was observed at different chemical shifts in the spectra more downfield than the signal of HCO_2H product (see arrows in Figure 23).

As shown in Figure 24, the current efficiencies η of the electrolysis experiments using **10f** conducted for different lengths of time were very similar and varied between 3 and 11%. The overall charge Q increased linearly, while the concentration of formic acid product and therby X_{observed} increased linearly with increasing time, further confirming the stability of this system in the electrocatalytic conversion of CO_2. If the catalytically active species were not stable, the formic acid concentration would not have grown linearly and the current would have decreased with longer electrolysis time

resulting in a nonlinear increase of the charge.

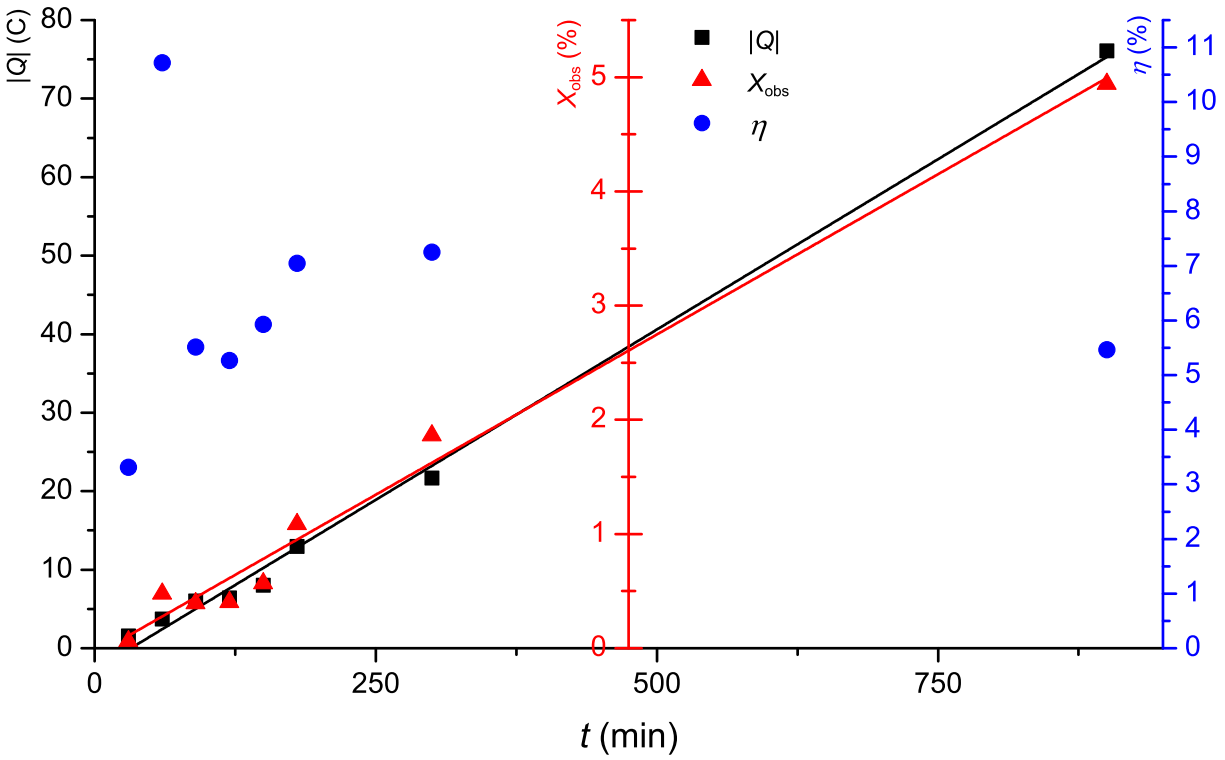

Figure 24: X_{observed}, $|Q|$ and η as a function of time in the electrolysis experiments at $E_{\text{app}} = -1.80$ V *vs* Ag/AgCl in solvent mixture *ii* using complex **10j**.

3.3.3.2 Experiments conducted for $t = 5$ and 15 h To achieve a more accurate picture of the catalytic activity of complexes **10a-10j**, product concentrations were determined in duplicates after $t = 5$ and 15 h of electrolysis and turnover frequencies (TOF) were calculated by linear regression of these four product concentrations (see Experimental Part Figure 39 and Table 13). Figure 25 summarizes the TOFs obtained using pre-catalysts **10a-10j** in the electrocatalytic CO_2 reduction towards formic acid. In general, complexes **10a**, **10b** and **10j**, which are reduced at the most negative potentials, show lower activity than complexes **10c-10i**, which display more positive reduction potentials. All complexes containing substituted bipyridines performed better in MeCN/MeOH (1:1 v/v) than parent complex **10a**. The standard errors of the TOF values are still relatively high and vary up to 25%. Current efficiencies were very low, typically between 5-20%, which is similar to the reported values of complex **10a** (see Experimental Part Table 14).[42]

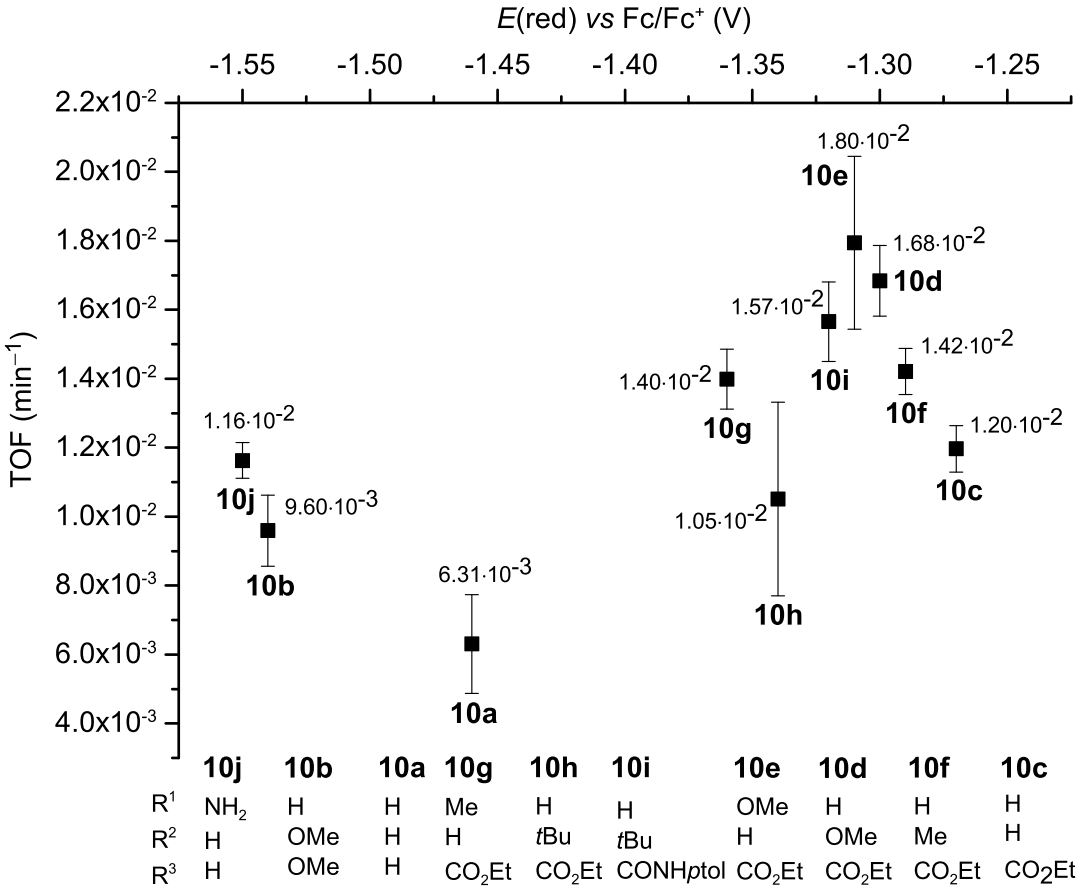

Figure 25: TOFs of complexes **10a-10j** in the electrocatalytic reduction of CO_2 to HCO_2H in MeCN/MeOH 1:1, v/v.

From the comparison of results presented in Figure 25 and Figure 18 it becomes clear that single data points after $t = 3$ h of electrolysis produce inaccurate data and more reliable activities are obtained from the measurements conducted for $t = 5$ and 15 h. As shown in Figure 25, the activity first decreases with growing reduction potential (or in other words with decreasing availability of the electrons on the metal center) for compounds **10j**, **10b** and **10a**, which is followed by an increase in TOFs for compounds that have higher E_{red} than -1.36 V. However, after $E_{red} = -1.31$ V for compound **10e**, the TOF values are decreasing again with increasing E_{red}. Substituents in the 6,6′ position on the bpy may have a positive influence on the catalytic activity: **10j** containing the 6-amino bpy ligand is the most active from the catalyst series on the most negative part of the E_{red} series and **10e** is actually one of the most active catalysts bearing a bpy ring with methoxy group on the 6′ position.

From the catalyst screening experiments we can conclude that

- the developed methodology including electrolysis experiments in a self-built divided cell as well

as solvent suppression ^{1}H NMR analysis displays relatively high experimental errors between 5-25%

- formaldehyde product was only observed in solvent mixture MeCN/MeOH 1:1 v/v and its formation was not reproducible after exchanging the used MeCN source, indicating the role of a unknown solvent impurity in the HCHO formation process
- the catalysis was selective towards the formation of HCO_2H (and HCHO) and only traces of H_2 and CO were observed after electrolysis for $t = 3$ h
- analysis of the time-current graphs show that using $[Cp^*Ir(bpy)Cl]^+$ complexes as catalysts, up to 75 and 81% of corrected current efficiencies η_{corr} could be obtained in solvent mixtures *i* and *ii*, respectively
- in solvent *ii* more product was formed than in solvent *i* in all cases
- the concentration of HCO_2H product and the consumed charge increased linearly over time for complexes **10f** and **10j**, confirming stability of the catalytically active species up to $t = 15$ h
- in the $t = 5$ and 15 h experiments overall current efficiencies η were as low as 5-15%, similar to the η reported by Deronzier for complex **10a**[42]
- all new complexes synthesized during the scope of this thesis showed better activity than parent compound **10a**
- acitvities of complexes **10a-10j** were influenced by both their electronic and structural features and a straightforward correlation between activity and reduction potential of the iridium centers was not observed

4 Additional investigations

We shortly investigated the possibilities to prepare surface functionalyzed silica to accomodate the [Cp*Ir(bpy)Cl]Cl complexes. The idea was to use 3-aminopropyl-triethoxysilane (APTES) linker to attach the bpy ligands on mesoporous silica surfaces and then add the catalyst precursor to form the supported Ir complex (Scheme 49).

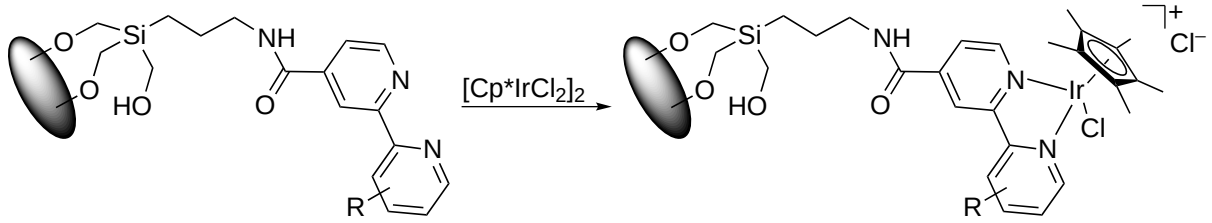

Scheme 49: Schematic representation of the immobilization of $[Cp^*Ir(bpy)Cl]^+$ on mesoporous silica surface.

Similar approaches have been reported on surface immobilized transition metal complexes for different catalytic transformations including electrocatalytic CO_2 reduction.[69,182,221,222,223] We attempted the preparation of APTES functionalized bpy ligands as depicted in Scheme 50.

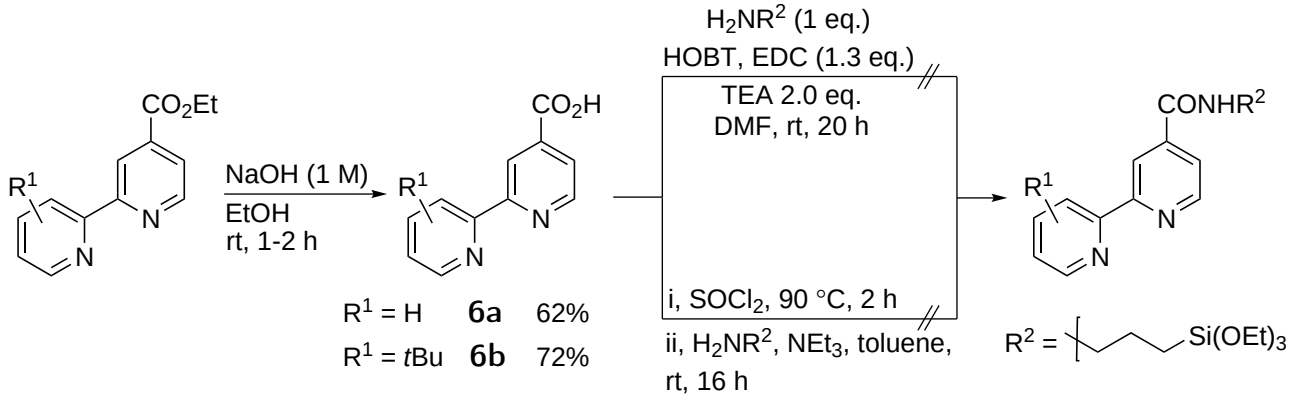

Scheme 50: Attempts to prepare APTES functionalyzed bpy ligands.

Unfortunately, APTES functionalized products could not be observed when using these methods starting from substrates **6a** and **6b**. Isolation of the reaction mixture components could not be achieved, probably due to strong interactions between the triethoxysilane groups with the silica gel even after its deactivation. However, when aluminium oxide standing phase was used for column chromatography, no product could be recovered either.

Ir complexes are also frequently used in **hydrogenation of carbonyl compounds and imines, as well as transfer hydrogenation reactions**.[224,225,226,179,227,228,229,230] We did some preliminary

studies on the applicability of the [Cp*Ir(bpy)Cl]Cl complexes in homogeneous hydrogenation of carbonyl compounds, using benzaldehyde and cyclohexanone substrates (Scheme 51).

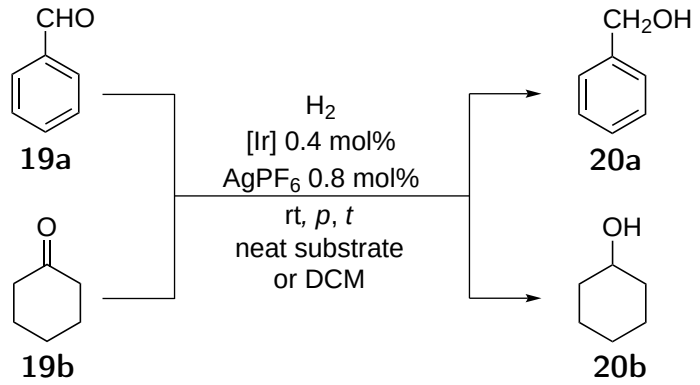

Scheme 51: Preliminary investigations on the hydrogenation of carbonyl compounds were conducted using benzaldehyde and cyclohexanone substrates.

The catalysts showed excellent reactivities with full conversion after $t = 5$ h and up to TON = 250 in neat substrates under 50 bar of H_2 pressure at room temerature using 0.4 mol% Ir catalyst (Table 9). Interestingly, when $AgPF_6$ salt was not added to the reaction mixture, no catalysis was observed emphasizing the importance of Cl^- dissociation from the Ir center to create an open coordination site.

Table 9: Initial condition screening experiments in the hydrogenation of **19a** and **19b** in neat substrate (0.5 mmol) in the presence of Ir complex (0.002 mmol, 0.4 mol%).

Entry	Complex	AgPF6 (mol %)	Substrate	p (bar)	t (h)	Product (%)
1	**10a**	–	**19b**	1	5	0
2	**10h**	–	**19b**	1	5	0
3	**10d**	–	**19b**	1	5	0
4	**10a**	–	**19a**	50	5	0
5	**10a**	0.8	**19a**	50	12	$>$ 99
6	**10a**	0.8	**19b**	50	12	$>$ 99
7	**10d**	0.8	**19a**	50	12	$>$ 99
8	**10d**	0.8	**19b**	50	12	$>$ 99
9	**10j**	–	**19a**	50	12	0
10	**10j**	0.8	**19a**	50	12	$>$ 99
11	**10j**	0.8	**19b**	50	12	$>$ 99

Hydrogenation of **19a** was further investigated at lower H_2 pressure using catalysts **10a-10j**. Table 10 shows the results of two to three runs of hydrogenation experiments under identical conditions (p = 20 bar, T = rt, t = 5 h), and the average yields of **20a** product with experimental errors in neat substrate, as well as single runs in *d*-DCM. In the absence of solvent, the product was obtained in moderate to excellent yields. Using omplexes **10b**, **10d**, **10e** and **10j** resulted in the best yields

of **20a**, whereas **10g** was the least active in the hydrogenation reaction. When hydrogenation was carried out on a substrate solution in *d*-DCM (0.83 M), the conversions dropped significantly in the case of most complexes, except for **10b**, **10d**, **10e**. Similarly, lowering the pressure to 10 bar, less product was formed during 5 h of reaction time (see Experimental part Table 17).

Table 10: Hydrogenation of **19a** using 0.4 mol% of complexes **10a-10b** and 0.8 mol% $AgPF_6$, under 20 bar of H_2 pressure at rt for 5 h in neat substrate or *d*-DCM (0.6 mL).

Complex	Yield of benzyl alcohol **20a** (%)[a]				
	no solvent				*d*-DCM
	run 1	run 2	run 3	Average	run 1
10a	93	81	74	83±10	54
10b	> 99	> 99	–	> 99±0	> 99
10c	60	60	37	52±13	22
10d	> 99	> 99	> 99	> 99±0	96
10e	> 99	> 99	87[b]	96±6	> 99
10f	74	> 99	–	87±18	63
10g	30	32	21	28±6	10
10h	82	99	63	81±18	61
10i	62	12[c]	57	60±4	78
10j	> 99	16[c]	97	98±1	32

[a]Yield determined by ^1H NMR directly from reaction mixture. 0.5 mmol substrate was used. [b]Run 4 >99% yield. [c]5 mmol substrate was used.

5 Conclusions & outlook

A variety of [Cp*Ir(bpy)Cl]$^+$ type complexes bearing unsymmetrically substituted bipyridines were synthesized and characterized. The redox potentials of the complexes in Ar saturated MeCN correlate with the electron donating and π accepting properties of the ligands as expected. All complexes are active in the electrocatalytic reduction of CO_2 in MeCN/H_2O (95:5, v/v). However, there is no straightforward correlation between redox potentials of the complexes and their catalytic activity under controlled potential electrolysis conditions, emphasizing that the catalytic performance is not determined by one single property but rather depends on numerous factors. In MeCN/MeOH (1:1, v/v) the complexes show an increased activity towards the formation of HCO_2H and occasionally formaldehyde was observed as by-product. H_2 and CO were not observed in substantial amounts. The present work shows that the catalytic activity of the new iridium-bipyridine complexes in the electrocatalytic reduction of CO_2 can be influenced by the substitution pattern of the bipyridine ligand. The new catalysts described in this work displayed up to three times higher TOFs than complex **10a**. Nevertheless, the turnover frequencies of these catalysts as well as the current efficiencies of the electrocatalysis are still fairly low and very similar to reported values for complex **10a**.[42] Obviously, for practical applications it will be necessary to improve the catalytic performance by several orders of magnitude. Therefore, I would recommend to focus in future work on the mechanistic understanding of this reaction which would provide knowledge for the molecular design of improved catalysts, as well as further optimization of the controlled potential electrolysis experiments to improve current effciencies.

There are several aspects considering an **improved cell design and electrolysis conditions**, which might result in better current efficiencies and overall yields in this electrocatalytic CO_2 reduction. In such electrolysis experiments the organic solvent is responsible for the dissolution of the catalyst and the reactant whereas H_2O or a protic organic solvent (MeOH) are essential as H^+ sources. Solvents should ideally be stable under reductive conditions and not too acidic, to prevent the formation of H_2 by protonation of the Ir−H species. Finally, the solvents should be compatible with all materials used in the cell (cell compartmnet, O-rings and membrane). MeCN and MeOH were good choices of solvents, because CO_2 is better soluble in these than in H_2O resulting in a higher concentration of substrate when using mixtures of MeCN/H_2O and MeCN/MeOH than only H_2O. All of these solvents were stable at the potential used in the electrolysis experiments, judged by CVs of the solvent mixtures.

In solvent *ii*, more product formation was observed than in solvent *i*. This could be explained not only by the better solubility of CO_2 in solvent *ii*, but also other factors such as MeOH acting as H^+ source or facilitating catalysis by solvent effects. The contribution of such solvent effects can be tested by using MeCN/MeOH solvent mixtures containing different amounts of MeOH. As the solubility of CO_2 in MeCN and MeOH is very similar, if changes were observed they would probably be brought about by other solvent effects. Ideally, pure MeOH would be a good option for future investigations. However, this would mean that another conductive salt has to be applied, because Bu_4NPF_6 is only slightly soluble in MeOH. As for the protonation of the Ir−H species, many solvents would probably be compatible, since these Ir−H species might actually be realtively stable towards acids. For example, species **14** was described to be stable in aqueous solutions between 1.0 < pH < 6.0 at 25 °C.[179] However, the reduced Ir−H species **14e** may be indeed more basic, therefore empirical data would be needed to further evaluate the possibility of using different protic solvents in this context.

Investigation of the catalytic reaction at different potentials would be another reasonable way to proceed. The light blue area in Figure 19 shows the potential region interesting for electrolysis experiments. This area is between the potential where the one electron reduction of the Ir−H is seen (−1.50 V) until the already tested applied potential (E_{app} = −1.80 V). The catalytic current wave is present within this potential range (−1.50 - −1.80 V *vs* Ag/AgCl) and therefore it is plausible that if the reactions were carried out at more positive potentials than −1.80 V, product would still be formed and less side-reactions would happen and therefore an increased current efficiency towards HCO_2H would be observed.

The conductive electrolyte may also play a significant role in electrolysis by lowering the resistance of the organic solution and thereby facilitating the current flow during electrolysis. Tetraalkylammonium salts are frequently used in aprotic organic solvents for electrochemical applications. If MeOH is used in further electrolysis experiments, perchlorate salts would be ideal as conductive electrolytes due to their good solubility. Lithium salts, like $LiClO_4$ would be escpecially interesting, because Li^+ can act as Lewis acid in the catalytic reaction, activating the CO_2 molecule and stabilizing the transition state between species **14e** and **14f**. Recently, an example of such stabilizing effect has been described by Hazari and Schneider in their studies on Fe catalyzed HCO_2H dehydrogentation.[231] The authors described that addition of catalytic amounts of Lewis acid promoted the

formic acid dehydrogenation using Fe pincer complexes. In these experiments alkali and alkali earth salts were used as additives and the best results were obtained with $LiBF_4$. The proposed pathway in the decarboxylation step is shown in Scheme 52. The authors indicated that the reverse reaction, hydrogenation of CO_2, was also promoted by the addition of Lewis acids.

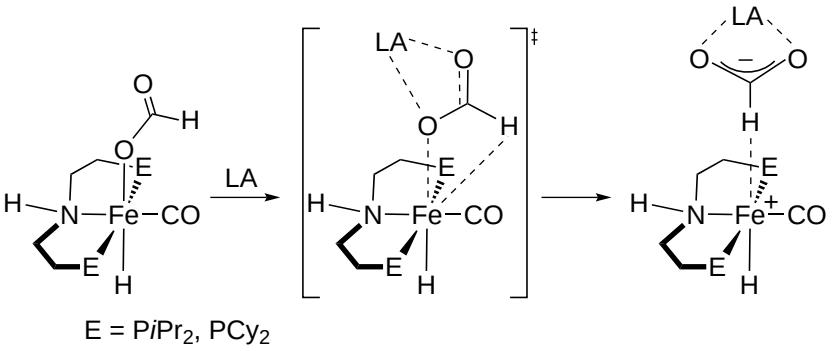

Scheme 52: Proposed pathway of Lewis acid mediated formic acid decarboxlation reaction catalyzed by Fe pincer complexes according to Hazari and Schneider.[231]

Another point to consider is the half reaction in the anodic half cell that not only provides the kinetics for an efficient electron flow, but possibly also H^+-s that diffuse to the cathodic half cell and are consumed in the CO_2 reduction cycle. The rate of the oxidation process should be equal to the rate of the reduction to facilitate maximum electrocatalytic efficiency. The $[Cp^*Ir(bpy)Cl]^+$ type complexes are efficicent water oxidation catalysts with significantly higher TOFs towards O_2 than what we observed for HCO_2H formation in our system.[232,212,214] Similar complexes were active in dehydrogenative alcohol oxidation to produce aldehydes.[233,229] Therefore it is unlikely that the rate of the CO_2 reduction is limited by the oxidation process in the anodic half cell in our setup using the solvent mixtures *i* and *ii* containing H_2O or MeOH. Nevertheless, there are several oxidation catalysts available to probe in the anodic half cell once the solvent oxidation process becomes limiting.

To gain more information on the **kinetics of the catalytic reaction and the possible mechanistic pathways**, a thorough study would be necessary. Considering the proposed catalytic cycle in Scheme 46, the neutral Ir(I) species **12** is very reactive and is protonated fast to form **14a** indicating that this is not the rate determining step.[201] Measuring the product formation over time at different Ir complex concentrations would give us information on the rate *vs* concentration relationship and directly the order of the reaction in this reagent. If the proposed catalytic cylce is valid, a first order dependence is expected. When measuring the rate *vs* concentration of the Ir−H compound **14**, the same first order kinetics is expected, which would indicate that the Ir−H **14** is a catalytic

intermediate and a mononuclear Ir species is present in the rate determining step of the cycle. The Ir(III)−H species **14** can be obtained by reduction of **10a** using sodium cyanoborohydride reagent in a mixture of EtOH and H_2O.[195] I expect an analogous procedure to be successful in the reduction of complexes **10b-10j** to the respective hydrides, because $NaBH_3CN$ is a mild and selective reducing agent that leaves ester functionalities intact.[234,235,236] We already attempted to prepare **14a** and **14d** using various methods summarized in Table 15.

Further spectroelectrochemistry experiments would be useful to determine the order of the CO_2 insertion/bipyridine reduction steps. Relying on previous reports and CV experiments, we assumed that the reduction event *e* that is seen in CO_2 saturated MeCN/H_2O, 9:1, *v*/*v* (condition C in Figure 10) is the one electron reduction of the bpy ligand in compound **14**. However, there is no experimental evidence that this is true for all newly prepared Ir complexes. As described in Section 3, complexes **10c**, **10d**, **10e**, **10f**, **10h** and **10i** only show event *e* under condition C, but not in the absence of CO_2 in Ar saturated MeCN/H_2O, 9:1, *v*/*v* (D). In such cases, one could imagine a direct reaction of **14** with CO_2 to give **14g**, whose one electron reduction could also be respoonsible for event *e* on the CVs under CO_2 atmosphere (C). If the relevant Ir−H compounds **14** are available for some of the new complexes, the order of the CO_2 insertion could be tested by ^{1}H NMR and SEC experiments under condition B.

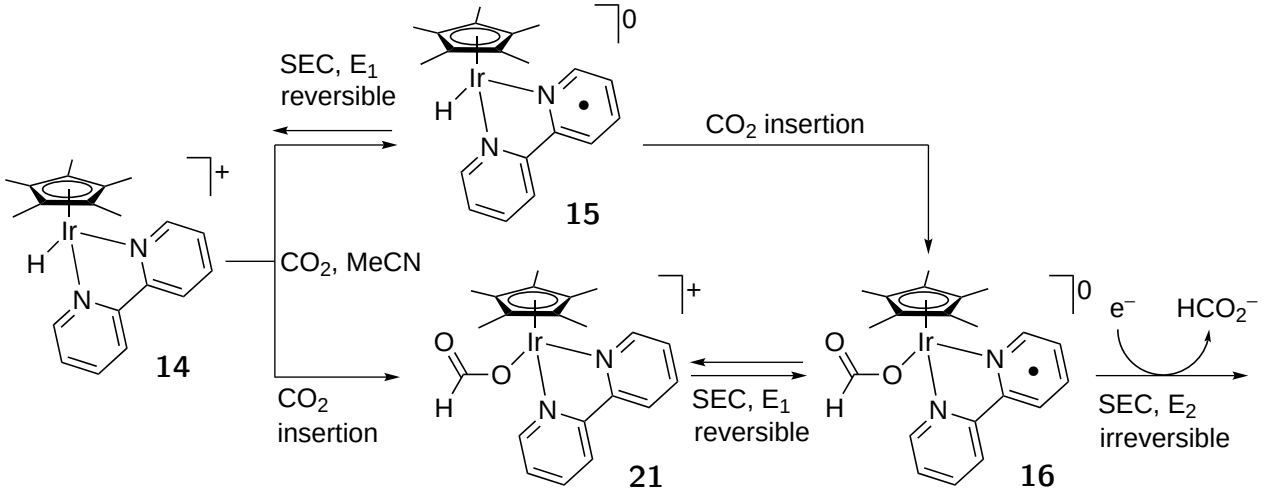

Scheme 53: Possible electrochemical pathways starting from Ir−H in CO_2 saturated solvent. Spectroelectrochemistry could be used to distinguish between the intermediates involved in the processes.

In this context I recommend the preparation of Ir−H derivatives of **10d** and **10g**, which were already used in the SEC measurements in Ar saturated MeCN (Figure 8) and showed different behavior in the CV measurements considering event *e* under condition D. Scheme 53 depicts the two possible

electrochemical pathways starting from the Ir−H compounds. The different species associated with a reversible redox process at E_1 could possibly be distinguished by their UV absorption spectra.

According to the mechanism in Scheme 46, we expected complexes with higher reduction potentials to be less catalytically active in case the CO_2 insertion were rate determining. On the contrary, if formate dissociation were the slow step, an easier reduced Ir center which corresponds to a less electron donating bpy, would facilitate the second electron bpy reduction and formate dissociation step. Since a direct trend in the catalytic activity *vs* the reduction potential of the Ir(III) center was not observed using catalysts **10a-10j**, either the mechanism in Scheme 46 does not apply in our setup under the described electrocatalytic conditions, or the rate determining step changes with the nature of the catalyst. The possibility of different rate determining steps depending on catalysts structures could be further investigated using DFT calculations.

Finally, further studies on the immobilization of the catalysts on electrode surfaces would be interesting for future investigations, if the previously suggested optimizations deliver higher catalyst activities and efficiencies. As our attempts failed to deliver APTES functionalized ligands so far, for future work I suggest first the preparation of an APTES functionalized surface and the subsequent addition of an activated carboxylic acid derivative of bpys.

6 Experimental part

6.1 General methods

Chemicals were purchased from commercial suppliers and used as received unless otherwise noted. Column chromatography was performed on *Merck Silica Gel 60* (230−400 mesh). ^{1}H and ^{13}C NMR spectra were recorded at room temperature using a *Jeol ECX 400*, *Jeol ECP500*, *Bruker AVANCE III 500* and *Bruker AVANCE III 700*. Data were processed with *MestReNova Software Version: 7.1.2-10008*. The chemical shifts (δ) are reported in parts per million (ppm) relative to tetramethylsilane and coupling constants (J) in Hertz (Hz). Data is reported as follows: s = singlet, d = doublet, t = triplet, q = quartet and m = multiplet. High resolution ESI-MS spectra were recorded on an *Agilent 6210 ESI-TOF*, *Agilent Technologies*. The applied charge is reported as positive (+). The spray charge was set to 4 kV. The defractor charge is given in Volt (V). Data are reported in mass to charge (m/z). GC-MS spectra were recorded on a *Saturn 2100* from *Varian Inc.* with a range of m/z 20 to 650. IR spectra were recorded on a *Nicolet Avatar 320 FT-IR* with a ZnSe optical window. The absorption bands, $\nu_{\max}$ are given in wave numbers (cm^{-1}), intensities are reported as follows: s = strong, m = medium, w = weak. Melting points were measured on a *BÜCHI 510 melting point* and are uncorrected.

6.2 Synthesis of 2-bromo-4-*tert*-butylpyridine

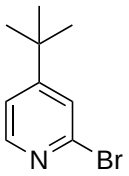

3a

The reaction was performed under an inert gas atmosphere and exclusion of water. 2-(Dimethylamino)-ethanol (4.80 mL, 47.8 mmol) was dissolved in hexane (125 mL) and cooled to 0 °C. *n*-Butyllithium (38.3 mL, 95.6 mmol, 2.5M in hexane) was added slowly and the mixture was kept at 0 °C for 15 min. 4-*tert*-Butylpyridine (3.23 g, 23.9 mmol, dissolved in 50 mL hexane) was added and the solution was stirred at 0 °C for 1 h. After cooling to −78 °C, tetrabromomethane (27.3 g, 82.3 mmol, dissolved in 125 mL THF) was added and the mixture was stirred at −78 °C for 30 min. The mixture was warmed to 0 °C, water (100 mL) was added and the layers were separated. The aqueous layer was extracted with diethyl ether (3x 100 mL). The combined organic layers were dried over

$MgSO_4$. Column chromatography (silica gel, 10 cm, hexane/ethyl acetate 0 *v/v %* 1000 mL, 1 *v/v %* 600 mL, 2 *v/v %* 800 mL, 5 *v/v %* 1200 mL) yielded 2.65 g of **3a** (12.4 mmol, 52%) as a brown oil.

^{1}H NMR (400 MHz, $CDCl_3$): δ (ppm) = 8.25 (d, J = 5.5 Hz, 1H, H-6) 7.44 (s, 1H, H-3), 7.22 (dd, J = 5.1, 1.7 Hz, 1H, H-5), 1.29 (s, 9H, CH_3 of *t*Bu).

^{13}C NMR (126 MHz, $CDCl_3$) δ (ppm) = 163.3 (C-4), 149.8 (C-6), 142.6 (C-2), 125.1 (C-3), 120.1 (C-5), 35.0 ($\underline{C}(CH_3)_3$), 30.3 (CH_3 of *t*Bu).

HRESI-MS: (+, 200V) *m/z*: $[M + H]^+$ 214.0246 (48) calc. 214.0231, $[M + Na]^+$ 236.0059 (100%) calc. 236.0045, $[M + K]^+$ 253.9787 (24) calc. 251.9770, $[2M + Na]^+$ 451.0209 (14) calc. 451.0184.

6.3 Synthesis of 4-(ethoxycarbonyl)pyridine *N*-oxide

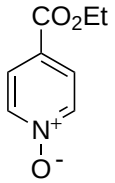

2a

H_2O_2 (41.0 mL, 397 mmol, 30% in water) was slowly added to a solution of ethyl isonicotinate (50.0 g, 331 mmol) in acetic acid (60 mL). The reaction mixture was stirred at 70 °C for 24 h. Acetic acid was partially removed *in vacuo* and dichloromethane (150 mL) was added. Sat. aq. Na_2CO_3 (150 mL) was added until the mixture became slightly basic. The organic layer was separated and the aqueous layer was extracted with dichloromethane (3x 150 mL). The combined organic layers were washed with sat. aq. NaCl (100 mL) and dried over $MgSO_4$. Removal of the solvent *in vacuo* yielded 50.5 g (302 mmol, 91%) of **2a** as a slightly yellow solid.

^{1}H NMR (400 MHz, $CDCl_3$): δ (ppm) = 8.18 (d, J = 7.3 Hz, 2H, H-2, H-6), 7.84 (d, J = 7.3 Hz, 2H, H-3, H-5), 4.36 (q, J = 7.1 Hz, 2H, $O\underline{CH_2}CH_3$), 1.36 (t, J = 7.1 Hz, 3H, $OCH_2\underline{CH_3}$).

^{13}C NMR (126 MHz, $CDCl_3$) δ (ppm) = 163.4 (CO_2Et), 139.5 (C-Ar), 126.9 (C-Ar), 126.5 (C-Ar), 62.0 ($O\underline{CH_2}CH_3$), 14.3 ($OCH_2\underline{CH_3}$).

6.4 Synthesis of bipyridine *N*-oxides

6.4.1 General Procedure A

Pyridine *N*-oxide (2 equiv.), $Pd(OAc)_2$ (5.0 mol%) and K_3PO_4 (2 equiv) were weighed in a Teflon capped vial or Schlenk flask. Under an argon atmosphere (glove box) P(*t*Bu)$_3$ (6.0 mol%) dissolved in toluene (so that the halopyridine concentration was 0.5 M) was added. Halopyridine (1 equiv) was added via syringe (if solid, the halopyridine was added in the beginning) and the reaction mixture was stirred for 15 min at r.t. and 24 h at 120 °C. After cooling to r.t. the reaction mixture was directly purified by column chromatography (d = 6 cm, l = 35 cm SiO_2 for 10 mmol halopyridine, deactivated, acetone/hexane, 0: 100 *v/v* - 100: 0 *v/v* in 10% increments).

6.4.2 4-Ethoxycarbonyl-2,2′-bipyridine *N*-oxide

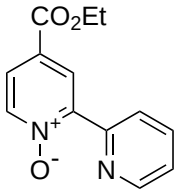

4a

According to General Procedure A: 4-(ethoxycarbonyl)pyridine *N*-oxide (33.4 g, 200 mmol), 2-bromopyri-dine (15.8 g, 100 mmol), toluene (170 mL). $Pd(OAc)_2$ (225 mg, 1.0 mmol), P(*t*Bu)$_3$ (243 mg, 1.2 mmol), K_3PO_4 (85 g, 400 mmol) was added at the beginning, after 24 h $Pd(OAc)_2$ (225 mg, 1.0 mmol), P(*t*Bu)$_3$ (243 mg, 1.2 mmol) was added again and the reaction heated for another 24 h. Purification by column chromatography (d = 8.5 cm, l = 40 cm SiO_2, deactivated, acetone/hexane, 0: 100 *v/v*-50: 50 *v/v*, R_f = 0.31 for 40: 60 *v/v*) gave **4a** as pale brown solid (14.9 g, 61 mmol, 61%) and 2,2′:6′,2″-terpyridine *N*′-oxide **8a** as white solid (2.9 g, 9 mmol, 18%, R_f = 0.46 for 40: 60 *v/v*).

4-Ethoxycarbonyl-2,2′-bipyridine *N*-oxide **4a**: ^{1}H NMR (400 MHz, $CDCl_3$): δ (ppm) = 8.77 (1H, d,J = 8.1 Hz, ArH-3′), 8.74 (2H, d, J = 2.8 Hz, ArH-3,6′ overlapping signals), 8.30 (1H, d, J = 6.7 Hz, ArH-6), 7.84 (1H, dd, J = 6.7, 2.8 Hz, ArH-5), 7.82 (1H, td, J = 7.9, 1.9 Hz, ArH-4′), 7.35 (1H, ddd, J = 7.4, 4.6, 0.9 Hz, ArH-5′), 4.40 (2H, q, J = 7.2 Hz, CH_2), 1.39 (3H, t, J = 7.2 Hz, CH_3) using COSY.

^{13}C NMR (100 MHz, $CDCl_3$): δ (ppm) = 163.6 (CO), 149.5, 148.9, 147.3, 140.8, 136.2, 128.2, 126.8,

125.2, 124.9, 124.5 (ArC), 61.8 (CH_2), 14.2 (CH_3).

HRESI-MS: (+, 200V) *m/z*: $[M + H]^+$ 245.0922 (100%) calc. 245.0921, $[M + Na]^+$ 267.0745 (100%) calc. 267.0740, $[2M + Na]^+$ 511.1596 calc. 511.1588.

IR ν_{max} (cm^{-1}): 3053 (w), 2980 (w), 1716(s, C=O), 1617 (m), 1581 (w), 1455 (m), 1412 (m), 1390 (w), 1366 (m), 1312 (m), 1259 (s), 1240 (s), 1224 (s), 1173 (w), 1152 (w), 1109 (m), 1057 (w), 1018 (m), 991 (w), 925 (w), 925 (w), 863 (w), 836 (w), 790 (m), 767 (m), 743 (m), 714 (m), 651 (m).

M.p.: 91-92 °C.

6.4.3 4′-*tert*-Butyl-4-ethoxycarbonyl-2,2′-bipyridine *N*-oxide

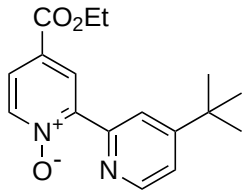

4b

According to General Procedure A: 4-(ethoxycarbonyl)pyridine *N*-oxide (3.1 g, 18.7 mmol), 2-bromo-4-*tert*-butylpyridine (1.9 g, 8.80 mmol), $Pd(OAc)_2$ (210 mg, 0.94 mmol), $P(tBu)_3$ (227 mg, 1.12 mmol), K_3PO_4 (7.9 g, 37 mmol) toluene (25 mL). Purification by column chromatography (SiO_2 , deactivated, acetone/hexane, 0: 100 *v/v*-100: 0 *v/v*, Rf = 0.43 for 30: 70 *v/v*) gave **4b** as brown oil (1.51 g, 5.0 mmol, 57%) and 4,4″-bis-*tert*-butyl-4′-ethoxycarbonyl-2,2′:6′,2″-terpyridine N′-oxide **8f** (140 mg, 0.32 mmol, 7%, R_f = 0.46 for 30: 70 *v/v*).

4′-*tert*-Butyl-4-ethoxycarbonyl-2,2′-bipyridine *N*-oxide **4b**: ^{1}H NMR (500 MHz, $CDCl_3$) δ (ppm) = 8.80 (1H, dd, J = 1.9, 0.7 Hz, ArH-3′), 8.72 (1H, d, J = 2.6 Hz, ArH-3), 8.65 (1H, dd, J = 5.3, 0.7 Hz, ArH-6′), 8.30 (1H, d, J = 6.7 Hz, ArH-6), 7.83 (1H, dd, J = 6.8, 2.6 Hz, ArH-5), 7.35 (1H, dd, J = 5.2, 1.9 Hz, ArH-5′), 4.40 (q, J = 7.2 Hz, 2H, CH_2), 1.39 (t, J = 7.2 Hz, 3H, CH_3), 1.36 (s, 9H, $C(CH_3)_3$) using COSY and HMBC.

^{13}C NMR (126 MHz, $CDCl_3$) δ (ppm) = 163.8, 160.5, 149.5, 149.1, 147.9, 141.0, 128.6, 127.0, 124.9, 122.6, 121.8 (ArC), 62.0 (CH_2), 35.1($\underline{C}(CH_3)_3$), 30.6 ($C(\underline{CH_3})_3$), 14.4 (CH_3) using DEPT.

HRESI-MS: (+, 200V) m/z: $[M + H]^+$ 301.1538 calc. 301.1547, $[M + Na]^+$ 323.1345 calc. 323.1366, $[M + K]^+$ 339.1097. calc. 339.1111.

IR ν_{max} (cm^{-1}): 3320 (broad peak, m), 2961 (s), 2933 (s), 2864 (s), 2672 (s), 2613 (s), 1977 (w), 1708 (m), 1634 (s), 1563 (w), 1505 (w), 1463 (s), 1367 (m), 1275 (m), 1222 (m), 1115 (m), 1082 (m), 990 (m), 929 (m), 848 (m), 737 (m), 665 (s).

6.4.4 4-Ethoxycarbonyl-4′-methyl -2,2′-bipyridine *N*-oxide

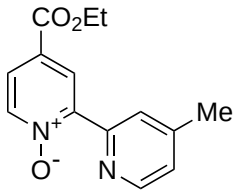

4e

According to General Procedure A: 4-(ethoxycarbonyl)pyridine *N*-oxide (571 mg, 3.41 mmol), 2-bromo-4-methylpyridine (294 mg, 1.71 mmol), $Pd(OAc)_2$ (12.9 mg, 0.085 mmol), $P(tBu)_3$ (20.6 mg, 0.102 mmol), K_3PO_4 (474 mg, 3.41 mmol) toluene (2 mL). Purification by column chromatography (SiO_2 , deactivated, acetone/hexane, 0: 100 *v/v*-100: 0 *v/v* gave **4e** as light brown solid (371 mg, 1.43 mmol, 84%)

^{1}H NMR (400 MHz, $CDCl_3$) δ (ppm) = 8.68 (d, J = 2.6 Hz, 1H, Ar-H), 8.49 (bs, 1H, Ar-H), 8.47 (d, J = 4.9 Hz, 1H, Ar-H), 8.19 (d, J = 6.7 Hz, 1H, Ar-H), 7.72 (dd, J = 6.8, 2.6 Hz, 1H, Ar-H), 7.05 (d, J = 4.9 Hz, 1H, Ar-H), 4.27 (q, J = 7.1 Hz, 1H, CH_2), 2.30 (s, 1H), 1.26 (t, J = 7.1 Hz, 1H, CH_3). ^{1}H NMR data matched reported values.[184]

6.5 Reduction of the bipyridine *N*-oxides

6.5.1 General Procedure B

The bipyridine *N*-oxide was dissolved in ethanol and Pd/C was added. The reaction mixture was degassed (3x vacuum/ argon) and to the evacuated mixture H_2 (atm) was added from a baloon. Depending on the conversion followed by TLC, additional 5-8 wt% Pd/C was added. The reaction mixture was filtered over celite and washed with ethanol (100 mL). Evaporation of the solvent gave the corresponding bipyridine. If the conversion was not complete, the product was separated from

the bipyridine *N*-oxide by silica gel column chromatography (eluent gradient to hexane/acetone 7:3 *v/v*).

6.5.2 4-Ethoxycarbonyl-2,2′-bipyridine

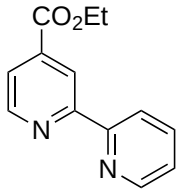

5a

According to the General Procedure B: 4-ethoxycarbonyl-2,2′-bipyridine *N*-oxide **4a** (1500 mg, 6.1 mmol), Pd/C (10 wt%, 650 mg, 0.61 mmol), ethanol (40 mL) for 2 h. Product **5a** was obtained as white solid after separation from the starting material by column chromatography (1250 mg, 5.5 mmol, 90%).

^{1}H NMR (400 MHz, $CDCl_3$): δ (ppm) = 8.89 (1H, s, ArH), 8.78 (1H, d, J = 4.9 Hz, ArH), 8.68 (1H, d, J = 7.8 Hz, ArH), 8.37 (1H, d, J = 7.9 Hz, ArH), 7.83 (1H, dd, J = 5.1, 1.6 Hz, ArH), 7.79 (1H, td, J = 7.9, 1.9 Hz, ArH), 7.29 (1H, dd, J = 7.4, 5.8 Hz, ArH), 4.41 (2H, q, J = 7.2 Hz, CH_2), 1.39 (3H, t, J = 7.0 Hz, CH_3).

^{13}C NMR (100 MHz, $CDCl_3$): δ (ppm) = 165.1 (CO), 157.1, 155.2, 149.7, 149.2, 138.7, 136.9, 124.0, 122.7, 121.1, 120.2 (ArC), 62.7 (CH_2), 14.1 (CH_3).

HRESI-MS: (+, 200V) m/z: $[M + H]^+$ 229.1000 calc. 229.0972.

IR ν_{max}/cm^{-1}: 3061 (w), 2961 (w), 1723(s, C=O), 1584 (m), 1556 (m), 1458 (m), 1442 (w), 1396 (m), 1367 (w), 1303 (m), 1291 (m), 1271 (m), 1255 (s), 1226 (s), 1173 (w), 1114 (w), 1089 (m), 1066 (w), 1016 (m), 994 (w), 925 (w), 895 (w), 860 (w), 799 (m), 759 (s), 744 (m), 730 (s), 683 (m), 659 (m).

M.p.: 48 °C.

6.5.3 4′-*tert*-Butyl-4-ethoxycarbonyl-2,2′-bipyridine

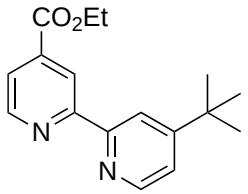

5b

According to the General Procedure B: 4′-*tert*-butyl-4-ethoxycarbonyl-2,2′-bipyridine *N*-oxide **4b** (1100 mg, 3.66 mmol), Pd/C (2.4 wt%, 95.2 mg, 0.895 mmol), ethanol (10 mL) for 2 h. Additional Pd/C (2.6 wt%, 100.0 mg, 0.096 mmol) was added after 2 and 4 h reaction time. Product **5b** was obtained as white solid after separation from the starting material by column chromatography (633.4 mg, 2.22 mmol, 61%).

^{1}H NMR (500 MHz, $CDCl_3$) δ (ppm) = 8.89 (dd, J = 1.6, 0.9 Hz, 1H, H-3), 8.79 (dd, J = 5.0, 0.9 Hz, 1H, H-6), 8.59 (dd, J = 5.2, 0.7 Hz, 1H, H-6′), 8.42 (dd, J = 2.0, 0.8 Hz, 1H, H-3′), 7.83 (dd, J = 5.0, 1.6 Hz, 1H, H-5), 7.30 (dd, J = 5.2, 2.0 Hz, 1H, H-5′), 4.41 (q, J = 7.1 Hz, 2H, CH_2), 1.39 (t, J = 7.1 Hz, 3H, CH_2 $\underline{CH_3}$), 1.36 (s, 9H, $C(CH_3)_3$) using COSY and HMBC.

^{13}C NMR (126 MHz, $CDCl_3$) δ (ppm) = 165.4(CO), 161.2, 157.8, 155.3, 149.9, 149.3, 138.9, 122.7, 121.4, 120.6, 118.3 (ArC), 61.8 (CH_2), 35.1 $\underline{C}(CH_3)_3$, 30.7 $C(\underline{CH_3})_3$, 14.4 (CH_2CH_3) using DEPT.

HRESI-MS: (+, 200V) m/z: $[M + H]^+$ 285.1642 (100%) calc. 285.1598, $[M + Na]^+$ 307.1455 calc. 307.1417, $[2M + Na]^+$ 591.2992. calc. 591.2942.

IR ν_{max}/cm^{-1}: 3726, 3708, 3676, 3649, 3627, 3596, 3566 (w), 3440, 3063, 2964, 2904, 2870 (w), 2360 (s), 2341 (m), 1726 (s), 1591, 1559, 1547 (m), 1458, 1433, 1393 (m), 1371 (s), 1318, 1299 (m), 1282, 1260, 1224 (s), 1172 (w), 1132, 1106, 1095, 1070, 1019 (m), 993, 925 (w), 907, 862, 844 (m), 806 (w), 771 (s), 755, 732, 715, 683, 668 (m), 652 (s).

M. p.: 50 °C.

6.5.4 4-Ethoxycarbonyl-4′-methyl-2,2′-bipyridine

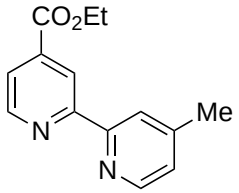

5e

According to the General Procedure B: 4-ethoxycarbonyl-4′-methyl-2,2′-bipyridine *N*-oxide **4e** (215 mg, 0.83 mmol), Pd/C (10 wt%, 87 mg, 0.08 mmol), ethanol (20 mL) for 4 h. Product **5e** was obtained after flush column chromatography (short silica gel bed, hexane/acetone eluent) as colourless solid (189 mg, 0.78 mmol, 94%).

^{1}H-NMR (500 MHz, $CDCl_3$) δ (ppm) = 8.91 (dd, J = 1.7, 0.9 Hz, 1H), 8.80 (dd, J = 4.9, 0.9 Hz, 1H), 8.57 (dd, J = 5.0, 0.7 Hz, 1H), 8.23 (dt, J = 1.5, 0.8 Hz, 1H), 7.86 (dd, J = 5.0, 1.6 Hz, 1H), 7.16 (ddd, J = 5.0, 1.7, 0.8 Hz, 1H), 4.43 (q, J = 7.1 Hz, 2H), 2.44 (d, J = 0.7 Hz, 3H), 1.42 (t, J = 7.2 Hz, 3H).

^{13}C NMR (126 MHz, $CDCl_3$) δ (ppm) = 165.4 (CO), 157.5, 155.2, 145.0, 149.2, 148.6, 139.0, 125.3, 123.0, 122.3, 120.7 (ArC), 62.0 (CH_2), 21.4 (Ar-CH_3), 14.4 ($CH_2\underline{CH_3}$).

IR ν_{max}/cm^{-1}: 3100, 3055, 3002, 2973, 2907, 1949 (w), 1716 (s), 1675 (w), 1604, 1590, 1556(m), 1475 (w), 1455 (s), 1425 (w), 1399 (m), 1362 (s), 1315 (m), 1295, 1272, 1257, 1236, 1187 (s), 1139. 1123 (w), 1113 (m), 1093 (s), 1066 (w), 1020 (s), 990 (m), 966 (w), 925 (m), 913 (w), 899, 865 (m), 832 (s), 800 (m), 775, 732 (s), 729 (m), 685 (s), 667 (m).

M. p.: 50 °C.

6.5.5 4-Ethoxycarbonyl-6′-methyl-2,2′-bipyridine

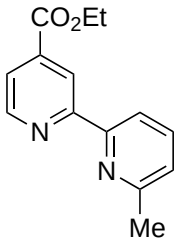

5c

According to the General Procedure B: 4-ethoxycarbonyl-6′-methyl-2,2′-bipyridine *N*-oxide **4c** (355 mg, 1.38 mmol), Pd/C (8.0 wt%, 116.8 mg, 0.110 mmol), ethanol (10 mL) for 2 h. Product **5c** was obtained as brown oil (313 mg, 1.29 mmol, 94%).

^{1}H NMR (500 MHz, $CDCl_3$) δ (ppm) = 8.85 (dd, J = 1.6, 0.8 Hz, 1H, H-3), 8.71 (dd, J = 5.0, 0.8 Hz, 1H, H-6), 8.10 (d, J = 7.8 Hz, 1H, H-3′), 7.75 (dd, J = 5.0, 1.6 Hz, 1H, H-5), 7.61 (t, J = 7.7 Hz, 1H, H-4′), 7.09 (d, J = 7.6 Hz, 1H, H-5′), 4.36 (q, J = 7.1 Hz, 2H, CH_2), 2.56 (s, 3H, Ar- CH_3), 1.35 (t, J = 7.1 Hz, 3H, CH_2 $\underline{CH_3}$) using COSY and HMBC.

^{13}C NMR (126 MHz, $CDCl_3$) δ (ppm) = 165.4 (CO), 158.2, 157.7, 154.8, 149.9, 138.7, 137.1, 123.7, 122.6, 120.4, 118.3 (ArC), 61.8 (CH_2), 24.6 (CH_3), 14.3 ($CH_2\underline{CH_3}$) using HMQC.

HRESI-MS: (+, 200V) *m/z*: $[M + H]^+$ 243.1164 calc. 243.1134, $[M + Na]^+$ 265.0987 (100%) calc. 265.0953, $[M + K]^+$ 281.0727. calc. 281.0692.

IR ν_{max} (cm^{-1}): 3059, 2980, 2927, 2872 (w), 1724 (s), 1602 (w), 1585, 1576, 1557, 1460 (m), 1399 (s), 1367, 1311 (m), 1285, 1255, 1247, 1218, 1173, 1155 (w), 1120 (s), 1091, 1018 (m), 996, 928, 907 (w), 863, 806 (m), 763 (s), 738, 731 (m), 709 (w), 684 (m), 658 (w).

6.5.6 4-Ethoxycarbonyl-4′-methoxy-2,2′-bipyridine

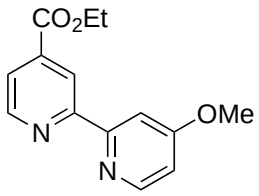

5f

According to the General Procedure B: 4-ethoxycarbonyl-4′-methoxy-[2,2′-bipyridine] *N*-oxide **4f** (860 mg, 3.13 mmol), Pd/C (2.5 wt%, 85.4 mg, 0.080 mmol), ethanol (15 mL) for 2 h. Additional Pd/C (3.0 wt%, 100.0 mg, 0.096 mmol) was added after 2 and 4 h reaction time. Product **5f** was obtained as brown solid (773 mg, 2.99 mmol, 96%).

^{1}H NMR (500 MHz, $CDCl_3$) δ (ppm) = 8.84 (dd, J = 1.7, 0.9 Hz, 1H, H-3′), 8.71 (dd, J = 5.0, 0.9 Hz, 1H, H-6′), 8.44 (dd, J = 5.4, 0.3Hz, 1H, H-6), 7.90 (d, J = 2.5 Hz, 1H, H-3), 7.79 (dd, J = 5.0,

1.6 Hz, 1H, H-5′), 6.78 (dd, J = 5.7, 2.6 Hz, 1H, H-5), 4.36 (q, J = 7.2 Hz, 2H, CH_2), 3.86 (s, 3H, OCH_3), 1.35 (t, J = 7.1 Hz, 3H, CH_3) using COSY and HMBC.

^{13}C NMR (126 MHz, $CDCl_3$) δ (ppm) = 166.7 (CO), 165.3, 157.2, 157.1, 150.4, 149.8, 138.8, 123.0, 120.5, 111.1, 106.4 (ArC), 61.8 (CH_2), 55.4 (OCH_3), 14.3 (CH_3) using HMQC.

HRESI-MS: (+, 200V) m/z: $[M + H]^+$ 259.1118 (100%) calc. 259.1077.

IR ν_{max} (cm^{-1}): 3071, 3006, 2977, 2963, 2930, 2871, 2855, 2839 (w), 1720 (s), 1679 (w), 1588 (s), 1490, 1462, 1449, 1425, 1394, 1365 (m), 1321, 1305, 1290 (s), 1257, 1236 (m), 1204, 1184 (s), 1113, 1096 (m), 1062 (s), 1030, 1010 (m), 990, 919 (w), 862, 828, 797 (s), 770, 747 (s), 727, 683, 664 (m).

M. p.: 58 °C.

6.5.7 4-Ethoxycarbonyl-6′-methoxy-2,2′-bipyridine

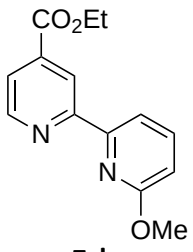

5d

According to the General Procedure B: 4-ethoxycarbonyl-6′-methoxy-2,2′-bipyridine N-oxide **4d** (1050 mg, 3.84 mmol), Pd/C (2.5 wt%, 100.0 mg, 0.096 mmol), ethanol (20 mL) for 2 h. Additional Pd/C (2.5 wt%, 100.0 mg, 0.096 mmol) was added after 2 and 4 h reaction time. Product **5d** was obtained as white solid after separation from the starting material by column chromatography (761 mg, 2.95 mmol, 77%).

^{1}H NMR (500 MHz, $CDCl_3$) δ (ppm) = 8.90 (dd, J = 1.7, 0.9 Hz, 1H, H-3), 8.79 (dd, J = 5.0, 0.8 Hz, 1H, H-6), 8.02 (dd, J = 7.5, 0.8 Hz, 1H, Ar′), 7.83 (dd, J = 5.0, 1.7 Hz, 1H, H-5), 7.71 (dd, J = 8.2, 7.4 Hz, 1H, Ar′), 6.81 (dd, J = 8.2, 0.8 Hz, 1H, Ar′), 4.45 (q, J = 7.1 Hz, 2H, CH_2), 4.07 (s, 3H, OCH_3), 1.43 (t, J = 7.1 Hz, 3H, CH_2 CH_3) using COSY and HMBC.

^{13}C NMR (126 MHz, $CDCl_3$) δ (ppm) = 165.50 (CO), 163.75, 157.30, 152.72, 149.84, 139.56, 138.78, 122.60, 120.44, 114.09, 111.75 (ArC), 61.90 (CH_2), 53.47 (OCH_3), 14.32 (CH_3).

HRESI-MS: (+, 200V) *m/z*: $[M + H]^+$ 259.1073 (100%) calc. 259.1077, $[M + Na]^+$ 281.0890 calc. 281.0902.

IR ν_{max} (cm^{-1}): 3088, 3064, 3019, 2999, 2987, 2975, 2945, 2910, 2874 (w), 2360, 2341 (m), 1728 (s), 1603 (w), 1588 (m), 1577 (s), 1560 (m), 1477, 1471 (s), 1437 (m), 1393 (s), 1362 (m), 1298, 1268 (s), 1241 (m), 1145 (w), 1133 (s), 1112, 1100, 1066 (m), 1028, 989, 925, 919, 876, 862, 804 (m), 764 (s), 747, 701, 687, 653 (m).

M. p.: 88 °C.

6.6 Synthesis of amino-4-(2′-pyridyl) pyridine

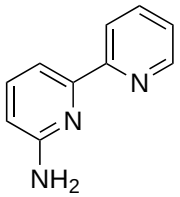

5h

Bipyridine *N*-oxide (150 mg, 0.87 mmol), pyridine (145 mg, 1.83 mmol) and diphenylphosphorylazide (599 mg, 2.18 mmol) were added to a Schlenck tube under Ar atmosphere. The mixture was heated at 120 °C for 24 h. After addition of methanol the white precipitate was filtered and dried and 6-azido-2,2′-bipyridine was obtained (128 mg, 0.65 mmol, 75%) and characterized by ^{1}H NMR. 6-Azido-2,2′-bipyridine (1 equiv.) was dissolved in ethanol and Pd/C (10 wt%, 0.10 equiv.) was added. The reaction mixture was degassed (3x vacuum/argon) and to the evacuated mixture H_2 (1 atm) was added. The reaction was followed by TLC and when completed the mixture was filtered over celite and washed with ethanol. Evaporation of the solvent gave compound **5h** as white solid (31 mg, 0.18 mmol, 72%).

^{1}H NMR (500 MHz, $CDCl_3$) δ (ppm) = 8.65 (ddd, J = 4.8, 1.8, 0.9 Hz, 1H), 8.24 (dt, J = 8.0, 1.1 Hz, 1H), 7.76 (td, J = 7.7, 1.8 Hz, 1H), 7.68 (dd, J = 7.6, 0.8 Hz, 1H), 7.61 − 7.52 (m, 1H), 7.26

(ddd, 1H with $CDCl_3$ peak), 6.56 (dd, J = 8.1, 0.8 Hz, 1H), 5.24 − 4.29 (broad peak, 2H). The ^{1}H NMR spectrum of 6-amino-2,2′-bipyridine **5h** matched reported data.[191]

6.7 Synthesis of 4′-*tert*-butyl-4-carboxylic acid-2,2′-bipyridine

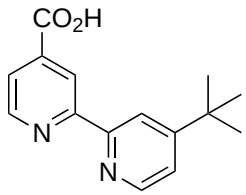

6b

A solution of 4′-*tert*-butyl-4-ethoxycarbonyl-2,2′-bipyridine **5b** (1.32 g, 4.6 mmol) in ethanol (14 mL) was mixed with NaOH (14 mL, 1 M) for 1 h at rt. The ethanol was removed in *vacuo* and to the remaining aqueous solution 1 M HCl was added dropwise to set the pH at 4. The product was filtered, washed with small amounts of H_2O and dried in *vacuo*. Product **6b** was obtained as brown solid in 72% yield (3.33 g, 13.0 mmol).

^{1}H NMR (500 MHz, $CDCl_3$) δ (ppm) = 9.45 (d, J = 1.2 Hz, 1H, H-3), 8.98 (d, J = 5.5 Hz, 1H, H-5′), 8.89 (d, J = 4.9 Hz, 1H, H-5), 8.64 (d, J = 1.9 Hz, 1H, H-3′), 8.01 (dd, J = 4.9, 1.4 Hz, 1H, H-6), 7.55 (dd, J = 5.5, 2.0 Hz, 1H, H-6′), 1.44 (s, 9H, C($\underline{CH_3}$)$_3$).

^{13}C NMR (126 MHz, $CDCl_3$) δ (ppm) = 193.7 (CO_2H), 166.8, 164.0, 154.5, 150.2, 147.6, 141.1, 123.8, 122.7, 122.1, 120.1, (ArC), 35.6 $\underline{C}(CH_3)_3$, 32.9, 30.6 30.7 C($\underline{CH_3}$)$_3$, 19.6 (CH_3).

HRESI-MS: (+, 200V) m/z: $[M + H]^+$ 257.1272 calc. 257.1290, $[M + Na]^+$ 279.1090 calc. 279.1109, $[M + K]^+$ 295.0829 calc. 295.0849.

IR ν_{max} (cm^{-1}): 3137 (w), 2965, 2901, 2864 (m), 2435 (w, broad peak), 2286 (w), 1768, 1714, 1611, 1597 (s), 1563, 1548, 1460, 1429, 1395, 1371 (m), 1283, 1254, 1232, 1197 (s), 1141, 1121, 1095 (w), 1074, 1012, 993 (m), 933, 920 (w), 898, 856, 837 (m), 770, 747, 717, 676, 665, 651 (s).

6.8 Synthesis of 4-carboxylic acid-2,2′-bipyridine

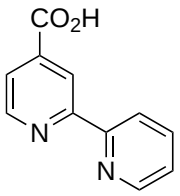

6a

A solution of 4-ethoxycarbonyl-2,2′-bipyridine **5a** (0.600 g, 2.63 mmol) in ethanol (8 mL) was mixed with NaOH (8 mL, 1 M) for 1 h at rt. The ethanol was removed in *vacuo* and to the remaining aqueous solution 1 M HCl was added dropwise to set the pH at 4. The product was filtered, washed with small amounts of H_2O and dried in *vacuo*. Product **6a** was obtained as brown solid in 95% yield (0.500 g, 2.50 mmol).

^{1}H NMR (500 MHz, $CDCl_3$) δ (ppm) = 8.83 (1H, s), 8.81 (1H, d, J = 5.0 Hz), 8.7 (1H, d, J = 4.8 Hz), 8.33 (1H, d, J = 7.9 Hz), 7.95 (1H, td, J = 7.8, 1.6 Hz), 7.92 (1H, dd, J = 5.0, 1.5 Hz), 7.33 (1H, dd, J = 7.74, 5.2 Hz).

^{13}C NMR (126 MHz, d-MeOD) δ (ppm) = 187.8 (COOH), 157.4, 155.0, 149.88, 149.0, 139.9, 137.6, 124.4 , 123.1, 121.4, 120.4 (ArC).

IR ν_{max} (cm^{-1}): 1699(s, COOH), 1592(s), 1561(s), 1463(s), 1384(m), 1206(m), 1249(m), 1227(m), 1162(w), 1129(w), 1070(m), 1005(s), 988(m), 926(m), 9098(m), 856(m), 791(m), 758(s), 727(m), 668(m), 637(m).

6.9 Synthesis of 4′-*tert*-butyl-*N*-*p*-tolyl-2,2′-bipyridine-4-carboxamide

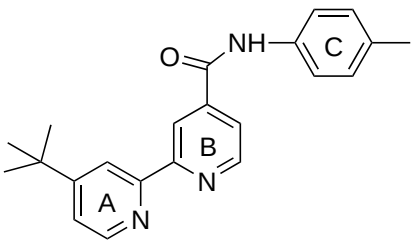

5g

In a dry Schlenk flask 4′-*tert*-butyl-2,2′-bipyridine-4-carboxylic acid **6b** (50 mg, 0.2 mmol) was added and the atmosphere was exchanged to Ar. Dry DMF (3 mL), coupling reagents HOBt (34 mg, 0.25 mmol) and *N*-(3-dimethylaminopropyl)-*N*′-ethylcarbodiimide hydrochloride, EDC (49 mg, 0.25 mmol), and *p*-toluidine (20.9 mg, 0.2 mmol) were added. The mixture was stirred for 2 h at room, temperature. DMF was removed and the crude product was purified by column chromatography (d = 1.5 cm, l = 30 cm SiO_2 deactivated with 100 mL NEt_3 solution (20 *v*/*v*% in hexane), eluent was acetone/hexane, 0: 1 *v*/*v* - 1: 1 *v*/*v* in 10% increments of 100 mL eluent) to obtain 4′-(*tert*-butyl)-*N*-(*p*-tolyl)-2,2′-bipyridine-4-carboxamide **5g** in 99% yield (69 mg, 0.2 mmol).

^{1}H NMR: ($CDCl_3$, 500 MHz): δ (ppm) = 8.78 (d, J = 4.8 Hz, 1H, Ar-B), 8.70 (s, 1H, Ar-B), 8.54 (d, 5.2 Hz, 1H, Ar-A), 8.45 (s, 1H, Ar-A), 8.43 − 8.36 (broad peak, 1H, NH), 7.79 (dd, 4.8, 2.0 Hz, 1H, Ar-B), 7.54 (d, = 8.1 Hz, 2H, Ar-C), 7.34-7.33 (m, 1H, Ar-A), 7.14 (d, = 8.0 Hz, 2H, Ar-C), 2.33 (s, 3H, Ar-CH_3), 1.38 (s, 9H, -$C(CH)_3$).

^{13}C NMR: ($CDCl_3$, 126 MHz): δ (ppm) = 163.9 (CO), 161.6, 157.3, 155.2, 150.3, 149.1, 143.2, 135.0, 134.8, 129.7, 121.9, 121.6, 120.7, 118.5, 117.4 (ArC), 35.1 ($\underline{C}(CH_3)_3$), 30.7 ($C(\underline{CH_3})_3$), 21.0 (CH_3, *p*Tol).

HRESI-MS: (+, 200V) *m*/*z*: $[M + H]^+$ 346.1889 (100%) calc. 346.1914, $[M_2 + Na]^+$ 713.3518 calc. 713.3575.

IR ν_{max} (cm^{-1}): = 3291 (m), 3190, 3126, 3056, 3031, 3001 (w), 2960 (m), 2917, 2862, 2361, 2336 (w), 1651, 1590, 1541, 1515 (s), 1474, 1456, 1408, 1372, 1357 (m), 1301, 1280 (w), 1267 (m), 1099, 1076, 1020, 993, 923, 905, 875 (w), 840, 813, 805 (s), 765, 753, 718, 701, 683, 668 (m).

6.10 Synthesis of terpyridine *N*-oxides

6.10.1 General Procedure C for the preparation of terpyridine *N*-oxides from bipyridine *N*-oxides

Bipyridine *N*-oxide (1 equiv), $Pd(OAc)_2$ (5.0 mol%) and K_3PO_4 (2 equiv) were weighed in a teflon capped vial. Under an argon atmosphere (glove box) $P(tBu)_3$ (6.0 mol%) dissolved in toluene (0.5 M, based on bipyridine *N*-oxide) was added. Halopyridine (1.2 equiv) was added via syringe (if solid the halopyridine was added in the beginning) and the reaction mixture was stirred for 15 min at r.t. and 24 h at 120 °C. After cooling to r.t. the reaction mixture was directly purified by column chromatography (d = 2.5 cm, l = 25 cm SiO_2, deactivated, acetone/hexane, 0: 100 *v/v*-100: 0 *v/v* in 10% increments).

6.10.2 General Procedure D for the preparation of terpyridine *N*-oxides from pyridine *N*-oxides

Pyridine *N*-oxide (1 equiv), $Pd(OAc)_2$ (10.0 mol%) and K_3PO_4 (2 equiv) were weighed in a teflon capped vial. Under an argon atmosphere (glove box) $P(tBu)_3$ (12.0 mol%) dissolved in toluene (0.5 M, based on pyridine *N*-oxide) was added. Halopyridine (2.4 equiv) was added via syringe (if solid the halopyridine was added in the beginning) and the reaction mixture was stirred for 15 min at r.t. and 24 h at 120 °C. After cooling to r.t. the reaction mixture was directly purified by column chromatography (d = 2.5 cm, l = 25 cm SiO_2, deactivated, acetone/hexane, 0: 100 *v/v* -100: 0 *v/v* in 10% increments).

6.10.3 2,2′:6′,2″-Terpyridine *N*′-oxide

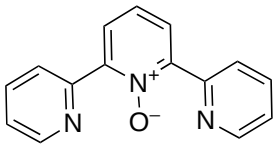

8l

According to General Procedure D: pyridine *N*-oxide (95 mg, 1.0 mmol), 2-bromopyridine (380 mg, 2.4 mmol), toluene (2 mL). $Pd(OAc)_2$ (22.5 mg, 0.1 mmol), $P(tBu)_3$ (24.3 mg, 0.12 mmol), K_3PO_4 (425 mg, 2.0 mmol). Purification by column chromatography (SiO_2, deactivated, acetone/hexane, 0: 100 *v/v* -100: 0 *v/v* , R_f = 0.52 for 40: 60 *v/v*) gave **8l** as white solid (66 mg, 0.26 mmol, 26%) and 2,2′-bipyridine *N*-oxide **4g** as pale brown solid (85.5 mg, 0.50 mmol, 50%, R_f = 0.26 for 40: 60 *v/v*).

The NMR spectra of **4g**[184] and **8l**[237] matched the reported data.

2,2′-Bipyridine *N*-oxide **4g**

^{1}H NMR (400 MHz, $CDCl_3$) δ (ppm) = 8.86 (1H, d, J = 8.1 Hz, ArH-3′), 8.70 (1H, d, J = 5.8 Hz, ArH-6′), 8.29 (1H, dd, J = 6.5, 0.7 Hz, ArH-3), 8.15 (1H, dd, J = 8.0, 1.9 Hz, ArH-6), 7.80 (1H, td, J = 7.8, 1.9 Hz, ArH-4′), 7.30-7.37 (2H, m, ArH-5,5′), 7.24 (1H, td, J = 6.5, 2.1 Hz, ArH-4) using COSY.

^{13}C NMR (126 MHz, $CDCl_3$) δ (ppm) = 149.5, 149.3, 147.2, 140.6, 136.2, 127.8, 125.7, 125.4, 125.2, 124.2 (ArC).

HRESI-MS: (+, 200V) *m/z*: $[M+H]^+$ 173.0697 calc. 173.0709, $[M+Na]^+$ 195.0517 (100%) calc. 195.0529.

IR ν_{max} (cm^{-1}): 3400 (w), 3054 (w), 1668 (w), 1609 (w), 1582 (m), 1569 (m), 1484 (m), 1461 (s), 1440 (s), 1412 (s), 1309 (m), 1250, 1229 (s), 1149 (m), 1111 (w), 1095 (w), 1059 (w), 1031 (s), 990 (m), 848 (s), 765 (s), 747 (s), 719 (s).

2,2′:6′,2″-Terpyridine *N*′-oxide **8l**

^{1}H NMR (500 MHz, $CDCl_3$) δ (ppm) = 8.75 (2H, ddd, J = 4.8, 1.7, 0.9 Hz, ArH), 8.69 (2H, d, J = 8.1 Hz, ArH), 8.07 (2H, d, J = 7.9 Hz, ArH), 7.81 (2H, td, J = 7.8, 1.8 Hz, ArH), 7.47 (1H, t, J = 7.9 Hz, ArH), 7.35 ppm (2H, ddd, J = 7.5, 4.8, 1.1 Hz, ArH).

^{13}C NMR (126 MHz, $CDCl_3$) δ (ppm) = 150.6, 149.5, 148.3, 136.1, 127.8, 125.8, 125.5, 124.2 (ArC).

6.10.4 4′-Nitro-2,2′:6′,2″-terpyridine *N*′-oxide

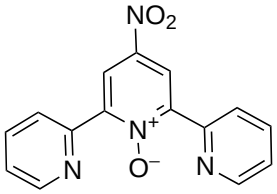

8k

According to General Procedure D: 4-nitroropyridine *N*-oxide (140 mg, 1.0 mmol), 2-bromopyridine (380 mg, 2.4 mmol), toluene (2 mL). $Pd(OAc)_2$ (22.5 mg, 0.1 mmol), P(*t*Bu)$_3$ (24.3 mg, 0.12 mmol), K_3PO_4 (425 mg, 2.0 mmol). Purification by column chromatography (SiO_2, deactivated, acetone/hexane, 0: 100 *v*/*v* -100: 0 *v*/*v* , R_f = 0.80 for 40: 60 *v*/*v*) gave **8k** as yellow solid (8 mg, 0.03 mmol, 3%) and 4-nitro-2,2′-bipyridine N-oxide **4h** as yellow solid (47 mg, 0.22 mmol, 22%, R_f = 0.38 for 30: 70 *v*/*v*).

4-Nitro-2,2′-bipyridine N-oxide **4h**

^{1}H NMR (400 MHz, $CDCl_3$) δ (ppm) = 9.15 (1H, d, J = 3.3 Hz, ArH-3), 8.88 (1H, d, J = 8.1 Hz, ArH-3′), 8.78 (1H, d, J = 4.9 Hz, ArH-6′), 8.35 (1H, d, J = 7.2 Hz, ArH-6), 8.05 (1H, dd, J = 7.2, 3.3 Hz, ArH-5), 7.87 (1H, td, J = 7.9, 1.6 Hz, ArH-4′), 7.42 (1H, dd, J = 7.7, 4.9 Hz, ArH-5′).

^{13}C NMR (126 MHz, $CDCl_3$) δ (ppm) = 149.7, 148.2, 147.5, 142.4, 141.9, 136.6, 125.3, 125.0, 122.5, 118.8 ppm (ArC).

HRESI-MS: (+, 200V) *m*/*z*: $[M+H]^+$ 218.0557 calc. 218.0560, $[M+Na]^+$ 240.0378 (100%) calc. 240.0380.

IR ν_{max} (cm^{-1}): 3056 (m), 2925 (w), 2855 (w), 1605 (m), 1584 (m), 1522 (s), 1509 (s), 1467 (m), 1457 (m), 1446 (m), 1406 (w), 1337 (s), 1289 (s), 1275 (s), 1235 (s), 1214 (s), 1611 (w), 1115 (s), 1053 (w), 1037 (w), 990 (w), 911 (m), 897 (s), 838 (m), 790 (m), 760 (m), 747 (s), 710 (m), 664 (s), 654 (s).

M.p.: 172-175 °C.

4′-Nitro-2,2′:6′,2″-terpyridine *N*′-oxide **8k**

^{1}H NMR (500 MHz, $CDCl_3$) δ (ppm) = 8.82-8.78 (2H, m, ArH), 8.76 (2H, s, ArH), 8.61 (2H, dt, J = 8.0, 1.1 Hz, ArH), 7.99 (2H, td, J = 7.8, 1.8 Hz, ArH), 7.56 (2H, ddd, J = 7.6, 4.7, 1.1 Hz, ArH).

HRESI-MS: (+, 200V) *m*/*z*: $[M+Na]^+$ 317.0634 (100%) calc. 317.0646.

6.10.5 4,4″-Bis-*tert*-butyl-4′-ethoxycarbonyl-2,2′:6′,2″-terpyridine *N*′-oxide

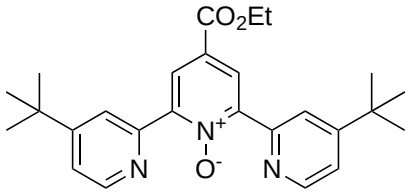

8f

According to General Procedure D: 4-(ethoxycarbonyl)pyridine *N*-oxide **2a** (167 mg, 1.0 mmol), 2-bromo-4-*tert*-butylpyridine **3a** (514 mg, 2.4 mmol), toluene (2 mL). $Pd(OAc)_2$ (22.5 mg, 0.1 mmol), $P(t\mathrm{Bu})_3$ (24.3 mg, 0.12 mmol), K_3PO_4 (425 mg, 2.0 mmol). Purification by column chromatography (SiO_2 , deactivated, acetone/hexane, 0: 100 *v/v*-100: 0 *v/v*) gave **8f** as brown solid (39 mg, 0.09 mmol, 9%, R_f = 0.46 for 30: 70 *v/v*) and 4′-*tert*-butyl-4-ethoxycarbonyl-2,2′-bipyridine *N*-oxide **4b** as brown oil (150 mg, 0.50 mmol, 50%, Rf = 0.43 for 30: 70 *v/v*).

^{1}H NMR (500 MHz, $CDCl_3$) δ (ppm) = 8.67 (2H, d, J = 5.3 Hz, ArH-6,6″), 8.52 (2H, s, ArH-3′,5′), 8.49 (2H, d, J = 1.8, ArH-3,3″), 7.36 (2H, dd, J = 5.3, 1.9 Hz, ArH-5,5″), 4.40 (2H, q, J = 7.1 Hz, CH_2), 1.38 (3H, t, J = 7.2 Hz, CH_3), 1.34 (18H, s, $C(CH_3)_3$).

^{13}C NMR (176 MHz, $CDCl_3$) δ (ppm) = 164.0 (CO), 160.4, 150.2, 149.6, 149.1, 127.8, 126.5, 122.8, 122.8, 121.6 (ArC), 61.9 (CH_2), 35.1 ($\underline{C}(CH_3)_3$), 30.4 ($C(\underline{CH_3})_3$), 14.4 (CH_3).

HRESI-MS: (+, 200V) *m/z*: $[M+H]^+$ 434.2444 (100%) calc. 434.2444.

IR ν_{max} (cm^{-1}): 2961 (s), 2902 (s), 2866 (s), 1951 (w), 1731 (w), 1689 (w), 1592 (s), 1581 (s), 1547 (s), 1465 (s), 1392 (s), 1374 (s), 1363 (s), 1285 (m), 1266 (m), 1201 (m), 1136 (m), 1114 (m), 1074 (m), 1025 (m), 994 (m), 929 (m), 904 (m), 841 (s), 773 (w), 748 (w), 727 (s), 684 (s), 668 (s).

M.p.: 125-130 °C.

6.10.6 4-*tert*-Butyl-4′-ethoxycarbonyl- 2,2′:6′,2″-terpyridine *N*′-oxide

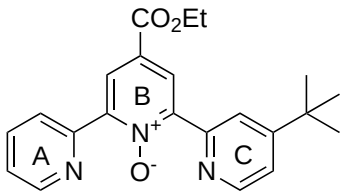

8b

According to General Procedure C: Starting from **4a**: 4-ethoxycarbonyl-2,2′-bipyridine *N*-oxide **4a** (122 mg, 0.5 mmol), 2-bromo-4-*tert*-butyl-pyridine (129 mg, 0.6 mmol), toluene (1 mL). $Pd(OAc)_2$ (5.6 mg, 0.025 mmol), P(*t*Bu)$_3$ (6.1 mg, 0.03 mmol), K_3PO_4 (212 mg, 1.0 mmol). Purification by column chromatography (SiO_2 , deactivated, acetone/hexane, 0: 100*v*/*v*-100: 0*v*/*v*, R_f = 0.50 for 30: 70*v*/*v*) gave **8b** as brown oil (134 mg, 0.36 mmol, 71%) and unreacted bipyridine *N*-oxide **4a** as brown solid (32 mg, 0.14 mmol, 29%).

Starting from **4b**: 4′-*tert*-butyl-4-ethoxycarbonyl-2,2′-bipyridine *N*-oxide **4b** (150 mg, 0.5 mmol), 2-bromopyridine (95 mg, 0.6 mmol), toluene (1 mL). $Pd(OAc)_2$ (5.6 mg, 0.025 mmol), P(*t*Bu)$_3$ (6.1 mg, 0.03 mmol), K_3PO_4 (212 mg, 1.0 mmol). Purification by column chromatography gave **8b** as brown oil (104 mg, 0.28 mmol, 55%) and unreacted bipyridine *N*-oxide **4b** as brown oil (43 mg, 0.14 mmol, 28%).

^{1}H NMR (500 MHz, $CDCl_3$): δ (ppm) = 8.77 (1H, ddd, J = 4.8, 1.8, 0.9 Hz, ArH-A), 8.67 (1H, dd, J = 5.2, 0.8 Hz, ArH-C), 8.59 − 8.57 (2H, m, ArH-B), 8.57 − 8.54 (2H, m, ArH-A, ArH-C), 7.82 (1H, dt, J = 8.6, 1.8 Hz, ArH-A), 7.39 − 7.31 (2H, m, ArH-A, ArH-C), 4.41 (2H, q, J = 7.1 Hz, CH_2), 1.39 (3H, t, J = 7.1 Hz, CH_3), 1.35 (9H, s, $C(CH_3)_3$) using COSY.

^{13}C NMR (176 MHz, $CDCl_3$): δ (ppm) = 163.9 (CO), 160.4, 150.2, 150.0, 149.8, 149.6, 149.1, 148.7, 136.2, 127.9, 127.6, 126.6, 125.6, 124.4, 122.7, 121.6 (ArC), 61.9 (CH_2), 35.1 ($\underline{C}(CH_3)_3$), 30.7 ($C(\underline{CH_3})_3$), 14.4 (CH_3).

HRESI-MS: (+, 200V) *m*/*z*: $[M+H]^+$ 378.1791 calc. 378.1812, $[M+Na]^+$ 400.1611 (100%) calc. 400.1632, $[M+K]^+$ 416.1351 calc. 416.1371, $[2M+Na]^+$ 777.3323 calc. 777.3371.

IR ν_{max} (cm^{-1}): 3725 (w), 3709 (w), 3700 (w), 3625 (w), 3596 (w), 3084 (w), 3056 (w), 2963 (m),

2935 (m), 2904 (m), 2870 (m), 2356 (m), 2338 (m), 1717 (s, C=O), 1621 (s), 1588 (s), 1568 (s), 1463 (s), 1412 (w), 1379 (m), 1363 (m), 1333 (m), 1244 (s), 1146 (m), 1111 (m), 1065 (m), 1019 (m), 992 (m), 903 (m), 848 (m), 791 (m), 765 (m), 742 (m), 710 (m), 668 (m), 655 (m).

6.10.7 4′-Ethoxycarbonyl-6-trifluoromethyl-2,2′:6′,2″-terpyridine N′-oxide

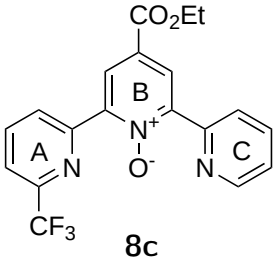

8c

According to General Procedure C: Starting from **4i**: 4-ethoxycarbonyl-6′-trifluoromethyl-2,2′- bipyridine *N*-oxide **4i** (156 mg, 0.5 mmol), 2-bromopyridine (95 mg, 0.6 mmol), toluene (1 mL). $Pd(OAc)_2$ (5.6 mg, 0.025 mmol), $P(t\mathrm{Bu})_3$ (6.1 mg, 0.03 mmol), K_3PO_4 (212 mg, 1.0 mmol). Purification by column chromatography (SiO_2 , deactivated, acetone/hexane, 0: 100 *v/v*-100: 0 *v/v*, R_f = 0.55 for 40: 60 *v/v*) gave **8c** as yellow solid (134 mg, 0.344 mmol, 69%) and unreacted bipyridine *N*-oxide **4i** as brown solid (29 mg, 0.09 mmol, 19%).

Starting from: 4-Ethoxycarbonyl-2,2′-bipyridine *N*-oxide **4a** (122 mg, 0.5 mmol), 2-bromo-6- (trifluoromethyl)pyridine (136 mg, 0.6 mmol), toluene (1 mL). $Pd(OAc)_2$ (5.6 mg, 0.025 mmol), $P(t\mathrm{Bu})_3$ (6.1 mg, 0.03 mmol), K_3PO_4 (212 mg, 1.0 mmol). Purification by column chromatography (SiO_2 , deactivated, acetone/hexane, 0: 100 *v/v*-100: 0 *v/v*, R_f = 0.55 for 40: 60 *v/v*) gave **8c** as yellow solid (29 mg, 0.07 mmol, 15%). 2^{nd} run: 15 mg, 0.04 mmol, 8% and unreacted bipyridine *N*-oxide **4a** as brown solid (1^{st} run: 98 mg, 0.40 mmol, 80%, 2^{nd} run: 94 mg, 0.38 mmol, 77%).

^{1}H NMR (500 MHz, $CDCl_3$): δ (ppm) = 8.86 (1H, d, J = 8.1 Hz, ArH-A), 8.79 (1H, ddd, J = 4.8, 1.7, 0.9 Hz, ArH-C), 8.68 (1H, d, J = 2.7 Hz, ArH-B), 8.67 (1H, d, J = 2.7 Hz, ArH-B), 8.56 (1H, d, J = 8.0 Hz, ArH-C), 8.01 (1H, t, J = 7.9 Hz, ArH-A), 7.84 (1H, td, J = 7.8, 1.8 Hz, ArH-C), 7.76 (1H, d, J = 7.8 Hz, ArH-A), 7.40 (1H, ddd, J = 7.5, 4.8, 1.1 Hz, ArH-C), 4.45 (2H, q, J = 7.1 Hz, CH_2), 1.42 (3H, t, J = 7.1 Hz, CH_3) using COSY.

^{13}C NMR (176 MHz, $CDCl_3$): δ (ppm) = 163.7 (C=O), 150.3, 149.54, 149.51, 148.4, 148.2 (q, J^{C-F} = 36 Hz, ArC-6), 147.3, 137.6, 136.5, 128.3, 128.1, 128.0, 127.0, 125.6, 124.6, 121.3 (q, J^{C-F} = 274

Hz, CF_3), 120.9 (q, J^{C-F} = 2.7 Hz, ArC-5), 62.0 (CH_2), 14.2 (CH_3).

^{19}F NMR (471 MHz, $CDCl_3$): δ (ppm) = -67.81 (s, CF_3).

HRESI-MS: (+, 200V) *m/z*: $[M+H]^+$ 390.1090 calc. 390.1066, $[M+Na]^+$ 412.0910 (100 %) calc. 412.0885.

IR ν_{max} (cm^{-1}): 3072 (w), 2925 (w), 2848 (w), 1730 (m, C=O), 1622 (w), 1589 (w), 1471 (w), 1432 (w), 1410 (w), 1390 (w), 1364 (w), 1343 (s), 1325 (w), 1255 (s), 1187 (m), 1129 (s), 1049 (w), 1018 (m), 993 (w), 931 (w), 910 (w), 876 (w), 861 (w), 820 (m), 788 (w), 763 (m), 738 (w), 673 (w), 656 (w).

M.p.: 147 °C.

6.10.8 4″-*tert*-Butyl-4′-ethoxycarbonyl-5-methoxy-2,2′:6′,2″-terpyridine N′-oxide

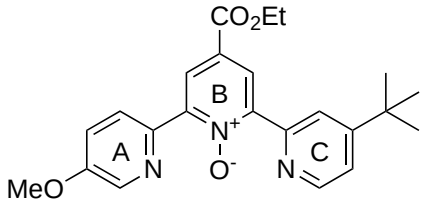

8g

According to General Procedure C: 4′-*tert*-butyl-4-ethoxycarbonyl-2-2′-bipyridine *N*-oxide **4b** (150 mg, 0.5 mmol), 2-bromo-5-methoxypyridine (113 mg, 0.6 mmol), toluene (1 mL). $Pd(OAc)_2$ (5.6 mg, 0.025 mmol), P(*t*Bu)$_3$ (6.1 mg, 0.03 mmol), K_3PO_4 (212 mg, 1.0 mmol). Purification by column chromatography (SiO_2 , deactivated, acetone/hexane, 0: 100 *v/v*-100: 0 *v/v*, Rf = 0.55 for 30: 70 *v/v*) gave **8g** as orange oil (4.1 mg, 0.01 mmol, 2%) and unreacted bipyridine *N*-oxide **4b** as brown oil (120 mg, 0.40 mmol, 80%).

^{1}H NMR (500 MHz, $CDCl_3$): δ (ppm) = 8.69 (1H, dd, J = 9.6, 0.7 Hz, ArH-C), 8.67 (1H, dd, J = 6.1, 0.8 Hz, ArH-A), 8.64 (1H, dd, J = 2.8, 0.7 Hz, ArH-B), 8.52 − 8.48 (2H, m, ArH-B, ArH-A), 8.46 (1H, dd, J = 3.7, 0.7 Hz, ArH-C), 7.36 (1H, dd, J = 5.3, 1.9 Hz, ArH-C), 7.30 (1H, dd, J = 8.9, 3.0 Hz, ArH-A), 4.41 (2H, q, J = 7.1 Hz, CH_2), 3.93 (3H, s, OCH_3), 1.40 (3H, t, J = 7.2, 3H, CH_3), 1.36 (9H, s, $C(CH_3)_3$) using COSY and HMBC.

^{13}C NMR (176 MHz, $CDCl_3$): δ (ppm) = 164.1 (CO), 160.4, 156.2, 150.3, 149.6, 149.1, 142.1, 138.0, 127.2, 127.1, 126.6, 126.2, 122.7, 121.5, 119.6 (ArC), 61.9 (CH_2), 55.8 (OCH_3), 35.1 ($\underline{C}(CH_3)_3$), 30.7 ($C(\underline{CH_3})_3$), 14.4 (CH_3) using DEPT.

HRESI-MS (+, 200V) *m/z*: $[M+H]^+$ 408.1909 calc. 408.1918, $[M+Na]^+$ 430.1729 (100%) calc. 430.1737, $[M+K]^+$ 446.1470 calc. 446.1477, $[2M+Na]^+$ 837.3548 calc. 837.3582.

IR ν_{max} (cm^{-1}): 2964 (m), 2899(w), 2864(w), 2837(w), 1720(s, C=O), 1620(w), 1588(m), 1554(w), 1467(m), 1380(m), 1363(m), 1335(m), 1245(s, R_3N+-O-), 1179(w), 1117(m), 1065(w), 1022(m), 911(w), 878(w), 833(w), 766(w), 730(w), 708(w), 658(w).

6.10.9 4″-*tert*-Butyl-4′-ethoxycarbonyl-6-methoxy-2,2′:6′,2″-terpyridine N′-oxide

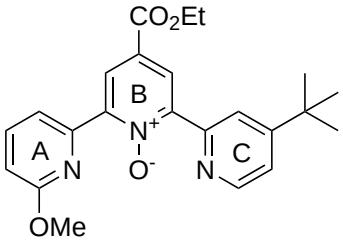

8d

According to General Procedure C: 4-ethoxycarbonyl-6′-methoxy-2,2′-bipyridine *N*-oxide **4d** (137 mg, 0.5 mmol), 2-bromo-4-*tert*-butyl-pyridine (129 mg, 0.6 mmol), toluene (1 mL). $Pd(OAc)_2$ (5.6 mg, 0.025 mmol), P(*t*Bu)$_3$ (6.1 mg, 0.03 mmol), K_3PO_4 (212 mg, 1.0 mmol). Purification by column chromatography (SiO_2 , deactivated, acetone/hexane, 0: 100*v/v*-100: 0*v/v*, Rf = 0.65 for 30: 70*v/v*) gave **8d** as orange solid (131 mg, 0.32 mmol, 64% yield) and unreacted bipyridine *N*-oxide **4d** as brown solid (44 mg, 0.16 mmol, 32%).

^{1}H NMR (500 MHz, $CDCl_3$): δ (ppm) = 8.76 (1H, d, J = 2.7 Hz, ArH-B), 8.66 (1H, dd, J = 5.3, 0.8 Hz, ArH-C), 8.52 (1H, dd, J = 2.0, 0.8 Hz, ArH-C), 8.51 (1H, d, J = 2.7 Hz, ArH-B), 8.41 (1H, dd, J = 7.5, 0.8 Hz, ArH-A), 7.70 (1H, t, J = 7.5 Hz, ArH-A), 7.35 (1H, dd, J = 5.3, 1.9 Hz, ArH-C), 6.83 (1H, dd, J = 8.3, 0.8 Hz, ArH-A), 4.41 (2H, q, J = 7.1 Hz, CH_2), 4.02 (3H, s, OCH_3), 1.40 (3H, t, J = 7.1 Hz, CH_3), 1.35 (9H, s, $C(CH_3)_3$) using COSY and HMBC.

^{13}C NMR (176 MHz, $CDCl_3$): δ (ppm) = 164.2 (CO), 163.6, 160.3, 150.2, 149.5, 148.4, 146.5, 139.1,

127.5, 127.2, 126.2, 122.7, 121.5, 118.6, 112.4 (ArC), 61.9 (CH_2), 53.6 (OCH_3), 35.1 ($\underline{C}(CH_3)_3$), 30.7 ($C(\underline{CH_3})_3$), 14.4 (CH_3) using DEPT.

HRESI-MS (+, 200V) *m/z*: $[M + H]^+$ 408.1915 calc. 408.1918, $[M + Na]^+$ 430.1736 (100%) calc. 430.1737, $[2M + Na]^+$ 837.3558 calc. 837.3582.

IR ν_{max} (cm^{-1}): 3091 (w), 3061 (w), 2967 (m), 2930 (m), 2906 (m), 2867 (m), 1719 (s, C=O), 1621 (m), 1575 (m), 1549 (m), 1470 (s), 1422 (m), 1404 (m), 1390 (m), 1378 (m), 1363 (m), 1332 (m), 1307 (m), 1255 (s), 1150 (m), 1130 (m), 1112 (m), 1075 (m), 1027 (s), 985 (m), 915 (m), 866 (m), 850 (m), 807 (s), 765 (s), 726 (m), 710 (m), 657 (m).

M.p.: 98-100 °C.

6.10.10 4″-*tert*-Butyl-4′-ethoxycarbonyl-4-methoxy-2,2′:6′,2″-terpyridine N′-oxide

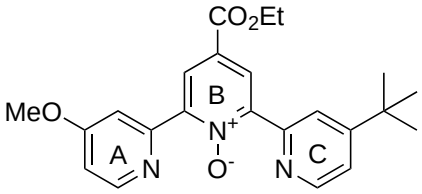

8e

According to General Procedure C: 4-ethoxycarbonyl-4′-methoxy-2,2′-bipyridine *N*-oxide **4f** (137 mg, 0.5 mmol), 2-bromo-4-*tert*-butyl-pyridine (129 mg, 0.6 mmol), toluene (1 mL). $Pd(OAc)_2$ (5.6 mg, 0.025 mmol), P(*t*Bu)$_3$ (6.1 mg, 0.03 mmol), K_3PO_4 (212 mg, 1.0 mmol). Purification by column chromatography (SiO_2 , deactivated, acetone/hexane, 0: 100 *v/v*-100: 0 *v/v*, Rf = 0.43 for 30: 70 *v/v*) gave **8e** as brown oil (136 mg, 0.33 mmol, 67%) and unreacted bipyridine *N*-oxide **4f** as brown solid (36 mg, 0.13 mmol, 26%).

^{1}H NMR (500 MHz, $CDCl_3$): δ (ppm) = 8.65 (1H, dd, J = 5.3, 0.8 Hz, ArH-C), 8.60 (1H, d, J = 2.7 Hz, ArH-B), 8.56-8.54 (2H, m, ArH-B, ArH-A), 8.51 (1H, dd, J = 1.9, 0.8 Hz, ArH-C), 8.16 (1H, d, J = 2.53 Hz, ArH-A), 7.35 (1H, dd, J = 5.3, 1.9 Hz, ArH-C), 6.88 (1H, dd, J = 5.7, 2.6 Hz, ArH-A), 4.40 (2H, q, J = 7.1 Hz, CH_2), 3.87 (3H, s, OCH_3), 1.38 (3H, t, J = 7.1 Hz, CH_3), 1.34 (9H, s, $C(CH_3)_3$) using COSY and HMBC.

^{13}C NMR (176 MHz, $CDCl_3$): δ (ppm) = 165.9 (CO), 163.9, 160.4, 151.5, 150.6, 150.1, 149.6, 149.2, 148.6, 127.8, 127.7, 126.6, 122.7, 121.6, 111.3, 111.2 (ArC), 61.9 (CH_2), 55.5 (OCH_3), 35.1 ($\underline{C}(CH_3)_3$), 30.6 ($C(\underline{CH_3})_3$), 14.4 (CH_3) using DEPT.

HRESI-MS (+, 200V) *m/z*: $[M + H]^+$ 408.1892 calc. 408.1918, $[M + Na]^+$ 430.1716 (100%) calc. 430.1737, $[M + K]^+$ 446.1449 calc. 446.1477.

IR ν_{max} (cm^{-1}): 3088 (w), 3060 (w), 2955 (w), 2908 (w), 2864 (w), 2357 (w), 2219 (w), 1714 (s, C=O), 1624 (m), 1588 (s), 1565 (m), 1468 (m), 1435 (m), 1376 (m), 1357 (m), 1328 (m), 1301 (m), 1240 (s), 1202 (s), 1197 (s), 1174 (w), 1136 (w), 1108 (w), 1059 (w), 1021 (s), 990 (w), 913 (m), 901 (m), 862 (m), 844 (m), 829 (m), 801 (w), 763 (m), 729 (m), 706 (m).

6.11 Synthesis of terpyridines from terpyridine *N*-oxides

6.11.1 General Procedure E for the reduction of terpyridine *N*-Oxides

The terpyridine *N*-oxide (1 equiv.) was dissolved in ethanol and Pd/C (10 wt%, 0.1 equiv.) added. The reaction mixture was degassed (3x vacuum/argon) and under vacuum H_2 (atm) with a hydrogen balloon added. After full conversion of the substrate was achieved, as judged by TLC, the reaction mixture was filtered over celite and washed with ethanol (100 mL). Removal of the solvent *in vacuo* gave the corresponding terpyridine.

6.11.2 4-*tert*-Butyl-4′-ethoxycarbonyl-2,2′:6′,2″-terpyridine

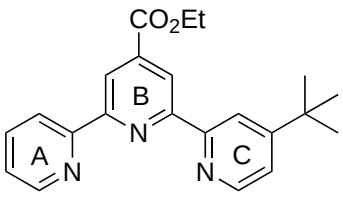

9a

According to General Procedure E: 4-*tert*-butyl-4′-ethoxycarbonyl-2,2′:6′,2″-terpyridine N′-oxide **8b** (201 mg, 0.53 mmol), Pd/C (10 wt%, 57 mg, 0.053 mmol), ethanol (8 mL) for 1 h. Concentration gave **9a** as brown oil (185 mg, 0.51 mmol, 97%).

^{1}H NMR (400 MHz, $CDCl_3$): δ (ppm) = 8.95-8.91 (2H, m, ArH), 8.67 (1H, d, J = 4.7 Hz, ArH), 8.60-8.55 (2H, m, ArH), 8.53 (1H, dd, J = 7.9, 1.0 Hz, ArH), 7.82 (1H, dd, J = 7.4, 1.7 Hz, ArH), 7.32-7.25 (2H, m, ArH), 4.42 (2H, q, J = 7.2 Hz, CH_2), 1.40 (3H, t, J = 7.1 Hz, CH_3), 1.36 (9H, s, $C(CH_3)_3$).

^{13}C NMR (126 MHz, $CDCl_3$): δ (ppm) = 165.4 (CO), 160.9, 156.9, 156.4, 155.5, 155.3, 149.2, 140.0, 136.9, 124.1, 121.3, 121.1, 120.5, 120.2, 118.1 (ArC), 61.7 (CH_2), 34.9 ($\underline{C}(CH_3)_3$), 30.6 ($C(\underline{CH_3})_3$), 14.3 (CH_3).

HRESI-MS (+, 200V) m/z: $[M+H]^+$ 362.1853 calc. 362.1869, $[M+Na]^+$ 384.1685 calc. 384.1683, $[M+K]^+$ 400.1462 calc. 400.1422.

IR ν_{max} (cm^{-1}): 3665 (w), 3092 (w), 3058 (w), 2964 (w), 2904 (w), 2869 (w), 2227 (w), 1971 (w), 1726 (s, C=O), 1584 (m), 1562 (m), 1548 (m), 1469 (m), 1445 (w), 1434 (w), 1408 (w), 1382 (s), 1370 (m), 1339 (m), 1284 (m), 1270 (m), 1253 (s), 1230 (s), 1173 (w), 1132 (m), 1106 (m), 1092 (m), 1070 (m), 1020 (m), 993 (m), 904 (m), 883 (m), 843 (m), 832 (w), 798 (m), 772 (s), 756 (m), 731 (s), 718 (s), 677 (s), 660 (s).

6.11.3 4,4″-Bis-*tert*-butyl-4′-ethoxycarbonyl-2,2′:6′,2″-terpyridine

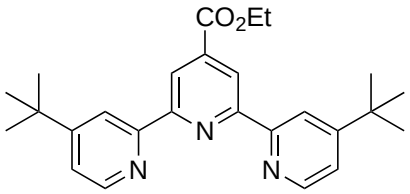

9e

According to General Procedure E: 4,4″-bis-*tert*-butyl-4′-ethoxycarbonyl-2,2′:6′,2″-terpyridine N'-oxide **8f** (130 mg, 0.3 mmol), Pd/C (10 wt%, 32 mg, 0.03 mmol), ethanol (10 mL) for 1 h. Concentration gave **9e** as grey solid (119 mg, 0.285 mmol, 95%).

^{1}H NMR (400 MHz,): δ (ppm) = 8.96 (2H, s, ArH-3′,5′), 8.72 (1H, dd, J = 2.0, 0.8 Hz, ArH-3,3′), 8.64 (1H, dd, J = 5.2, 0.7 Hz, ArH-6,6′), 7.36 (1H, dd, J = 5.2, 1.9 Hz, ArH-5,5′), 4.46 (2H, q, J = 7.2 Hz, CH_2), 1.44 (3H, t, J = 7.3 Hz, CH_3), 1.42 (9H, s, $C(CH_3)_3$).

^{13}C NMR (126 MHz, $CDCl_3$): δ (ppm) = 165.54 (CO), 160.93, 156.65, 155.50, 149.35, 140.27, 121.46, 120.21, 118.28 (ArC), 61.81(CH_2), 35.05 ($\underline{C}(CH_3)_3$), 30.60 ($C(\underline{CH_3})_3$), 14.45 (CH_3).

HRESI-MS (+, *m/z*): $[M+H]^+$ 418.2475 calc. 418.2495, $[M+Na]^+$ 440.2296 calc. 440.2314, $[2M+Na]^+$ 857.4694 calc. 857.4730.

IR ν_{max} (cm^{-1}): 3095 (w), 3057 (w), 2957 (m), 2895 (w), 2866 (w), 2357 (w), 2323 (w), 1718 (m, C=O), 1585 (m), 1561 (w), 1544 (m), 1473 (m), 1463 (m), 1437 (w), 1425 (w), 1387 (w), 1367 (s), 1353 (m), 1327 (w), 1301 (w), 1287 (w), 1279 (w), 1260 (s), 1224 (s), 1170 (w), 1131 (m), 1103 (m), 1067 (m), 1022 (m), 997 (w), 991 (w), 964 (w), 918 (w), 900 (m), 867 (w), 854 (w), 840 (m), 824 (w), 800 (w), 778 (s), 752 (w), 745 (w), 716 (m), 676 (m), 666 (m), 642 (m).

M.p.: 137-141 °C.

6.11.4 4″-*tert*-Butyl-4′-ethoxycarbonyl-6-methoxy-2,2′:6′,2″-terpyridine

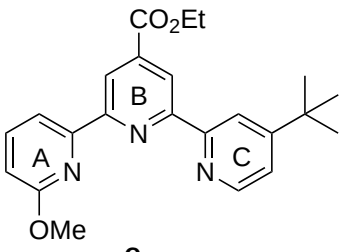

9c

According to General Procedure E: 4″-*tert*-butyl-4′-ethoxycarbonyl-6-methoxy-2,2′:6′,2″-terpyridine N′-oxide **8d** (117 mg, 0.29 mmol), Pd/C (10 wt%, 31 mg, 0.029 mmol), ethanol (10 mL) for 1 h. Concentration gave **9c** as red solid (112 mg, 0.286 mmol, 99%).

^{1}H NMR (500 MHz, $CDCl_3$): δ (ppm) = 8.92 (1H, d, J = 1.4 Hz, ArH-B), 8.91 (1H, d, J = 1.5 Hz, ArH-B), 8.64-8.58 (2H, m, ArH-C), 8.17 (1H, d, J = 7.4 Hz, ArH-A), 7.74 (1H, t, J = 8.1 Hz, ArH-A), 7.34-7.32 (1H, m, ArH-C), 6.80 (1H, d, J = 8.2 Hz, ArH-A), 4.46 (2H, q, J = 7.1 Hz, CH2), 4.07 (3H, s, OCH_3), 1.44 (3H, t, J = 7.2, CH_3), 1.40 (9H, s, $C(CH_3)_3$) using COSY and HMBC.

^{13}C NMR (126 MHz, $CDCl_3$): δ (ppm) = 165.7 (CO), 163.7, 161.1, 156.9, 156.4, 155.5, 152.9, 149.3, 139.9, 139.4, 121.4, 120.2, 120.2, 118.3, 113.9, 111.7 (ArC), 61.8 (CH_2), 53.4 (OCH_3), 35.1 ($\underline{C}(CH_3)_3$),

30.7 (C($\underline{C}H_3$)$_3$), 14.4 (CH_3) using DEPT.

HRESI-MS (+, 200V) m/z: $[M+Na]^+$ 414.1792 calc. 414.1794.

IR ν_{max} (cm^{-1}): 3853 (w), 3838 (w), 3727 (w), 3708 (w), 3649 (w), 3628 (w), 3596 (w), 3567 (w), 3087 (w), 2975 (w), 2953 (w), 2905 (w), 2868 (w), 2360 (s), 2341 (s), 2273 (w), 1719 (m, C=O), 1654 (w), 1605 (w), 1578 (m), 1560 (m), 1551 (m), 1508 (w), 1467 (m), 1446 (m), 1431 (w), 1402 (m), 1390 (m), 1376 (m), 1339 (w), 1298 (m), 1269 (m), 1252 (m), 1239 (m), 1162 (w), 1133 (m), 1106 (m), 1082 (w), 1035 (m), 999 (w), 987 (m), 938 (w), 917 (w), 900 (m), 868 (m), 853 (w), 841 (m), 809 (m), 771 (m), 752 (m), 738 (m), 720 (m), 700 (m), 678 (m), 669 (m), 657 (m).

M.p.: 84-85 °C.

6.11.5 4″-*tert*-Butyl-4′-ethoxycarbonyl-4-methoxy-2,2′:6′,2″-terpyridine

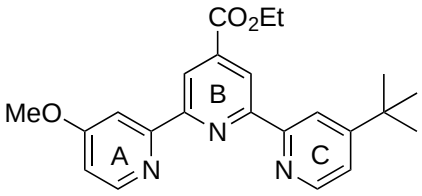

9d

According to General Procedure E: 4″-*tert*-butyl-4′-ethoxycarbonyl-4-methoxy-2,2′:6′,2″-terpyridine N′-oxide **8e** (144 mg, 0.35 mmol), Pd/C (10 wt%, 38 mg, 0.035 mmol), ethanol (10 mL) for 1 h. Concentration gave **9d** as green solid (127 mg, 0.32 mmol, 92%).

^{1}H NMR (500 MHz, $CDCl_3$): δ (ppm) = 8.95 (2H, s, ArH-B), 8.64 (1H, dd, J = 5.3, 0.6 Hz, ArH-A), 8.62 (1H, dd, J = 2.0, 0.7 Hz, ArH-A), 8.55 (1H, d, J = 5.6 Hz, ArH-C), 8.18 (1H, d, J = 2.6 Hz, ArH-C), 7.36 (1H, dd, J = 5.2, 2.0 Hz, ArH-A), 6.89 (1H, dd, J = 5.7, 2.6 Hz, ArH-C), 4.46 (2H, q, J = 7.1 Hz, CH_2), 3.98 (3H, s, OCH_3), 1.44 (3H, t, J = 7.2 Hz, CH_3), 1.41 (9H, s, C(CH_3)$_3$) using COSY.

^{13}C NMR (126 MHz, $CDCl_3$): δ (ppm) =166.74 (CO), 165.45, 161.04, 157.40, 156.86, 156.19, 155.43, 150.57, 149.35, 140.21, 121.44, 120.76, 120.45, 118.27, 110.78, 106.85 (ArC), 61.84 (CH_2), 55.19 (OCH_3), 35.07 ($\underline{C}$(CH_3)$_3$), 30.66(C($\underline{CH_3}$)$_3$), 14.44 (CH_3) using DEPT.

HRESI-MS (+, 200V) *m/z*: $[M+H]^+$ 392.1956 calc. 392.1974, $[M+Na]^+$ 414.1776 calc. 414.1794.

IR ν_{max} (cm^{-1}): 3087 (w), 3056 (w), 2961 (w), 2899 (w), 2865 (w), 2361 (w), 2280 (w), 1721 (s, C=O), 1585 (s), 1558 (m), 1546 (m), 1487 (m), 1473 (m), 1432 (w), 1400 (w), 1372 (s), 1333 (m), 1297 (m), 1280 (m), 1260 (m), 1226 (s), 1200 (s), 1176 (m), 1133 (m), 1105 (m), 1064 (w), 1022 (m), 990 (w), 903 (m), 885 (w), 867 (m), 848 (m), 829 (m), 806 (w), 778 (s), 750 (m), 731 (s), 718 (s), 690 (s), 677 (m), 665 (m), 636 (m).

M.p.: 118-120 °C.

6.12 Complex synthesis

General Procedure F: to a dry Schlenk tube pentamethylcyclopentadienyl iridium dichloride dimer $[IrCp^*Cl_2]_2$ was added. The iridium precursor was dissolved in DCM (dry from solvent drying system). In another Schlenk tube the ligand was added and the atmosphere was exchanged (3x vacuum/argon). The ligand was dissolved in dry DCM and was added to the solution of the precursor. The mixture was stirred at room temperature for 2 days. The work up differed depending on the behavior of the compound in DCM solution.

6.12.1 [(η^5-Pentamethylcyclopentadienyl)(2,2′-bipyridine)chloroiridium]chloride

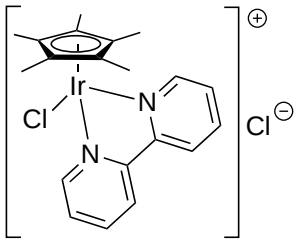

10a

According to the General Procedure F: 2,2′-bipyridine (25.2 mg, 0.16 mmol) in 1 mL DCM, $[IrCp^*Cl_2]_2$ (64.2 mg, 0.08 mmol), in 1 mL DCM for 2.5 days. The product precipitated from DCM and was filtered and dried under vacuum. Product **10a** was obtained as yellow solid (87.8 mg, 0.16 mmol, > 99 %).

^{1} H NMR (500 MHz, Methanol-d4) δ (ppm) = 8.99 (ddd, J = 5.8, 1.4, 0.7 Hz, 2H), 8.65 − 8.61 (m, 2H), 8.28 (td, J = 7.8, 1.5 Hz, 2H), 7.84 (ddd, J = 7.4, 5.6, 1.3 Hz, 2H), 1.71 (s, 15H, Cp*, CH_3).

^{13}C NMR (126 MHz, Methanol-d4) δ (ppm) = 155.5, 151.8, 140.3, 128.7, 123.9 (ArC), 89.6 (Cp*, tert-C), 7.2 (Cp*, CH_3).

HRESI-MS: (+, 200V) *m/z*: $[M]^+$ 519.1175 (100%) calc. 519.1179.

IR ν_{max} (cm^{-1}): 3400 (w, broad peak), 3107, 3069, 3036, 3019, 2962, 2907, 1632 (w), 1603 (m), 1567, 1491, 1464 (w), 1445 (m), 1422, 1386, 1330 (w), 1310, 1259 (s), 1164 (w), 1084, 1072, 1018 (s), 914, 865 (w), 784 (s), 729, 686, 675, 661 (m).

M.p.: decomposes > 250 °C.

UV-Vis (MeCN) $\lambda_{max}(\varepsilon)$ = 252 (19200), 293 (11020), 315 sh, 353 (2200) nm.

6.12.2 [(η^5-Pentamethylcyclopentadienyl)(4,4′-dimethoxy-2,2′-bipyridine)chloroiridium] chloride

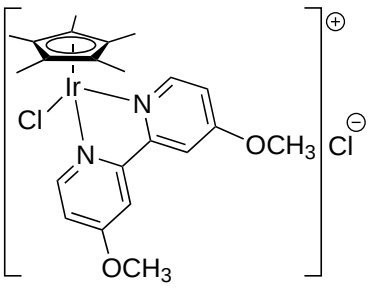

10b

According to the General Procedure F: 4,4′-dimethoxy-2,2′-bipyridine (38.9 mg, 0.18mmol) in 1 mL DCM, $[IrCp^*Cl_2]_2$ (64.1 mg, 0.08 mmol), in 1 mL DCM for 2.5 days. After the reaction DCM was removed and water was added. The solution was filtered over celite to remove the excess ligand. After removal of water, product **10b** was obtained as yellow solid (97.6 mg, 0.16 mmol, > 99 %).

^{1} H NMR (400 MHz, d-DCM) δ (ppm) = 8.99 (dd, J = 2.8, 0.8 Hz, 2H), 8.45 (dd, J = 6.6, 0.8 Hz, 2H), 7.17 - 7.13 (m, 2H), 4.27 (s, 6H, OCH_3), 1.62 (s, 15H, Cp*, CH_3). The ^{1} H NMR spectrum of 2 is in good agreement with reported data.[58]

UV-Vis (MeCN) $\lambda_{max}(\varepsilon)$ (nm) = 230 (35000), 265 (sh), 300 (7500), 345 (3700).

6.12.3 [(η^5-Pentamethylcyclopentadienyl)(4-ethoxycarbonyl-2,2′-bipyridine) chloroiridium] chloride

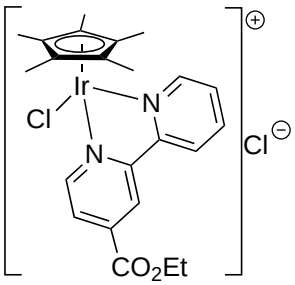

10c

According to the General Procedure F: 4-ethoxycarbonyl-2,2′-bipyridine (41.1 mg, 0.18mmol) in 1 mL DCM, $[IrCp^*Cl_2]_2$ (63.7 mg, 0.08mmol), in 1 mL DCM for 3 days. After the reaction was completed, the solvent was evaporated and the excess ligand was removed by washing with hexane. Product **10c** was obtained as orange solid (100 mg, 0.16 mmol, 89 %).

^{1}H NMR (400 MHz, d-DCM) δ (ppm) = 9.07 (dt, J = 5.8, 0.7 Hz, 1H), 8.96 (d, J = 1.6 Hz, 1H), 8.94 − 8.90 (m, 1H), 8.75 (d, J = 8.0 Hz, 1H), 8.33 (td, J = 7.6, 1.3 Hz, 1H), 8.28 (ddd, J = 5.8, 1.7, 0.6 Hz, 1H), 7.96 − 7.86 (m, 1H), 4.50 (q, J = 7.1 Hz, 2H, CH_2), 1.72 (s, 15H, Cp*, CH_3), 1.45 (t, J = 7.1 Hz, 3H, $CH_2\underline{CH_3}$).

^{13}C NMR (176 MHz, d-DCM) δ (ppm) = 162.7 (CO), 156.4, 154.5, 152.4, 151.7, 141.3, 140.8, 129.7, 128.0, 125.0, 123.4 (ArC), 90.0 (Cp*,*t*C), 63.3 (CH_2), 14.0 ($CH_2\underline{CH_3}$), 8.7 (Cp*, CH_3).

HRESI-MS: (+, 200V) m/z: $[M]^+$ 591.1402 (100%) calc. 591.1390.

IR ν_{max} (cm^{-1}): 3346 (broad peak, w), 3111, 3067, 2981, 2914 (w), 1722 (s), 1604, 1554 (w), 1471, 1415, 1384, 1366, 1328 (m), 1299, 1258, 1239 (s), 1169 (m), 1122, 1105 (s), 1072, 1055 (w), 1028, 1012 (s), 902, 857, 794 (m), 767, 719, 700, 656 (s).

M.p.: decomposes > 270 °C.

UV-Vis (MeCN) $\lambda_{max}(\varepsilon)$ (nm) = 229 (22200), 301 (13300), 323 (sh), 366 (3320).

6.12.4 [(η^5-Pentamethylcyclopentadienyl)(4-ethoxycarbonyl-4′-methoxy-2,2′-bipyridine) chloroiridium] chloride

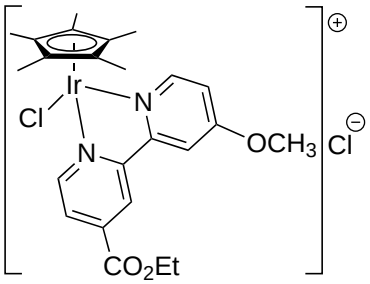

10d

According to the General Procedure F: 4-ethoxycarbonyl-4′-methoxy-2-2′-bipyridine (46.5 mg, 0.180 mmol) in 3 mL DCM, $[IrCp^*Cl_2]_2$ (63.7 mg, 0.080 mmol), in 1 mL DCM for 1.5 days. After the reaction DCM was removed and water was added. The solution was filtered over celite to remove the excess ligand. After removal of water, product **10d** was obtained as orange crystalline solid (101.4 mg, 0.154 mmol, 97 %).

^{1}H NMR (500 MHz, d-DCM) δ (ppm) = 9.11 (dd, J = 1.8, 0.7 Hz, 1H), 9.06 (dd, J = 5.9, 0.7 Hz, 1H), 8.72 (d, J = 6.5 Hz, 1H), 8.28 (d, J = 2.7 Hz, 1H), 8.26 (dd, J = 5.8, 1.7 Hz, 1H), 7.47 (dd, J = 6.6, 2.7 Hz, 1H), 4.51 (q, J = 7.1 Hz, 2H, CH_2), 4.21 (s, 3H, OCH_3), 1.71 (s, 15H, Cp*, CH_3), 1.46 (t, J = 7.2 Hz, 3H, $CH_2\underline{CH_3}$).

^{13}C NMR (126 MHz, d-DCM) δ (ppm) = 168.7 (CO), 163.0, 156.7, 155.9, 152.5, 152.3, 141.3, 128.0, 123.7, 115.7, 111.7 (ArC), 89.5 (Cp*, tC), 63.2 (CH_2), 58.1 (OCH_3), 14.1 ($CH_2\underline{CH_3}$), 8.7 (Cp*, CH_3).

HRESI-MS: (+, 200V) m/z: $[M]^+$ 621.1482 (100%) calc. 621.1496.

IR ν_{max} (cm^{-1}): 3353 (broad peak), 3115, 3075, 2981, 2920, 2562, 2412, 2379, 2348, 2285, 2174, 2097, 2041 (w), 1724, 1615 (s), 1558 (m), 1487 (s), 1456 (m), 1416 (s), 1386, 1368 (m), 1307, 1285, 1265, 1237 (s), 1185, 1123, 1075 (m), 1036, 1012, 956 (s), 917 (m), 854 (s), 797, 770 (m), 704, 670 (s).

M.p.: decomposes > 250 °C.

UV-Vis (MeCN) $\lambda_{max}(\varepsilon)$ (nm) = 220 (31100), 303 (10600), 323 (5600), 366 (3080).

6.12.5 [(η^5-Pentamethylcyclopentadienyl)(4-ethoxycarbonyl-6′-methoxy-2,2′-bipyridine) chloroiridium] chloride

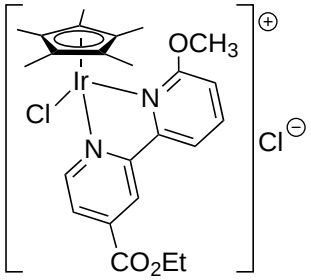

10e

According to the General Procedure F: 4-ethoxycarbonyl-6′-methoxy-2-2′-bipyridine (41.3 mg, 0.160 mmol) in 1 mL DCM, $[IrCp^*Cl_2]_2$ (63.7 mg, 0.080 mmol), in 1 mL DCM for 2 days. After the reaction DCM was removed. Product **10e** was obtained as dark orange crystalline solid without further purification (105.0 mg, 0.160 mmol, > 99 %).

^{1}H NMR (400 MHz, d-DCM) δ (ppm) = 9.05 (dd, J = 5.9, 0.6 Hz, 1H), 8.82 (d, J = 1.3 Hz, 2H), 8.35 (t, J = 8.1 Hz, 1H), 8.28 (dd, J = 7.8, 1.0 Hz, 1H), 8.21 (dd, J = 5.9, 1.7 Hz, 1H), 7.60 (dd, J = 8.4, 1.1 Hz, 1H), 4.45 (q, J = 7.1 Hz, 2H, CH_2), 4.22 (s, 3H, OCH_3), 1.60 (s, 15H, Cp*, CH_3), 1.41 (t, J = 7.1 Hz, 3H, $CH_2\underline{CH_3}$).

^{13}C NMR (126 MHz, d-DCM) δ (ppm) = 164.7 (CO), 162.9, 157.2, 152.7, 144.2, 141.0, 127.6, 123.3, 117.8, 111.7 (ArC), 89.9 (Cp*, tC), 63.2 (CH_2), 58.8 (OCH_3), 14.1 ($CH_2\underline{CH_3}$), 9.3 (Cp*,CH_3).

HRESI-MS: (+, 200V) m/z: $[M]^+$ 621.1481 (100%) calc. 621.1496.

IR ν_{max} (cm^{-1}): 3371 (broad peak), 3079, 2982, 2924 (w), 1726 (CO) (s), 1604 (m), 1573, 1557 (w), 1492 (s), 1457, 1432, 1387, 1369, 1337 (m), 1289, 1262, 1244 (s), 1183 (w), 1143, 1126, 1110, 1097, 1035 (m), 922, 858 (w), 810, 768, 744, 729 (m), 696 (w).

M.p.: 112 °C.

UV-Vis (MeCN) $\lambda_{max}(\varepsilon)$ (nm) = 313 sh (3320), 326 (4080), 341 (3640), 376 (900).

6.12.6 [(η^5-Pentamethylcyclopentadienyl)(4-ethoxycarbonyl-4′-methyl-2,2′-bipyridine) chloroiridium] chloride

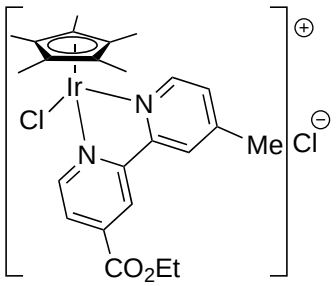

10f

According to the General Procedure F: 4-ethoxycarbonyl-4′-methyl-2-2′-bipyridine (43.6 mg, 0.180 mmol) in 1 mL DCM, $[IrCp^*Cl_2]_2$ (63.7 mg, 0.080 mmol), in 1 mL DCM for 1.5 days. After the reaction DCM was removed and water was added. The solution was filtered over celite to remove the excess ligand. After removal of water, product **10f** was obtained as yellow crystalline solid (108.5 mg, 0.165 mmol, > 99 %).

^{1}H NMR (700 MHz, d-DCM) δ (ppm) = 9.11 (dd, J = 5.8, 0.7 Hz, 1H), 8.96 (d, J = 1.3 Hz, 1H), 8.78 (d, J = 5.8 Hz, 1H), 8.59 (d, J = 1.7 Hz, 1H), 8.30 (dd, J = 5.8, 1.7 Hz, 1H), 7.73 − 7.71 (m, 1H), 4.53 (q, J = 7.1 Hz, 2H, $\underline{CH_2}CH_3$), 2.73 (s, 3H, CH_3), 1.74 (s, 15H, Cp*), 1.48 (t, J = 7.2 Hz, 3H, $CH_2\underline{CH_3}$)ppm.

^{13}C NMR (176 MHz, d-DCM) δ (ppm) = 163.4(CO), 157.1, 154.6, 154.0, 153.1, 151.4, 141.7, 130.9, 128.5, 126.1, 123.8 (ArC), 90.4 (Cp*, tC), 63.8 (CH_2), 21.8 (Ar-CH_3, 14.6 ($CH_2\underline{CH_3}$), 9.2 (Cp*, CH_3).

HRESI-MS: (+, 200V) *m/z*: $[M]^+$ 605.1598 (100%) calc. 605.1541.

IR ν_{max} (cm^{-1}): 3305, 2962, 2919 (m), 2161, 1979 (w), 1722 (s), 1619, 1556, 1476, 1449, 1406, 1385, 1366, 1321 (m), 1298, 1260, 1238 (s), 1210 (m), 1172 (w), 1110 (s), 921, 851 (m), 770, 756 (s), 722, 702, 666 (m).

M.p.: 95 °C.

UV-Vis (MeCN) $\lambda_{max}(\varepsilon)$ (nm) = 230 (16600), 304 (12200), 327 (sh), 367 (3640).

6.12.7 [(η^5-Pentamethylcyclopentadienyl)(4-ethoxycarbonyl-6′-methyl-2,2′-bipyridine) chloroiridium] chloride

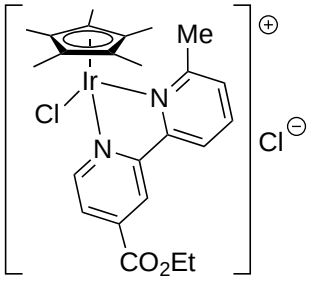

10g

According to the General Procedure F: 4-ethoxycarbonyl-6′-methyl-2-2′-bipyridine (38.8 mg, 0.160 mmol) in 1 mL DCM, $[IrCp^*Cl_2]_2$ (63.7 mg, 0.080 mmol), in 1 mL DCM for 2 days. After the reaction DCM was removed. Product **10g** was obtained as dark brown solid without further purification (101.8 mg, 0.159 mmol, 99%).

^{1}H NMR (500 MHz, d-DCM) δ (ppm) = 9.11 (d, J = 5.8 Hz, 1H), 8.90 (d, J = 1.7 Hz, 1H), 8.68 (dd, J = 8.0, 1.2 Hz, 1H), 8.28 − 8.22 (m, 2H), 7.80 (d, J = 7.7 Hz, 1H), 4.47 (q, J = 7.1 Hz, 2H, CH_2), 3.05 (s, 3H, Ar-CH_3), 1.53 (s, 15H, Cp*, CH_3), 1.43 (t, J = 7.1 Hz, 3H, $CH_2\underline{CH_3}$).

^{13}C NMR (126 MHz, d-DCM) δ (ppm) = 162.9, 162.9 157.4, 154.5, 153.6, 141.6, 141.0, 129.2, 127.5, 123.0, 122.4 (Ar), 89.8 (Cp*, tC), 63.2 (CH_2), 27.9 (Ar-CH_3), 14.1 ($CH_2\underline{CH_3}$), 9.0 (Cp*,CH_3).

HRESI-MS: (+, 200V) m/z: $[M]^+$ 605.1546 (100%) calc. 605.1547.

IR ν_{max} (cm^{-1}): 3377 (broad peak), 2981, 2926, 2367, 2341 (w), 1727 (s), 1607, 1558, 1482 (w), 1444, 1385 (m), 1329 (w), 1293, 1270 (s), 1235 (m), 1176 (w), 1133, 1111 (m), 1089 (w), 1024 (m), 949, 919, 861, 810 (w), 769 (m), 744, 719, 694, 680, 670, 661, 654 (w).

M.p.: decomposes > 220 °C.

UV-Vis (MeCN) $\lambda_{max}(\varepsilon)$ (nm) = 287 (4200), 312 (4340), 321 (4200), 335 (sh), 362 (1000).

6.12.8 [(η^5-Pentamethylcyclopentadienyl)(4′-tert-butyl-4-ethoxycarbonyl-2,2′-bipyridine) chloroiridium] chloride

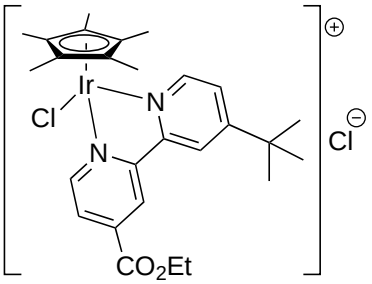

10h

According to the General Procedure F: 4′-*tert*-butyl-4-ethoxycarbonyl-2-2′-bipyridine (56.9 mg, 0.189 mmol) in 1 mL DCM, $[IrCp^*Cl_2]_2$ (67.1 mg, 0.084 mmol), in 1 mL DCM for 2 days. After the reaction DCM was removed and water was added. The solution was filtered over celite to remove the excess ligand. After removal of water, product **10h** was obtained as orange crystalline solid (114 mg, 0.167 mmol, 99 %).

^{1}H NMR (500 MHz, d-DCM) δ (ppm) = 9.16 (dd, J = 5.8, 0.7 Hz, 1H), 8.89 (d, J = 1.7 Hz, 1H), 8.83 (d, J = 6.0 Hz, 1H), 8.41 (d, J = 2.0 Hz, 1H), 8.33 (dd, J = 5.9, 1.7 Hz, 1H), 7.87 (dd, J = 6.0, 2.1 Hz, 1H), 4.51 (q, J = 7.1 Hz, 2H,CH_2), 1.73 (s, 15H, Cp*, CH_3), 1.47 (s, 9H, $C(CH_3)_3$), 1.45 (t, J = 7.2 Hz, 3H, $CH_2\underline{CH_3}$).

^{13}C NMR (126 MHz, d-DCM) δ (ppm) = 165.7 (CO), 163.0, 156.4, 154.2, 153.0, 151.3, 141.1, 128.2, 127.0, 123.0, 121.6 (ArC), 90.0 (Cp*, tC), 63.3 (CH_2), 35.9 $\underline{C}(CH_3)_3$, 30.2 $(CH_3)_3$, 14.1 $(CH_3)_3$), 8.7 (Cp*, CH_3).

HRESI-MS: (+, 200V) m/z: $[M]^+$ 647.2005 (100%) calc. 647.2016. IR ν_{max} (cm^{-1}): 3559, 3350 (broad peak), 3215, 3108 (w), 2963, 2914 (m), 2871, 2756, 2545, 2359, 2341, 1983 (w), 1725 (CO) (s), 1616 (m), 1556 (w), 1478, 1465 (m), 1407 (s), 1388, 1368, 1322 (m), 1303, 1263, 1240 (s), 1208, 1173 (w), 1147, 1132, 1123, 1113, 1047 (m), 1028 (s), 912 (w), 857 (m), 799 (w), 770, 728 (s), 697 (m), 667 (w).

M.p.: 119 °C.

UV-Vis (MeCN) $\lambda_{max}(\varepsilon)$ (nm) = 231 (23300), 300 (5200), 329 (sh), 353 (2200).

6.12.9 [(η^5-Pentamethylcyclopentadienyl)(4′-(tert-butyl)-N-(p-tolyl)-2,2′-bipyridine) chloroiridium] chloride

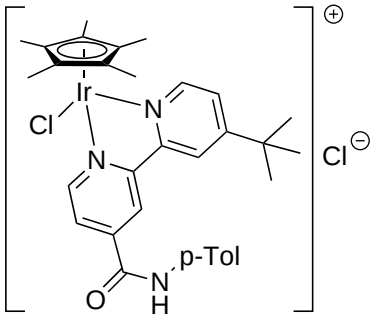

10i

According to the General Procedure F: 4′-(tert-butyl)-N-(p-tolyl)-2,2′-bipyridine-4-carboxamide **5i** (38.9 mg, 0.113mmol) in 1 mL DCM, $[IrCp^*Cl_2]_2$ (44.8 mg, 0.056mmol), in 1 mL DCM for 2 days. After the reaction DCM was removed and water was added. The solution was filtered over celite to remove the excess ligand. After removal of water, product **10i** was obtained as orange crystalline solid (83.0 mg, 0.112 mmol, 99 %).

^{1}H NMR (400 MHz, d-DCM) δ (ppm) = 11.98 (s, 1H, NH), 10.65 (s, 1H, Ar-1), 9.63 (d, J = 2.0 Hz, 1H, Ar-2), 8.84 (d, J = 5.9 Hz, 1H, Ar-1), 8.61 (dd, J = 6.0, 0.5 Hz, 1H, Ar-2), 8.46 (dd, J = 5.9, 1.8 Hz, 1H, Ar-1), 8.11 (d, J = 8.5 Hz, 2H, Ar-*p*-Tol), 7.64 (dd, J = 6.0, 2.0 Hz, 1H, Ar-2), 7.14 (d, J = 8.2 Hz, 2H, Ar-*p*-Tol), 2.32 (s, 3H, CH_3, *p*-Tol), 1.66 (s, 15H, Cp*, CH_3), 1.53 (s, 9H, $C(CH_3)_3$).

^{13}C NMR (126 MHz, d-DCM) δ (ppm) = 166.5 (CO), 160.8, 156.4, 155.4, 150.9, 150.0, 145.6, 136.4, 134.3, 129.0, 128.1, 125.5, 124.9, 123.6, 121.8 (ArC), 89.2 (Cp*, tC), 36.4 $\underline{C}(CH_3)_3$, 30.4 $(\underline{CH_3})_3$, 20.8 (CH_3, *p*-Tol), 8.6 (Cp*, CH_3).

HRESI-MS: (+, 200V) m/z: $[M]^+$ 708.2310 (100%) calc. 708.2333. IR ν_{max} (cm^{-1}): 3177, 3102 (w), 2959, 2922 (m), 2869, 2359, 2342 (w), 1662 (s), 1601 (m), 1536, 1512 (s), 1480, 1456 (m), 1405 (s), 1383 (m), 1323 (s), 1302 (m), 1258 (s), 1243, 1207, 1147, 1111, 1081 (m), 1027 (s), 926, 873, 847 (m), 819, 803, 751 (s), 723, 713, 699, 667 (m).

M.p.: decomposes > 260 °C.

UV-Vis (MeCN) $\lambda_{max}(\varepsilon)$ = 231 (25600), 299 (2340), 323 (1500), 358 (780) nm.

6.12.10 [(η^5-Pentamethylcyclopentadienyl)(6-amino-2,2′-bipyridine) chloroiridium] chloride

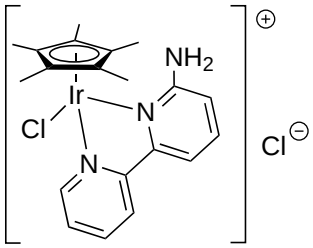

10j

According to the General Procedure F: 6-amino-2,2′-bipyridine ligand **5j** (36.0 mg, 0.21 mmol) in 1 mL DCM, $[IrCp^*Cl_2]_2$ (68.7 mg, 0.09 mmol), in 1 mL DCM for 2.5 days.The product precipitated from DCM and was filtered and dried under vacuum. Product **10j** was obtained as bright yellow solid (87.0 mg, 0.15 mmol, 83 %).

^{1} H NMR (700 MHz, MeOH-d4) δ (ppm) = 8.92 (ddd, J = 5.6, 1.4, 0.7 Hz, 1H), 8.41 (d, J = 8.0 Hz, 1H), 8.21 (ddd, J = 8.1, 7.6, 1.5 Hz, 1H), 7.83 (dd, J = 8.4, 7.4 Hz, 1H), 7.79 − 7.73 (m, 2H), 7.07 (dd, J = 8.4, 1.0 Hz, 1H), 1.63 (s, 15H, Cp*, CH_3).

^{13}C NMR (176 MHz, MeOH-d4) δ (ppm) = 160.3, 157.1, 152.0, 151.9, 140.0, 139.8, 127.5, 123.1, 113.6, 112.7 (ArC), 89.2 (Cp*, tC), 7.5 (Cp*, CH_3).

HRESI-MS: (+, 200V, m/z): $[M]^+$ 534.1293 (100%) calc. 534.1288.

IR ν_{max} (cm^{-1}): 3612, 3535, 3466, 3365, 3268, 3239, 3215, 3113, 3093, 3011 (w), 1634, 1604 (m), 1566 (w), 1492, 1469, 1449 (m), 1421, 1402, 1385 (w), 1314 (m), 1278, 1263, 1195, 1152, 1113, 1097, 1078, 1031, 1017, 992, 922, 909 (w), 817 (m), 790 (s), 753, 731 (w), 687 (m).

M.p.: decomposes > 220 °C.

UV-Vis (Acetonitrile) $\lambda_{max}(\varepsilon)$ = 235 (44200), 287 (1320), 369 (960), 403 (1560) nm.

6.12.11 [(η^5-Pentamethylcyclopentadienyl)(2,2′-bipyridine)(acetonitrile)iridium]bis-hexafluorophosphate

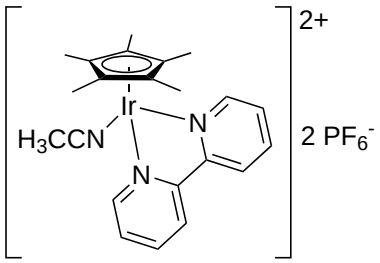

11a

AgPF6 (54.8 mg, 0.22 mmol) was weighed in a Schlenk tube in the glove box. Complex **10a** (60 mg, 0.11 mmol) was added and upon addition of 2 mL dry acetonitrile, white precipitate was immediately formed. The mixture was stirred overnight at 50 °C. The precipitate was filtered off under Ar atmosphere and the solution was concentrated. **11a** was recrystallized from the grey crude product by slow diffusion of Et_2O into a solution of MeCN. Product **11a** was obtained as white solid (54.2 mg, 0.07 mmol, 61 %).

^{1}H NMR (500 MHz, CD_3CN) δ (ppm) = 8.93 (ddd, J = 5.6, 1.4, 0.7 Hz, 2H), 8.52 (d, J = 8.2 Hz, 2H), 8.35 (td, J = 7.8, 1.2 Hz, 2H), 7.90 (ddd, J = 7.5, 5.7, 1.3 Hz, 2H), 1.68 (s, 15H).

^{13}C NMR (126 MHz, CD_3CN) δ (ppm) = 152.5, 141.8, 129.7, 124.8, 117.4, 92.5, 7.8.

HRESI-MS: (+, 200V) m/z: $[M]^{2+}$ 262.5921 (100%) calc. 262.5873.

IR ν_{max} (cm^{-1}): 3648, 3628, 3129, 3101, 3018, 2953 (w), 2359, 2342, 2314, 2287 (w, CN stretching), 1654, 1611, 1500, 1474, 1451, 1427, 1391, 1372, 1328, 1315, 1246, 1166, 1129, 1113, 1076, 1034 (w), 823, 767 (s), 741, 727, 668 (m).

6.13 Cyclic voltammetry

6.13.1 General description

Electrochemical experiments were performed using a potentiostat/galvanostat PGSTAT (*Metrohm*). The three-electrode system consisted of a glassy carbon working electrode 3.0 mm ID, 6.0 mm OD (*ALS*), a Pt wire counter electrode (*ALS*) and a $Ag/AgNO_3$ non aqueous reference electrode (10 mM $Ag/AgNO_3$, 0.1 M Bu_4NPF_6 in acetonitrile, 0.54 V *vs* NHE from *ALS*) in a one compartment cell. Electrodes were purchased from *C3 Prozess- und Analysentechnik GmbH*. Compounds **10a-10j** were added to the cell that was consecutively flushed with Ar for 5 min. Conditions: a. dry acetonitrile was added and Ar was bubbled through the solution for 5-10 min; b. the solution was saturated with CO2; c. 1 mL distilled water was added to the solution and it was saturated with Ar or CO_2. Saturation by gases was achieved by bubbling the corresponding gas through the solution for 10 minutes through a Teflon tube. The tube was then removed from the solution and fixed on the top to maintain the required atmosphere above the solution.

6.13.2 CVs of complex 10a

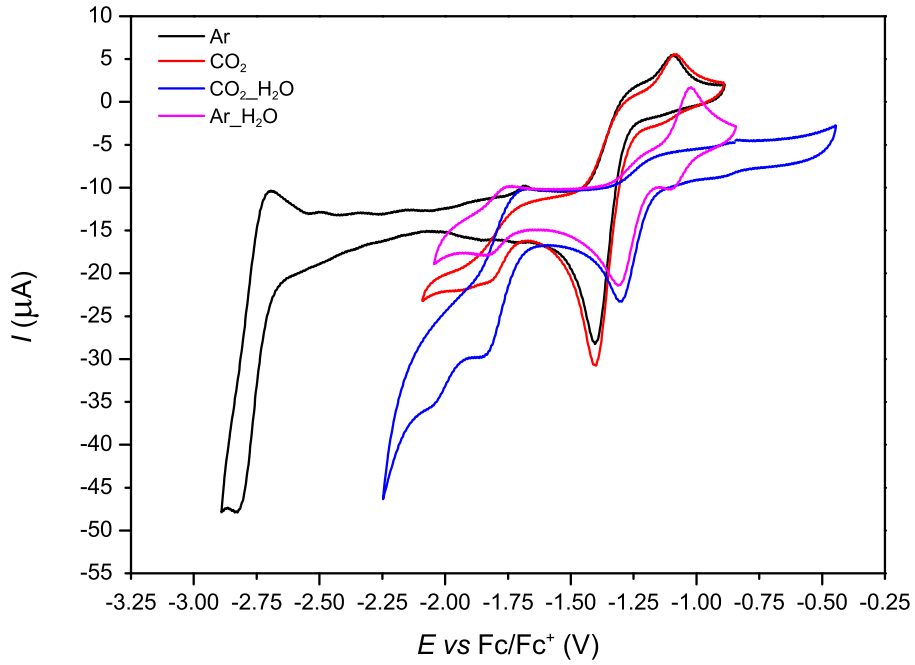

Figure 26: CVs under different conditions. Ar: Ar saturated MeCN; CO_2: CO_2 saturated MeCN; CO_2_H_2O: CO_2 saturated MeCN/H_2O (9:1, *v*/*v*); Ar_H_2O: Ar saturated MeCN/H_2O (9:1, *v*/*v*).

6.13.3 CVs of complex 10b

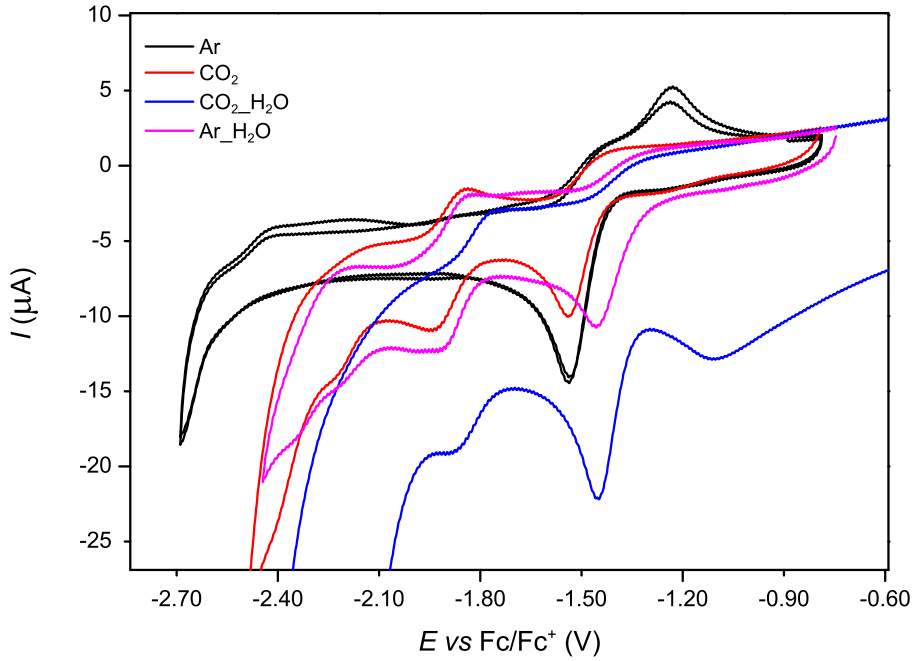

Figure 27: CVs under different conditions. Ar: Ar saturated MeCN; CO_2: CO_2 saturated MeCN; CO_2_H_2O: CO_2 saturated MeCN/H_2O (9:1, *v*/*v*); Ar_H_2O: Ar saturated MeCN/H_2O (9:1, *v*/*v*).

6.13.4 CVs of complex 10c

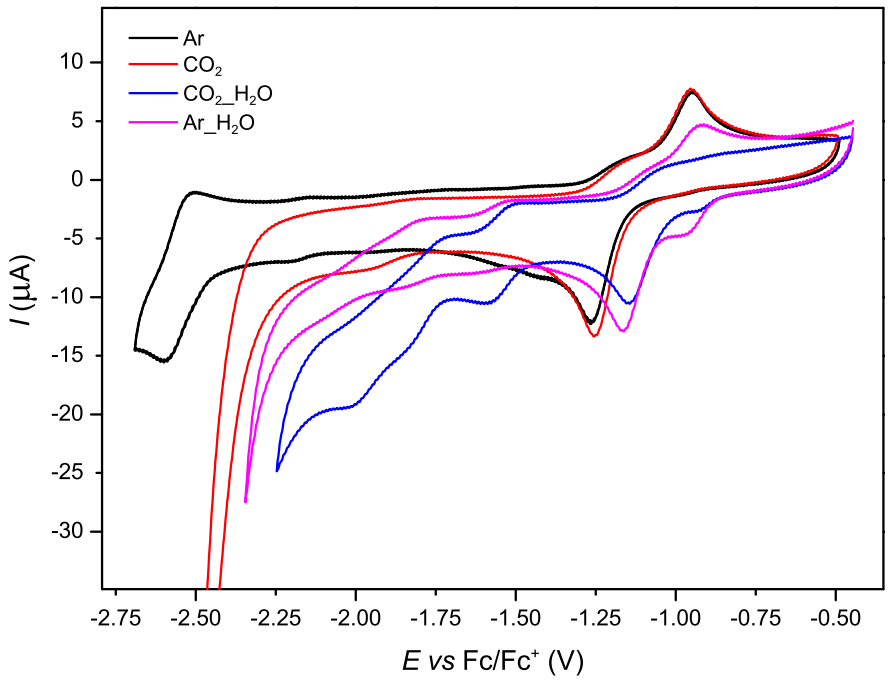

Figure 28: CVs under different conditions. Ar: Ar saturated MeCN; CO_2: CO_2 saturated MeCN; CO_2_H_2O: CO_2 saturated MeCN/H_2O (9:1, *v*/*v*); Ar_H_2O: Ar saturated MeCN/H_2O (9:1, *v*/*v*).

6.13.5 CVs of complex 10d

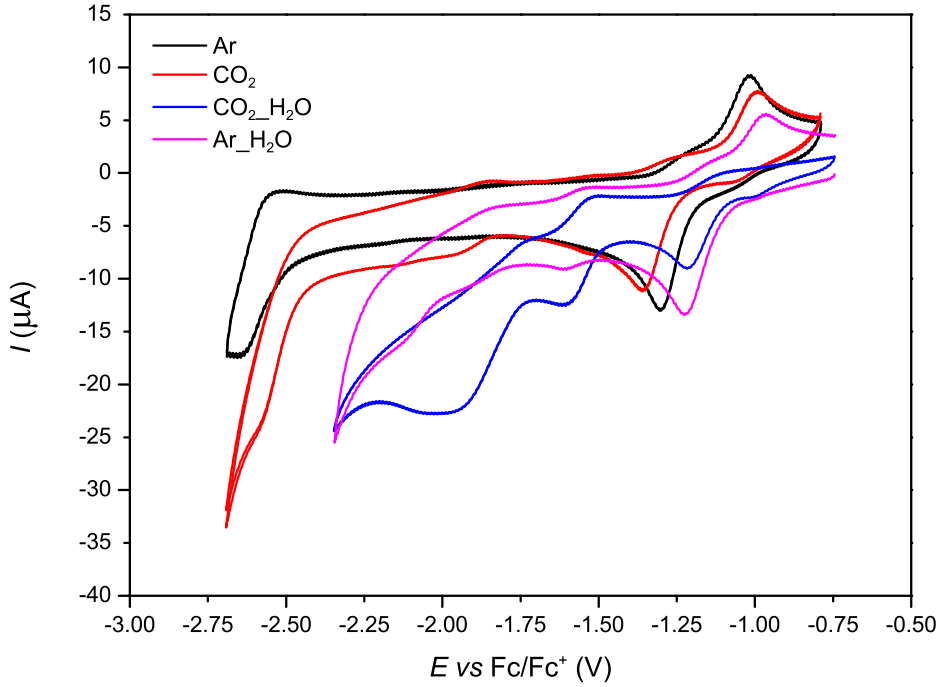

Figure 29: CVs under different conditions. Ar: Ar saturated MeCN; CO_2: CO_2 saturated MeCN; CO_2_H_2O: CO_2 saturated MeCN/H_2O (9:1, *v*/*v*); Ar_H_2O: Ar saturated MeCN/H_2O (9:1, *v*/*v*).

6.13.6 CVs of complex 10e

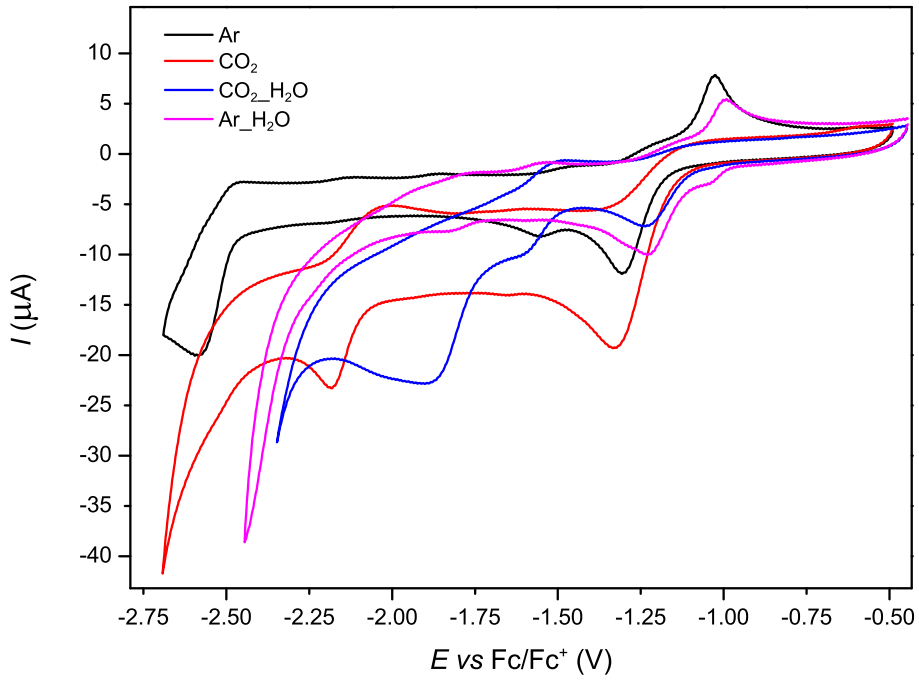

Figure 30: CVs under different conditions. Ar: Ar saturated MeCN; CO_2: CO_2 saturated MeCN; CO_2_H_2O: CO_2 saturated MeCN/H_2O (9:1, *v*/*v*); Ar_H_2O: Ar saturated MeCN/H_2O (9:1, *v*/*v*).

6.13.7 CVs of complex 10f

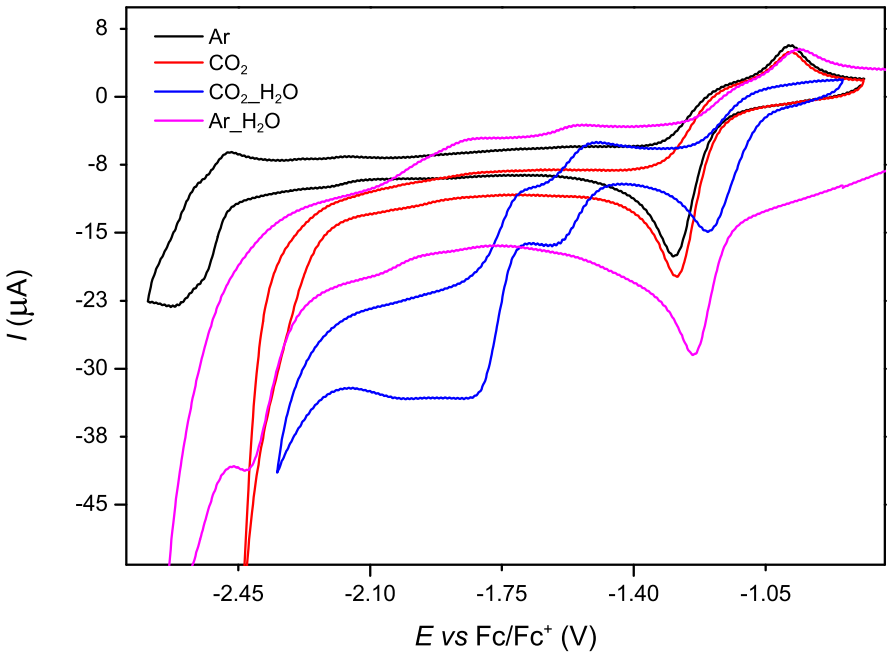

Figure 31: CVs under different conditions. Ar: Ar saturated MeCN; CO_2: CO_2 saturated MeCN; CO_2_H_2O: CO_2 saturated MeCN/H_2O (9:1, *v*/*v*); Ar_H_2O: Ar saturated MeCN/H_2O (9:1, *v*/*v*).

6.13.8 CVs of complex 10g

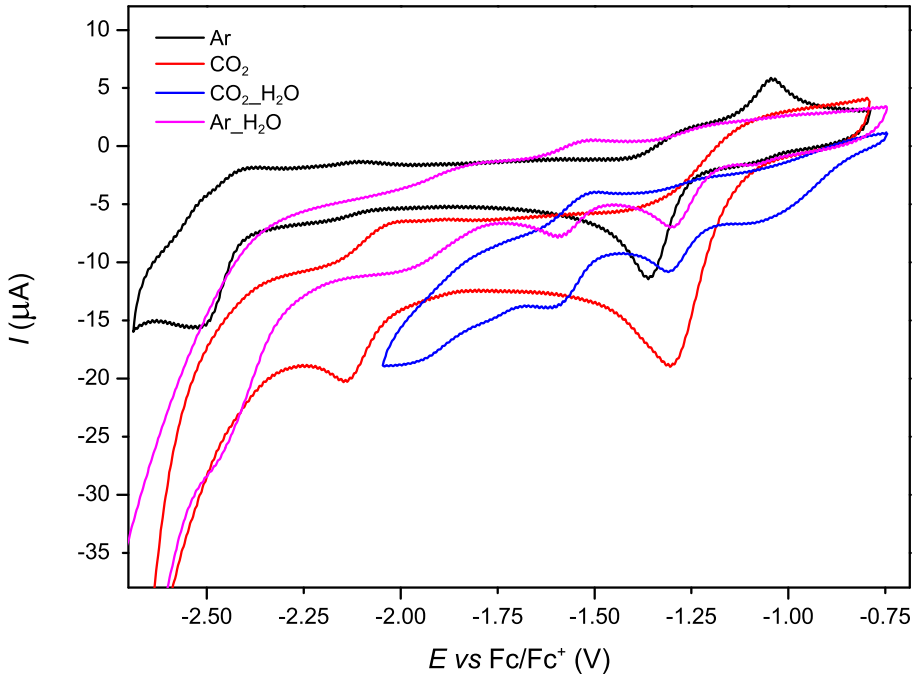

Figure 32: CVs under different conditions. Ar: Ar saturated MeCN; CO_2: CO_2 saturated MeCN; CO_2_H_2O: CO_2 saturated MeCN/H_2O (9:1, *v*/*v*); Ar_H_2O: Ar saturated MeCN/H_2O (9:1, *v*/*v*).

6.13.9 CVs of complex 10h

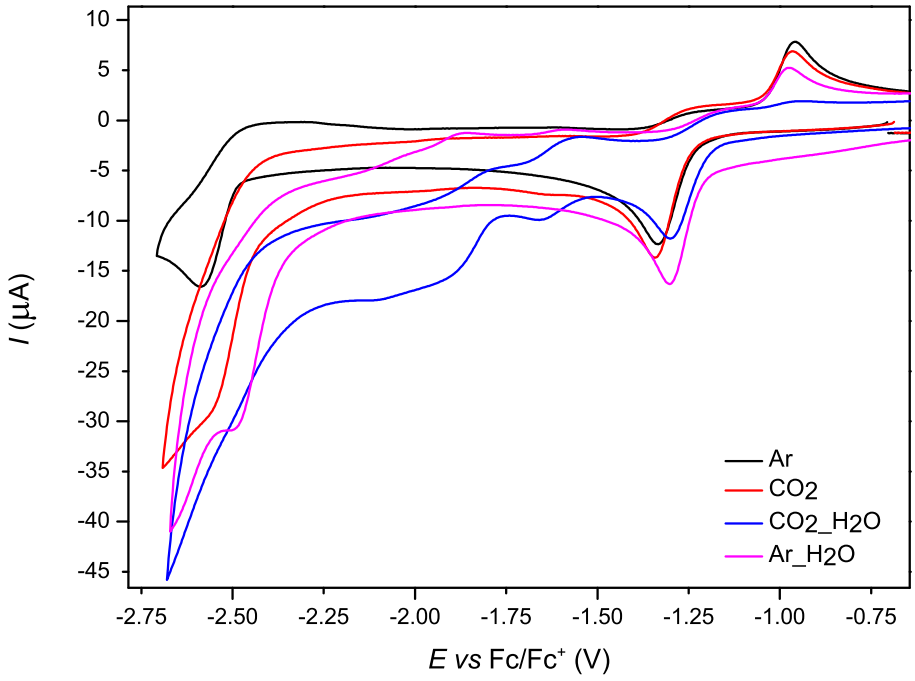

Figure 33: CVs under different conditions. Ar: Ar saturated MeCN; CO_2: CO_2 saturated MeCN; CO_2_H_2O: CO_2 saturated MeCN/H_2O (9:1, *v*/*v*); Ar_H_2O: Ar saturated MeCN/H_2O (9:1, *v*/*v*).

6.13.10 CVs of complex 10i

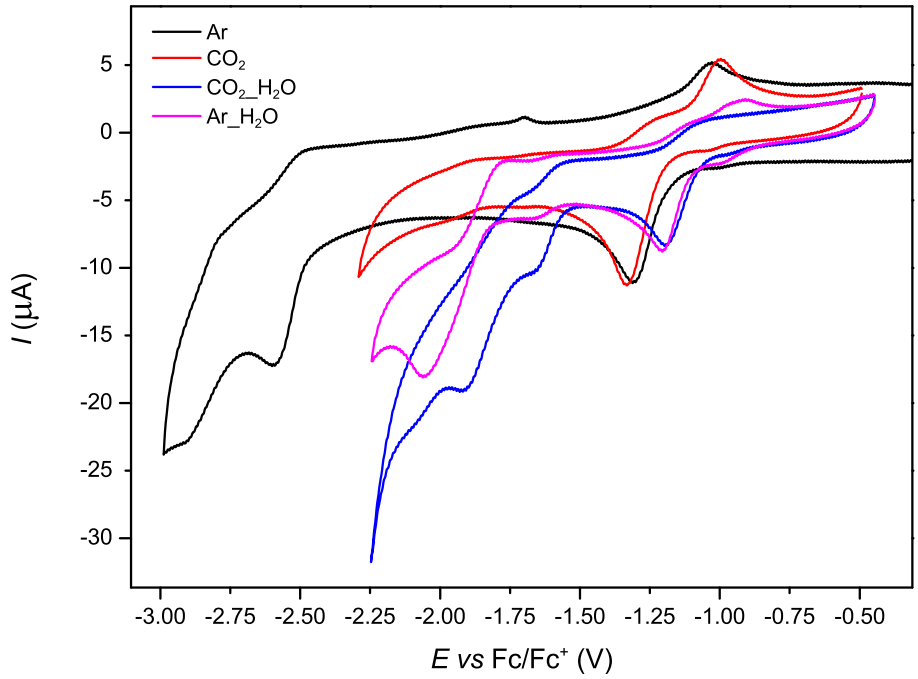

Figure 34: CVs under different conditions. Ar: Ar saturated MeCN; CO_2: CO_2 saturated MeCN; CO_2_H_2O: CO_2 saturated MeCN/H_2O (9:1, *v*/*v*); Ar_H_2O: Ar saturated MeCN/H_2O (9:1, *v*/*v*).

6.13.11 CVs of complex 10j

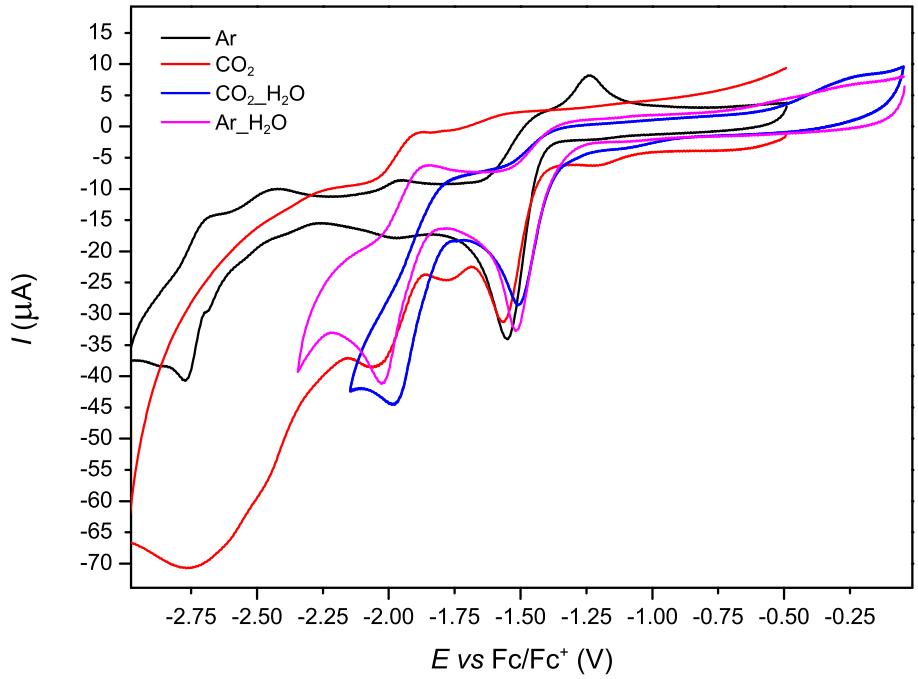

Figure 35: CVs under different conditions. Ar: Ar saturated MeCN; CO_2: CO_2 saturated MeCN; CO_2_H_2O: CO_2 saturated MeCN/H_2O (9:1, *v*/*v*); Ar_H_2O: Ar saturated MeCN/H_2O (9:1, *v*/*v*).

6.14 Electrolysis experiments

6.14.1 Electrolysis cell parameters

Table 11: Main properties of the two cell types.

Property	Cell type 1	Cell type 2
Material	glass	Teflon
V_{tot} (mL)	1.2	1.5
Membrane	Nafion N324	Nafion N324
WE	GC, 25×25×3 mm	GC, 25×25×3 mm
RE	Ag wire	Ag/AgCl LF-2, d = 2 mm
CE	Pt sheet	GC, 25×25×3 mm
Seal	Teflon	FKM O-ring 12.5×3 mm
A (cm^2)	1.19	1.19
A/V_{tot} (cm^2/mL)	1.0	0.76
Top seal	rubber septa NS 5	rubber septa NS 5
Used in	optimization experiments	catalyst screening

6.14.2 Optimization experiments

Optimization experiments were performed using a potentiostat PhSTAT302N (*Metrohm*) or potentiostat/galvanostat PGSTAT (*Metrohm*) in a gas-tight two-compartment cell (cell type 1) separated by Nafion membrane N324 (purchased from *Ion Power, GmbH*). The three electrode system consisted of glassy carbon plate working and counter electrodes 25x25x3 mm (*HTW GmbH*) and Ag wire reference electrode (*ALS Accessories*). The counter electrode was separated from the working and reference electrodes. The total volume of each compartment was 1.2 mL. The surface of glassy carbon working electrode exposed to the solution during catalysis was 1.19 cm^2. The GC and Pt electrodes were washed with *cc*HNO_3 between the measurements.

A solution of catalyst ($c_{\mathrm{Ir}} = 1.3$ mM), conductive salt and additive in the investigated solvent mixture were degassed (3x) and saturated with CO_2. (When $AgPF_6$ was used as additive, precipitate was observed at the bottom of the flask and the solution was taken from above the solid.) The electrolysis cell was flushed with CO_2 and the cell compartments were closed with septa. Catalyst solutions were filled to the cell compartments with a syringe. The reference electrode was placed into the cathodic cell solution through the septum. The electrolysis potential (E_{app}) was set at a PGSTAT (Metrohm) potentiostat and the reaction was run for $t = 3$ h. After electrolysis, samples from both half cells (0.7 mL) were taken with a syringe and ^{1}H NMR samples were prepared with a known amount of *p*-xylene standard (50 μL of a 10 mL dilution in MeCN of typically 10-12 mg *p*-xylene). HCO_2H and HCHO amounts were determined as given below.

$$n_{\mathrm{HCO_2H}} = \frac{Int_{\mathrm{HCO_2H}}}{Int_{\mathrm{pxyl}}} \cdot 4 \cdot n_{\mathrm{pxyl}} \cdot \frac{V_{\mathrm{tot}}}{V_{\mathrm{NMR}}} \ (\mu\mathrm{mol}) \tag{20}$$

$$n_{\mathrm{HCHO}} = \frac{Int_{\mathrm{HCHO}}}{Int_{\mathrm{pxyl}}} \cdot 2 \cdot n_{\mathrm{pxyl}} \cdot \frac{V_{\mathrm{tot}}}{V_{\mathrm{NMR}}} \ (\mu\mathrm{mol}) \tag{21}$$

6.14.3 Product analysis

6.14.3.1 Gas analysis To quantify CO and H_2 evolved during the electrocatalysis, the reaction mixtures were transferred from the electrochemical cell to a small glass tube (3.2 mL) sealed with a septum *via* a syringe. After equilibration between the gases dissolved in the solvent and in headspace above the solution was established, 250 μL gas from the headspace were injected in a gas chromatograph (*Shimadzu GC-17A* with thermal conductivity detector and *Resteks ShinCarbon* packed column ST 80/100 (2 m, 1/8″ OD, 2 mm ID)) and CO or H_2 were quantified using calibration curves. The measurement errors for the amount of CO and H_2 are estimated to be 2% and 10%, respectively not considering loss of gas *via* withdrawal of the samples from the electrolysis cell. CO and H_2 dissolved in the solvent were not considered, thus, the TON of CO or H_2 are only related to the amount detected in the gas phase above the solution. Furthermore, electrocatalytic experiments were done without the catalyst, but under the same conditions. There, a small amount of CO, but no H_2, could be detected. The given TON of CO were then corrected by these values.

6.14.3.2 Formaldehyde analysis From the electrolysis reaction mixture in the cathodic half cell 0.5 mL sample was taken. The formaldehyde amount in the sample was known from the ^{1}H

NMR integration with *p*-xylene as internal standard. Milli-Q water was added and the precipitated Bu_4NPF_6 was filtered off. This was repeated until no more precipitation was observed (up to 2.5 mL H_2O). Afterwards, 5 equivalents of DNPH reagent was added in the form of the following solution: c_{DNPH} = 0.02 M, c_{HCl} = 2.0 M in aqueous solution. The mixture was shaken after the addition of the orange reagent. A yellow colour indicating product formation was not observed because of the low concentration of the formaldehyde in the sample. Ammonia in MeOH (7.0 M) was added to neutralize the solution. The product was extracted with 1 mL toluene. Samples were taken from the toluene phase and injected to the GC-MS. Results were compared with those in the *Varian* MS library.

The dependence of the HCHO formation on the presence of water as possible impurity in MeCN was also investigated. However, HCHO was not observed when 1, 3 and 5% H_2O was added to the 1:1 mixture of MeOH/MeCN. The stock solutions were prepared from 2.96 mg of **10a**, 38.7 mg Bu_4NPF_6, and 4 mL solvent containing 1. 1980 μL MeCN, 1980 μL MeOH and 40 μL H_2O; 2. 1940 μL MeCN, 1940 μL MeOH and 120 μL H_2O; 3. 1900 μL MeCN, 1900 μL MeOH and 200 μL H_2O.

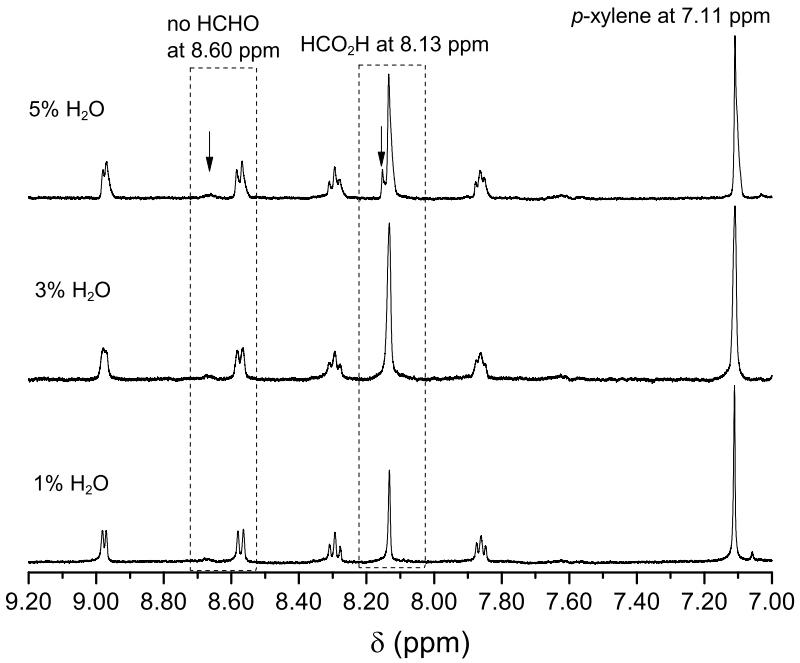

Figure 36: ^{1}H NMR spectra of the reaction mixture taken from the cathodic half cell after electrolysis for t = 2 h at E_{app} = −1.80 V *vs* Ag/AgCl. Conditions: c_{Ir} = 1.3 mM, V_{tot} = 1.5 mL, solvent mixture: MeOH/MeCN/H_2O 1:1:y, v/v, where y is the amount of added water.

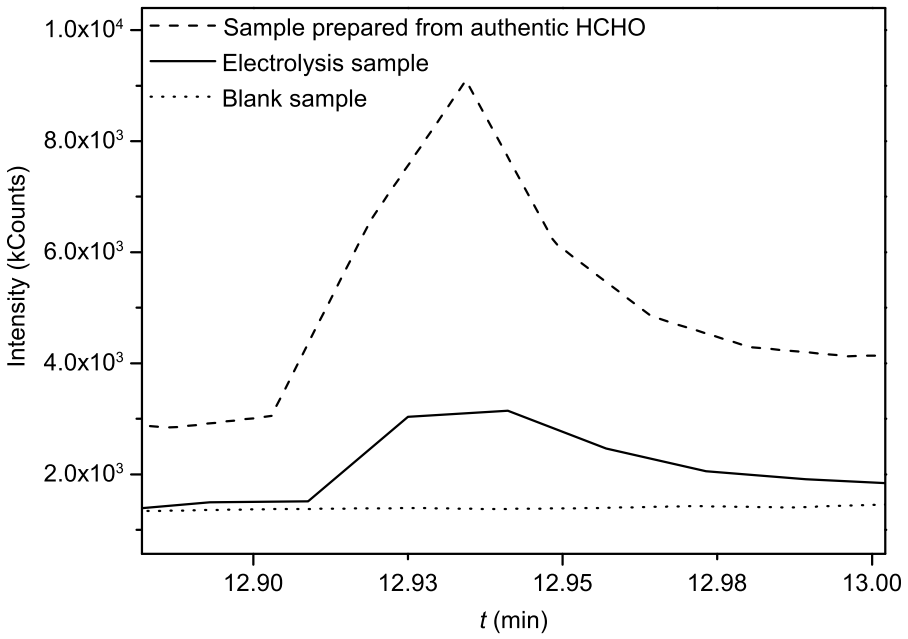

Figure 37: Gas chromatograms of **18** from a sample prepared from authentic formaldehyde; an electrolysis sample; and a blank sample with electrolyte solution.

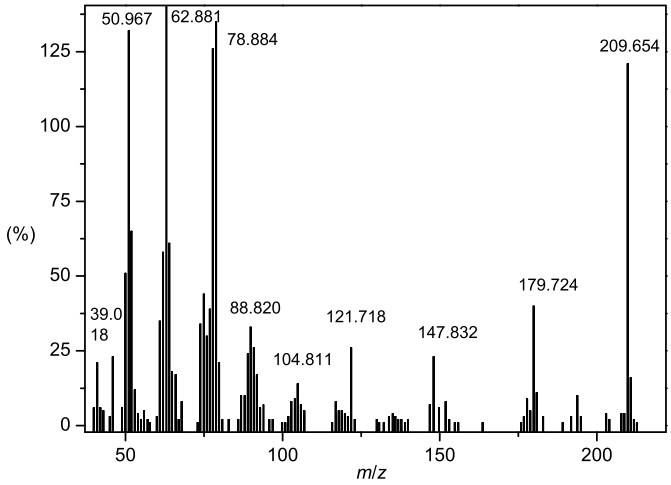

(a) sample prepared from electrolysis solution

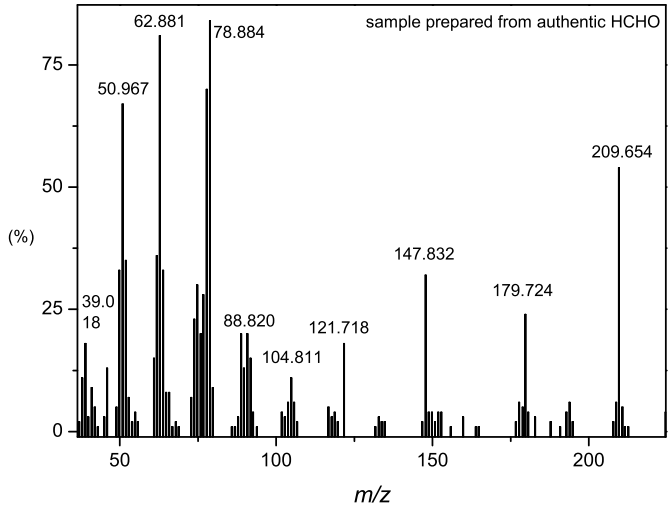

(b) sample prepared from authentic HCHO

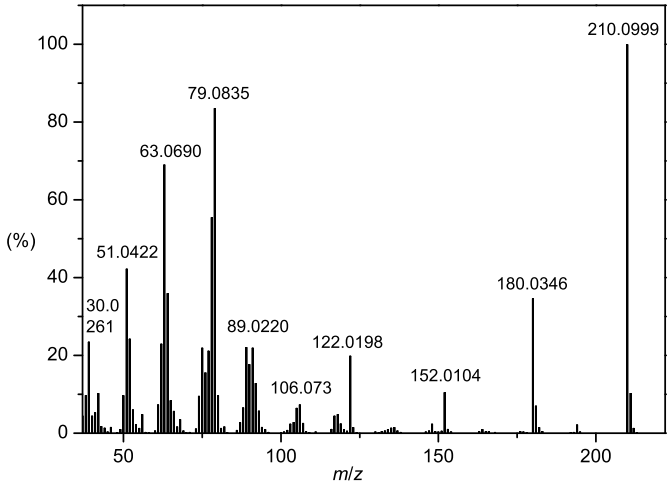

(c) spectrum obtained from the *Varian* MS library

Figure 38: The mass spectrum obtained of **18** prepared from (a) the electrolysis solution, (b) authentic HCHO and (c) obtained from the *Varian* MS library.

6.14.4 Catalyst screening experiments

Electrolysis experiments were performed using a potentiostat PhSTAT302N (*Metrohm*) or potentiostat/galvanostat PGSTAT (*Metrohm*) in a gas-tight two-compartment cell (cell type 2) separated by Nafion membrane N324 (purchased from *Ion Power, GmbH*). The three electrode system consisted of glassy carbon plate working and counter electrodes 25x25x3 mm (*HTW GmbH*) and Ag/AgCl leak free reference electrode LF-1-65-T, 1 mm OD, 63-66mm total length 40-43 mm long barrel (*Innovative Instruments Inc.*). The counter electrode was separated from the working and reference electrodes. The total volume of each compartment was 1.5 mL. The surface of glassy carbon working electrode exposed to the solution during catalysis was 1.19 cm^2. The GC electrodes were washed with organic solvent and polished with polishing cloth between the measurements.

A solution of catalyst (c_{Ir} = 1.399 mM) and conductive salt ($c_{\mathrm{Bu_4NPF_6}}$ = 25.0 mM) in MeCN/MeOH 1:1, v/v were degassed (3x) and saturated with CO_2. The electrolysis cell was flushed with CO_2 and the cell compartments were closed with septa. Catalyst solutions were filled to the cell compartments with a syringe. The reference electrode was placed into the cathodic cell solution through the septum. The potential $E_{\mathrm{app}} = -1.80$ V was set at a PGSTAT (Metrohm) potentiostat and the reaction was run for t = 5 or 15 h at rt. After electrolysis, samples from both half cells (0.7 mL) were taken with a syringe and ^{1}H NMR samples were prepared with a known amount of *p*-xylene standard (50 μL of a 10 mL dilution in MeCN of typically 10-12 mg *p*-xylene). HCO_2H concentrations were determined as given below.

$$n_{(-/+)} = \frac{Int_{\mathrm{HCO_2H}}}{Int_{\mathrm{xyl}}} \cdot 4 \cdot c_{\mathrm{xyl}} \cdot V_{\mathrm{xyl}}\ (\mu\mathrm{mol}) \tag{22}$$

$$c_{\mathrm{tot}} = \frac{n_{(-)} + n_{(+)}}{V_{\mathrm{NMR(-)}} + V_{\mathrm{NMR(+)}}}\ (\mu\mathrm{mol} \cdot \mathrm{mL}^{-1}) \tag{23}$$

In the following, data for the determination of TOFs from the experiments conducted for t = 5 and 15 h are presented, as well as current efficiencies of experiments stopped at t = 15 h. Conditions: $E_{\mathrm{app}} = -1.80$ *vs* Ag/AgCl, c_{Ir} = 1.399 mM, V_{tot} = 1.5 mL, solvent: MeCN/MeOH 1:1, v/v, at r.t.

Table 12: Summary of HCO_2H concentrations obtained from the electrolysis experiments conducted for $t = 5$ and 15 h and the corresponding total charge determined from the time-current graphs.

	c_{tot}(i) (μmol·mL^{-1})				Q_i (C)			
	$t = 5$ h		$t = 15$ h		$t = 5$ h		$t = 15$ h	
Complex	c_1	c_2	c_3	c_4	Q_1	Q_2	Q_3	Q_4
10a	3.95	1.85	8.86	7.54	-9.44	-6.21	-18.38	-13.57
10b	3.88	3.62	10.95	12.66	-8.18	-9.42	-15.21	-35.99
10c	5.06	5.65	15.88	14.92	-29.02	-23.18	-67.3	-65.67
10d	4.19	5.31	19.54	18.23	-14.62	-20.80	-49.93	-47.41
10e	3.68[a]	4.74	23.07	18.83	-7.67[a]	-13.52	-48.20	-37.21
10f	6.10	5.41	17.21	21.37	-20.21	-16.80	-58.61	-52.64
10g	7.71	8.76	20.47	19.47	-18.97	-21.84	-61.88	-52.36
10h	6.32	5.25	11.53	17.77	-14.2	-12.73	-36.90	-36.19
10i	7.24	7.15	21.30	19.38	-18.19	-15.72	-50.87	-57.35
10j	6.40	5.29	14.33	20.54	-21.65	-19.09	-76.08	-51.52

[a] measurement was stopped at $t = 3$ h.

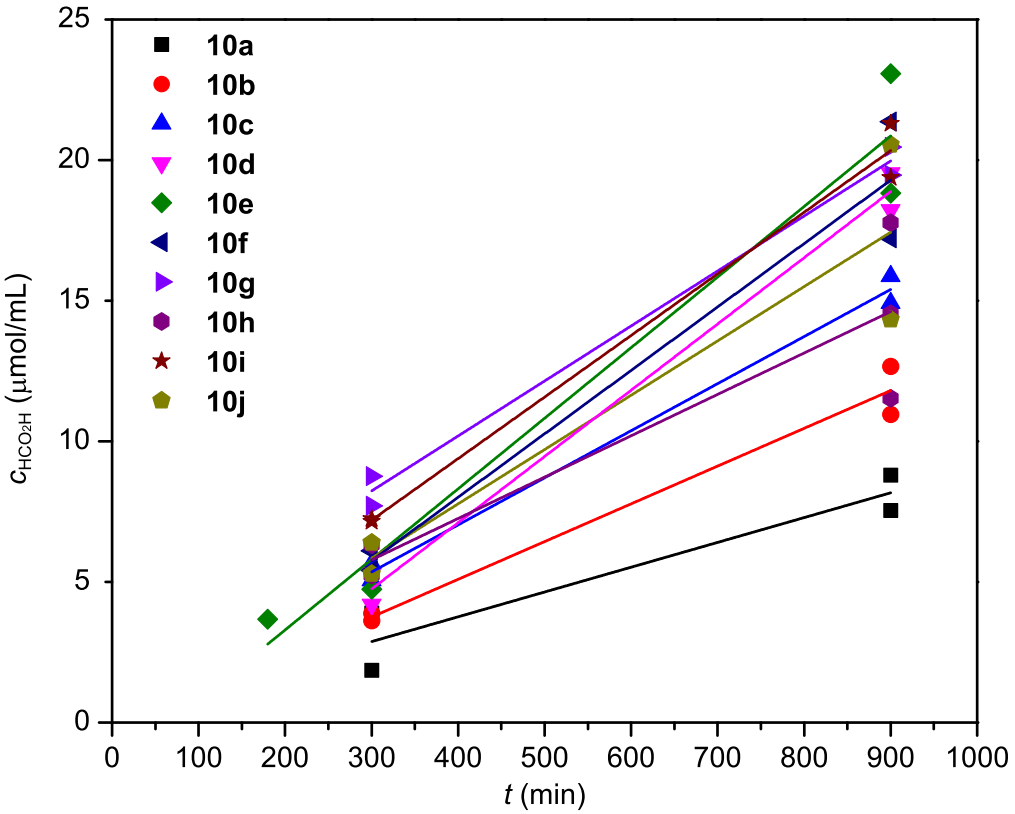

Figure 39: Linear fits on the four concentration data points (see values in Table 12) obtained in duplicates from experiments conducted for $t = 5$ and 15 h.

Table 13: TOFs of complexes **10a** - **10j**.

Complex	data points	$\Delta c_{tot}/\Delta t \cdot 10^2$ (μmol·mL^{-1}·min^{-1})	$(\Delta c_{tot}/\Delta t)_{er} \cdot 10^2$	TOF·10^2 ± TOF$_{er}$ · 10^2 (min^{-1})
10a	4	0.88	0.20	0.63 ± 0.14
10b	4	1.34	0.14	0.96 ± 0.10
10c	4	1.67	0.09	1.20 ± 0.07
10d	4	2.36	0.14	1.68 ± 0.10
10e	4	2.51	0.35	1.79 ± 0.25
10f	10	1.99	0.09	1.42 ± 0.07
10g	4	1.96	0.12	1.40 ± 0.09
10h	4	1.48	0.53	1.05 ± 0.38
10i	4	2.19	0.16	1.57 ± 0.12
10j	10	1.63	0.07	1.16 ± 0.05

Table 14: TONs and current efficiencies of complexes **10a** - **10j**.

Complex	Measurement 1			Measurement 2		
	TON_{NMR}	TON_{el}	η (%)	TON_{NMR}	TON_{el}	η (%)
10a	6.3	45.4	14.0	5.4	33.5	16.1
10b	7.8	37.6	20.8	9.1	88.9	10.2
10c	11.4	165.4	6.9	10.7	162.0	6.6
10d	14.0	123.4	11.3	13.0	117.2	11.1
10e	16.5	119.2	13.9	13.5	92.0	14.7
10f	12.3	130.0	9.5	15.3	144.9	10.6
10g	14.7	153.0	9.6	13.9	129.5	10.8
10h	8.3	91.1	9.1	12.7	89.4	14.2
10i	15.2	125.7	12.1	13.9	141.7	9.8
10j	15.4	133.4	11.5	10.7	197.0	5.5

Calculations for Table 14 are according to the following equations:

$$\mathrm{TON_{NMR}} = \frac{c_{\mathrm{tot}}}{c_{\mathrm{Ir}}} \tag{24}$$

$$\mathrm{TON_{el}} = \frac{Q}{2 \times F \times c_{\mathrm{Ir}} \times V_{\mathrm{tot}}} \tag{25}$$

$$\eta = \frac{\mathrm{TON_{NMR}}}{\mathrm{TON_{el}}} \times 100\ (\%) \tag{26}$$

6.14.5 Attempts to prepare the Ir−H compounds

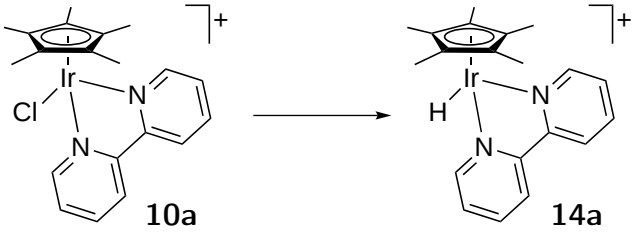

Table 15: Attempts to prepare Ir−H species **14**.

Entry	Solvent	Reagent 1	Reagent 2	Temperature (°C)	Product
1	THF	$AgPF_6$	Red-Al	70	no
2	THF	–	Red-Al	50	no
3	MeCN, THF	–	Red-Al	rt	no
4	H_2O	$AgPF_6$	HCO_2NH_4	70	no
5	DCM	$AgPF_6$	H_2, 20 bar	rt	no
6[a]	MeOH, H_2O	–	$NaBH_3CN$	rt	yes

Procedure also tested using compound **10d** as starting material.

Procedure, entry 1: [Cp*Ir(bpy)Cl]Cl (25.0 mg, 1 eq.) was added to $AgPF_6$ (35.0 mg, 3 eq.) and under an Ar atmosphere 1.7 mL dry THF was added. The Ir complex slowly dissolved at 70°C in 30-45 min. The mixture became a dark brown slurry upon heating. Upon addition of 20 μL Red-Al (70 w/w% in toluene, 1.5 eq.) the mixture turned violet and then immedaiately black. After evaporation of the volatiles the insoluble black residue was not analyzed.

Procedure, entry 2: [Cp*Ir(bpy)Cl]Cl (50.0 mg, 1 eq.) was dissolved in dry THF. 25 μL Red-Al (70 w/w% in toluene, 1.0 eq.) was added and the mixture was heated to 50°C. After 3 h reaction time the light yellow solution contained some white precipitate. The solid was filtered off and from both residues samples were taken for ^{1}H NMR measurements. Product **14** was not observed.

Procedure, entry 3: [Cp*Ir(bpy)Cl]Cl (17.3 mg, 1 eq.) was dissolved in a MeCN/THF mixture (5 mL). Upon addition of 8.6 μL Red-Al, the mixture turned immediately black and then slowly to dark red. After 45 min stirring the solvents were evaporated and the solid was washed with dry THF. The orange solid was analyzed by ^{1}H NMR and ESI-MS measurements, but no hydride formation was observed.

Procedure, entry 4: [Cp*Ir(bpy)Cl]Cl (25.0 mg, 1 eq.) was added to $AgPF_6$ (23.0 mg, 2 eq.) and under an Ar atmosphere 3 mL H_2O was added. The mixture was heated overnight at 70°C after which grey precipitate was observed in a bright yellow solution. The precipitate was filtered off over celite and the solvent was evaporated. The light yellow solid was dried under vacuum overnight. The solid was dissolved in 3 mL H_2O and the mixture was heated to 70°C. HCO_2NH_4 (1.3 g, 20 mmol, 444 eq.) in 10 mL H_2O was slowly added upon which the solution became darker and black precipitate formed. The mixture was cooled down in an ice bath to precipitate the formed product and the solid was filtered off under Ar. The black solid residue was washed with $CHCl_3$ to obtain an orange solution. After evaporation of $CHCl_3$, the orange solid was analyzed by ^{1}H NMR and ESI-MS, but no product was observed.

Procedure, entry 5: in a 10 mL reaction vial [Cp*Ir(bpy)Cl]Cl (10.0 mg, 1 eq.) was add to $AgPF_6$ (9.8 mg, 2.2 eq.) in the glove box. In a Schlenk tube lutidine (1.93 mg, 1 eq.) was flushed with Ar and 3 mL dry DCM was added. The reaction vial with the complex/$AgPF_6$ mixture was placed in the autoclave and the cap was removed to add the lutidine solution under Ar flow. The autoclave was closed hand tight, flushed with Ar and transferred to the high pressure lab. The autoclave was closed pressure tight and 20 bar H_2 was added. After 3 h of stirring at rt, the pressure was released and the autoclave was flushed with Ar. The dark brown reaction mixture was transferred to a Schlenk tube and the solvent was evaporated. The ^{1}H NMR of the crude showed no ligand peaks in D_2O. d-MeCN was added and the slurry was filtered under Ar. The ^{1}H NMR of the filtrate contained ligand peaks, but the hydride peak was not observed.

Procedure, entry 6: in a 25 mL Schlenk flask, Ir complex (0.036 mmol, 1 eq.) was dissolved in a mixture of MeOH and H_2O. The solution was degassed and saturated with Ar. $NaBH_3CN$ (11.3 mg, 0.18 mmol, 5 eq.) was added and the mixture was stirred at rt for 38 h. After the reaction, the homogeneous solution was concentrated to about 1 mL of aqueous solution, to which saturated

KPF_6 solutions was added to precipitate the product. The solid was filtered under air and washed with Et_2O. The product was dried in *vacuo* and analyzed.

[(η^5-Pentamethylcyclopentadienyl)(2,2′-bipyridine) hydridoiridium] hexafluorophosphate 14a was prepared as given in "Procedure, entry 6" starting from **10a** (20 mg). Approximetly 15 mg yellow powder was obtained and characterized by ^{1}H NMR and ESI-MS. The solid was air-stable and soluble in DCM, MeOH, acetone. It was insoluble in H_2O and Et_2O. The complex decomposed in MeCN.

^{1}H NMR (500 MHz, Methanol-d4) δ (ppm) = 9.12 (d, J = 5.6 Hz, 1H), 9.09 (d, J = 5.7 Hz, 1H), 8.99 (d, J = 5.7 Hz, 1H), 8.72 (d, J = 7.9 Hz, 1H), 8.69 (d, J = 8.1 Hz, 1H), 8.64 (d, J = 8.1 Hz, 1H), 8.39 − 8.34 (m, 2H), 8.34 − 8.29 (m, 1H), 7.92 − 7.83 (m, 2H), 1.86 (s, 5H), 1.75 (s, 5H), 1.74 (s, 5H), −10.65 (m, 1H).

HRESI-MS: (+, 200V) m/z: $[M]^+$ 485.1599 (100%) calc. 485.1569.

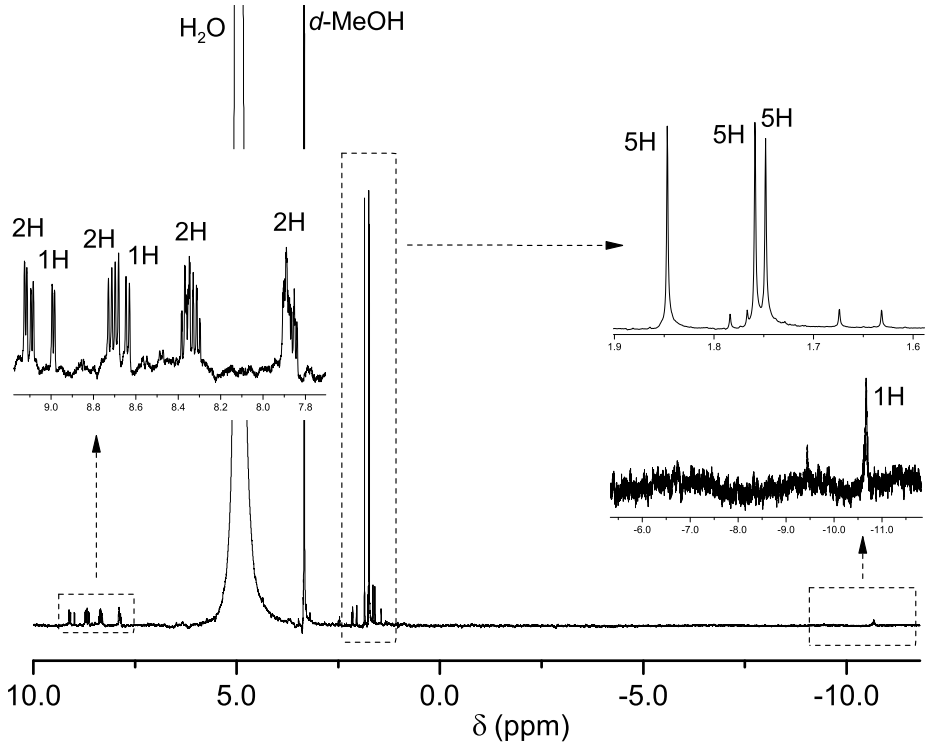

Figure 40: ^{1}H NMR spectrum of the formed product in procedure, enrty 6 in Table 15 starting from complex **10a**.

[(η^5-Pentamethylcyclopentadienyl)(4-ethoxycarbonyl-4′-methoxy-2,2′-bipyridine) hydridoiridium] hexafluorophosphate 14d was prepared as given in "Procedure, entry 6" starting from

10d (23.6 mg). Approximetly 15 mg dark red powder was obtained and characterized by ^{1}H NMR and ESI-MS. The solid was air-stable and soluble in DCM, MeOH, acetone. It was insoluble in H_2O and Et_2O. The complex decomposed in MeCN.

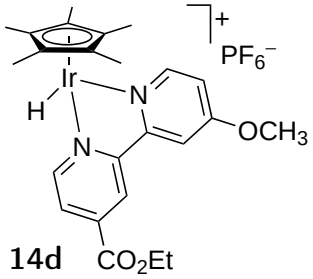

^{1}H NMR (500 MHz, Methanol-d4+drops od d-acetone) δ (ppm) = 9.25 (d, J = 5.9 Hz, 1H), 9.09 (d, J = 1.3 Hz, 1H), 8.89 (d, J = 6.6 Hz, 1H), 8.37 (d, J = 2.7 Hz, 1H), 8.28 (dd, J = 5.8, 1.7 Hz, 1H), 7.45 (dd, J = 6.6, 2.8 Hz, 1H), 3.60 (q, J = 7.1 Hz, 2H), 2.10 (m, 9H, CH_2CH_3+d-acetone) 1.73 (s, 15H), -10.24 (s, 1H).

HRESI-MS: (+, 200V) m/z: $[M]^+$ 587.1961 (100%) calc. 587.1880.

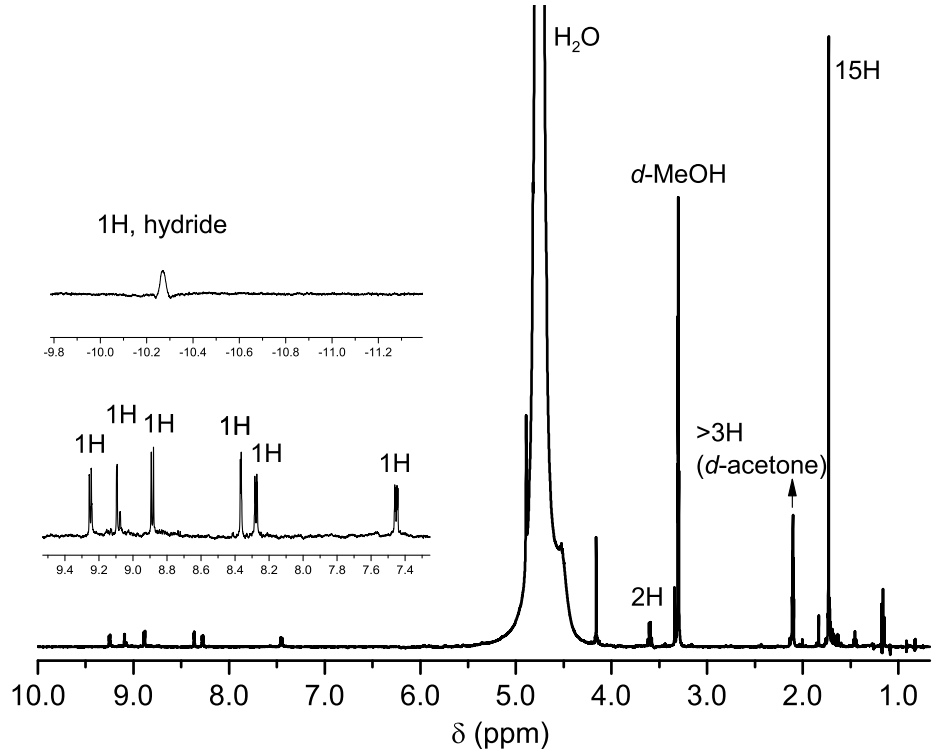

Figure 41: ^{1}H NMR spectrum of the formed product in procedure, entry 6 in Table 15 starting from complex **10d**.

6.14.5.1 CVs and DPVs of 10d and 14d Due to decomposition of **14a** and **14d** in MeCN solvent, DPVs of **10d** and **14d** were recorded in MeOH/THF, 1:1, v/v in the presence of Bu_4NPF_6 conductive salt (0.1 M) between $E = 0.00$ and -1.40 V *vs* $Ag/AgNO_3$. At $E = -1.40$ V solvent decomposition was observed. CVs were recorded with 100 mV/s scan rate. In Ar and CO_2 saturated MeOH/THF, 1:1, v/v, $E_{Fc/Fc^+} = 0.13$ V and 0.12 V *vs* $Ag/AgNO_3$, respectively.

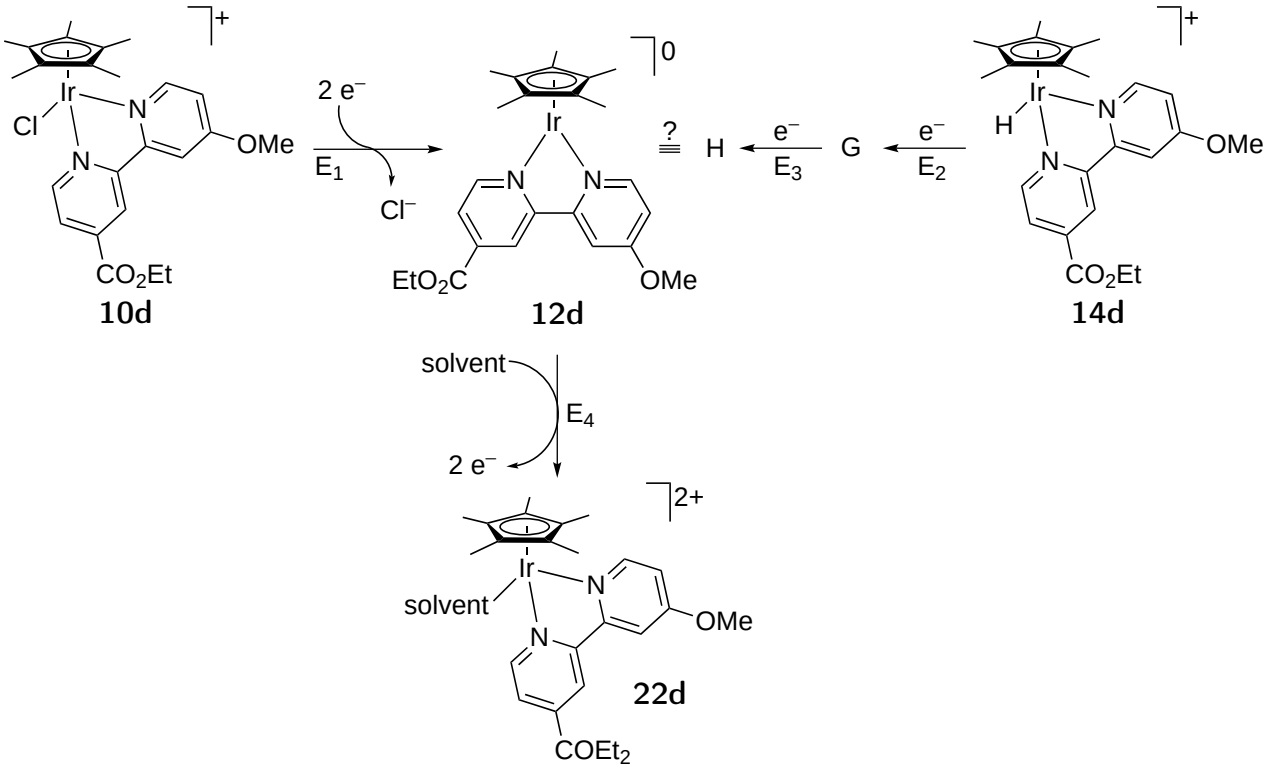

Scheme 54: Observed redox events of **10d** and **14d** in Ar saturated MeOH/THF, 1:1, v/v.

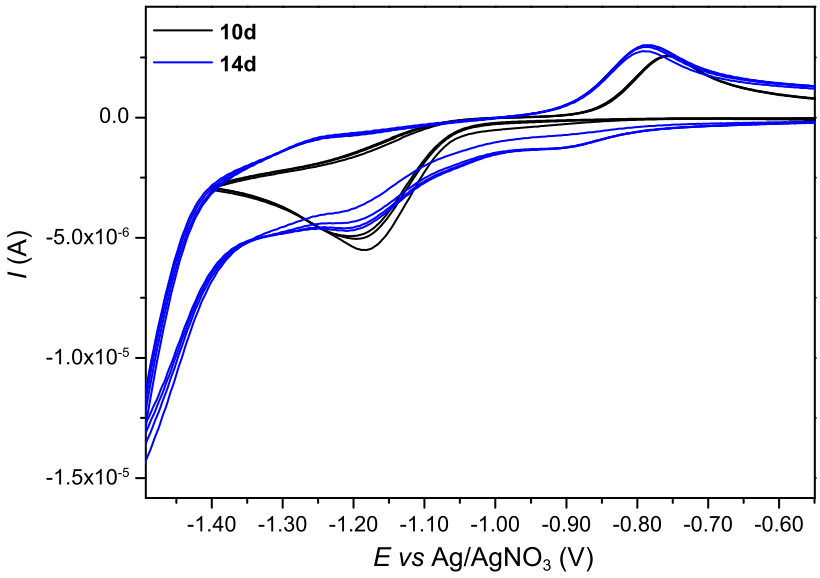

Figure 42: CVs of **10d** and **14d** in Ar saturated MeOH/THF, 1:1, v/v.

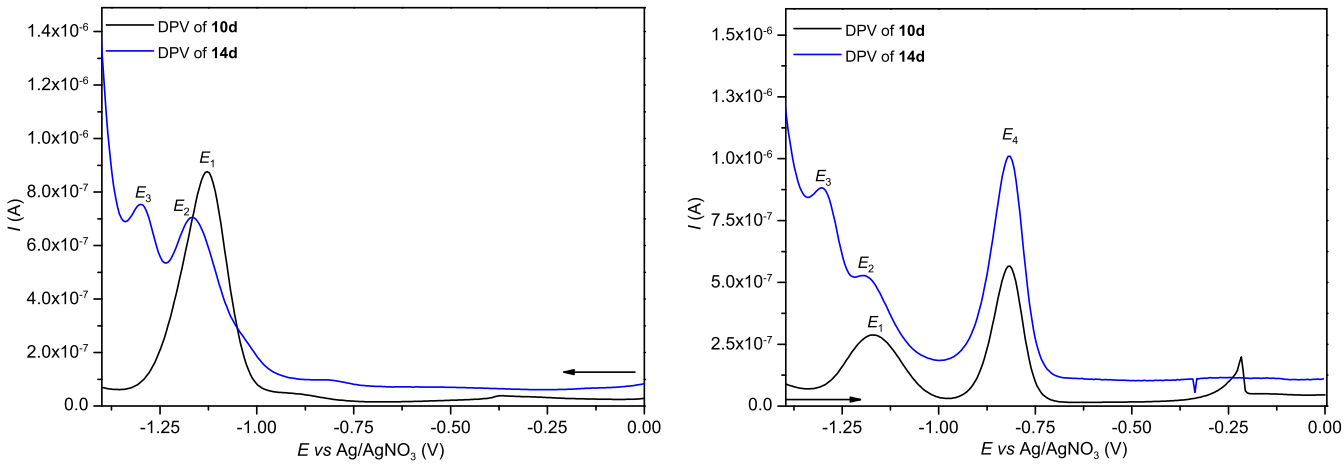

Figure 43: DPVs of **10d** and **14d** in Ar saturated MeOH/THF, 1:1, v/v on the reductive and oxidative scan between $E = 0.00$ and -1.40 V *vs* $Ag/AgNO_3$.

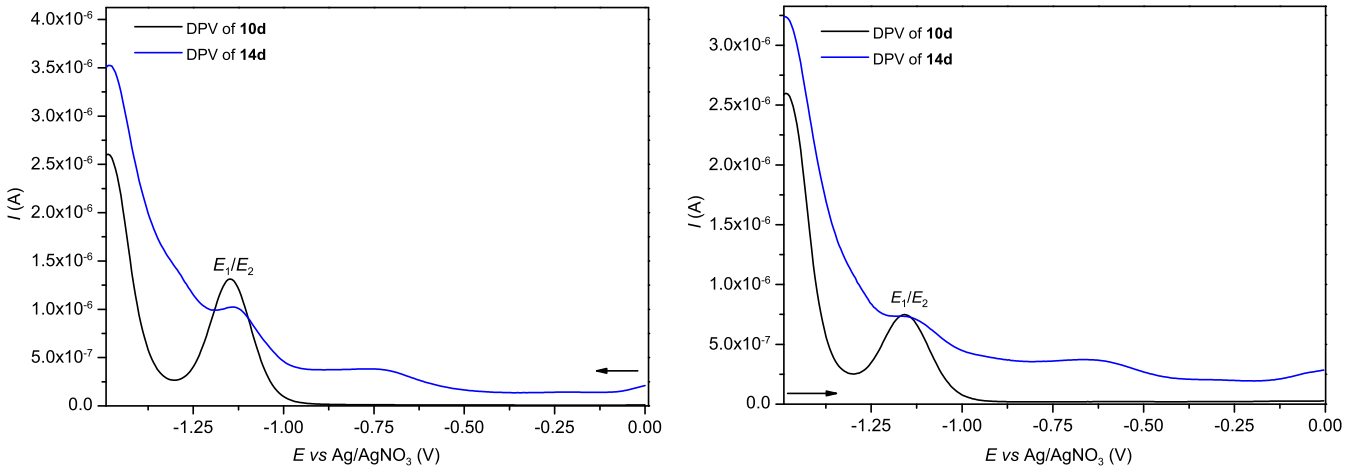

Figure 44: DPVs of **10d** and **14d** in CO_2 saturated MeOH/THF, 1:1, v/v on the reductive and oxidative scan between $E = 0.00$ and -1.40 V *vs* $Ag/AgNO_3$.

Table 16: Potential values of the redox events of **10d** and **14d** in Ar saturated MeOH/THF, 1:1, v/v.

	Redox event			
Compound	E_1 (V)	E_2 (V)	E_3 (V)	E_4 (V)
10d	-1.13	–	–	-0.82
14d	–	-1.17	-1.30	-0.82

6.15 Hydrogenation of carbonyl compounds

6.15.1 Catalyst screening experiments

To a 4 mL vial iridium complex (0.002 mmol) and $AgPF_6$ (0.004 mmol, 1.0 mg) were added in the glove box. The vials (typically 8 vials a time) were placed in a 250 mL Schlenk flask with NS 29 glass joint and transferred from the glove box to the autoclave. After addition of the Ar-degassed substrate (0.5 mmol) under constant Ar stream, the vials were capped with perforated plastic caps and placed in the autoclave. The autoclave was closed hand tight, flushed with Ar and transferred to the high pressure lab. The autoclave was closed pressure tight and was flushed with H_2 three times before adjusting the required H_2 pressure. When 1 atm H_2 pressure was used, the reaction was carried out using a balloon filled with H_2 connected to the Schlenk-flask. The reaction mixtures were stirred for 5-12 h at rt. After the pressure was released and the autoclave was flushed with Ar, the samples were diluted with $CDCl_3$ and filtered over celite to directly carry out ^{1}H NMR analysis to determine conversions.

Table 17: Hydrogenation experiments in neat substrate or diluted solutions. Conditions: $p = 10$ bar, $T =$ rt, $t = 5$ h, Ir complex 0.4 mol%, $AgPF_6$ 0.6 mol%, substrate 0.5 mmol neat or $c_{substrate} = 5$ M.

Entry	Complex	Substrate	Solvent	Yield
1	**10d**	**19a**	–	64
2	**10d**	**19b**	–	50
3	**10d**	**19a**	d-DCM	10
4	**10j**	**19a**	–	53
5	**10j**	**19b**	–	50
6	**10j**	**19a**	d-DCM	<1
7	**10h**	**19a**	–	44
8	**10h**	**19b**	–	33
9	**10h**	**19a**	d-DCM	10
10	$[Cp^*IrCl_2]_2$	**19a**	–	4

Bibliography

[1] M. L. O. NOAA-ESRL, *Earth's CO_2 Home Page*, `http://co2now.org/`, Accessed in November 2014.

[2] P. Friedlingstein, R. M. Andrew, J. Rogelj, G. P. Peters, J. G. Canadell, R. Knutti, G. Luderer, M. R. Raupach, M. Schaeffer, D. P. van Vuuren, C. Le Quere, *Nat. Geosci.* **2014**, *7*, 709–715.

[3] W. D. U.S. Energy Information Administration, US Department of Energy, *Carbon Dioxide Emissions From Energy Consumption*, `http://www.eia.gov/totalenergy/data/annual/index.cfm`, Accessed in June 2014.

[4] S. D. Kenarsari, D. Yang, G. Jiang, S. Zhang, J. Wang, A. G. Russell, Q. Wei, M. Fan, *RSC Adv.* **2013**, *3*, 22739–22773.

[5] P. G. Jessop, T. Ikariya, R. Noyori, *Chem. Rev.* **1995**, *95*, 259–272.

[6] E. E. Benson, C. P. Kubiak, A. J. Sathrum, J. M. Smieja, *Chem. Soc. Rev.* **2009**, *38*, 89–99.

[7] M.-A. Courtemanche, M.-A. Légaré, L. Maron, F.-G. Fontaine, *J. Am. Chem. Soc.* **2013**, *135*, 9326–9329.

[8] F.-G. Fontaine, M.-A. Courtemanche, M.-A. Légaré, *Chem. - Eur. J.* **2014**, *20*, 2990–2996.

[9] S. N. Riduan, Y. Zhang, J. Ying, *Angew. Chem. Int. Ed.* **2009**, *48*, 3322–3325.

[10] W. Wang, S. Wang, X. Ma, J. Gong, *Chem. Soc. Rev.* **2011**, *40*, 3703–3727.

[11] P. G. Jessop, F. Joó, C.-C. Tai, *Coord. Chem. Rev.* **2004**, *248*, 2425 – 2442.

[12] N. A. M. Razali, K. T. Lee, S. Bhatia, A. R. Mohamed, *Renewable Sustainable Energy Rev.* **2012**, *16*, 4951 – 4964.

[13] J. Qiao, Y. Liu, F. Hong, J. Zhang, *Chem. Soc. Rev.* **2014**, *43*, 631–675.

[14] J. Schneider, H. Jia, J. T. Muckerman, E. Fujita, *Chem. Soc. Rev.* **2012**, *41*, 2036–2051.

[15] C. Costentin, M. Robert, J.-M. Saveant, *Chem. Soc. Rev.* **2013**, *42*, 2423–2436.

[16] J. L. Inglis, B. J. MacLean, M. T. Pryce, J. G. Vos, *Coord. Chem. Rev.* **2012**, *256*, 2571 – 2600.

[17] K. Kobayashi, K. Tanaka, *Phys. Chem. Chem. Phys.* **2014**, *16*, 2240–2250.

[18] A. Corma, H. Garcia, *J. Catal.* **2013**, *308*, 168 – 175.

[19] D. T. Whipple, P. J. A. Kenis, *J. Phys. Chem. Lett.* **2010**, *1*, 3451–3458.

[20] M. Schulz, M. Karnahl, M. Schwalbe, J. G. Vos, *Coord. Chem. Rev.* **2012**, *256*, 1682 – 1705.

[21] R. Reithmeier, C. Bruckmeier, B. Rieger, *Catalysts* **2012**, *2*, 544–571.

[22] B. Kumar, M. Llorente, J. Froehlich, T. Dang, A. Sathrum, C. P. Kubiak, *Annu. Rev. Phys. Chem.* **2012**, *63*, 541–569.

[23] S. N. Habisreutinger, L. Schmidt-Mende, J. K. Stolarczyk, *Angew. Chem. Int. Ed.* **2013**, *52*, 7372–7408.

[24] Y.-N. Li, L.-N. He, Z.-F. Diao, Z.-Z. Yang in *CO2 Chemistry, Vol. 66* (Eds.: M. Aresta, R. van Eldik), Academic Press, **2014**, pp. 289 – 345.

[25] S. Navalón, A. Dhakshinamoorthy, M. Álvaro, H. Garcia, *ChemSusChem* **2013**, *6*, 562–577.

[26] D. L. DuBois, A. Miedaner, R. C. Haltiwanger, *J. Am. Chem. Soc.* **1991**, *113*, 8753–8764.

[27] M. Hammouche, D. Lexa, M. Momenteau, J. M. Saveant, *J. Am. Chem. Soc.* **1991**, *113*, 8455–8466.

[28] J. M. Smieja, C. P. Kubiak, *Inorg. Chem.* **2010**, *49*, 9283–9289.

[29] M. Bourrez, F. Molton, S. Chardon-Noblat, A. Deronzier, *Angew. Chem. Int. Ed.* **2011**, *50*, 9903–9906.

[30] J. W. Raebiger, J. W. Turner, B. C. Noll, C. J. Curtis, A. Miedaner, B. Cox, D. L. DuBois, *Organometallics* **2006**, *25*, 3345–3351.

[31] M. Beley, J.-P. Collin, R. Ruppert, J.-P. Sauvage, *J. Chem. Soc. Chem. Commun.* **1984**, 1315–1316.

[32] W. Zhu, R. Michalsky, O. Metin, H. Lv, S. Guo, C. J. Wright, X. Sun, A. A. Peterson, S. Sun, *J. Am. Chem. Soc.* **2013**, *135*, 16833–16836.

[33] Z. Chen, C. Chen, D. R. Weinberg, P. Kang, J. J. Concepcion, D. P. Harrison, M. S. Brookhart, T. J. Meyer, *Chem. Commun.* **2011**, *47*, 12607–12609.

[34] J. M. Smieja, M. D. Sampson, K. A. Grice, E. E. Benson, J. D. Froehlich, C. P. Kubiak, *Inorg. Chem.* **2013**, *52*, 2484–2491.

[35] S. Sato, T. Morikawa, T. Kajino, O. Ishitani, *Angew. Chem. Int. Ed.* **2013**, *52*, 988–992.

[36] T. W. Woolerton, S. Sheard, E. Reisner, E. Pierce, S. W. Ragsdale, F. A. Armstrong, *J. Am. Chem. Soc.* **2010**, *132*, 2132–2133.

[37] H. Ishida, H. Tanaka, K. Tanaka, T. Tanaka, *J. Chem. Soc. Chem. Commun.* **1987**, 131–132.

[38] T. Ono, N. Planas, P. Miró, M. Z. Ertem, E. C. Escudero-Adán, J. Benet-Buchholz, L. Gagliardi, C. J. Cramer, A. Llobet, *ChemCatChem* **2013**, *5*, 3897–3903.

[39] L. González-Sebastián, M. Flores-Alamo, J. J. García, *Organometallics* **2013**, *32*, 7186–7194.

[40] J. H. Jeon, P. M. Mareeswaran, C. H. Choi, S. I. Woo, *RSC Adv.* **2014**, *4*, 3016–3019.

[41] H. Takeda, H. Koizumi, K. Okamoto, O. Ishitani, *Chem. Commun.* **2014**, *50*, 1491–1493.

[42] C. Caix, S. Chardon-Noblat, A. Deronzier, *J. Electroanal. Chem.* **1997**, *434*, 163 – 170.

[43] H. Ishida, K. Tanaka, T. Tanaka, *Organometallics* **1987**, *6*, 181–186.

[44] C. M. Bolinger, N. Story, B. P. Sullivan, T. J. Meyer, *Inorg. Chem.* **1988**, *27*, 4582–4587.

[45] K. Nakata, T. Ozaki, C. Terashima, A. Fujishima, Y. Einaga, *Angew. Chem. Int. Ed.* **2014**, *53*, 871–874.

[46] S. Bontemps, L. Vendier, S. Sabo-Etienne, *J. Am. Chem. Soc.* **2014**, *136*, 4419–4425.

[47] C. Li, X. Yuan, K. Fujimoto, *Appl. Catal. A* **2014**, *469*, 306 – 311.

[48] D. J. Boston, Y. M. F. Pachón, R. O. Lezna, N. R. de Tacconi, F. M. MacDonnell, *Inorg. Chem.* **2014**, *53*, 6544–6553.

[49] Q. Liu, Y. Zhou, W. Tu, S. Yan, Z. Zou, *Inorg. Chem.* **2014**, *53*, 359–364.

[50] S. Rani, N. Bao, S. C. Roy, *Appl. Surf. Sci.* **2014**, *289*, 203 – 208.

[51] M. Czaun, A. Goeppert, J. Kothandaraman, R. B. May, R. Haiges, G. K. S. Prakash, G. A. Olah, *ACS Catal.* **2014**, *4*, 311–320.

[52] X. Gu, Z.-H. Lu, H.-L. Jiang, T. Akita, Q. Xu, *J. Am. Chem. Soc.* **2011**, *133*, 11822–11825.

[53] S. Enthaler, J. von Langermann, T. Schmidt, *Energy Environ. Sci.* **2010**, *3*, 1207–1217.

[54] F. Joó, *ChemSusChem* **2008**, *1*, 805–808.

[55] S. Enthaler, *ChemSusChem* **2008**, *1*, 801–804.

[56] Y. Himeda, N. Onozawa-Komatsuzaki, H. Sugihara, H. Arakawa, K. Kasuga, *Organometallics* **2004**, *23*, 1480–1483.

[57] Y. Himeda, N. Onozawa-Komatsuzaki, H. Sugihara, K. Kasuga, *J. Am. Chem. Soc.* **2005**, *127*, 13118–13119.

[58] Y. Himeda, N. Onozawa-Komatsuzaki, H. Sugihara, K. Kasuga, *Organometallics* **2007**, *26*, 702–712.

[59] W.-H. Wang, J. F. Hull, J. T. Muckerman, E. Fujita, Y. Himeda, *Energy Environ. Sci.* **2012**, *5*, 7923–7926.

[60] Y.-y. Ohnishi, T. Matsunaga, Y. Nakao, H. Sato, S. Sakaki, *J. Am. Chem. Soc.* **2005**, *127*, 4021–4032.

[61] R. Tanaka, M. Yamashita, K. Nozaki, *J. Am. Chem. Soc.* **2009**, *131*, 14168–14169.

[62] C. Federsel, R. Jackstell, M. Beller, *Angew. Chem. Int. Ed.* **2010**, *49*, 6254–6257.

[63] R. Tanaka, M. Yamashita, L. W. Chung, K. Morokuma, K. Nozaki, *Organometallics* **2011**, *30*, 6742–6750.

[64] T. J. Schmeier, G. E. Dobereiner, R. H. Crabtree, N. Hazari, *J. Am. Chem. Soc.* **2011**, *133*, 9274–9277.

[65] N. D. McNamara, J. C. Hicks, *ChemSusChem* **2014**, *7*, 1114–1124.

[66] Z. Xu, N. D. McNamara, G. T. Neumann, W. F. Schneider, J. C. Hicks, *ChemCatChem* **2013**, *5*, 1769–1771.

[67] P. Kang, C. Cheng, Z. Chen, C. K. Schauer, T. J. Meyer, M. Brookhart, *J. Am. Chem. Soc.* **2012**, *134*, 5500–5503.

[68] P. Kang, T. J. Meyer, M. Brookhart, *Chem. Sci.* **2013**, *4*, 3497–3502.

[69] P. Kang, S. Zhang, T. J. Meyer, M. Brookhart, *Angew. Chem. Int. Ed.* **2014**, *53*, 8709–8713.

[70] L. Li, S. Zhang, L. Xu, J. Wang, L.-X. Shi, Z.-N. Chen, M. Hong, J. Luo, *Chem. Sci.* **2014**, *5*, 3808–3813.

[71] B. P. Sullivan, T. J. Meyer, *J. Chem. Soc. Chem. Commun.* **1984**, 1244–1245.

[72] B. Sullivan, T. Meyer, *Organometallics* **1986**, *5*, 1500–1502.

[73] J. R. Pugh, M. R. M. Bruce, B. P. Sullivan, T. J. Meyer, *Inorg. Chem.* **1991**, *30*, 86–91.

[74] E. Graf, W. Leitner, *J. Chem. Soc. Chem. Commun.* **1992**, 623–624.

[75] J. C. Tsai, K. M. Nicholas, *J. Am. Chem. Soc.* **1992**, *114*, 5117–5124.

[76] C. Ovalles, C. Fernández, D. J. Darensbourg, *J. Mol. Catal.* **1994**, *93*, 125 – 136.

[77] M. S. Ahlquist, *J. Mol. Catal. A: Chem.* **2010**, *324*, 3 – 8.

[78] X. Yang, *ACS Catal.* **2011**, *1*, 849–854.

[79] S. Ogo, R. Kabe, H. Hayashi, R. Harada, S. Fukuzumi, *Dalton Trans.* **2006**, 4657–4663.

[80] C. Hou, J. Jiang, S. Zhang, G. Wang, Z. Zhang, Z. Ke, C. Zhao, *ACS Catal.* **2014**, *4*, 2990–2997.

[81] S. E. Clapham, A. Hadzovic, R. H. Morris, *Coord. Chem. Rev.* **2004**, *248*, 2201 – 2237.

[82] L. Cao, C. Sun, N. Sun, L. Meng, D. Chen, *Dalton Trans.* **2013**, *42*, 5755–5763.

[83] Y. Himeda, S. Miyazawa, T. Hirose, *ChemSusChem* **2011**, *4*, 487–493.

[84] B. Loges, A. Boddien, F. Gaertner, H. Junge, M. Beller, *Top. Catal.* **2010**, *53*, 902–914.

[85] Y. Himeda, *Green Chem.* **2009**, *11*, 2018–2022.

[86] S. Fukuzumi, *Eur. J. Inorg. Chem.* **2008**, 1351–1362.

[87] A. Boddien, F. Gärtner, C. Federsel, P. Sponholz, D. Mellmann, R. Jackstell, H. Junge, M. Beller, *Angew. Chem. Int. Ed.* **2011**, *50*, 6411–6414.

[88] G. Papp, J. Csorba, G. Laurenczy, F. Joó, *Angew. Chem. Int. Ed.* **2011**, *50*, 10433–10435.

[89] J. F. Hull, Y. Himeda, W.-H. Wang, B. Hashiguchi, R. Periana, D. J. Szalda, J. T. Muckerman, E. Fujita, *Nat. Chem.* **2012**, *4*, 383–388.

[90] C. Kaes, A. Katz, M. W. Hosseini, *Chem. Rev.* **2000**, *100*, 3553–3590.

[91] Q. Wang, C. Chen, *Tetrahedron Lett.* **2008**, *49*, 2916 – 2921.

[92] H.-L. Kwong, H.-L. Yeung, C.-T. Yeung, W.-S. Lee, C.-S. Lee, W.-L. Wong, *Coord. Chem. Rev.* **2007**, *251*, 2188 – 2222.

[93] G. Chelucci, R. P. Thummel, *Chem. Rev.* **2002**, *102*, 3129–3170.

[94] A. Winter, G. R. Newkome, U. S. Schubert, *ChemCatChem* **2011**, *3*, 1384–1406.

[95] T. Wada, H. Maki, T. Imamoto, H. Yuki, Y. Miyazato, *Chem. Commun.* **2013**, *49*, 4394–4396.

[96] C. M. Moore, N. K. Szymczak, *Chem. Commun.* **2013**, *49*, 400–402.

[97] N. Kaveevivitchai, R. Zong, H.-W. Tseng, R. Chitta, R. P. Thummel, *Inorg. Chem.* **2012**, *51*, 2930–2939.

[98] M. Grätzel, *Acc. Chem. Res.* **2009**, *42*, 1788–1798.

[99] L. Sun, L. Hammarstrom, B. Akermark, S. Styring, *Chem. Soc. Rev.* **2001**, *30*, 36–49.

[100] A. Juris, V. Balzani, F. Barigelletti, S. Campagna, P. Belser, A. von Zelewsky, *Coord. Chem. Rev.* **1988**, *84*, 85 – 277.

[101] M. Ichikawa, S. Mochizuki, H.-G. Jeon, S. Hayashi, N. Yokoyama, Y. Taniguchi, *J. Mater. Chem.* **2011**, *21*, 11791–11799.

[102] C.-Y. Liu, A. J. Bard, *J. Am. Chem. Soc.* **2002**, *124*, 4190–4191.

[103] C. Bazzicalupi, A. Bencini, S. Puccioni, B. Valtancoli, P. Gratteri, A. Garau, V. Lippolis, *Chem. Commun.* **2012**, *48*, 139–141.

[104] A. Wild, A. Winter, M. D. Hager, U. S. Schubert, *Chem. Commun.* **2012**, *48*, 964–966.

[105] Z. Huang, J. Du, J. Zhang, X.-Q. Yu, L. Pu, *Chem. Commun.* **2012**, *48*, 3412–3414.

[106] U. S. Schubert, C. Eschbaumer, *Angew. Chem. Int. Ed.* **2002**, *41*, 2892–2926.

[107] A. Wild, A. Winter, F. Schlutter, U. S. Schubert, *Chem. Soc. Rev.* **2011**, *40*, 1459–1511.

[108] K. A. Williams, A. J. Boydston, C. W. Bielawski, *Chem. Soc. Rev.* **2007**, *36*, 729–744.

[109] E. C. Constable, *Chem. Soc. Rev.* **2007**, *36*, 246–253.

[110] F. Krohnke, *Synthesis* **1976**, 1–24.

[111] H. Bönnemann, *Angew. Chem. Int. Ed.* **1978**, *17*, 505–515.

[112] G. Chelucci, M. Cabras, A. Saba, *J. Heterocycl. Chem.* **1994**, *31*, 1289–1291.

[113] A. Goswami, K. Ohtaki, K. Kase, T. Ito, S. Okamoto, *Adv. Synth. Catal.* **2008**, *350*, 143–152.

[114] Y.-k. Sugiyama, S. Okamoto, *Synthesis* **2011**, 2247–2254.

[115] S. Okamoto, *Heterocycles* **2012**, *85*, 1579+.

[116] Y. Wakatsuki, H. Yamazaki, *Tetrahedron Lett.* **1973**, *14*, 3383 – 3384.

[117] Bonneman.H, Brinkman.R, Schenklu.H, *Synthesis* **1974**, 575–577.

[118] G. R. Pabst, K. Schmid, J. Sauer, *Tetrahedron Lett.* **1998**, *39*, 6691 – 6694.

[119] G. R. Pabst, J. Sauer, *Tetrahedron Lett.* **1998**, *39*, 6687 – 6690.

[120] G. R. Pabst, J. Sauer, *Tetrahedron* **1999**, *55*, 5067 – 5088.

[121] G. R. Pabst, O. C. Pfüller, J. Sauer, *Tetrahedron* **1999**, *55*, 5047 – 5066.

[122] S. Diring, P. Retailleau, R. Ziessel, *Tetrahedron Lett.* **2007**, *48*, 8069 – 8073.

[123] M. Altuna-Urquijo, A. Gehre, S. P. Stanforth, B. Tarbit, *Tetrahedron* **2009**, *65*, 975 – 984.

[124] B. Shi, W. Lewis, I. B. Campbell, C. J. Moody, *Org. Lett.* **2009**, *11*, 3686–3688.

[125] S. P. Stanforth, B. Tarbit, M. D. Watson, *Tetrahedron* **2004**, *60*, 8893 – 8897.

[126] J. Dash, H.-U. Reissig, *Chem. - Eur. J.* **2009**, *15*, 6811–6814.

[127] P. Hommes, P. Jungk, H.-U. Reissig, *Synlett* **2011**, 2311–2314.

[128] G. R. Newkome, A. K. Patri, E. Holder, U. S. Schubert, *Eur. J. Org. Chem.* **2004**, *2004*, 235–254.

[129] M. Hapke, L. Brandt, A. Lützen, *Chem. Soc. Rev.* **2008**, *37*, 2782–2797.

[130] R. N. Dhital, C. Kamonsatikul, E. Somsook, H. Sakurai, *Catal. Sci. Technol.* **2013**, *3*, 3030–3035.

[131] T. M. Cassol, F. Demnitz, M. Navarro, E. A. Neves, *Tetrahedron Lett.* **2000**, *41*, 8203 – 8206.

[132] M. Heller, U. S. Schubert, *J. Org. Chem.* **2002**, *67*, 8269–8272.

[133] C. A. Panetta, H. J. Kumpaty, N. E. Heimer, M. C. Leavy, C. L. Hussey, *J. Org. Chem.* **1999**, *64*, 1015–1021.

[134] P. F. H. Schwab, F. Fleischer, J. Michl, *J. Org. Chem.* **2002**, *67*, 443–449.

[135] E. Negishi, A. O. King, N. Okukado, *J. Org. Chem.* **1977**, *42*, 1821–1823.

[136] T. Sakamoto, Y. Kondo, N. Murata, H. Yamanaka, *Tetrahedron* **1993**, *49*, 9713 – 9720.

[137] C. Bolm, M. Ewald, M. Felder, G. Schlingloff, *Chem. Ber.* **1992**, *125*, 1169–1190.

[138] H.-L. Kwong, W.-S. Lee, *Tetrahedron: Asymmetry* **1999**, *10*, 3791 – 3801.

[139] S. L. Hargreaves, B. L. Pilkington, S. E. Russell, P. A. Worthington, *Tetrahedron Lett.* **2000**, *41*, 1653 – 1656.

[140] F. Trécourt, B. Gervais, M. Mallet, G. Quéguiner, *J. Org. Chem.* **1996**, *61*, 1673–1676.

[141] N. Murata, T. Sugihara, Y. Kondo, T. Sakamoto, *Synlett* **1997**, 298–&.

[142] P. Nshimyumukiza, D. Cahard, J. Rouden, M.-C. Lasne, J.-C. Plaquevent, *Tetrahedron Lett.* **2001**, *42*, 7787 – 7790.

[143] S. A. Savage, A. P. Smith, C. L. Fraser, *J. Org. Chem.* **1998**, *63*, 10048–10051.

[144] A. Lützen, M. Hapke, *Eur. J. Org. Chem.* **2002**, *2002*, 2292–2297.

[145] T. Ishiyama, K. Ishida, N. Miyaura, *Tetrahedron* **2001**, *57*, 9813 – 9816.

[146] K. Deshayes, R. D. Broene, I. Chao, C. B. Knobler, F. Diederich, *J. Org. Chem.* **1991**, *56*, 6787–6795.

[147] S. R. L. Fernando, U. S. M. Maharoof, K. D. Deshayes, T. H. Kinstle, M. Y. Ogawa, *J. Am. Chem. Soc.* **1996**, *118*, 5783–5790.

[148] H. Matondo, N. Ouhaja, S. Souirti, M. Baboulene, *Main Group Met. Chem.* **2002**, *25*, 163–167.

[149] S. J. Durrant, J. L. Pinder, J.-D. Charrier, J.-M. Jimenez, G. Brenchley, P. N. Collier, D. Kay, A. Miller, F. Pierard, S. Ramaya, S. Sadiq, H. C. Twin, *Heterocycles* **2006**, *70*, 509+.

[150] A. Bouillon, J.-C. Lancelot, J. S. de Oliveira Santos, V. Collot, P. R. Bovy, S. Rault, *Tetrahedron* **2003**, *59*, 10043 – 10049.

[151] N. A. Jones, J. W. Antoon, A. L. Bowie, J. B. Borak, E. P. Stevens, *J. Heterocycl. Chem.* **2007**, *44*, 363–367.

[152] C. Guetz, A. Luetzen, *Synthesis* **2010**, 85–90.

[153] M. Heller, U. Schubert, *Eur. J. Org. Chem.* **2003**, 947–961.

[154] J. Li, T. Sato, H. Li, M. Higuchi, *Synthesis* **2011**, 1361–1364.

[155] M. Heller, U. Schubert, *Synlett* **2002**, 751–754.

[156] R. Fallahpour, *Synthesis* **2003**, 155–184.

[157] P. Hommes, C. Fischer, C. Lindner, H. Zipse, H.-U. Reissig, *Angew. Chem. Int. Ed.* **2014**, *53*, 7647–7651.

[158] U. S. Schubert, C. Eschbaumer, *Org. Lett.* **1999**, *1*, 1027–1029.

[159] U. S. Schubert, C. Eschbaumer, M. Heller, *Org. Lett.* **2000**, *2*, 3373–3376.

[160] K.-L. Wu, C.-H. Li, Y. Chi, J. N. Clifford, L. Cabau, E. Palomares, Y.-M. Cheng, H.-A. Pan, P.-T. Chou, *J. Am. Chem. Soc.* **2012**, *134*, 7488–7496.

[161] S.-H. Yang, K.-L. Wu, Y. Chi, Y.-M. Cheng, P.-T. Chou, *Angew. Chem. Int. Ed.* **2011**, *50*, 8270–8274.

[162] N. Kuhl, M. N. Hopkinson, J. Wencel-Delord, F. Glorius, *Angew. Chem. Int. Ed.* **2012**, *51*, 10236–10254.

[163] P. B. Arockiam, C. Bruneau, P. H. Dixneuf, *Chem. Rev.* **2012**, *112*, 5879–5918.

[164] C. S. Yeung, V. M. Dong, *Chem. Rev.* **2011**, *111*, 1215–1292.

[165] T. W. Lyons, M. S. Sanford, *Chem. Rev.* **2010**, *110*, 1147–1169.

[166] D. A. Colby, R. G. Bergman, J. A. Ellman, *Chem. Rev.* **2010**, *110*, 624–655.

[167] X. Chen, K. M. Engle, D.-H. Wang, J.-Q. Yu, *Angew. Chem. Int. Ed.* **2009**, *48*, 5094–5115.

[168] L. Ackermann, R. Vicente, A. R. Kapdi, *Angew. Chem. Int. Ed.* **2009**, *48*, 9792–9826.

[169] F. Bellina, R. Rossi, *Tetrahedron* **2009**, *65*, 10269–10310.

[170] J. A. Bull, J. J. Mousseau, G. Pelletier, A. B. Charette, *Chem. Rev.* **2012**, *112*, 2642–2713.

[171] G. Yan, A. J. Borah, M. Yang, *Adv. Synth. Catal.* **2014**, *356*, 2375–2394.

[172] S. H. Cho, S. J. Hwang, S. Chang, *J. Am. Chem. Soc.* **2008**, *130*, 9254+.

[173] L. Ackermann, S. Fenner, *Chem. Commun.* **2011**, *47*, 430–432.

[174] L. Campeau, S. Rousseaux, K. Fagnou, *J. Am. Chem. Soc.* **2005**, *127*, 18020–18021.

[175] S. I. Gorelsky, D. Lapointe, K. Fagnou, *J. Am. Chem. Soc.* **2008**, *130*, 1084810849.

[176] H.-Y. Sun, S. I. Gorelsky, D. R. Stuart, L.-C. Campeau, K. Fagnou, *J. Org. Chem.* **2010**, *75*, 8180–8189.

[177] S. I. Gorelsky, D. Lapointe, K. Fagnou, *J. Org. Chem.* **2012**, *77*, 658–668.

[178] Y. Tan, F. Barrios-Landeros, J. F. Hartwig, *J. Am. Chem. Soc.* **2012**, *134*, 3683–3686.

[179] T. Abura, S. Ogo, Y. Watanabe, S. Fukuzumi, *J. Am. Chem. Soc.* **2003**, *125*, 4149–4154.

[180] T. Kaminski, P. Gros, Y. Fort, *Eur. J. Org. Chem.* **2003**, *2003*, 3855–3860.

[181] K. D. Dubois, H. He, C. Liu, A. S. Vorushilov, G. Li, *J. Mol. Catal. A: Chem.* **2012**, *363-364*, 208−−213.

[182] C. Liu, K. D. Dubois, M. E. Louis, A. S. Vorushilov, G. Li, *ACS Catal.* **2013**, *3*, 655–662.

[183] C. del Pozo, A. Corma, M. Iglesias, F. Saánchez, *Organometallics* **2010**, *29*, 4491–4498.

[184] S. Duric, C. C. Tzschucke, *Org. Lett.* **2011**, *13*, 2310–2313.

[185] D. Wenkert, R. B. Woodward, *J. Org. Chem.* **1983**, *48*, 283–289.

[186] R. Balicki, M. Cybulski, G. Maciejewski, *Synth. Commun.* **2003**, *33*, 4137–4141.

[187] R. Balicki, *Synthesis* **1989**, *1989*, 645–646.

[188] Y. Mikami, A. Noujima, T. Mitsudome, T. Mizugaki, K. Jitsukawa, K. Kaneda, *Chem. – Eur. J.* **2011**, *17*, 1768–1772.

[189] R. L. Shook, A. S. Borovik, *Inorg. Chem.* **2010**, *49*, 3646–3660.

[190] J. M. Keith, *J. Org. Chem.* **2006**, *71*, 9540–9543.

[191] J. Yin, B. Xiang, M. A. Huffman, C. E. Raab, I. W. Davies, *J. Org. Chem.* **2007**, *72*, 4554–4557.

[192] W. H. Henderson, J. M. Alvarez, C. C. Eichman, J. P. Stambuli, *Organometallics* **2011**, *30*, 5038–5044.

[193] W. Herrmann, C. Brossmer, K. Ofele, C. Reisinger, T. Priermeier, M. Beller, H. Fischer, *Angew. Chem. Int. Ed.* **1995**, *34*, 1844–1848.

[194] S. Duric, F. D. Sypaseuth, S. Hoof, E. Svensson, C. C. Tzschucke, *Chem. – Eur. J.* **2013**, *19*, 17456–17463.

[195] M.-T. Youinou, R. Ziessel, *J. Organomet. Chem* **1989**, *363*, 197 – 208.

[196] K. Hasan, L. Donato, Y. Shen, J. D. Slinker, E. Zysman-Colman, *Dalton Trans.* **2014**, *43*, 13672–13682.

[197] Y. Li, N. Dandu, R. Liu, Z. Li, S. Kilina, W. Sun, *J. Phys. Chem. C* **2014**, *118*, 6372–6384.

[198] P. Alam, M. Karanam, D. Bandyopadhyay, A. R. Choudhury, I. R. Laskar, *Eur. J. Inorg. Chem.* **2014**, *2014*, 3710–3719.

[199] V. V. Pavlishchuk, A. W. Addison, *Inorg. Chim. Acta* **2000**, *298*, 97 – 102.

[200] C. Caix, S. Chardon-Noblat, A. Deronzier, R. Ziessel, *J. Electroanal. Chem.* **1993**, *362*, 301 – 304.

[201] M. Ladwig, W. Kaim, *J. Organomet. Chem* **1992**, *439*, 79 – 90.

[202] A. J. Bard in *Potential Sweep Methods*, John Wiley, **2001**, pp. 228–232.

[203] V. S. Thoi, Y. Sun, J. R. Long, C. J. Chang, *Chem. Soc. Rev.* **2013**, *42*, 2388–2400.

[204] G. Jacobs, D. Severin, *Pet. Sci. Technol.* **1997**, *15*, 103–125.

[205] S. Davies, R. Linforth, S. Wilkinson, K. Smart, D. Cook, *Biotechnol. Biofuels* **2011**, *4*, 28.

[206] A. W. Smallwood, *Am. Ind. Hyg. Assoc. J.* **1978**, *39*, 151–153.

[207] S. Moret, P. J. Dyson, G. Laurenczy, *Dalton Trans.* **2013**, *42*, 4353–4356.

[208] I. Berregi, G. del Campo, R. Caracena, J. I. Miranda, *Talanta* **2007**, *72*, 1049 – 1053.

[209] G. del Campo, I. Berregi, R. Caracena, J. Zuriarrain, *Talanta* **2010**, *81*, 367 – 371.

[210] J. Burakevich, J. O. Jr., *Anal. Chim. Acta* **1971**, *54*, 528 – 530.

[211] S. H. Smallcombe, S. L. Patt, P. A. Keifer, *J. Magn. Reson. Ser. A* **1995**, *117*, 295 – 303.

[212] D. G. H. Hetterscheid, J. N. H. Reek, *Angew. Chem. Int. Ed.* **2012**, *51*, 9740–9747.

[213] D. J. Wasylenko, R. D. Palmer, C. P. Berlinguette, *Chem. Commun.* **2013**, *49*, 218–227.

[214] R. H. Crabtree, *Chem. Rev.* **2012**, *112*, 1536–1554.

[215] E. Pretsch, T. Clerc, J. Seibl, W. Simon, *Tables of Spectral Data for Structure Determination of Organic Compounds*, Springer, Berlin Heidelberg, **1989**.

[216] V. P. Taori, R. Bandari, M. R. Buchmeiser, *Chem. - Eur. J.* **2014**, *20*, 3292–3296.

[217] P. M. Zimmerman, Z. Zhang, C. B. Musgrave, *Inorg. Chem.* **2010**, *49*, 8724–8728.

[218] S. Matsuoka, K. Yamamoto, T. Ogata, M. Kusaba, N. Nakashima, E. Fujita, S. Yanagida, *J. Am. Chem. Soc.* **1993**, *115*, 601–609.

[219] J. J. Carroll, J. D. Slupsky, A. E. Mather, *J. Phys. Chem. Ref. Data* **1991**, *20*, 1201–1209.

[220] N. Schüler, K. Hecht, M. Kraut, R. Dittmeyer, *J. Chem. Eng. Data* **2012**, *57*, 2304–2308.

[221] L. Deiana, L. Ghisu, S. Afewerki, O. Verho, E. V. Johnston, N. Hedin, Z. Bacsik, A. Córdova, *Adv. Synth. Catal.* **2014**, *356*, 2485–2492.

[222] A. T. Dickschat, F. Behrends, S. Surmiak, M. Weiss, H. Eckert, A. Studer, *Chem. Commun.* **2013**, *49*, 2195–2197.

[223] P. W. van Leeuwen, A. J. Sandee, J. N. Reek, P. C. Kamer, *J. Mol. Catal. A: Chem.* **2002**, *182-183*, 107 – 123.

[224] B. Štefane, F. Požgan, *Catal. Rev.* **2014**, *56*, 82–174.

[225] C. Wang, B. Villa-Marcos, J. Xiao, *Chem. Commun.* **2011**, *47*, 9773–9785.

[226] R. Malacea, R. Poli, E. Manoury, *Coord. Chem. Rev.* **2010**, *254*, 729 – 752.

[227] S. Ogo, N. Makihara, Y. Watanabe, *Organometallics* **1999**, *18*, 5470–5474.

[228] R. Kawahara, K.-i. Fujita, R. Yamaguchi, *J. Am. Chem. Soc.* **2012**, *134*, 3643–3646.

[229] R. Kawahara, K.-i. Fujita, R. Yamaguchi, *Angew. Chem. Int. Ed.* **2012**, *51*, 12790–12794.

[230] K.-i. Fujita, N. Tanino, R. Yamaguchi, *Org. Lett.* **2007**, *9*, 109–111.

[231] E. A. Bielinski, P. O. Lagaditis, Y. Zhang, B. Q. Mercado, C. Würtele, W. H. Bernskoetter, N. Hazari, S. Schneider, *J. Am. Chem. Soc.* **2014**, *136*, 10234–10237.

[232] T. Zhang, K. E. deKrafft, J.-L. Wang, C. Wang, W. Lin, *Eur. J. Inorg. Chem.* **2014**, *2014*, 698–707.

[233] R. Kawahara, K.-i. Fujita, R. Yamaguchi, *J. Am. Chem. Soc.* **2012**, *134*, 3643–3646.

[234] R. F. Borch, M. D. Bernstein, H. D. Durst, *J. Am. Chem. Soc.* **1971**, *93*, 2897–2904.

[235] R. Calabretta, C. Gallina, C. Giordano, *Synthesis* **1991**, 536–539.

[236] R. Zimmer, T. Arnold, K. Homann, H. Reissig, *Synthesis* **1994**, 1050–1056.

[237] R.-A. Fallahpour, M. Neuburger, *Eur. J. Org. Chem.* **2001**, *2001*, 1853–1856.

Curriculum vitae

The curriculum vitae is not available in the online version due to data protection.

Der Lebenslauf ist in der Online-Version aus Gründen des Datenschutzes nicht enthalten.

List of publications

- F. D. Sypaseuth, C. Matlachowski, M. Weber, M. Schwalbe, C. C. Tzschucke, Electrocatalytic Carbon Dioxide Reduction Using Cationic Cp*-Iridium Complexes Bearing Unsymmetrically Substituted Bipyridine Ligands, submitted

- D. Konning, T. Olbrisch, F. D. Sypaseuth, C. C. Tzschucke, M. Christmann, Oxidation of allylic and benzylic alcohols to aldehydes and carboxylic acids, *Chem. Commun.* **2014**, *50*, 5014-5016

- J. J. M. Weemers, F. D. Sypaseuth, P. S. Bäuerlein, W. N. P. van der Graaff, I. A. W. Filot, M. Lutz, C. Müller, Development of a Benzimidazole-Derived Bidentate P,N-Ligand for Enantioselective Iridium-Catalyzed Hydrogenations, *Eur. J. Org. Chem.* **2014**, 350-362

- S. Duric, F. D. Sypaseuth, S. Hoof, E. Svensson, C. C. Tzschucke, Synthesis of Asymmetrically Substituted Terpyridines by Palladium-Catalyzed Direct C−H Arylation of Pyridine N-Oxides, *Chem. - Eur. J.* **2013**, 19, 17456-17463

Acknowledgment

First of all, I would like to thank UniCat and BIG-NSE for giving me the opportunity and financial support to start my PhD project in catalysis in the exciting city of Berlin. I am grateful to my PhD advisor, Prof. Dr. C. Christoph Tzschucke for giving me an interesting and challenging topic and his guidance during the years I spent in his group. Special thanks goes to Prof. Dr. Christian Müller, who is not only the second reviewer of my thesis, but also the advisor of my MSc project. Professor Müller, thanks for your guidance, advices, encouraging thoughts and continuous help in the last four years!

I would also like to thank Dr. Matthias Schwalbe for the fruitful collaboration and his always friendly and positive attitude. I thank Corinna Matlachowski and Pierre Wrzolek for the nice atmosphere and for making me feel welcome in the AG Schwalbe every time I visited. I thank Prof. Dr. Reinhard Schomäcker for his useful ideas, feedback and support during my PhD work and the opportunity to try some hydrogenation reactions in his labs.

I am very grateful to my (former) colleagues and friends in the AG Tzschucke. Ralf Albrecht, Michal Andrä, Sasa Duric, Swantje Wiebalck, Emma Svensson, Anja Sokolowski, Shanshan Liu and Sina Zucker: you made my lab and social life even more exciting and fun and I wish you all the best in the future! I thank Stefan Hentschel for his help with some of the experiments presented in this thesis. I am happy to have supervised talented students during my PhD. Alicja Boduch, Tom Sauer and Lisa Suntrup, thanks for the great work you have done! Lisa, good luck with your PhD in the AG Sarkar, I am going to miss our lunch breaks together!

I also thank the AG Müller for the nice lunch breaks, barbeques and scientific discussions we had. Special thanks goes to Dr. Jelena Wiecko and Manuela Weber for their help with the measurement and data analysis of the crystal structures reported in this thesis and to Marlene Bruce Vázquez del Mercado for her friendship!

I would like to thank Naina Deibel for carrying out and analyzing the spectroelectrochemistry measurements, for our scientific discussions as well as the nice dinner conversations; Karsten Meyer and Alexander Schökel for their valuable insight on electrochemistry and their patience for sharing it with me.

I thank Dr. Andreas Schäfer for his continuous help with the NMR measurements, Dr. Andreas Springer and Thomas Kolrep for their ideas on the formaldehyde analysis. I sincerely thank the collective NMR and MS service department for supporting my work every day.

Thanks to Melanie Göth, Tobias Seitz, Sven Hahn and Michael Giulbudagian for the nice atmosphere

in the OC lab course which made time go faster now that I look back. I also thank the OC boss Herr Lehmann for readily answering all my chemistry questions meanwhile improving my German skills. The whole BIG-NSE family "led by" Dr. J.P. Lonjaret deserves a huge THANK YOU from my side. I have enjoyed all the events together: Durga Puja, Chinese and Iranian cultural eves, bike tours, CatSlam, Christmas parties, social evenings all accompanied by happy faces and beer! I am happy to have spent not only the BIG-NSE inital phase but also many meaningful moments with my scientifically and otherwise talented batchmates:): Daniel Gallego, Gengwen Tan, Laura Vieweg, Linyu Jiao, Matthias Parthey, Moritz Baar, Hong Nhan Nong, Patrick Littlewood, Setarehalsadat Sadjadi and Xunhua Zhao! I also thank Laura Carito for teaching me the Colombian dance during the world cup. This should be a skill useful in the future!

I thank Nieke Aerts for her friendship and I appreciate all the time we spent together while exploring Berlin life! It was great to share our happy and sad moments and I hope we will do this in the future too. I thank my former colleagues and friends in the Netherlands Sabriye and Hans Fredriksson, Leen Broeckx, Iris de Krom, Samaneh Kheyrroz, Henriette Nowothnick, Remco Aerts, Michele Koper, Marloes Verbruggen, Marieke Steenbeeke and Irma Bouwman for their hospitality during my visits in Eindhoven and for their visits in Berlin to explore the city together. It is very nice that we kept in touch and shared our (PhD) experience with each other.

I would also like to thank all the members of my football team, FSV Hansa 07, who managed to motivate me to come out and play on a weekly basis during my PhD work, greatly contributing to the maintenance of my work-life balance. Thanks for teaching me all the nice words in German :) and introducing me to Schrottwichteln. Thanks goes to Jonathan Mouat for the many excellent running sessions and for being such a good neighbor.

Finally I am thanking my family who supported me from afar and who waited patiently for my irregular calls in the last couple of months. Anyu és Nyuszi, köszönöm hogy gondoskodtatok arról az évek során, hogy meg legyen a lehetőségem ezt az utat választani! Nagyon sokat köszönhetek Nektek és tudom, hogy nélkületek, nem jutottam volna eddig. Apu, köszönöm azt a két izgalmas gimis nyarat Budapesten, ami rádöbbentett, hogy nem is akarnék máshol tanulni! Köszönöm hogy ott voltál abban a három és fél évben és segítettél hogy otthon érezzem magam a nagyvárosban is. Klaudia, köszönöm hogy számíthattam rád a budapesti évek alatt és hogy olyan sokszor meglátogattál külföldön is! Remélem ez ezután is így lesz majd, és ülünk még a bárpultnál társalogva, finom koktélt iszogatva a jövőben is sokszor:). Dorina, Te pedig felnőttél miközben én csak kémiát tanultam:). Köszönöm, hogy meglátogattál nyáron, igazán jól éreztem magam és végre megismerhettelek

egy kicsit jobban is:). Remélem Te is hamar megtalálod azt ami legjobban érdekel és egy sikeres út áll előtted. Ha gyakorolnád a németet (vagy ha nem), bármikor szívesen látunk!
Ich möchte mich bedanken bei der Familie Sonntag für die unendliche Unterstützung und die liebevollen Familientreffen in den letzten drei Jahren. Es war immer sehr lustig mit Euch zusammen Zeit zu verbringen und ich habe gelernt, dass im Leben wie in der Chemie nicht alles so einfach ist wie es aussieht. Ich hoffe, wir sehen uns öfter in der Zukunft um noch mehr schöne Erfahrungen zu erleben! Ihr seid für mich alle Lieb und wir sehen uns bald!
Micha, the last lines are for you! It seems we have survived two thesis writing periods:). Not bad! I am most grateful for all your support in the last couple of years and wish us an exciting future together with many opportunitites!